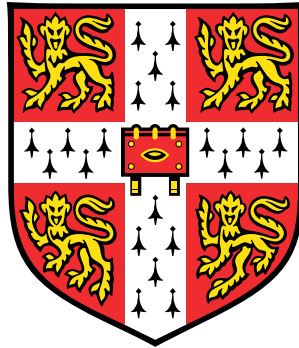


GALACTIC STRUCTURE WITH GIANT STARS

JAMES RICHARD GRADY



Corpus Christi College
University of Cambridge

March 2021

This dissertation is submitted for the degree of Doctor of Philosophy

ABSTRACT

The content of this thesis derives from three projects conducted during my Ph.D, focusing on both the Milky Way and the Magellanic Clouds. I deploy long period variables, especially Miras, as chronometers to study the evolution of Galactic structure over stellar age. I study red giants in the Magellanic Clouds, assign them photometric metallicities and map large scale trends both in their chemistry and proper motions.

In Chapter 1 I provide an overview of the historical observations that underpin our current understanding of the Galactic components. Specifically, I detail those pertaining to the Galactic bulge, the Galactic disc and the Magellanic Clouds as it is these that constitute the main focus of the work in this thesis.

In Chapter 2 I collate a sample of predominately oxygen-rich Mira variables and show that gradients exist in their pulsation period profiles through the Galaxy. Under the interpretation that the period of Miras correlates inversely with their stellar age, I find age gradients consistent with the inside-out disc formation scenario.

I develop such analysis further in Chapter 3: seizing on the Miras provided by *Gaia* DR2, I observe them to trace the Galactic bulge/bar and disc. With the novel ability to slice both components chronologically at once, the old disc is seen to be stubby; radially constricted and vertically extended. The younger disc is vertically thinner and more extensive radially, providing further observational evidence for inside-out formation of the Milky Way disc. The longer period and hence younger bulge Miras show a clear bar-like morphology bearing the classic X-shape. The old, short period bulge Miras appear to constitute a separate population, decoupled from the inclined bar with little evidence for having buckled.

Chapter 4 details a chemo-kinematic analysis of red giants residing in the Magellanic Clouds. I utilise optical and infra-red photometry to assign photometric metallicity estimates to the giants. The metallicity structure in the larger Cloud correlates with known stellar overdensities induced from historic perturbations. I observe the smaller Cloud to be disrupting, identifying stellar debris trailing the dwarf.

DECLARATION

This thesis is the result of my own work and includes nothing which is the outcome of work done in collaboration except as declared below and specified in the text¹:

- Chapter 2 is based on the work published under the title: "Age gradients throughout the Galaxy with long-period variables" in Monthly Notices of the Royal Astronomical Society; Grady, Belokurov, and Evans (2019).
- Chapter 3 is based on the work published under the title "Age demographics of the Milky Way disc and bulge" in Monthly Notices of the Royal Astronomical Society; Grady, Belokurov, and Evans (2020).
- Chapter 4 is based on the work published under the title "Magellanic Mayhem: Metallicities and Motions" in The Astrophysical Journal; Grady, Belokurov, and Evans (2021).

It is not substantially the same as any that I have submitted, or, is being concurrently submitted for a degree or diploma or other qualification at the University of Cambridge or any other University or similar institution. I further state that no substantial part of my dissertation has already been submitted, or, is being concurrently submitted for any such degree, diploma or other qualification at the University of Cambridge or any other University of similar institution. It does not exceed the prescribed 60,000 word limit.

Cambridge, March 2021

James Richard Grady

¹ Where appropriate, I maintain the use of the proverbial "we" so as to be consistent with the published works that form this thesis.

For Dad

ACKNOWLEDGMENTS

I would like to sincerely thank my supervisors, Prof. N. Wyn Evans and Prof. Vasily Belokurov, for their continual guidance throughout my time studying in Cambridge. Both have provided me with a great deal of advice and encouragement in my studies, layered with good humour. I would also like to thank all members of the Streams group. Their suggestions and comments have always been fruitful and the group meetings have provided stimulating topics of discussion and inquiry. I thank Sergey Kuposov for maintaining the Whole Sky Database, a truly invaluable resource for any astronomer. I further thank the administrative staff within the Institute for their prompt and effective support. Acknowledgement is owed to the Science and Technologies Facilities Council who provided the funding for my research.

I would like to thank my fellow students at the Institute; I have made some great friends. Many an evening we have spent laughing and conversing in some of Cambridge's fine pubs! A necessary antidote to the rigours of research.

Further thanks goes to Corpus Christi College for hosting me during my time here in Cambridge. I have enjoyed partaking in the unique collegiate life offered by this University. It has also been a pleasure to represent the College in my sporting efforts, having had great fun in turning out regularly for the football and cricket teams alongside a thoroughly enjoyed spell of rowing.

Above all, I thank my family. Unfailing in your love and support, you have kept me going. Thank you.

CONTENTS

1	INTRODUCTION	1
1.1	The Milky Way in Context	1
1.2	The Galactic Bulge	2
1.2.1	Bulge Morphology	3
1.2.2	Stellar Ages in the Bulge	4
1.2.3	Bulge Metallicity Distribution	5
1.2.4	Bulge Kinematics	6
1.3	The Galactic Disc	8
1.3.1	Disc Dichotomy	9
1.3.2	Formation of the Discs	11
1.3.3	Disc Substructure	13
1.4	The Magellanic Clouds	14
1.4.1	Large Magellanic Cloud	15
1.4.2	Small Magellanic Cloud	17
1.4.3	Magellanic Interactions	17
1.5	Long Period Variables	19
1.5.1	What is a Long Period Variable?	19
1.5.2	Useful characteristics of Long Period Variables	20
1.6	Thesis Structure	21
2	AGE GRADIENTS THROUGHOUT THE GALAXY WITH LONG PERIOD VARIABLES	23
2.1	Data	23
2.1.1	Mira Selection	24
2.1.2	O-rich LPV Distributions	27
2.1.3	Distance Determination and Validation	28
2.2	Galactic Age Gradients	31
2.2.1	Miras outside of the Galactic disc	36
2.2.2	Satellite Galaxy and Globular Cluster Associations	41
2.3	Summary	44
3	AGE DEMOGRAPHICS OF THE MILKY WAY DISC AND BULGE	47
3.1	Data	47
3.1.1	Selecting Miras	48
3.1.2	Miras in the Large Magellanic Cloud	49
3.1.3	Galactic Sample	50
3.2	Stellar Density Profiles	52
3.2.1	Modelling the Galactic Disc and Bulge	52
3.2.2	Simulated data	56
3.3	Results	58

3.3.1	Miras in the Disc	59
3.3.2	Miras in the Bulge	65
3.4	Summary	72
4	MAGELLANIC MAYHEM: METALLICITIES AND MOTIONS	75
4.1	Data	75
4.2	Regression Analysis	80
4.2.1	Regression Performance	83
4.2.2	Regression Predictions	83
4.3	Metallicity Maps	86
4.3.1	Metallicity Gradients	91
4.3.2	Slicing the Clouds by Metallicity	98
4.3.3	SMC shape and disruption	102
4.3.4	Old stellar Bridge	108
4.4	Summary	112
5	CONCLUSIONS AND OUTLOOK	115
5.1	Conclusions	115
5.2	Outlook	117
A	APPENDIX	121
A.1	Mira Cluster Associations	121
A.2	Density profile likelihood	122
A.3	Model M2 Residuals	123
	BIBLIOGRAPHY	125

LIST OF FIGURES

Figure 1.1	APOGEE giant abundance trends	10
Figure 1.2	Magellanic main sequence stars and red giants.	16
Figure 1.3	Epoch photometry of <i>Gaia</i> LPVs.	20
Figure 2.1	Selection criteria for O-rich LPV candidates from the CRTS and ASAS-SN data sets.	25
Figure 2.2	Period-luminosity diagram for <i>Gaia</i> LPVs in the LMC.	26
Figure 2.3	Visual amplitude histograms of selected and rejected O-rich candidates.	27
Figure 2.4	Spatial distributions of O-rich LPVs in CRTS and ASAS-SN.	28
Figure 2.5	Distance estimate validation using the LMC and the Sgr Stream.	29
Figure 2.6	Location of O-rich LPVs in Galactocentric cylindrical coordinates.	30
Figure 2.7	Dependence of Mira age with period using Galactic and Magellanic clusters.	31
Figure 2.8	Spatial footprint of O-rich LPVs as a function of pulsation period.	32
Figure 2.9	Profiles of median LPV pulsation period through the Galaxy.	33
Figure 2.10	Period profiles of ASAS-SN stars through the disc at different heights from the plane.	34
Figure 2.11	Decomposition of LPVs sub-groups in on-sky projection.	37
Figure 2.12	Difference in spatial extent between short and long period LPVs.	38
Figure 2.13	Distribution of old, short-period LPV stars in the Milky Way halo as viewed by CRTS.	40
Figure 2.14	Great circle counts of LPVs.	41
Figure 2.15	Dwarf galaxy and globular cluster associations.	42
Figure 3.1	<i>Gaia</i> +2MASS LPVs in Galactic projection.	48
Figure 3.2	Mira selection in <i>Gaia</i> DR2.	49
Figure 3.3	Mira period-luminosity diagram.	50
Figure 3.4	Miras in the Galaxy at different periods.	51
Figure 3.5	Luminosity function of Mira sample.	54
Figure 3.6	Simulated data modelling.	57

Figure 3.7	Marginalised posterior distributions for density model parameters. 58
Figure 3.8	Evolution of recovered model parameters as a function of Mira pulsation period 60
Figure 3.9	Model residuals in Galactocentric (X,Y) projection for disc+bulge. 62
Figure 3.10	Model residuals in Galactocentric (X,Z) projection for disc+bulge. 63
Figure 3.11	Model residuals in Galactocentric (Y,Z) projection for disc+bulge. 64
Figure 3.12	Model residuals in Galactocentric (X,Z) projection for disc only. 65
Figure 3.13	Model residuals in Galactocentric (Y,Z) projection for disc only. 67
Figure 3.14	Model residuals in Galactocentric (X,Y) projection for disc only. 69
Figure 3.15	X-shape of Miras in the bulge. 71
Figure 4.1	Magellanic RGB stars and RR Lyrae. 77
Figure 4.2	<i>Gaia</i> +2MASS+WISE red giants in Magellanic Stream coordinates. 78
Figure 4.3	Colour magnitude diagrams in the <i>Gaia</i> +2MASS+WISE photometric systems. 79
Figure 4.4	APOGEE training data CMDs and [Fe/H]-colour correlations. 81
Figure 4.5	Model learning curve. 82
Figure 4.6	Model prediction performance. 84
Figure 4.7	Predicted metallicities as a function of WISE colour $W1 - W2$. 85
Figure 4.8	Metallicity distribution function of the Clouds. 87
Figure 4.9	Stellar densities, metallicities and extinction in the LMC+SMC 89
Figure 4.10	Metallicity gradient in the LMC. 92
Figure 4.11	Bar-aligned metallicity profiles of the Clouds. 93
Figure 4.12	Metallicity structure in the LMC. 95
Figure 4.13	Proper motion dispersion histograms of LMC sub-structure. 96
Figure 4.14	Changing morphology of the Clouds with metallicity. 98
Figure 4.15	Mean motions and dispersions in μ_L in three metallicity bins. 100
Figure 4.16	Mean motions and dispersions in μ_B in three metallicity bins. 101
Figure 4.17	Distorted shape of the SMC. 103

Figure 4.18	Disrupted motions in the SMC.	104
Figure 4.19	Trailing tail of the SMC.	105
Figure 4.20	Metallicity structure across the old stellar bridge.	109
Figure 4.21	<i>Gaia</i> RR Lyrae lying between the Clouds.	111
Figure 5.1	Sagittarius giant distance estimates	119
Figure A.1	Model M2 residuals in Galactocentric (X, Y) projection.	123
Figure A.2	Model M2 residuals in Galactocentric (X, Z) projection.	124
Figure A.3	Model M2 residuals in Galactocentric (Y, Z) projection.	124

LIST OF TABLES

Table 2.1	Distant O-rich LPV candidates.	39
Table 2.2	Candidate Mira associations with Galactic dwarf spheroidals and distant globular clusters.	43
Table 3.1	Inference of model parameters from simulated data.	57
Table 3.2	Inferred model parameters of the Galactic disc and bulge.	59
Table 4.1	Error in our regression predictions across four metallicity bins.	83
Table A.1	LMC pairs of clusters and Mira shown in Fig. 2.7.	121
Table A.2	Milky Way pairs of clusters and Mira shown in Fig. 2.7.	121

ACRONYMS

AGB	Asymptotic Giant Branch
APOGEE	The Apache Point Observatory Galactic Evolution Experiment
ARGOS	Abundances and Radial velocity Galactic Origins Survey
ASAS-SN	All-Sky Automated Survey for Supernovae
BP	Boxy-peanut
BRAVA	Bulge Radial Velocity Assay
C-rich	Carbon rich
CMD	Colour magnitude diagram
GC	Galactic Centre
LMC	Large Magellanic Cloud
LPV	Long period variable
MB	Magellanic Bridge
MDF	Metallicity Distribution Function
MS	Magellanic Stream
MW	Milky Way
OLR	Outer Lindblad Resonance
O-rich	Oxygen rich
OGLE	Optical Gravitational Lensing Experiment
PL	Period-luminosity
RC	Red Clump
RG	Red Giant
RGB	Red Giant Branch
RRL	RR Lyrae
SEGUE	Sloan Extension for Galactic Understanding and Exploration
SDSS	Sloan Digital Sky Survey
Sgr	Sagittarius
SMC	Small Magellanic Cloud
SRV	Semi-regular variable
SVR	Support Vector Regression
VVV	Vista Variables in the Via Lactea
2MASS	The Two Micron All-Sky Survey

INTRODUCTION

1.1 THE MILKY WAY IN CONTEXT

Our Galaxy, the Milky Way (MW), is a spiral galaxy that may be typically characterised by three broad components: a central bulge, a flattened disc and a diffuse halo. The stellar content of these components differ in their age, chemistry, structural morphology as well as in their kinematics. Under this basic framework, one can consider the bulge and halo to host the older stars in our Galaxy, with the younger stars mainly residing in the disc. Central to the Galaxy is the massive black hole Sagittarius A*, with an estimated mass of $\sim 4 \times 10^6 M_{\odot}$ as determined by Gillessen et al. (2009) in their analysis of stellar orbits close to the Galactic centre (GC).

The bulge is boxy, triaxial and bar like, with its major axis offset from the Solar – Galactic Centre line (bar angle) by $\sim 20^{\circ} - 30^{\circ}$; a non-axisymmetric contributor to the Galactic potential. The orbits of stars in the bulge are complex though the structure as a whole is observed to rotate cylindrically. The metallicity distribution function (MDF) in the bulge is complex, with a mixture of populations observed from super-solar values and down to metal poor values of $[Fe/H] < -1$ (see e.g. Ness et al., 2013a). In a rudimentary sense, the disc can be described as a collection of stars moving coherently on near circular orbits around the GC, never straying too far from the plane of the Galaxy. Ages of stars in the disc are varied, encompassing those that are newly born through to stars that are billions of years old. The now classic work of Gilmore and Reid (1983) found the vertical stellar density profile of the disc to be well modelled by a double exponential. A ‘thin’ disc component with scale height ~ 0.3 kpc and a ‘thick’ disc component with scale height ~ 1 kpc was identified. The disc hosts the majority of the Galaxy’s stellar content, with Licquia and Newman (2015) estimating a mass of $\sim 5 \times 10^{10} M_{\odot}$ compared to $\sim 0.9 \times 10^{10} M_{\odot}$ for the bulge. The stellar content of the halo is relatively small at $\sim 10^9 M_{\odot}$ but its extent is large, reaching out to $r > 100$ kpc¹ from the GC. The stellar density follows a power law with index ~ -2.5 out to 20 kpc, falling off more rapidly beyond this, with much of the outer halo is spherically distributed. Halo denizens are metal

¹ Throughout this thesis, unless otherwise stated, I will denote Galactocentric spherical radius by r and Galactocentric cylindrical radius by R .

poor and ancient, with ages surpassing 10 Gyr, and the motions of these stars is largely disordered, following orbits of all orientations. However, stratification on metallicity has led to an observational dichotomy: there appears to be an inner, metal-rich component that is mildly prograde in its motion alongside an outer, more metal-poor one that is retrograde (see e. g. Nissen and Schuster, 2010).

The Milky Way is a primary component of the Local Group, a galactic system comprised of gravitationally bound spirals and dwarfs. The other principal member is the Andromeda galaxy (M31), orbited by the dwarfs M32 and M33. Similarly, the Milky Way hosts its own collection of satellite galaxies, notably the Large and Small Magellanic Clouds visible by eye in the southern sky; two interacting dwarf galaxies located approximately 50 kpc and 60 kpc away respectively. Our closest satellite, however, is the Sagittarius Dwarf galaxy (Sgr), residing behind the bulge at a heliocentric distance of $\sim 25 - 30$ kpc. Its motion is nearly perpendicular to the stellar disc northwards and is striking in its disruption, with tidal tails spanning much of the sky and populating the stellar halo; a clear indication that the stellar halo is not a homogeneous component. Indeed it is observed to be littered with remnants and stellar debris as the MW has cannibalised dwarf satellites over its history. Invaluable tracers of the outer halo, their kinematics are exploited in determining the total mass of the MW estimated of order $\sim 1 \times 10^{12} M_{\odot}$ (see e. g. Callingham et al., 2019; Deason et al., 2021), the mass budget being dominated by dark matter.

1.2 THE GALACTIC BULGE

The bulge was first recognised as a distinct component of our Galaxy by Baade (1946) in observing a high density of aged stellar populations towards the GC (see also Stebbins and Whitford, 1947). The bulge has garnered much interest in order to ascertain the origin of this structure, with two main theories existing. One posits the bulge formed as a consequence of successive mergers at early stages in the Galaxy's history. The competing scenario sees the bulge form secularly, born out of natural dynamical evolution of the stellar disc. These differing formation scenarios yield distinct structures that, following the convention of Kormendy and Kennicutt (2004), are called classical bulges and pseudo-bulges respectively. Consequently, the structural nature of the MW bulge has been much studied to ascertain its exact nature. A number of observational distinctions between the two bulge types have been found in external galaxies; the Sérsic index of stellar light in pseudo-bulges is generally observed to be less than 2 (i.e.

near exponential), whereas that of classical bulges is almost always greater than 2 (see e.g. Fisher and Drory, 2008). The velocity dispersion profiles of classical bulges are centrally peaked, with pseudo-bulge profiles flattening centrally, and are generally observed with central velocity dispersions exceeding $\sim 100 \text{ km s}^{-1}$ (see e.g. Fabricius et al., 2012). In projections of the fundamental plane, classical bulges are near indistinguishable from normal elliptical galaxies, with pseudo-bulges showing greater scatter about the projected relations. Ultimately, classical bulges closely resemble rotating elliptical galaxies, differing in the fact that they are surrounded by a stellar disc. Pseudo-bulge morphology is more varied, ranging from ‘boxy’ to ‘X-shaped’, and exist as the central portion of an elongated, flatter bar residing in the disc (see e.g. Erwin and Debattista, 2013).

I will consider four main characteristics of the MW bulge in this opening chapter, outlining the observations pertaining to each and how they contribute to our current understanding of the bulge and its formation:

- Morphology
- Stellar age
- Metallicity
- Kinematics

1.2.1 *Bulge Morphology*

Utilising data from the Cosmic Background Explorer (COBE) satellite, Dwek et al. (1995) confirmed the global nature of the Milky Way bulge to be ‘boxy’ and tri-axial in its morphology, complementing the barred structure observed by Weiland et al. (1994) in the same data set. Subsequent analysis of Red Clump (RC) giants towards the GC by McWilliam and Zoccali (2010) revealed a split in the stellar luminosity function, interpreted as the signature of an X-shaped bulge/boxy-peanut (BP) bulge. Drawing ~ 8 million bulge RC giants from the Vista Variables in the Via Lactea (VVV) survey, Wegg and Gerhard (2013) further established the MW inner bulge to be boxy, orientated with a bar angle of $27^\circ \pm 2^\circ$ and, at approximately 400 pc above Galactic plane, to display a prominent X-shape in its density distribution. Whilst such a morphology has been contested, with López-Corredoira et al. (2019) claiming that the split RC is a result of two distinct stellar populations, the spectacular WISE imaging of Ness and Lang (2016) reveals the X-shape clearly. The proper motion data from VVV as analyzed by Sanders et al. (2019) show differential motion between the

peaks, which argues strongly against population effects causing the X-shape; if population effects were to describe the split RC, each peak should have similar kinematics. Such a morphology is a clear indicator of a pseudo-bulge component central to the galaxy, formed out of the buckling instability known to affect barred structures and supported by resonant banana orbits (Williams et al., 2016). Compiling a RC sample from the The Two Micron All-Sky Survey (2MASS), VVV and UK Infrared Deep Sky Survey, Wegg, Gerhard, and Portail (2015) observed a smooth extension of stars from the inner bulge out into a longer, thinner bar lying at an angle of $\sim 28^\circ$. Thus the MW appears to harbour a central boxy bulge that itself is the vertical extension of a more extended, thinner bar, as observed in numerous external galaxies (see e.g. Bureau and Freeman, 1999; Erwin and Debattista, 2013; Savchenko et al., 2017).

This picture is complicated, however, by claims of ancient bulge stellar populations forming a distinct central component. Studying a sample of VVV RR Lyrae (RRL), Dékány et al. (2013) observed them to be distributed in a spheroidal, central fashion with no indication they trace the bar like structure seen in the RC giants. More recently, Prudil et al. (2019) combined data from the VVV and the Optical Gravitational Lensing Experiment (OGLE) IV to obtain a sample of $\sim 8,000$ bulge RRL, again finding no spatial correlation with the bar. Catchpole et al. (2016) studied a sample of bulge Mira variables, whose pulsation period correlates inversely with stellar age, and found a similar situation. Splitting their sample into older and younger sub-populations, through stratifying on period, they observed the likely younger Miras to be those that trace a tilted bar, with the more ancient Miras distributed centrally and smoothly. Interestingly, a recent analysis of $\sim 16,000$ OGLE+*Gaia* bulge RRL by Du et al. (2020) saw the metal poor RRL, $[\text{Fe}/\text{H}] < -1$ dex, to follow a smaller bar angle than the metal rich RRL orientated at $\sim 20^\circ - 30^\circ$, a value consistent with the RC structure. The possibility that these central metal-poor RRL are in fact an inner extension of the halo is debated and it is still unclear whether the true nature of the MW bulge is indeed composite.

1.2.2 *Stellar Ages in the Bulge*

The majority of stars in the MW bulge are old, as gleaned from dedicated photometric studies towards this region. Zoccali et al. (2003) utilised near infra-red observations to produce bulge colour magnitude diagrams (CMDs) from the Red Giant Branch (RGB) down to the main sequence turn off, a useful age indicator. In doing so, they concluded that the bulk of the bulge population studied, lying in a low

extinction region at $(\ell, b) \sim (0.3^\circ, 6^\circ)$, was ~ 10 Gyr old (see Valenti et al., 2013, for a similar analysis). Clarkson et al. (2008) studied the CMD of kinematically selected bulge stars observing a tight turnoff and a negligible upper main sequence, from which they concluded the majority of bulge stars bear ages of $\sim 11 \pm 3$ Gyr. A recent, data-driven analysis of $\sim 1,500$ APOGEE bulge stars by Sit and Ness (2020), covering a region of $|b| < 15^\circ$ and $-5^\circ < \ell < 15^\circ$, found the mean age of their bulge sample to be ~ 8 Gyr, significantly older than the disc stars in their sample whose mean age was ~ 4 Gyr. Similarly, Hasselquist et al. (2020) employed similar methods to a sample of $\sim 6,000$ metal rich bulge stars, finding the bulk of them to bear ages in excess of 8 Gyr. Interestingly, they also observed a non-negligible of younger stars, 2 – 5 Gyr, lying close to the plane. Bensby et al. (2017) obtained high resolution spectra of 90 bulge stars from which they obtained estimates of stellar age. Indeed, for the metal-rich portion of their sample ($[\text{Fe}/\text{H}] > -0.5$ dex) they observed a wide range of stellar ages spanning $\sim 2 - 10$ Gyr. Further, a portion of their sample bear super-solar metallicities and one third of these were determined to have ages less than 8 Gyr. Indeed, a bulge that formed secularly out of the disc might be expected to harbour a population of young stars.

1.2.3 *Bulge Metallicity Distribution*

Early metallicity measurements of bulge stars were derived from stellar spectra towards low extinction regions (see e.g. McWilliam and Rich, 1994; Ramírez et al., 2000; Sadler, Rich, and Terndrup, 1996), indicating the mean bulge population is metal rich, peaking around $[\text{Fe}/\text{H}] \sim 0$ dex. Early claims of a metallicity gradient within the bulge were made by Minniti et al. (1995) from low resolution spectroscopic observations of RGs, with stellar metallicity decreasing on increasing distance away from the bulge along the minor axis. Such gradients have been of observational interest as they could provide insight into the MW bulge formation process. For example, the vertical heating processes that transform a bar into a boxy pseudo-bulge may not be expected to act preferentially on the more metal poor stars.

Subsequently, Zoccali et al. (2008) measured the MDF of RGB stars at three fields along the bulge minor axis from high resolution spectroscopy. Giants presented metallicities in the range $-1.5 < [\text{Fe}/\text{H}] < 0.5$ with metal rich stars gradually disappearing on increasing latitude. Such a gradient was also observed by Ness et al. (2013a) who identified up to five Gaussian components in the MDF with the metal rich components dominating at lower latitudes, $b \sim -5^\circ$ and the sig-

nificance of metal poorer components increasing farther away from the plane down to $b \sim -15^\circ$. Substructure within the bulge MDF has also been identified by Rojas-Arriagada et al. (2014) from the *Gaia*-ESO survey observations wherein they identified two broad components: a narrow metal rich, super-solar component and a broader metal poor, sub-solar one. The relative weights of the two components evolves on moving away from the bulge, in turn producing a mean metallicity gradient and indicative of a composite bulge nature. Indeed, through observing the magnitude distribution of both components, they observe only the metal rich stars to present a bimodal profile, characteristic of an X-shaped bulge/bar (see Ness et al., 2012, also). Such a dichotomy is interesting given the morphological evidence of a secularly evolved MW bulge. The metal rich, X-shaped bulge stars are thought to be those originating in the MW disc, trapped by the bar potential and subsequently buckling to form the boxy/X-shape.

1.2.4 *Bulge Kinematics*

In considering the morphology, age and metallicity distribution of bulge stars, the picture appears somewhat complex; old, metal poor stars co-exist with old metal rich stars differing in their spatial distribution, compounded by the claims of non-negligible fractions of young stars residing in the bulge. Modern spectroscopic surveys have provided significant advances in our understanding of the dynamical characteristics of the bulge. It is understood that the MW bulge lies between a purely rotating system and one solely supported by velocity dispersion. The Bulge Radial Velocity Assay (BRAVA) (Howard et al., 2008; Kunder et al., 2012) obtained radial velocity measurements of giants along the bulge major and minor axes, finding evidence for cylindrical rotation, i.e. independent of vertical distance, a characteristic observed in external barred galaxies with pseudo-bulges (see e.g. Bureau and Freeman, 1999; Kormendy and Illingworth, 1982; Molaiezhad et al., 2016). Shen et al. (2010) compared the BRAVA data to N-body bar simulations tuned to represent the MW. From the kinematic data, they rule out the existence of a classical bulge component residing alongside a pseudo-bulge that forms secularly out of the the bar buckling instability.

The chemo-dynamical information provided by the Abundances and Radial velocity Galactic Origins Survey (ARGOS) allowed Ness et al. (2013b) to chemically dissect the bulge and study the kinematics of four metallicity bins: $[\text{Fe}/\text{H}] > 0$, $-0.5 < [\text{Fe}/\text{H}] < 0$, $-1 < [\text{Fe}/\text{H}] < -0.5$ and $[\text{Fe}/\text{H}] < -1$ labelled A, B, C and D re-

spectively. They observed stars in bins A – C to rotate cylindrically with the metal poorest stars, in bin D, rotating much more slowly at higher velocity dispersion. Studying the magnitude distribution of their stars, they observe stars in bins A and B to display the double peaked profile synonymous with a BP bulge. Further, these stars show similar, centrally peaked, dispersion profiles as a function of longitude with bin A being somewhat cooler. Stars in bin C are markedly different with flatter dispersion profiles independent of latitude. Ness et al. (2013b) posit that populations A and B share a common disc origin having buckled into the BP bulge. The metal poorer stars in bin C are suggested to represent the inner extension of the thick disc and those in bin D constituting the inner halo/an accreted population.

Du et al. (2020) studied the kinematics of bulge RRL drawn from the OGLE survey equipped with *Gaia* Data Release 2 (DR2) proper motion measurements, the latter allowing them to study the rotation curve for $\sim 16,000$ bulge stars. Indeed the motions of the RRL at differing latitudes were observed to be consistent with a cylindrically rotating bulge. Splitting their sample into metal poor, $[\text{Fe}/\text{H}] < -1$, and metal rich, $[\text{Fe}/\text{H}] > -1$, they observed the former sub-sample to rotate slowly with an angular velocity of $\sim 32 \text{ km s}^{-1} \text{ kpc}^{-1}$. In comparison the metal rich sub-sample was found to rotate at $\sim 40 \text{ km s}^{-1} \text{ kpc}^{-1}$, intermediate between the metal poor RRL and the RC giants analysed by Sanders et al. (2019).

Some insight into the apparent chemo-dynamical complexity of the bulge has been gleaned from modern simulations. Debattista et al. (2017) found that bars can efficiently separate disc populations in accordance with their initial velocity dispersions. Initially hotter stars form a vertically thicker, boxy bulge. Cooler stars are more strongly captured by the bar potential, subsequently buckling to form an X-shape. A continuous evolution in bulge properties with stellar age is observed ranging between the two extremes. Fragkoudi et al. (2018) explored a sample of barred galaxies in the Auriga cosmological suite of simulations to investigate the formation of BP bulges in MW like analogues. Indeed younger, metal-richer stars were observed to more strongly exhibit the buckled X-shape, with more ancient stars boxy, kinematically hotter and slower in rotation. They observe the analogues to best match the MW bulge properties are those in which the bulge predominately formed *in-situ*, experiencing a relatively quiescent recent history.

1.3 THE GALACTIC DISC

The Milky Way disc teems with complex structure and kinematic features that portray the turbulent history of formation, interaction and evolution. The detailed mechanisms of disc formation remain to be worked out, but the general picture is clear. Early infall of halo gas provides material that cools and settles into a disc in the inner regions of the galaxy. Gas accreted at later times falls onto the outer regions providing an ‘inside-out’ picture for the formation of the stellar disc (see e.g. Kepner, 1999; Larson, 1976; Mo, van den Bosch, and White, 2010). The Sun is located ~ 8 kpc from the GC with the circular velocity at this position measured to be $\sim 220 \text{ km s}^{-1}$. The disc is cold, with velocity dispersion measurements of order $\sim 20 - 30 \text{ km s}^{-1}$ observed locally, far outweighed by the bulk circular motion. Furthermore, a clear age dependence in stellar velocity dispersion has been observed (see e.g. Aumer and Binney, 2009; Holmberg, Nordström, and Andersen, 2009; Sanders and Das, 2018) with older stars being kinematically hotter; as disc stars age their orbits are ‘heated’, potentially through interactions with non-axisymmetric perturbations, giant molecular clouds or satellite galaxy infall (see e.g. Aumer, Binney, and Schönrich, 2016; Velazquez and White, 1999). Such interactions in effect increase the random motion of a star as it maintains its orbit at fixed angular momentum: *blurring*. Another secular process known to reorganise the disc is radial migration wherein the angular momentum of an orbit is now changed: *churning*. Orbital resonances induced by non-axisymmetric structure (e.g. spiral arms) are thought to seed such phenomena (Sellwood and Binney, 2002) and is observed as a strong effect in dynamical simulations (see e.g. Minchev et al., 2011; Roškar et al., 2008). It was determined by Frankel et al. (2020) to be dominant over blurring in the secular evolution of the MW. Stars harbour the chemical composition of the gas from which they were born, and those that radially migrate remain dynamically cold and act to flatten age/metallicity gradients through the disc.

The full extent of the MW’s disc is not fully constrained, though star forming molecular clouds have been observed out to $R \sim 20$ kpc (see e.g. Kobayashi et al., 2008) with claims of young stellar associations lying beyond $R \sim 15$ kpc (Carraro et al., 2010) and Cepheid variables observed to flare far from the plane at $R \sim 15 - 20$ kpc (Feast et al., 2014).

1.3.1 Disc Dichotomy

Gilmore and Reid (1983) first recognised the nature of the disc to be dual, introducing the notion of distinct thin and thick components both constituting the Galaxy’s stellar disc. More recent studies of the disc density profile have also found a distinction between the thin and thick discs in terms of both scale lengths and scale heights (see e.g. Jurić et al., 2008; Ojha, 2001; Yoachim and Dalcanton, 2006) with the distinction being purely geometric; the thick disc is both vertically and radially more extended than the thin disc. Further, such thick disc components are a common feature in other disc galaxies (see e.g. Comerón et al., 2012; Pohlen et al., 2007; Yoachim and Dalcanton, 2006). The Galaxy’s thick disc component has generally been observed as older (Kilic et al., 2017; Liu and Chaboyer, 2000) and kinematically hotter (Soubiran, Bienaymé, and Siebert, 2003; Yoachim and Dalcanton, 2006) than the thin disc.

Modern spectroscopic studies (see e.g. Adibekyan et al., 2011, 2012; Bensby, Feltzing, and Lundström, 2003; Hayden et al., 2015; Mishenina et al., 2004; Reddy, Lambert, and Allende Prieto, 2006) have revealed a chemical dichotomy within the disc. There exists a population of stars enhanced in $[\alpha/\text{Fe}]$ and deficient in $[\text{Fe}/\text{H}]$ comprising an older component. Conversely, there is a younger population enhanced in $[\text{Fe}/\text{H}]$ and deficient in $[\alpha/\text{Fe}]$. This is illustrated in Fig. 1.1 which shows APOGEE giants in the $[\alpha/\text{Fe}]$ vs $[\text{Fe}/\text{H}]$ plane; at fixed metallicity the $[\alpha/\text{Fe}]$ distribution is bi-modal. At $[\text{Fe}/\text{H}] \sim -0.2$ the high $[\alpha/\text{Fe}]$ sequence kinks, often labelled the ‘knee’, indicative of the delayed onset of Type Ia supernovae that subsequently become the dominant source of iron enrichment.

The work of Bovy et al. (2012) investigated the spatial structure of the disc through a sample of G-dwarfs from the Sloan Extension for Galactic Understanding and Exploration (SEGUE) survey. Having both $[\alpha/\text{Fe}]$ and $[\text{Fe}/\text{H}]$ information, they divided their sample into mono-abundance sub populations. The density profile of each sub-population was well modelled by a single exponential in both the radial and vertical directions. In this analysis, the scale length (height) decreases (increases) for older sub-populations, in stark contrast to the geometric thick and thin disc. Thus, it has now become common to refer to the α -rich and α -poor discs, in favour of the traditional thick and thin discs. Furthermore, given that $[\alpha/\text{Fe}]$ is a reasonable proxy for stellar age (see e.g. Fuhrmann, 1998; Schönrich and Binney, 2009b; Silva Aguirre et al., 2018; Wyse and Gilmore, 1988), the findings of Bovy et al. (2012) that the $[\alpha/\text{Fe}]$ enhanced (chemically old) stars are those most centrally concentrated and increasingly younger

The α elements are typically O, Mg, Si, S, Ca, Ti and are primarily produced in high mass stars ($M > 8 M_{\odot}$).

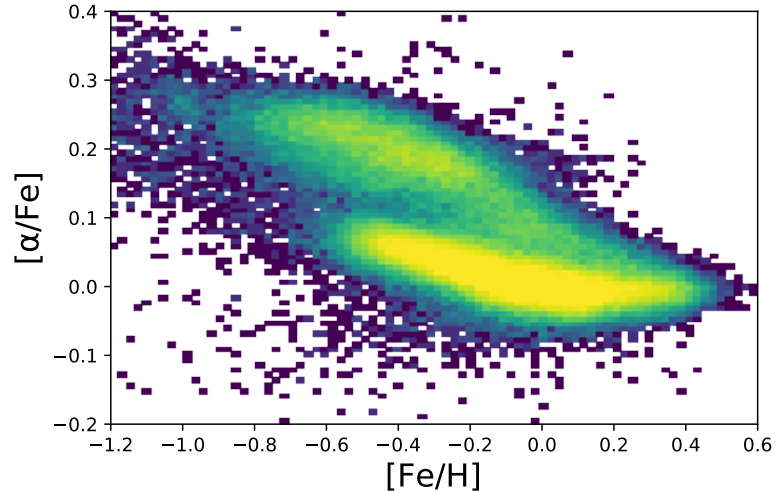


Figure 1.1: Density of giants in chemical abundance space from APOGEE. Two distinct sequences are clearly visible with clear bi-modality in $[\alpha/\text{Fe}]$.

stars are increasingly more radially extended is direct observational evidence of inside-out formation of the disc.

Hayden et al. (2015) collated a sample of $\sim 70,000$ giants from APOGEE DR12, mapping the distribution of stars in the $[\alpha/\text{Fe}]$ vs $[\text{Fe}/\text{H}]$ plane over an unprecedented volume of $3 \text{ kpc} < R < 15 \text{ kpc}$ and $|Z| < 2 \text{ kpc}$. Towards the inner galaxy at $R < 5 \text{ kpc}$, the low $[\alpha/\text{Fe}]$ sequence is absent. A single track is observed starting at high (low) $[\alpha/\text{Fe}]$ ($[\text{Fe}/\text{H}]$), breaking at the ‘knee’ and terminating at solar $[\alpha/\text{Fe}]$ and super solar metallicity. The metal rich end of this sequence dominates nearer the plane and is negligible at $|Z| > 1 \text{ kpc}$. Proceeding outwards radially, the form of the low $[\alpha/\text{Fe}]$ sequence becomes more apparent with the disc duality particularly clear locally. Near to the Sun, the relative fraction of low and high $[\alpha/\text{Fe}]$ stars varies on distance from the plane, with the latter becoming more dominant on increasing height. Furthermore, the locus of the low $[\alpha/\text{Fe}]$ sequence shifts to lower $[\text{Fe}/\text{H}]$ on increasing radial distance through the disc, driving a Galactic metallicity gradient. Towards the outer disc, beyond $R \sim 11 \text{ kpc}$ the high $[\alpha/\text{Fe}]$ sequence is virtually absent with low $[\alpha/\text{Fe}]$ stars dominating at all heights above and below the plane. The MDF of the outer disc is skewed positively, likely an effect of radial migration having driven metal rich inner disc stars outwards to larger radii. Interestingly, the high $[\alpha/\text{Fe}]$ sequence is remarkably similar at all radii for which it is observed, perhaps indicating that it is a well mixed system. Bovy et al. (2016) updated their previous work on disc structure utilising RC stars from APOGEE spanning the radial range of $4 \text{ kpc} < R < 15 \text{ kpc}$. Their results are consistent with those of Hayden et al. (2015); the $[\alpha/\text{Fe}]$ -rich stars are centrally concentrated

with a radial scale length of ~ 2 kpc. For the low $[\alpha/\text{Fe}]$ subset they observed more complex behaviour. Their radial density profiles peak at characteristic radii that increase on decreasing metallicity, consistent with the radial metallicity gradient in the disc. Furthermore, they observe the vertical scale height of the low $[\alpha/\text{Fe}]$ mono abundance populations to have a radial dependence; they flare in a manner interpreted to be indicative of radial migration and consistent with the observations of Hayden et al. (2015).

In essence, the inner and outer regions of the disc display very different chemical abundance patterns. Chemically old stars are vertically extended and confined to the inner regions of the Galaxy. Chemically young stars are largely confined to the plane but extend to a greater radial extent. In the outer disc they dominate the relative number density of the two sequences at all heights from the plane, flaring in this region.

1.3.2 Formation of the Discs

Whilst the $[\alpha/\text{Fe}]$ dichotomy of the disc has long been known and well mapped, its origin is still not fully understood with numerous chemo-dynamical models existing in the literature. A ‘two-infall’ scenario has been proposed wherein the thick disc forms out of early, rapid gas accretion with the thin disc forming at later times more steadily out of an extended period of gas in-fall (see e. g. Chiappini, Matteucci, and Gratton, 1997; Grisoni et al., 2017). Spitoni et al. (2019) utilised a sample of $\sim 1,000$ local RGs with both APOGEE chemical abundances and age estimates derived from asteroseismology (Silva Aguirre et al., 2018). They found good agreement in the abundance trends if the second accretion of primordial gas occurred ~ 9 Gyr ago, delayed relative to the initial infall by ~ 4 Gyr. Snaith et al. (2015) and Haywood et al. (2013) posit an alternative scenario in which the inner disc ($R < 10$ kpc) is a closed system – gas accretion occurs before any significant star formation. The outer disc is subject to accretion of primordial gas ~ 10 Gyr ago acting to dilute the *in-situ* gas. In order to reproduce the observed abundance trends, they find a cessation in star formation is required to produce the $[\alpha/\text{Fe}]$ dichotomy. State of the art simulations have been employed to gain insight into the formation mechanism of the double sequence and, in turn, the assembly history of the MW. Studying the highest resolution Auriga simulations, Grand et al. (2018) broadly observed the spatial evolution of the α sequences to agree with the APOGEE observations of Hayden et al. (2015): the low $[\alpha/\text{Fe}]$ sequence is more radially compact than the high $[\alpha/\text{Fe}]$ sequence. A dual pathway to the dichotomy was ob-

served regarding its formation in the inner and outer disc. Early gas rich mergers ignite an brief period of intense star formation and form the $[\alpha/\text{Fe}]$ -rich sequence. A quiescent period follows until Type Ia SN become prevalent, rapidly transitioning the gas to a low $[\alpha/\text{Fe}]$, high $[\text{Fe}/\text{H}]$ stage. Towards the outer disc ($R > 7$ kpc), a double $[\alpha/\text{Fe}]$ sequence was only observed in one of the simulations; that which saw two episodes of gas infall linked by a period of near zero star formation – a phenomenon they attribute to shrinking of the gaseous disc. Subsequent minor mergers of gas-rich satellites replenish the outer disc as well as diluting the ISM, seeding the formation of $[\alpha/\text{Fe}]$ -poor stars at low metallicities.

Such simulations are invaluable in light of the recent discovery that the MW did indeed suffer an early ($\sim 8 - 10$ Gyr ago) massive merger event (Belokurov et al., 2018; Deason et al., 2018; Myeong et al., 2018a,b,c). Building much of the stellar halo, it potentially formed the thick disc whilst simultaneously replenishing gas reserves from which the thin disc grew. Recently, Grand et al. (2020) analysed a set of Auriga simulations bearing a highly radially anisotropic halo component akin to the that in the MW – the ‘*Gaia* Sausage’. Prior to the merger, the MW analogue exhibits a proto-disc which is subsequently dynamically heated by the collision though maintaining its prograde, disc-like configuration. Owing to the rapid supply of gas a centrally concentrated starburst stellar population forms during the merger. Stars from both channels populate the $[\alpha/\text{Fe}]$ -rich sequence with subsequent rapid enrichment from the starburst. Post merger, the galaxy accretes metal poor gas from the circumgalactic medium, diluting the enriched gas and gradually grows the thin disc inside-out and upside-down.

As noted in Section 1.3, radial migration is an import consideration with regards to the evolution of the MW disc. Schönrich and Binney (2009a) proposed such a model that was broadly able to reproduce the local abundance trends. More recently, Sharma, Hayden, and Bland-Hawthorn (2020) developed an empirical chemical evolution model arguing that radial migration, specifically churning, is essential in forming the observed dichotomy. Whilst their model was tuned manually, they were able to reproduce the APOGEE observations of Hayden et al. (2015) without invoking separate evolutionary paths for the two sequences. Given that the MW did experience a historic massive merger, the details of the interplay between such an event and secular migratory processes are yet to be fully understood in the context of MW disc formation.

1.3.3 Disc Substructure

Analysing the spatial density distribution of main sequence Sloan Digital Sky Survey (SDSS) stars, Jurić et al. (2008) modelled the disc as a double exponential in standard fashion. Studying their model residuals revealed several substructures, notably the Virgo Overdensity and the Monoceros Ring; a ring-like stellar substructure located towards the Galactic anti-centre above the plane. Whilst N-body simulations have shown it is plausible such a structure was born out of the accretion of a satellite galaxy (see e. g. Guglielmo et al., 2018), it has also been suggested that it owes its origins to disc perturbations alone. Sheffield et al. (2018) estimated the fraction of RRL to M giants associated with the structure, informed by stellar kinematics, finding the value to be extremely low at ~ 0.02 and typical of the MW disc. This claim is bolstered by the chemical abundances obtained by Bergemann et al. (2018) for 14 stars towards this region, finding them to closely match the abundance patterns of disc stars. A similar analysis was conducted by Price-Whelan et al. (2015) regarding stars towards the Triangulum–Andromeda stellar overdensities, two halo structures located at large R (~ 30 kpc) and ~ 10 kpc below the plane. Again finding negligible RRL association, despite all known MW dwarfs containing at least some, they conjectured that such substructures constitute a population of kicked disc stars. On simulating a Sagittarius Dwarf like galaxy plunging through a MW like disc, corrugated ring like overdensities above and below the plane were induced; a tantalising indication that historic perturbations to the disc of the Galaxy may indeed eject stars from the plane and into the halo. As mentioned in Section 1.3, Feast et al. (2014) discovered five Cepheid Variables, usually disc residents, lying beyond 1 kpc vertically from the plane, indicative of flaring/warping in the outer disc.

The current era of *Gaia* has gone further in revealing the richness of MW disc substructure than ever before. Perhaps the most vivid demonstration has been provided by Antoja et al. (2018) who uncovered the $Z - V_Z$ phase space spiral of stars local to the Sun. Here we are afforded a glimpse into the phase mixing process currently ongoing in a disc that is out of equilibrium. This finding builds on that of Bennett and Bovy (2019) who identified oscillatory behaviour in stellar counts on increasing distance away from the plane: waves in the disc.

Equipped with a suite of N-body simulations mimicking the impact of a Sgr like dwarf on the MW, Laporte, Johnston, and Tzanidakis (2019) set out to first assess whether such a scenario could reproduce the structures observed towards the Galactic anti-centre. Indeed his-

toric pericentric passages of the dwarf are observed to induce Galactic ‘feathers’; stream like perturbations arching above and below the plane persisting for Gyrs. Analysing the same simulations in the inner disc, (Laporte et al., 2019) saw the Sgr like impact to produce a local phase spiral remarkably similar to that observed in the *Gaia* data. The simulated disc is perturbed globally after the most recent pericentric passage of the dwarf and they observe the phase spiral to exist from $R \sim 6$ kpc out to $R \sim 14$ kpc. Squashed in Z towards the inner disc, where the restoring force is greater, and less tightly wound in the outer disc where longer orbital timescales delay the progression of phase mixing. Encouragingly, Laporte et al. (2019) saw such behaviour in the *Gaia* DR2 phase spiral, with 6D phase space information afforded to them out to $R \sim 12$ kpc. Dissecting the spiral by age in the Solar neighbourhood, they observed the structure to be present over a range of ages ($\sim 0.5 - 9$ Gyr), corroborating earlier such claims by Tian et al. (2018) and indicative that it was seeded by a recent perturbation.

It thus appears that much of the substructure harboured by the MW disc can be understood through its historic interaction with the Sgr dwarf; stars can be kicked vertically, ‘feathers’ are drawn from the outer regions far from the plane and the disc is plunged into global disequilibrium for which *Gaia* has provided us a glimpse.

1.4 THE MAGELLANIC CLOUDS

The history of the Large and Small Magellanic Clouds is fraught with complex interactions and, being our nearest example of such a system, provides us with a vital laboratory for detailed study of interacting dwarf irregulars. Mass estimates of the Large Magellanic Cloud (LMC) yield a lower bound of $\sim 1.2 \times 10^{11} M_{\odot}$ and its smaller companion, the Small Magellanic Cloud (SMC), is estimated to have a total mass of $\sim 7 \times 10^9 M_{\odot}$ (Bekki and Stanimirović, 2009; Erkal and Belokurov, 2020). Both Clouds are gas rich systems, harbouring numerous sites of active star formation and giant molecular clouds. Their star formation histories are thought to be intimately linked through their mutual interactions. It has become increasingly evident that, given its high mass, the LMC has influence on the MW. For example, Erkal et al. (2019) determined the LMC capable of providing the gravitational perturbation necessary to produce the misalignment between the Orphan stream track and the velocity vectors of the stream’s denizens. Going further, Erkal et al. (2020) observe the southern (northern) halo to be blue-shifted (red-shifted) in its line of sight motion relative to the Sun, a signature they assign to stem from a downward accelera-

tion imparted onto the Galaxy by the LMC. Vasiliev, Belokurov, and Erkal (2021) arrived at a similar conclusion in studying the Sgr stream stellar orbits, finding a massive LMC in conjunction with the MW potential is required to accurately model the structure. In Chapter 4 I study the motions and metallicities of Magellanic giants, particularly in the context of their historic interactions with one another. Thus I here provide an overview of our current understanding of the Clouds, both individually and in relation to one another.

1.4.1 Large Magellanic Cloud

The LMC is generally well described by a planar disc, inclined by $\sim 20 - 30^\circ$ to our line of sight. Yet it still displays a host of deviations from this simple picture; it has long been observed to display one dominant spiral arm (see e.g. de Vaucouleurs, 1955; de Vaucouleurs and Freeman, 1972) as well as an off-centred stellar bar (e.g., Nikolaev et al., 2004; Zhao and Evans, 2000) and shell/ring like features (e.g. Choi et al., 2018b; Irwin, 1991; de Vaucouleurs, 1955). In a broad sense, the young stellar populations of the LMC exhibit a clumpy structure, largely congregating centrally around the bar and spiral arm, with little evidence for them residing in the outer regions (see e.g. Moni Bidin et al., 2017). The LMC interior is host to multiple star forming regions, most notably 30 Doradus, harbouring dense populations of young stellar objects and newly formed stars (see e.g. Cignoni et al., 2015; De Marchi et al., 2011; Ochsendorf et al., 2017; van Gelder et al., 2020). The recent morphological mapping of the Clouds by El Yousoufi et al. (2019) across a range of stellar ages shows the young main sequence stars and super-giants of the LMC primarily tracing a fragmented thin bar and spiral-like arms, along with clear overdensities associated with known star forming regions. On increasing stellar age, RC stars and red giants are observed to be distributed more smoothly, tracing a thicker bar and diminishing association with the spiral features. Comparison of the two panels in Fig. 1.2 highlights these morphological differences between LMC stellar populations as gleaned by *Gaia* EDR3 data.

Probing the planarity of the LMC using RC stars, Olsen and Salyk (2002) found an inner south-west region to display a prominent warp, curiously located in the portion of disc nearest to the SMC. More recently, Choi et al. (2018a) identified an outer RC warp in the Cloud, departing from the LMC plane by up to ~ 4 kpc towards the SMC. Towards the outer regions of the LMC, a plethora of substructure is observed with Mackey et al. (2016) first identifying a 10 kpc stellar arc located in the northern periphery of the LMC. The optical imaging of

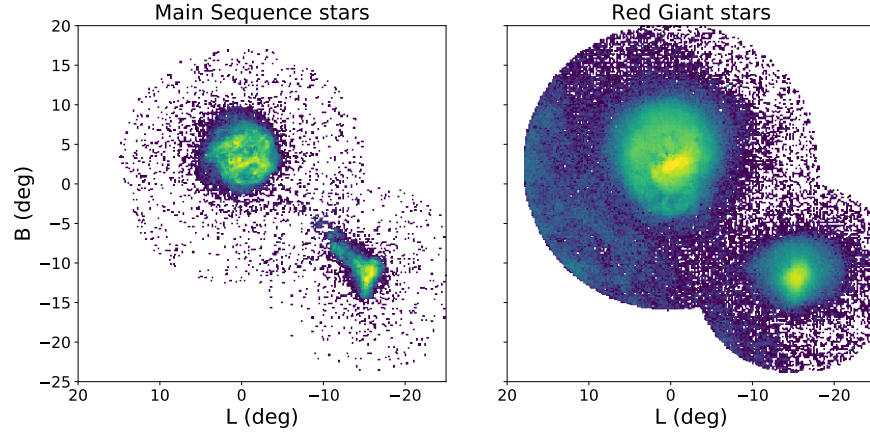


Figure 1.2: Spatial density of Magellanic main sequence and red giant stars in the left and right hand panels respectively, as observed by *Gaia*. In both instances, the LMC bar is visible. The northern spiral arms of the LMC are delineated by the main sequence stars who also trace a more tightly wound arm south of the bar. The stellar distribution is clumpy owing to dense regions of star formation and molecular clouds. The LMC RGs are more smoothly distributed though faint, wispy substructures are discernible in the northern and southern portions of the dwarfs disc. With regards to the SMC, relatively little structure is observed in the giants, with a dense core visible and a somewhat elongated on-sky morphology. Considering the main sequence stars however, the eastern wing is striking, reaching from the inner regions of the dwarf out to the outskirts of the LMC.

the Clouds by Besla et al. (2016) further revealed significant substructure in the northern portions of the LMC. The recent deep imaging of Mackey et al. (2018), in combination with that of the Dark Energy Survey (DES), revealed diffuse stellar substructures residing south of the LMC along with stellar disc truncation in the southern and western regions (see also Belokurov and Erkal, 2019). Interestingly, towards the northeast of the Cloud, Salem et al. (2015) observed the gas profile of the LMC to be truncated with no such observation seen in the stellar density profile. They interpreted this to be the result of ram pressure stripping of the LMC gas on its infall through the circumgalactic medium of the Milky Way; such effects have no bearing on the stellar morphology of the galaxy (see also Indu and Subramaniam, 2015; Piatti, 2018, for discussion). Belokurov and Erkal (2019) too observed the western stellar truncation of the LMC disc in *Gaia* giants, employing N-body simulations to probe the origin of such a feature from which they concluded that close LMC-SMC passages have the capacity to produce such a one-sided disc deformation.

1.4.2 *Small Magellanic Cloud*

The state of the metal-poorer SMC is even more complex and disordered, exhibiting a roughly triaxial ellipsoidal shape with substantial depth along various lines of sight (see e.g. Deb et al., 2015; Gardiner and Hawkins, 1991; Jacyszyn-Dobrzniecka et al., 2017; Muraveva et al., 2018; Scowcroft et al., 2016; Subramanian and Subramanian, 2012). There is evidence of stellar debris tidally stripped by the LMC lying in its eastern regions (Nidever et al., 2013; Subramanian et al., 2017). Centrally, the SMC displays a less prominent bar as well as an eastern wing structure first observed by Shapley (1940), departing from the northern end of the bar towards the LMC. Recent mapping of the SMC by El Youssoufi et al. (2019) has shown the morphology of the younger stellar populations to be highly irregular and largely limited to the SMC bar and eastern wing, tracing the perturbed gaseous reservoir of the SMC (Stanimirović, Staveley-Smith, and Jones, 2004), with recent star formation expected to have occurred in these regions (see e.g. El Youssoufi et al., 2019; Irwin, Demers, and Kunkel, 1990). In the left panel of Fig. 1.2, I show *Gaia* EDR3 main sequence stars, selected towards both Clouds from the CMD cuts of Gaia Collaboration et al. (2020). The eastern wing of the SMC is clear, protruding right through to the outermost regions of the LMC. The older stellar populations, on the other hand, display a much more homogeneous spatial distribution (see also Haschke, Grebel, and Duffau, 2012; Jacyszyn-Dobrzniecka et al., 2017; Zaritsky et al., 2000) and are offset from the younger populations, as observed by Mackey et al. (2018). Such distinctions are suggestive of historic perturbations to the SMC's gas supply. Furthermore, Olsen et al. (2011) discovered a population of giants residing in the LMC yet distinct in their kinematics with respect to the local field. This disparity was compounded by the fact that these stars were also significantly metal-poorer than would be expected for an LMC disc population, leading the authors to the conclusion that these stars in fact originated in the SMC, having been accreted onto the more massive dwarf.

1.4.3 *Magellanic Interactions*

The general features outlined above clearly demonstrate that we cannot consider the Clouds independently. Their present day morphology is directly influenced by historic, mutual interactions with a striking example being the existence of the Magellanic Bridge (MB). The structure was first observed by Hindman, Kerr, and McGee (1963) as a continuous structure of neutral hydrogen linking the two Clouds. Ir-

win, Kunkel, and Demers (1985) later discovered this gaseous bridge to be a site of recent star formation. They observed hundreds of blue main sequence stars to lie in the bridge region, coincident with the HI distribution. The young stellar bridge has also been observed more recently. For example, Casetti-Dinescu et al. (2012) map the bridge with OB stars selected using a combination of UV, optical and IR photometry. Mackey et al. (2017) trace young stellar associations, ages $\lesssim 30$ Myr, from the SMC wing to the outskirts of the LMC, suggesting that their spatial coincidence with the densest regions of HI gas between the Clouds points to these stars having formed *in-situ*. In addition, there is the $\sim 200^\circ$ long Leading Arm and trailing Magellanic Stream (MS) features associated with the system; purely gaseous in nature, they are strongly indicative of tidal stripping of the Clouds. The simulations of Diaz and Bekki (2012) and Besla et al. (2012) demonstrate that a historic close encounter between the Clouds is able to reproduce the general large scale features of the MS and Leading Arm. To reproduce the general characteristics of the gaseous MB, a more recent encounter seems to be required, with swathes of gas being stripped from the SMC into the MB region, hosting star formation, alongside stripped stellar debris.

Evidence for a stripped intermediate/old stars in the MB has been seen numerous times (see e.g. Bagheri, Cioni, and Napiwotzki, 2013; Carrera et al., 2017; Nidever et al., 2013; Skowron et al., 2014). The RR Lyrae stars selected from *Gaia* DR1 by Belokurov et al. (2017) revealed the presence of tidal tails around both the LMC and SMC. They traced a bridge of stars connecting the two Clouds. Studying the 3D structure of this bridge, they found a dual nature; the bridge exhibits one component displaying a smooth distance gradient from the SMC to the LMC, with the other at the mean distance of the LMC, indicative that the old stellar bridge is composite in stellar make up. That is, a large portion of the old stellar bridge is the trailing tail of the SMC, tidally stripped to closer heliocentric distances and towards the LMC. The leading arm is largely compressed on-sky, and elongated along our line of sight. Belokurov et al. (2017) went on to posit that a significant portion of the bridge is composed of LMC material, tidally dragged into the MB region. The follow-up studies by Mackey et al. (2018) and Belokurov and Erkal (2019) have confirmed the presence of a messy mix of extra-tidal sub-structure in this intra-Cloud region, sometimes referred to as "old Magellanic Bridge".

Based on Hubble Space Telescope (HST) observations, Zivick et al. (2018) showed a close encounter occurred of order 150 Myr ago, with an impact parameter of less than 10 kpc. The extent of the LMC disc is large, with Mackey et al. (2016) observing it to continue to ~ 18.5

kpc in the DES imaging of the Cloud. Thus it seems extremely likely that the LMC and SMC have undergone a recent direct collision. The Clouds appear to be on their first infall into the Milky Way (Besla et al., 2007), consistent with the notion that it is LMC-SMC interactions that are the main driver of the substructure we observe. Indeed, the deep photometry from the Survey of the Magellanic Stellar History (SMASH) analysed by Ruiz-Lara et al. (2020) found evidence for the long term stability of the LMC's spiral arm, dating its origin to more than 2 Gyr ago, and suggesting its independence from the MW interaction.

1.5 LONG PERIOD VARIABLES

The first two chapters of this thesis utilise long period variables (LPVs) and Miras in the study of Galactic structure. As such I present here a short summary of the nature of these stars and the useful properties they bear in relation to tracing galactic structure.

1.5.1 *What is a Long Period Variable?*

LPVs are pulsating red giant or supergiant stars which require many months or several years to complete one cycle. One of the most well-studied classes of LPVs are Miras, which are variable Asymptotic Giant Branch (AGB) stars. They are in the late stages of red giant evolution and will expel their envelopes to form planetary nebulae in a few million years. Typically, they have periods longer than 100 days, and amplitudes greater than 2.5 magnitudes at visual wavelengths (Gaposchkin, 1954; Habing and Olofsson, 2003). Giant variables of lower pulsation amplitude have been labelled the semi-regular variables (SRVs). In Fig. 1.3 I show three examples of *Gaia* DR2 LPV light curves for illustrative purposes. The upper light curve is visibly periodic over hundreds of days with a small visual amplitude; a likely SRV candidate. The middle and lower light curves show far greater visual amplitudes, exceeding 2 magnitudes, with long term periodicity characteristic of Mira type variables. Mira variables fall into two classes dependent on their surface chemistry: oxygen rich (O-rich) and carbon rich (C-rich). Miras have complex molecules present in their spectra with those that are O-rich showing H_2O , TiO , SiO and the C-rich presenting C_2 and CN (Matsunaga et al., 2017). Miras become carbon dominated in dredge up processes where inner shell burning induces thermal pulses, driving carbon from the stellar core towards the surface.

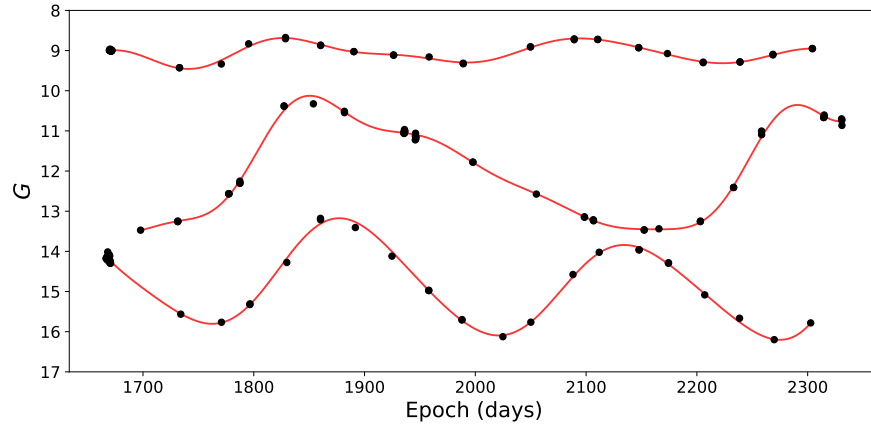


Figure 1.3: Three examples of *Gaia* DR2 LPV raw light curves drawn from the `vari_long_period_variable` and `epoch_photometry` table. Magnitude offsets of 0.3 mag have been applied for clarity for the upper and lower examples. The upper light curve is an example of an SRV, a low amplitude pulsator with a period of 247 days as determined by the *Gaia* pipeline. The middle and lower light curves show examples of Mira like LPVs; the visual amplitudes of these stars are in excess of 2.5 magnitudes and bear periods of 446 days and 256 days respectively. The solid red lines show a fit to the data that has been included purely to guide the eye.

1.5.2 Useful characteristics of Long Period Variables

LPVs are worthy of special study for a number of reasons. Firstly, they are representatives of the intermediate-age population. In particular, Miras are so intrinsically bright that they are detectable throughout the Galactic disc, bulge and halo (Habing and Olofsson, 2003), the Magellanic Clouds (Deason et al., 2017), the dwarf satellites (Sakamoto et al., 2012; Whitelock et al., 2009) and even in M31 and M33 (An et al., 2004), amongst other relatively distant galaxies (see e.g. Huang et al., 2018; Rejkuba, Minniti, and Silva, 2003; Rejkuba et al., 2003; Yuan et al., 2018). Secondly, LPVs provide an independent distance calibration via period-luminosity (PL) relations. For example, both oxygen rich, or O-Miras, and carbon rich, or C-Miras, obey period-luminosity-colour relations (Feast et al., 1989; Whitelock, Feast, and Van Leeuwen, 2008a). For O-Miras, the colour term in the PL relation is a very minor correction (Huang et al., 2018). Thirdly, LPVs are major contributors to the processed material currently entering the interstellar medium and an important source of enrichment. However, perhaps the most important property of LPVs such as Miras is that they provide good chronometers (Feast, 2009; Feast, Whitelock, and Menzies, 2006).

Accurate stellar ages have the potential to completely transform Galactic astronomy. The dissection of the Galaxy according to age would allow us to map its assembly and growth, as well as to study

secular processes that control its evolution. Unhappily, good stellar ages are usually hard to come by. The most successful attempts so far use a combination of spectroscopy and stellar evolutionary models. For example, the masses of red giants can be predicted from their photospheric carbon and nitrogen abundances, together with their spectroscopic stellar parameters. With the masses in hand, stellar evolutionary theory is then used to obtain ages, typically with errors of ~ 40 per cent (e.g., Martig et al., 2016a; Ness et al., 2016).

It has long been known empirically that O-Mira kinematics depend on their periods. For nearby O-Miras, the age and velocity dispersion relationship calibrated for stars in the solar neighbourhood can be used to derive a period-age relationship (Feast and Whitelock, 2000a; Feast, 2007). The period of a Mira increases with increasing luminosity, and hence mass. Thus, longer period Miras correspond to younger ages. Samples of O-rich Miras can therefore be used to determine age gradients in the Milky Way Galaxy and even, in the most propitious circumstances, date the populations. Additionally, the measured spread in near-infrared colours of O-rich Miras is substantially smaller than that observed in the C-rich counterparts (e.g. Matsuura et al., 2009; Whitelock et al., 2006; Yuan et al., 2017). One possible explanation of this phenomenon is that the O-Miras suffer less from varying levels of extinction due to circumstellar dust. If true, this makes them more trustworthy distance indicators than their C-rich peers.

1.6 THESIS STRUCTURE

The remaining chapters of this thesis detail the work undertaken during my Ph.D., with a research focus on discerning galactic structure with giants. They are structured as follows:

- **Chapter 2:** I investigate the ability of O-rich LPVs and Miras to act as Galactic chronometers, tracing them through the inner disc, out into the distant halo.
- **Chapter 3:** I utilise *Gaia* DR2 LPVs to study the spatial density profile of the bulge and disc. Seizing on the relationship between pulsation period and stellar age I dissect both components chronologically revealing marked evolution.
- **Chapter 4:** Drawing Magellanic giants from *Gaia* DR2, I assign photometric metallicity estimates to study the chemokinematical properties of the Clouds.

AGE GRADIENTS THROUGHOUT THE GALAXY WITH LONG PERIOD VARIABLES

This chapter is based on work originally published in Grady, Belokurov, and Evans (2019).¹

We assemble a sample of $\sim 2,200$ O-rich Miras and associated LPVs and highlight their importance for age-dating the components of the Galaxy. Our sample stretches from the Galactic bulge to the distant halo and we estimate $\sim 80\%$ of our selected sample to be comprised of O-rich LPVs. Given that the period of LPVs correlates with age, this offers a new way of determining age gradients throughout the Galaxy. We use our sample to show (i) disc O-rich LPVs have periods increasing on moving outwards from ~ 3 to 15 kpc, so the outer disc LPVs are younger than the inner disc, (ii) the transition from younger disc to halo LPVs occurs at $r \sim 15$ kpc and is marked by a plummeting in period, (iii) there exists a population of young O-Miras likely kicked from the disc to heights of order of $|Z| \sim 10$ kpc, (iv) great circle counts of old LPVs show evidence for distant debris agglomeration associated with the Magellanic Clouds.

2.1 DATA

This work exploits data from two primary sources, that of the Catalina Surveys and the All Sky Automated Survey for Supernovae (ASAS-SN). The Catalina Surveys catalog is comprised of two main components surveying the northern (Drake et al., 2014) and southern (Drake et al., 2017) sky respectively. The surveys in both hemispheres are analysed by the Catalina Real-Time Transient Survey (CRTS) in search of optical transient phenomena and we extract data from both sub-sets. Our sample of LPV candidates is then cross-matched with the 2MASS catalog to obtain JHK_s magnitudes, yielding a total of 960 unique sources. The ASAS-SN project is an all-sky optical survey with published classifications of variable stars (Jayasinghe et al., 2018). Cross-matching the ASAS-SN Mira candidates with 2MASS provides 1,831 sources for study. A cross-match radius of 1 arcsec was used in both instances. Magnitudes are dereddened with extinction coefficients of

¹ I note that Figs. 2.7 & 2.14 were created by Vasily Belokurov and appear here as they do in the published work.

$\mathcal{R}_J = 0.72$, $\mathcal{R}_H = 0.46$ and $\mathcal{R}_{K_s} = 0.306$ combined with the reddening values of Schlegel, Finkbeiner, and Davis (1998).

2.1.1 *Mira Selection*

C-Miras (and their allies, the Carbon stars) have been studied extensively before (e.g., Battinelli and Demers, 2014; Downes et al., 2004). They were exploited most recently by Huxor and Grebel (2015) to trace out structures in the stellar halo. In this study, we will focus on the less well-studied O-Miras, and their allies, the oxygen-rich LPVs.

The selection of our sample proceeds via the application of two main cuts. The work of Yuan et al. (2017) and Glass et al. (1995) shows that the colour indices of Mira increase as a function of period, itself a proxy for age. Glass et al. (1995) provides linear colour-period relations for O-Miras in the SAAO photometric system. For this work, the $J - H$ relation is converted into the 2MASS photometric system via the transformation of Carpenter (2001) as shown by the solid red line in the top two panels of Fig. 2.1. Associated errors of the original linear relations and colour transformations are combined to produce a $1-\sigma$ bound defining the selection cut for O-Mira from our sample. These are displayed as the dashed red lines in the upper panels of Fig. 2.1. We note that the photometric transformation of Miras can be affected by broad absorption bands (Glass et al., 1995). We use the colour-period relation of Yuan et al. (2017) purely as a guide for our selection and have checked that the applied photometric transformation has no significant effect on our results.

We observe that the oxygen-rich LPVs form a tight sequence with only a mild dependence on $J - H$ colour in these plots. To further rid our sample of C-Miras and other contaminants, a cut on amplitude in the V-band is applied. The work of Soszyński et al. (2009) reveals a distinction between O-rich and C-rich stars in amplitude-period space, on which we base our cut shown in the bottom row of Fig. 2.1. The CRTS catalog groups Miras and SRVs under the single classification of LPVs. Accordingly, we use our CRTS sample to define the cut in amplitude based on the higher potential for contamination and the fact that the ASAS-SN sample is predominantly an O-rich population, as evidenced by the top right panel of Fig. 2.1. The combined CRTS and ASAS-SN cleaned samples of O-rich LPVs consist of $\sim 2,200$ sources or $\sim 85\%$ of the original combined sample. We do not study the rejected sample of mainly C-rich LPVs any further in this chapter.

LPVs are known to exist on sets of sequences in period-luminosity space (e.g., Wood, 2000; Wood et al., 1999) depending on their vari-

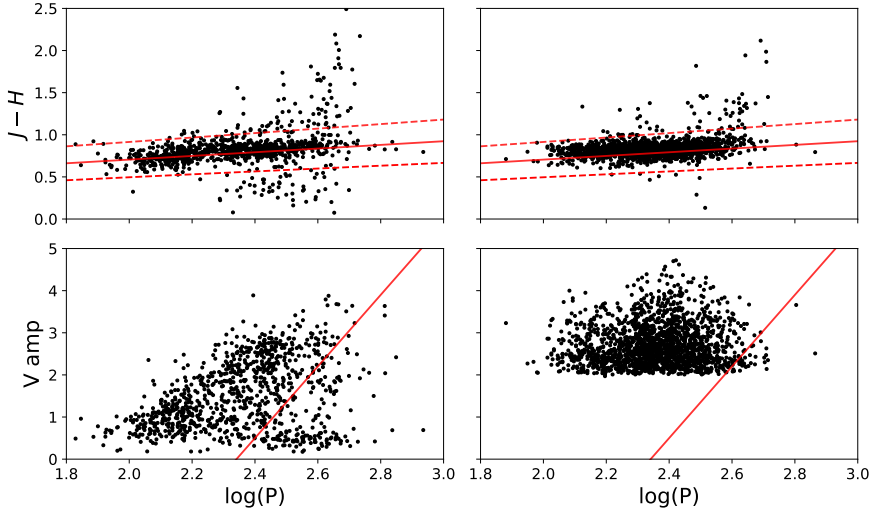


Figure 2.1: Red lines show the O-rich LPV and Mira selection cuts applied to our sample for the CRTS data (left column) and the ASAS-SN data (right column). Dashed red lines in the upper panels are the $1-\sigma$ bounds on the cut in colour-period space. Notice that the sequence of O-Miras is only weakly dependent on colour. The red line in the lower panel trims the sample by removing some contaminating C-Miras using a period-amplitude cut.

ability type and pulsation mode. The primary periods of Mira-like variables lie on the commonly called C and C' sequences (Ita et al., 2004; Spano et al., 2011) with C' lying at a lower period than C. Sequences A and B lie at lower periods still and are populated by the so-called OGLE small amplitude red giants or OSARGs (Soszynski et al., 2004b). Sequences D and E are populated by long secondary pulsators, whose nature is still unclear, as well as ellipsoidal and eclipsing binary systems (Soszynski et al., 2004a), with the latter two contained in a separate CRTS catalog not utilised in this work. Soszyński and Wood (2013) also found that there is a low amplitude population of semi-regular variables (SRVs) whose primary period lies between the C and C' sequences. Given that the selections of Fig. 2.1 produce a CRTS sample with a wide range of visual amplitudes, it is uncertain on which sequence our CRTS sources lie and to which class of LPVs they belong. The left panel of Fig. 2.2 shows sources from *Gaia*'s DR2 LPV catalog (Gaia Collaboration et al., 2018a, 2016; Mowlavi et al., 2018) chosen to lie within a 15° aperture of the LMC. Cross-matching with 2MASS reveals three distinct sequences existing in the K_s band, with the middle sequence corresponding to the Mira C sequence. Belokurov et al. (2017) defined a variability parameter (the “*Gaia* amplitude”) based on *Gaia*'s flux information as:

$$\text{Amp} = \log_{10} \left(\sqrt{N_{\text{obs}}} \frac{\sigma_{I_G}}{I_G} \right) \quad (2.1)$$

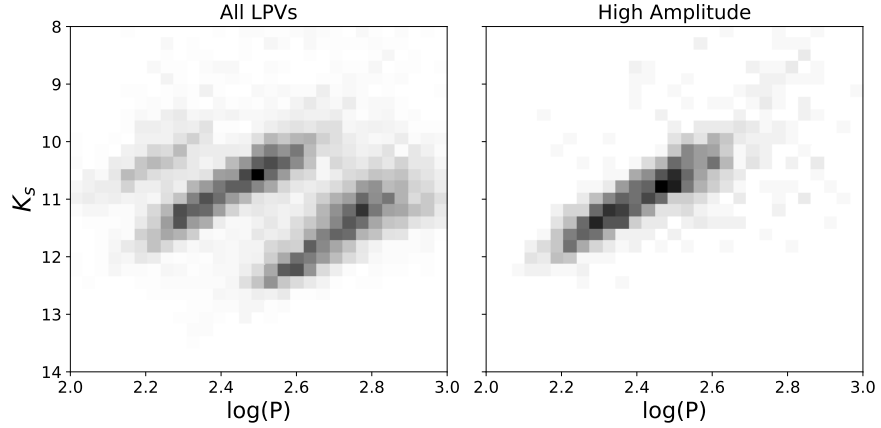


Figure 2.2: Dereddened K_s magnitudes and periods of *Gaia* DR2 LPVs within 15° of the LMC are shown. K_s magnitudes derive from a one arcsec aperture cross-match with 2MASS. *Left*: Three distinct PL sequences are seen. The panel displays all LPVs with no restriction of *Gaia* amplitude. *Right*: Sources with a *Gaia* amplitude > -0.55 are selected and shown. It is seen that such a selection cut primarily picks out the middle sequence of stars.

where $\sqrt{N_{\text{obs}}}$ is the number of observations, σ_{I_G} is the mean flux error in the G band and I_G is the mean flux in the G band. Requiring a *Gaia* amplitude greater than -0.55 isolates a sample of LPVs lying on a single PL sequence, as evident in Fig. 2.2. We produce a secondary cleaned CRTS sample for which we are more confident in that they lie on the Mira sequence and, therefore, have good distance estimates. We do so by cross-matching with the *Gaia* DR2 source catalog and enforcing that the *Gaia* amp > -0.55 . We also restrict the sample to visual amplitudes > 1 to further eliminate small amplitude variables. Application of these two cuts gives a cleaned CRTS sample with 287 members. We utilise this cleaned CRTS sample in Sec. 2.2, where we exploit the period age correlation of LPVs, the interpretation of which may be muddled if very low visual amplitude variables were inadvertently retained. For example, AGB variables residing in a common Magellanic Cloud globular cluster have been observed by Kamath et al. (2010) both at high and low amplitudes. They found stars with low amplitudes also had lower stellar periods, implying differing period age relations.

We have checked the effectiveness of our cleaned CRTS selection criteria through application on the OGLE LMC LPV catalog of Soszyński et al. (2009), cross-matched with *Gaia*+2MASS. We find $\sim 92\%$ of the selected sample to lie within 0.5 magnitudes of our PL relation (see Sec. 2.1.3). For stars with periods less than 150 days, this is even higher at $\sim 97\%$. We estimate our sample to be $\sim 70\%$ O-rich Miras and high amplitude LPVs based on these selections also. Thus, we are confident that our cleaned CRTS sample is suitable for the

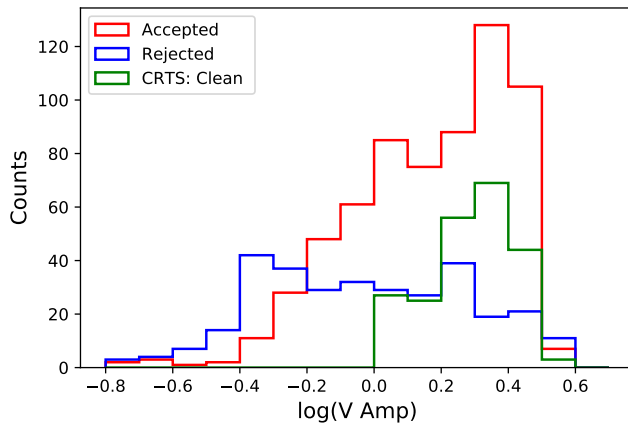


Figure 2.3: Amplitude histograms for the CRTS samples. Red shows the distribution of amplitudes of candidate LPVs that passed the cuts of Fig. 2.1 only. Green shows the effect of further enforcing the *Gaia* and visual amplitude criteria is to remove low amplitude variables. Blue shows the amplitudes of the sources rejected by the application of all the cuts. The bi-modality of the rejected sources is expected, as the contaminants are mainly from two disparate populations, the C-Miras and the semi-regular variables. (Bins of width 0.1 are implemented, and the logarithm here, and henceforth, is to the base 10.)

period age interpretation in the analysis of Sec. 2.2. Once the amplitude cuts are applied, we expect that the rejected sources display a bi-modal distribution in amplitude space given that they constitute two components: C-Miras and SRVs. Fig. 2.3 confirms that this to be the case and is consistent with the results of Soszyński et al. (2009) who studied the Mira amplitude distribution in the OGLE *I* band.

To summarise, we have produced three samples of O-rich LPVs: the CRTS and ASAS-SN samples from the selections of Fig. 2.1, along with the cleaned CRTS sample which is subjected to high *Gaia* and visual amplitudes cuts. The latter has been produced exclusively for the analysis of Sec. 2.2 and we estimate at least 70% of this sample are O-rich Mira and high amplitude LPVs.

2.1.2 O-rich LPV Distributions

The spatial distribution of our O-rich LPV sample is displayed in Fig. 2.4. The ASAS-SN O-Miras lie close to the Galactic plane with approximately 81% of the stars having $|b| < 10^\circ$. This enables us to probe the O-Mira structure within the Galactic disc. O-rich LPVs from the CRTS selection extend to much higher latitudes and thus grant us information on the halo component of the Galaxy. We immediately see in Fig. 2.4 a number of prominent substructures, including the LMC and the Sgr Stream. They are identified and removed from

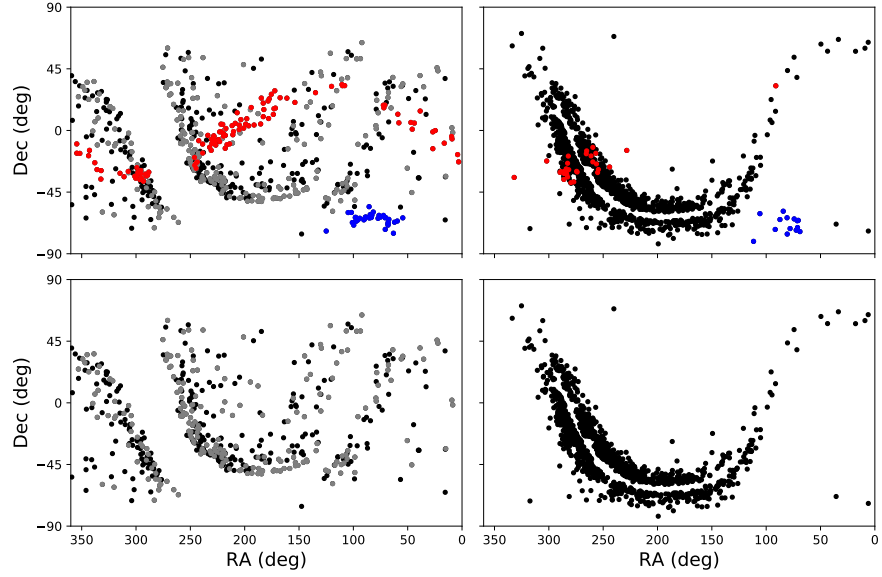


Figure 2.4: Spatial distributions of selected O-rich LPVs with (upper panel) and without (lower panel) prominent substructures in right ascension and declination for the CRTS (left) and ASAS-SN (right) surveys. Red and blue markers identify O-rich LPVs associated with the Sagittarius Stream and the Large Magellanic Cloud respectively. Grey markers indicate the cleaned CRTS selection with high *Gaia* and visual amplitudes. Notice that ASAS-SN sample is restricted mainly to the disc, but CRTS samples the halo as well. The percentage of the sample in the LMC and Sgr Stream is $\sim 2\%$ and 6% respectively.

our sample. Although interesting from the viewpoint of substructure studies, they are a nuisance here as our aim is to understand the relative ages of the mainstream Galactic populations.

We remove sources associated with the LMC by excising a 15° radii circle centred on the respective structure. Identifying Sgr Stream denizens requires a transformation into the Sgr Stream coordinates $(\Lambda_{\text{Sgr}}, B_{\text{Sgr}})$ of Belokurov et al. (2014). We remove stars with Sgr Stream latitude $|B_{\text{Sgr}}| < 10^\circ$ and heliocentric $D > 15$ kpc. The latter is needed as the Sgr Stream passes through the Galactic plane, yet we wish to retain the disc O-Miras. Once removed, our sample of O-rich LPVs is comprised of $\sim 2,000$ distinct sources, probing the Galactic thin and thick discs, bulge and halo.

2.1.3 Distance Determination and Validation

We calculate Mira distances using the empirical quadratic PL relation from eqn (1) of Yuan et al. (2017). We choose to work in the K_s band to minimise the effects of extinction. Recent estimation of the distance to the LMC from the work of Elgueta et al. (2016) yield values of 50.3 ± 0.5 kpc. We then select our CRTS O-rich LPV candidates (i.e.

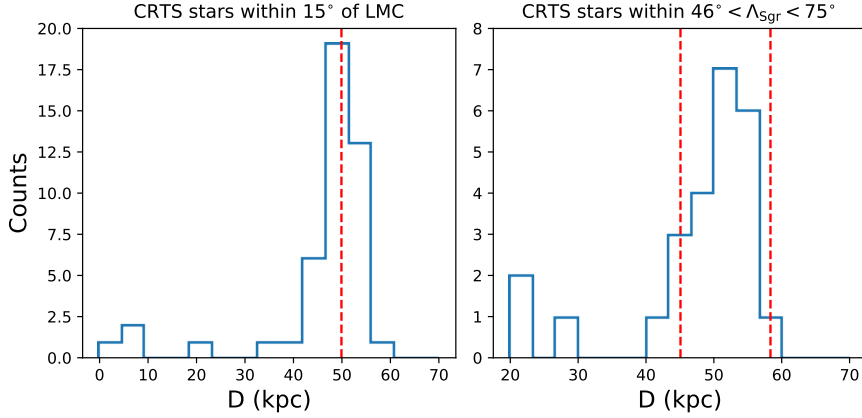


Figure 2.5: Histograms of heliocentric distances of CRTS sources accepted from the cuts of Fig. 2.1. *Left*: Distance histogram of the LMC CRTS LPVs. The red dotted line indicates 50 kpc. *Right*: Distance histogram of the Sgr Stream selected CRTS LPVs. The red dotted line indicates the distance to this section of the stream from Belokurov et al. (2014).

those within 15° of the dwarf’s centre), compute their distance and apply a small empirical correction (-0.17 mag) to the PL relation to produce a distance distribution peaked at the 50 kpc range. The distance distribution of these LPVs is shown in the left panel of Fig. 2.5. The median distance of the prominent peak is 49.8 kpc. The standard deviation approximated from the median absolute deviation of the LMC sample is ~ 4 kpc. This can be used as a typical distance error to stars in our sample, which, encouragingly, appears to be of order $\sim 10\%$. This method results in a final PL relation of:

$$M_{K_s} = -6.90 - 3.77 (\log P - 2.3) - 2.23 (\log P - 2.3)^2 - 0.17 \quad (2.2)$$

where P is the period in days and M_{K_s} is the absolute magnitude in the K_s band. This relation was independently validated on the test sample of *Gaia* DR2 LPV data seen in Fig. 2.2. It coincides with the middle sequence once shifted by the LMC distance modulus value of 18.452 from Elgueta et al. (2016). The sample of LMC *Gaia* LPVs all have G band magnitudes < 20 , for which *Gaia* is expected to be complete. So, selection biases will have minimal effect on our consistency check of the distance calibration. 2MASS is expected to be more than 99% complete at this latitude given the magnitude range of our test sample. We note that there appears to be no observational evidence of the O-rich Mira PL relation being strongly dependent on metallicity (Goldman et al., 2019; Whitelock et al., 1994). Consequently, it is reasonable to expect that distance estimates deriving from such a relation, calibrated by the LMC, should hold in our Galactic sample. As a further check, the distance to a populated section of the Sgr Stream

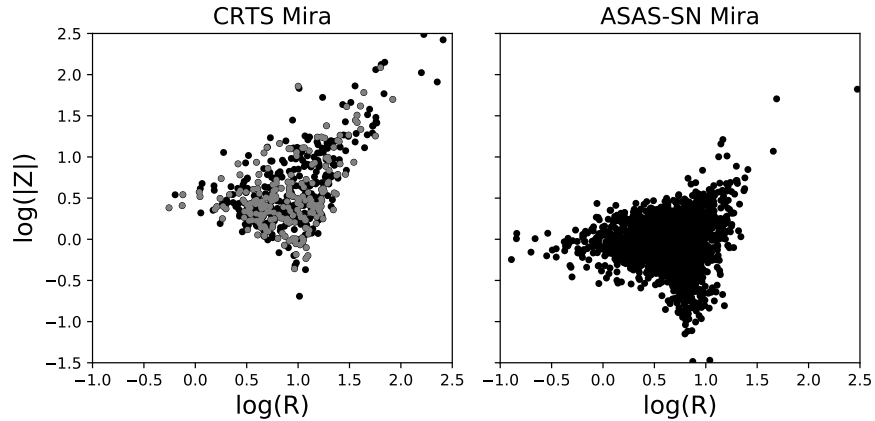


Figure 2.6: Locations of O-Miras and LPVs in CRTS (left) and ASAS-SN (right) using cylindrical radius R and vertical height $|Z|$ in kpc. Notice that the ASAS-SN O-Miras do not extend beyond a few kpc from the Galactic plane and so are predominantly thin and thick disc stars. The CRTS O-rich LPVs range in cylindrical radii from 0.3 kpc to more than 80 kpc, from the Galactic bulge into the distant halo. The LMC and Sgr Stream Mira have been removed from the sample in both panels of this figure. Grey CRTS markers highlight the cleaned high amplitude sample. The Sun is assumed to lie at $Z_{\odot} = 27$ pc.

was computed for the associated CRTS sample. The right panel of Fig. 2.5 shows the peak of the distribution to lie at ~ 50 kpc in agreement with the values in Table 1 of Belokurov et al. (2014) which quote distances of 45 - 58 kpc in the chosen Sgr Stream longitude range. We note that we have not used the cleaned CRTS sample, which by design lies on the middle sequence of Fig. 2.2, in our distance validation yet we still recover the appropriate structure and distance estimates. Taking the solar position as $R_{\odot} = 8$ kpc, we convert from Galactic (ℓ, b) and heliocentric distance to Galactocentric cylindrical polar coordinates (R, Z) . The panels of Fig. 2.6 compare the spatial distributions of O-Mira in the CRTS and ASAS-SN samples. In CRTS, the sample probes distances characteristic of the Galactic bulge right out to the far halo. By contrast, in ASAS-SN, we see a clustering of stars at low $|Z|$ around the solar neighbourhood, along with a sample largely confined to within a kiloparsec of the Galactic plane. The two samples are therefore highly complementary, with CRTS probing from the bulge to the halo, and ASAS-SN concentrating on the thin and thick discs.

Given the dependence of the Mira luminosity on its period, the completeness and contamination of the O-Mira selection must vary with distance. This is dictated by the distribution of the LPV stars in the space spanned by period, colour and amplitude as shown in Fig. 2.1. For example, the contamination from C-rich Mira stars and other LPVs with broader $J - H$ colour range increases sharply with period. Thus, because at fixed limiting magnitude the most distant

stars detectable are those with larger periods, it is possible to expect that contamination may increase with distance. On the other hand, the short-period O-Mira stars have lower amplitudes and thus may suffer a much faster drop in completeness with distance compared to the long-period counterparts.

2.2 GALACTIC AGE GRADIENTS

While the age of the Mira variables has typically been estimated by matching them to disc stellar populations with similar velocity dispersions (see e.g. Feast, 2009; Feast, 2007; López-Corredoira, 2017), we attempt to calibrate the Mira age-period relation by finding candidate LPVs in the LMC and the Milky Way star clusters with known ages. In the LMC, we rely on the Mira catalog by Soszyński et al. (2009) and the compendium of massive star clusters by Baumgardt et al. (2013). In the Galaxy, we use the combined ASAS-SN+CRTS sam-

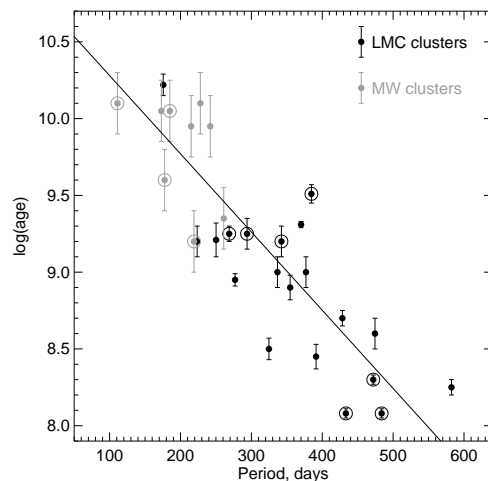


Figure 2.7: Dependence of the Miras age on its period. For the LMC, ages of the massive star clusters from Baumgardt et al. (2013) are used by cross-matching their positions with those of the LMC Miras in the catalog by Soszyński et al. (2009) with a 100 arcsec aperture. These measurements are complemented by age estimates of the Mira and LPV stars in the combined sample of ASAS-SN+CRTS in the vicinity of Galactic star clusters from the catalog of Kharchenko et al. (2016). The cross-match is carried out with a 9 arcmin aperture, only objects with the distance mismatch less than the half of the distance to the cluster are kept. The straight line indicates a linear fit to the data with 10.79 and -5.09×10^{-3} for the intercept and slope respectively. Circled data points are those that survive if the aperture is shrunk by a factor of two. We list the pairings in Appendix Tables A.1 and A.2.

ple of O-rich Mira and LPVs presented in this work and the catalog of star clusters by Kharchenko et al. (2016). Fig. 2.7 shows the age of the star cluster as a function of the period of the candidate Mira matched to its location. In agreement with previous similar studies (Kamath

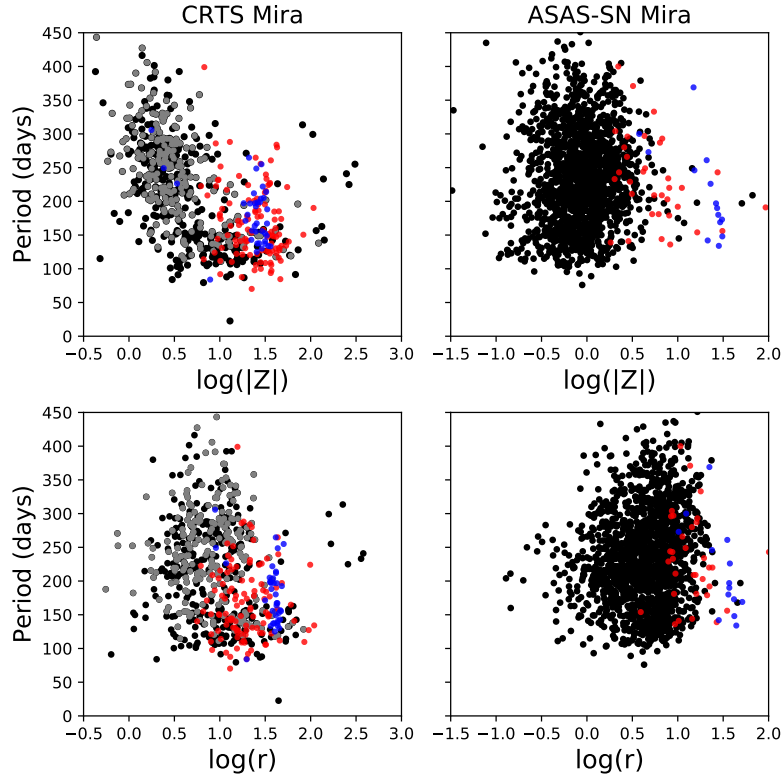


Figure 2.8: The set of four panels display the distribution of O-rich LPVs and Mira in period versus Galactic position with the main halo substructures. Red indicates Sgr Stream O-Mira, blue those of the LMC. Vertical height above/below the plane and spherical polar radius are represented by $|Z|$ and r respectively. Grey markers show the cleaned CRTS O-Mira to be more restricted to the plane as well as constituting a slightly longer period population.

et al., 2010; Nishida et al., 2000), the trend is clear albeit with considerable scatter. The shortest period Miras with $P < 200$ days do tend to live in clusters that are 8 – 10 Gyr old. On the other hand, Mira stars with periods of $P \sim 350$ days are found in much younger star cluster with ages of order of 1 Gyr.

We investigate the period distribution through the Galaxy for both the ASAS-SN and CRTS LPVs, as a function of spherical radius denoted r , with a view to tracing age gradients through the Galaxy. We plot Galactocentric spherical polar radius r and vertical height $|Z|$ above or below the Galactic plane as a function of period with a view to understanding the O-rich age distribution in both the disc and halo components of the Galaxy. This is shown with and without substructures in the four topmost and bottommost two panels of Fig. 2.8. The CRTS panels of these plots are the most interesting. They show that O-rich LPVs with short periods ($\lesssim 200$ days) reach much greater heights above the Galactic plane than those with long periods ($\gtrsim 300$ days). A similar pattern is seen in the plot of period versus spherical distance, with long period O-rich LPVs confined to within

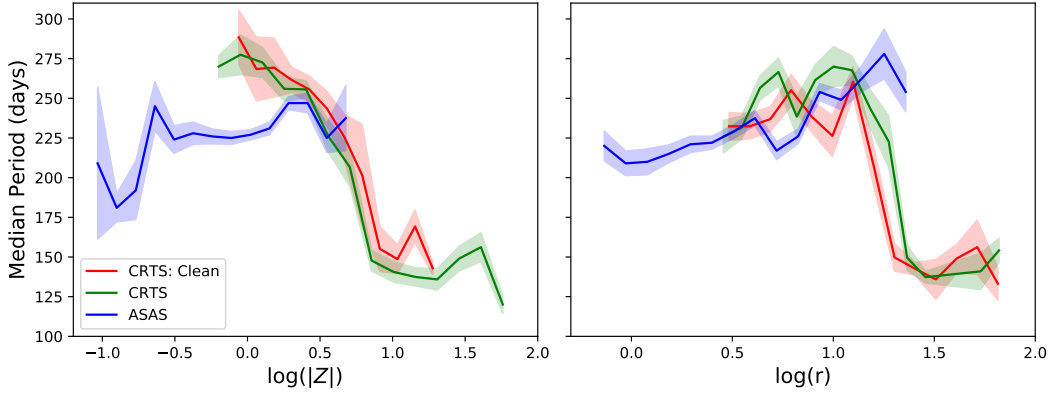


Figure 2.9: The median of O-Mira and LPV periods versus height above/below the Galactic plane $|Z|$ and spherical polar radius r in kpc. Distances have been binned with bins containing less than 5 stars omitted. Error bars indicate standard errors for each bin. Green and blue markers identify the CRTS and ASAS-SN samples resulting from the selections of Fig. 2.1 and removal of LMC and Sgr Stream. The red marker shows the cleaned CRTS sample, predominately an O-Mira population. Both CRTS samples show a transition from disc to halo population, marked by a sharp drop in period at $r \sim 15$ kpc in the profile. The disc O-Miras in ASAS-SN have periods that increase on moving outwards in radii from ~ 1 to 15 kpc.

the innermost $r \sim 15$ kpc of the Galaxy. Clearly, we are seeing the transition from a younger disc population into an older halo component. The age profile of the halo is rather flat, seemingly at odds with the recent claims of the negative age gradient in the halo by Carollo et al. (2016). Less transition is observed in the ASAS-SN counterpart owing to the limited sampling at high Galactic latitudes in this data set. The LMC and Sgr Stream O-Mira are seen to predominantly inhabit an intermediate to low period range representative of the stellar population these structures contain. The panels of Fig. 2.9 give the period distributions of the O-Miras and O-rich LPVs in vertical distance from the plane $|Z|$ and spherical polar radius r . Distances have been binned, with bins containing less than 5 stars being rejected, and prominent substructures removed. Median periods have been computed for each bin along with standard errors. The standard error on the median is formulated through appropriate scaling of the median absolute deviation. The CRTS Miras and LPVs appear to demonstrate a transition in populations at a Galactocentric distance of ~ 15 kpc as a clear break exists from high to low period. Notice that such behavior is exhibited by both CRTS samples. As the ASAS-SN Mira sample contains predominately disc O-Miras, it is interesting to note the positive correlation between Galactocentric radius and period given that period is a proxy for age. The implication here, then, is that the age of the O-Mira populated components of the disc decreases on mov-

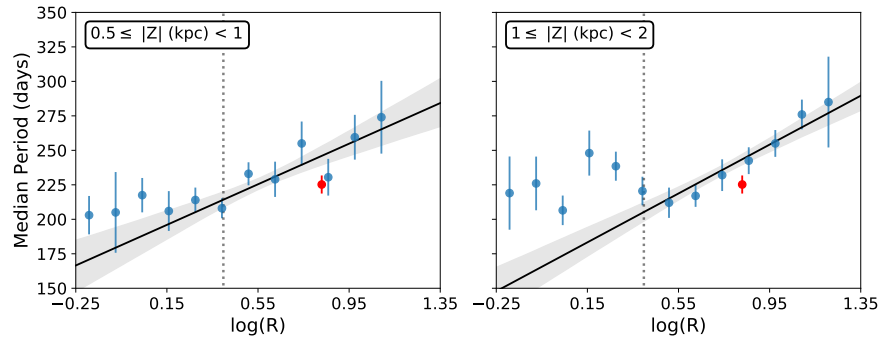


Figure 2.10: Relation between periods of ASAS-SN O-rich Miras and their distances above and within the plane with cuts in vertical distance. Red points mark solar neighbourhood Mira selected with the criteria of $\log(|Z|) < -0.5$. This selection was chosen given the distribution of ASAS-SN Mira in Fig. 2.6. The vertical black dashed line, at $R = 2.5$ kpc, marks the boundary between left lying bulge/bar regions and the disc to the right. Bins with less than 5 Mira are neglected.

ing outwards. We do not see any evidence of a sharp break in the radial profile of the median age of disc, as conjectured by Roškar et al. (2008). Their simulations suggest that the outer disc is deficient in young stars, but is populated by old stars which migrated from the inner disc. If such an upturn exists, then it must lie beyond ~ 15 kpc. In fact, Amôres, Robin, and Reylé (2017) have recently argued that the break may be at 16.1 ± 1.3 kpc on the basis of population synthesis applied to 2MASS data.

To probe any change in period gradient, the ASAS-SN O-Mira are further binned into two subgroups: $0.5 \leq |Z| < 1$ kpc and $1 \leq |Z| < 2$ kpc. We use cylindrical radius R in this instance to focus on the evolution of period throughout the Galactic disc. These cuts correspond to radial ranges of $0.25 \leq R < 18.4$ kpc and $0.67 \leq R < 21.7$ kpc respectively, as enforced by the footprint in Fig. 2.6. The panels of Fig. 2.10 clearly demonstrate that beyond 2.5 kpc the O-Mira population follows the trend of increasing median period with increasing Galactocentric distance. Quantifying by a linear fit yields radial period gradients of 74^{+22}_{-21} days/dex and 89^{+15}_{-17} days/dex for the two instances. At small radii (< 2.5 kpc), the trend is not present and the relationship between median period and distance is flat. This is possibly indicative of existence of the intermediate age Mira reported towards the bulge in the works of Catchpole et al. (2016), Blommaert and Groenewegen (2007) and Matsunaga et al. (2017), which are difficult to separate from the disc Miras.

Recent estimates, from the works of Ojha (2001), Jurić et al. (2008) and Jayaraman et al. (2013), for the scale of the thick disc are based on double exponential models with radial and vertical scale heights

in the ranges $h_R \sim 3.6 - 4$ kpc and $h_z \sim 0.8 - 1$ kpc. In a broad sense, the ASAS-SN LPVs in the panels of Fig. 2.10 would be expected to be mostly thick disc stars. It is interesting to note that radial age gradients at different $|Z|$ ranges have been observed by Martig et al. (2016b) in thick disk APOGEE RC stars, from $R \geq 4$ kpc onward. They see clear separations in age gradients between the $|Z|$ bins. That is, higher $|Z|$ bins constitute a clearly older population for given radius R in their sample, whereas the distinctive gradients in our sample are less well separated. However, their results are consistent with ours, as we both detect a younger stellar population as we move outward through the disc.

Additionally, the red marker in Fig. 2.10 corresponds to the datum derived from a solar neighbourhood selection of Mira. From Fig. 2.6, there is an appendage of Mira extending to low $|Z|$ at the Solar position. A cut selecting Mira with $\log |Z| < -0.5$ has been used to define the O-Miras in the solar region. This though leads to the surprising result that the solar neighbourhood O-Miras have median periods lower than the thick disc O-Miras, and hence are likely older! Although the origin of this result is not fully clear, there are indications that our solar neighbourhood sample is affected by survey systematics. In addition to the variation of the sample completeness and contamination with period as discussed in Sec. 2.1.3, other effects such as that linked to saturation may be taking place; saturation for ASAS-SN is at $V \sim 11$ and long period O-Miras are luminous so they are more likely to be saturated and not included in the selection. Finally, it is worth pointing out that, if only a sub-class of Miras is considered, such as O-rich stars, the period-based chronometry argument might only work for a limited range of ages. This is because the period-age relation is normally derived for a combination of both C- and O-rich Miras, however, their period distributions are rather different. It has been noticed (see e.g. Cioni et al., 2001; Feast et al., 1989; Lorenz et al., 2011) that O-rich stars are biased towards short periods while C-rich ones tend to have longer periods on average. Translated into age, these differences imply that O-rich Mira might significantly under-sample the younger populations of the Galactic disc.

Further, Feast (2009) notes that the period-age relation of C-Mira may be offset from O-Mira. Further, the LPVs associated with star clusters in Fig. 2.7 are a mixture of our O-rich selection along with contaminating C-rich or SRV stars. Nonetheless, a negative correlation between period and age is still expected, albeit with scatter. Whilst offsets may occur for differing types of Mira/LPVs, this work focuses on the global trends in age gradient. We have checked that our estimated contamination does not significantly affect the inter-

pretation of our age gradient results. Feast and Whitelock (2000b) have observed period-metallicity correlations for O-Mira in globular clusters. The LPV pulsation modelling of Trabucchi et al. (2021) suggests that the offset in metallicity between a value typical of an O-rich, Magellanic LPV and one of solar value can alter the fundamental pulsation period by up to $\sim 10\%$. Thus it seems reasonable to expect that metallicity variations do, to some degree, contribute to the gradients we observe in Figs. 2.9 and 2.10 though likely to a lesser degree than stellar age.

2.2.1 *Miras outside of the Galactic disc*

The CRTS sample used in this section has not been cleaned by the application of the high *Gaia* and visual amplitude cuts. It may seem that their distances are uncertain, given the ambiguity as to which period-luminosity sequence they lie on. However, we highlight several factors indicating otherwise. First, this sample was used in the calibration of our adopted PL relation from eqn (2.2). Selection of these stars towards the LMC and Sgr Stream section of Fig. 2.5 and application of eqn (2.2) clearly shows the distances have better than 10% accuracy. Reference to Fig. 2.2 shows a sequence of low luminosity and high period lying below the middle sequence on which low amplitude variables may sit. However, our visual amplitude selection of Fig. 2.1 specifically acts to remove high period, low amplitude stars. Using a value of $V_{\text{amp}} = 1$ as a reference, this selection removes all stars with $\log(P) \gtrsim 2.45$ which is precisely the region of periods in which the lower sequence sits. Therefore, whilst there may exist low amplitude LPVs in the sample used in this section, our selection acts to ensure they do not lie on the lower sequence and thus we are confident that we have not overestimated their distance. We note that the upper sequence is much less densely populated than the middle (by a factor of ~ 4) and that our distance estimates for any stars that do lie here will be lower bounds. For shorter period stars, we acknowledge that a fraction of them may possess underestimated distances as low amplitude contamination increases in this domain. However we primarily study these in relation to the longer period sample, noting differences in their spatial extent (see later in this section).

While the ASAS-SN sample is largely limited to $|Z| < 5$ kpc, the complementary CRTS LPVs probe a much larger range of Galactic heights, $5 \lesssim |Z| \lesssim 200$ kpc (and probably beyond). We first focus on the distribution of long-period pulsators in CRTS. According to Fig. 2.9, the bulk of the disc Miras in the ASAS-SN set have periods in excess of 170 days. Fig. 2.11 gives the view of the distribution of the

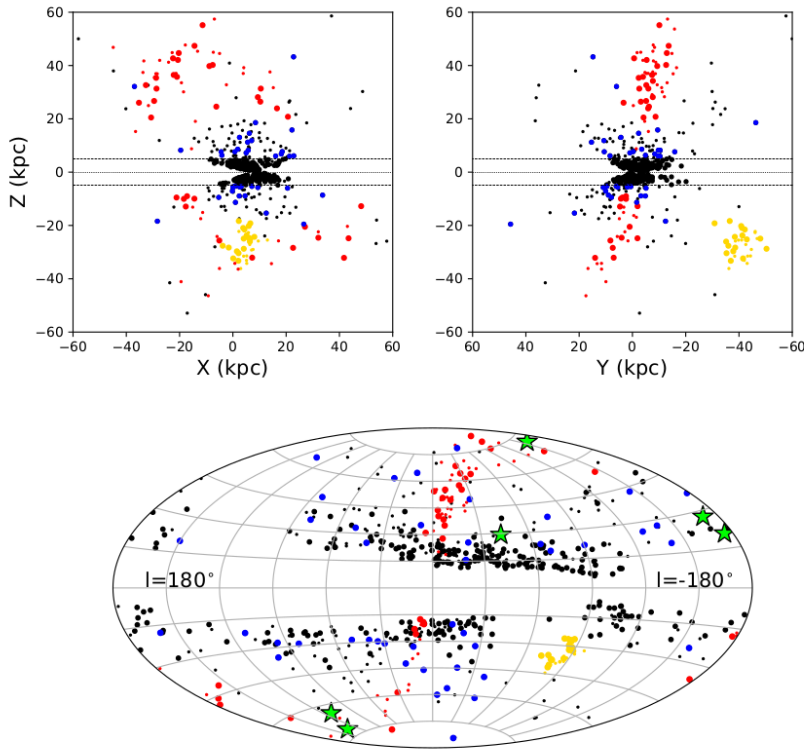


Figure 2.11: Distribution of CRTS LPV stars in the Galactic halo. Small dots represent LPVs with $P < 170$ days, large filled circles correspond to those with $P > 170$ days. Red symbols are stars projected to lie within the Sgr Stream and more than 15 kpc away from the GC. Yellow symbols mark the stars within 15° of the LMC. Blue (black) filled circles give the locations of long-period Mira stars above (below) $|Z| = 5$ kpc. Note that the blue symbols trace out a highly flattened, disc-like sub-sample of Miras and LPVs traveling to Galactic heights $5 < |Z| < 10$ kpc. Outside of this sub-group, the vast majority of long-period Miras at high Z belong either to the Sgr Stream or the LMC. *Top left:* Distribution of stars in Galactic X and Z . *Top right:* Distribution of stars in Galactic Y and Z . *Lower:* Distribution of stars on the sky in Galactic coordinates. Green stars mark the location of LPVs with Galactocentric radii in excess of ~ 90 kpc. Of these, the majority appear to be associates of the Sgr Stream.

population of the long-period (and thus likely younger) Mira stars across the Milky Way. Apart from the obvious disc denizens (filled black circles), three distinct groups can be identified in the figure. The first two are the stars belonging to the Sgr Stream (red filled circles) and the LMC (yellow filled circles). The last group (blue filled circles) is comprised of stars that follow the extent of the disc in X, Y dimensions but travel to heights as large as $|Z| \sim 10$ kpc. Their reach in $|Z|$ and R can be gleaned from Fig. 2.12, where their distribution (blue histograms) is compared to that of the short-period Miras (black histograms). Indeed, both long-period and short-period objects are detected as far as $R \sim 30$ kpc; however the (likely) younger CRTS LPVs do not wander beyond $|Z| \sim 10$ kpc. We therefore speculate that, if

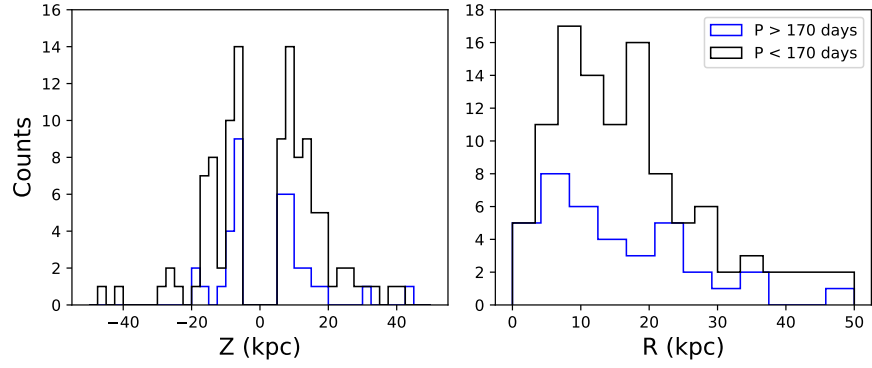


Figure 2.12: Difference in spatial extent between the old, i.e. shorter-period (black line) LPVs and the young, i.e. longer-period (blue line) ones as observed by CRTS. Stars belonging to the Sgr Stream and the LMC have been excluded. *Left*: Distribution of stars as a function of Galactic Z . Note that the longer-period LPV stars (blue line) appear to be mostly limited to $|Z| < 10$ kpc. *Right*: Distribution of stars as a function of Galactocentric cylindrical R . Note that both young and old, i.e. long- and short-period, stars extend as far as $R \sim 30$ kpc.

our distance estimates are valid, these objects represent a population of kicked disc stars. As of today, several prominent groups of high $|Z|$ disc stars are known, including those composed of M-giant stars, close relatives of Miras (Bergemann et al., 2018; Deason, Belokurov, and Koposov, 2018; Rocha-Pinto et al., 2004; Sheffield et al., 2018; Xu et al., 2015; de Boer, Belokurov, and Koposov, 2018). Strikingly, apart from the three obvious groups, such as the kicked disc population (blue) and the members of the Sgr Stream and the LMC (red and yellow), there are almost no young Miras in the Galactic halo.

However, we do find a total of 6 LPVs that extend to large distances, i.e. to Galactocentric distances in excess of ~ 90 kpc, and possess high *Gaia* amplitudes. In this regime, we find 91% of OGLE LMC LPVs (Soszyński et al., 2009) to lie within 0.5 magnitudes of our PL relation. Thus we are confident in our distance estimates for these stars in that they are highly likely to populate the Mira PL sequence. Further, these candidates were checked to bear colors consistent with Mira, again through comparison to the LPV catalog of Soszyński et al. (2009) and our own criteria in Fig. 2.1. The locations of these LPVs are marked with filled green stars in the right panel of Fig. 2.11 and are seen to extend out to ~ 130 kpc. These sources derive from the CRTS sample and their properties are listed in Table 2.1.

The latest tally of the record holders can be found in Bochanski et al. (2014). Table 1 of their paper lists all of the 9 stars with distances greater than 120 kpc known at the time. Of all large-distance candidates, the most securely identified are the horizontal branch stars. At least three independent samples of pulsating HB stars, or RR Lyrae,

CRTS ID	ℓ (deg)	b (deg)	J	H	K_s	Period (days)	V amp	D (kpc)
J003412.4-013154	113.04	-64.07	15.08	14.38	14.15	138	1.3	138 ± 11
J010520.9-091742	134.02	-71.87	14.30	13.59	13.28	190	1.2	115 ± 9
J072154.5+333020	184.85	20.49	13.76	12.95	12.66	224	2.1	104 ± 8
J080016.8+320949	188.96	27.75	14.75	14.08	13.81	134	1.1	122 ± 10
J112912.3+285815	202.32	71.79	14.03	13.36	13.07	151	1.9	90 ± 7
J135224.2-314452	317.79	29.36	14.62	13.86	13.62	128	1.0	97 ± 8

Table 2.1: Table of the six most distant LPVs in our sample, all deriving from the CRTS catalog. Listed are the CRTS ID's, Galactic coordinates, 2MASS magnitudes and periods. We also provide values of the visual amplitude and Galactocentric distance values. These Mira correspond to the green markers in the rightmost panel of Fig. 2.11. Distance errors are estimated from the dispersion of our LMC Mira distribution in Fig. 2.5.

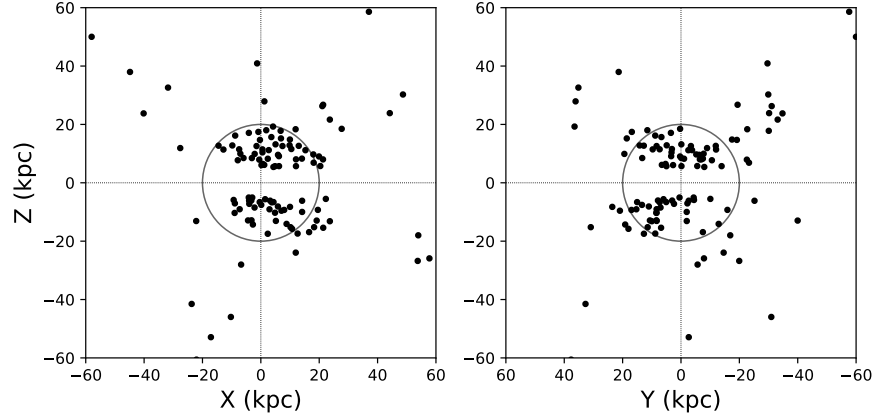


Figure 2.13: Distribution of old, short-period LPV stars in the Milky Way halo as viewed by CRTS. Stars belonging to the Sgr Stream, the LMC and those with $|Z| < 5$ kpc have been excluded. Note the marked drop in the density of old Mira stars outside of the grey circle, which has a radius of 20 kpc. *Left*: Distribution of stars projected onto the X, Z plane. *Right*: Distribution of stars projected onto the Y, Z plane.

have been published recently, each containing sizeable numbers of stars beyond 100 kpc (see Drake et al., 2013; Medina et al., 2018; Sesar et al., 2017). Additionally, blue HB stars can also be used as standard candles – albeit with somewhat lower accuracy – and thus used to trace the outskirts of the Galaxy. For example, Deason et al. (2012) uses a combination of deep multi-band photometry and VLT spectroscopy to detect BHBs at distances of order of 150 kpc. Finally, just like Miras, other stars around the AGB are good candidates for the most distant objects in the Galaxy owing to their spectacular luminosity. Accordingly, in the last two decades, Carbon stars and M-giants have been used routinely to scout the far reaches of the Milky Way (e.g. Bochanski et al., 2014; Deason et al., 2012; Koposov et al., 2015; Majewski et al., 2003; Maun, 2008; Maun, Gigoyan, and Kostandyan, 2018; Totten and Irwin, 1998).

The whereabouts of the old Miras, i.e. those with short period ($P < 170$ d) can be studied in Fig. 2.13. Their distribution appears to be broken into two components, a relatively smooth, compact one with $r < 20$ kpc (as indicated by black circle) and sparse lumpy one with $r > 20$ kpc. To investigate further the spatial properties of the distant old LPVs, we break them into three sub-samples, according to their Galactocentric distance, as shown in Fig. 2.14 in Galactic coordinates. Additionally, for all short-period pulsators with $r > 25$ kpc we carry out a great circle star count, following the ideas of (e.g. Ibata et al., 2001; Johnston, Hernquist, and Bolte, 1996; Lynden-Bell and Lynden-Bell, 1995; Mateu et al., 2011). In practice, for a given pole, we assign a Gaussian (with $\sigma = 6^\circ$) weight to each LPV according to

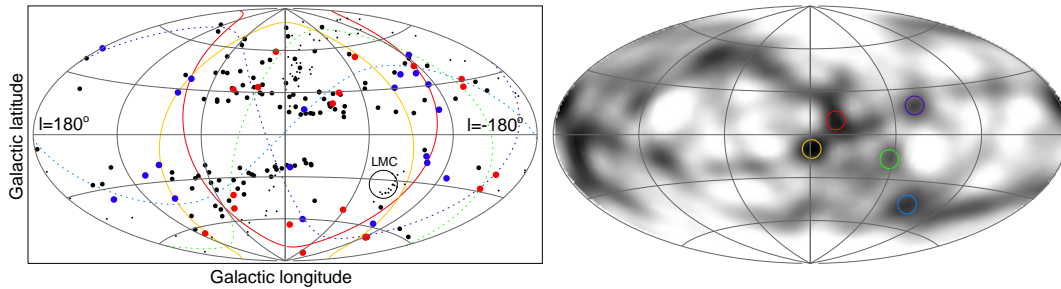


Figure 2.14: *Left*: Distribution of the CRTS LPVs with $P < 170$ d. Small black dots show the locations of stars in the Sgr Stream and the LMC. Filled black circles correspond to the stars with $R < 25$ kpc, while filled blue circles to the stars with $25 < R < 50$ kpc, and finally, red ones are those with $R > 50$ kpc. Red and yellow solid curves are the great circles corresponding to the two most significant over-densities in the plane of poles (see the right panel). These great circles pass close to the LMC (marked with a large empty black circle) and are aligned with the direction of the dwarf's motion. Dotted green, blue and violet show the great circles corresponding to the three other, less significant over-densities in the plane of poles. *Right*: Great circle pole density. The grey-scale value of each pixel of this map corresponds to the density of stars along the great circle with the pole at this pixel. Each great circle is represented by a pole (ℓ_0, b_0) together with its antipodes $(180 - \ell_0, -b_0)$. Stars are summed up with Gaussian weights according to their latitudinal distance from the equator of the great-circle coordinate frame with $\sigma = 6^\circ$. The two most obvious over-densities are marked with red and yellow. Other, less significant candidate over-densities are marked with green, blue and violet.

its latitude in the great circle coordinate system. The density of stars in the plane of poles is shown in the right panel of Fig. 2.14 in Galactic coordinates. The two most prominent over-densities are located near $(\ell, b) = (0^\circ, 0^\circ)$ and are marked with red and yellow empty circles. The corresponding great circles are over-plotted in the left panel. Interestingly, the two great circle pass very close to the LMC and are approximately aligned with the motion of the Cloud on the plane of the sky. This tentative detection of the Magellanic debris traced by LPVs is in agreement with the earlier study of Deason et al. (2017). Additionally, we identify three other, lower significance over-densities marked in green, blue and violet, whose corresponding great circles are shown in the left panel with dotted lines.

2.2.2 Satellite Galaxy and Globular Cluster Associations

Although AGB stars have been surveyed in the Local Group dwarf spheroidals (dSphs), the only confirmed detection of an O-Mira is in Sextans (Sakamoto et al., 2012). There are two C-Miras, but no O-Miras, so far found in Sculptor (Menzies et al., 2011). Whitelock et al.

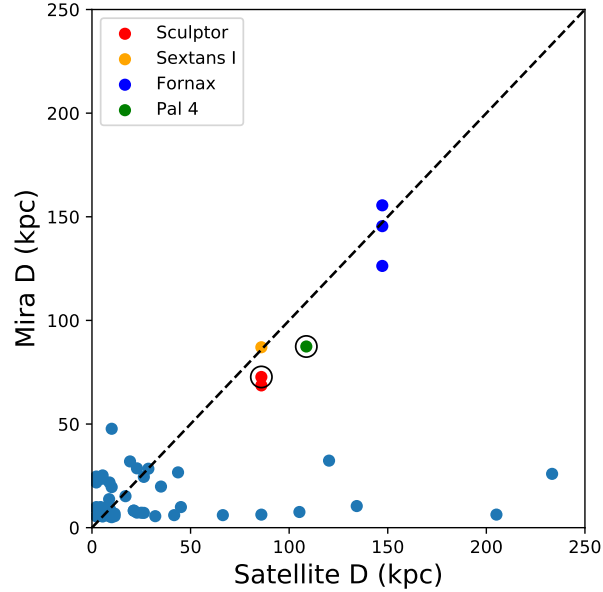


Figure 2.15: Possible associations of O-Mira with Local Group globular cluster and dwarf satellites. Labeled markers show Mira within 0.5° of known satellites and light blue markers within 2° . Circled markers are those for which the *Gaia* amplitude was applied yielding confident distance estimates. The heliocentric distance offset from satellites is shown as deviation from the linear line. These Mira derive from the CRTS subset.

(2009) report 6 C-Miras in Fornax – a further candidate (F51010 in their notation) is so blue that they were unable to determine from its colours whether it was C-rich or O-rich.

The spatial coordinates of the O-Mira candidates are compared against those of known objects within the Local Group. For this search, we utilise the CRTS O-rich LPV sample and search for associations by requiring the candidates to lie less than half a degree from the centres of globular clusters and dSphs in the Local Group. We use half a degree because many of these objects are expected to have extra-tidal stars. Given that Miras correspond to a short-lived phase of stellar evolution, they are intrinsically extremely rare and so any chance association is a priori very unlikely.

Potential associations exist with the Sculptor, Sextans I, and Fornax dSphs based on angular separation, as illustrated in Fig. 2.15. Circle markers indicate those that fulfill the criteria for a *Gaia* amplitude exceeding -0.55 . Our candidates are checked to all lie comfortably within the selections of Fig. 2.1 and thus are characteristic of O-rich Miras. The CRTS IDs, distances, periods and amplitudes of our candidates are listed in Table 2.2. It would be interesting to confirm the candidates with kinematic evidence, which may already be possible with proper motion data from the recent data release 2 of the *Gaia* satellite.

CRTS ID	Period (days)	V amp	Mira D (kpc)	Satellite	Satellite D (kpc)	Age (Gyr)	$\Delta\theta$ (deg)
J005958.9-332834*	196	1.1	72 \pm 6	Sculptor	86 \pm 6	6	0.2
J010120.8-335304	92	0.8	69 \pm 5	Sculptor	86 \pm 6	10	0.3
J101234.2-013440	120	1.1	87 \pm 7	Sextans (I)	86 \pm 4	10	0.1
J023822.6-343804	163	0.8	145 \pm 12	Fornax	147 \pm 12	9	0.4
J023910.7-343920	157	0.9	126 \pm 10	Fornax	147 \pm 12	10	0.3
J024045.9-343453	143	0.8	156 \pm 12	Fornax	147 \pm 12	10	0.2
J111320.6+221116	184	0.8	193 \pm 15	LeoII	233 \pm 14	7	0.05
J112912.3+285815*	151	1.9	87 \pm 7	Pal 4	100	10	0.02
J112914.6+285814	131	1.3	102 \pm 8	Pal 4	100	10	0.009

Table 2.2: The data on the candidate Mira associations with Galactic dwarf spheroidals and distant globular clusters. We provide the CRTS ID and heliocentric coordinates of the candidates, as well as heliocentric distance to the satellite and angular offset. Pal 4 distance estimates were obtained from Harris (1996) and the remaining satellites from McConnachie (2012). Tentative age estimates derive from the relation in Figure 2.7 and have been capped to 10 Gyr. Heliocentric coordinates are encoded in the CRTS ID and Mira distance errors are derived similarly to those in Table 2.1. Starred IDs marks associations possessing a *Gaia* amplitude > -0.55 .

We reproduce the detection of the O-Mira found by Sakamoto et al. (2012) in Sextans who report a distance of $79.8_{-9.9}^{+11.5}$ kpc, consistent with our distance estimate of 87 ± 7 kpc. We also identified an O-Mira located close to the Palomar 4 globular cluster. This is a young halo globular cluster that is likely to have been accreted by the Milky Way via the infall of its parent dwarf satellite. The O-Mira lies at a heliocentric distance of 87 kpc compared to a distance of Pal 4 of 109 kpc (Sohn et al., 2003). The latter authors carried out deep photometric searches in a field $1.3^\circ \times 0.9^\circ$ around Pal 4, and claimed evidence for the existence of extra-tidal tails and features. Although semi-regular variables are known in Pal 4, this is the first report of a possible Mira.

2.3 SUMMARY

This chapter has highlighted a neglected resource. The Miras are bright and can be traced throughout the Galaxy, and beyond. The carbon-rich or C-Miras have a long history of use as tracers of halo substructure (e.g., Downes et al., 2004; Huxor and Grebel, 2015). However the oxygen-rich, or O-Miras, have been less widely scrutinised yet they are at least as valuable. Their period and luminosity only weakly depends on colour, so the O-Miras are excellent distance indicators. Their period depends on age, with young O-Miras having the longest periods, thus they are useful chronometers. So, samples of Miras will enable us to detect age gradients throughout the Galaxy and to date the Galactic populations. Here, we have used the Catalina Surveys and the All Sky Automated Survey for Supernovae to extract a sample of $\sim 2,200$ O-rich LPVs, particularly Miras. They probe the Galactic bulge, thin and thick discs and the distant halo. In principle, they offer a unique resource to age-date all the structural components of the Galaxy.

We show that the disc O-Miras have periods increasing on moving outwards from ~ 1 to 15 kpc. As the period of O-Miras correlates inversely with age, this is a clear demonstration of the ‘inside out’ nature of the Galactic disc (e.g., Martig et al., 2016b). The outer disc O-Miras have median period ~ 275 days, as compared to the inner disc value of ~ 200 days. At least out to 15 kpc, there is no evidence of an upturn in the radial profile of the age of disc, as expected from models in which the outer disc is populated by old stars which migrated from the inner disc (Roškar et al., 2008). There are also hints of vertical variation, in the sense that O-Miras at higher $|Z|$ comprise an older population for given radius R in the inner disc. At small Galactocentric distances, within 2 – 3 kpc from the MW centre, age

gradients flatten out, signaling that the bulge contains a mix of stellar ages, in agreement with earlier studies (see e.g. Catchpole et al., 2016). Moving away from the centre, clearly visible in our data is the transition from younger disc to older halo O-Miras, which occurs at $r \sim 15$ kpc where the median O-Mira period plummets. The median period of the halo O-Miras is ~ 150 days (roughly 10 Gyrs).

O-Miras and other LPVs are also precious as tracers outside the Galactic disc. There is a population of long period, and hence young, O-rich LPVs that follow the extent of the Galactic disc, but lie at heights of up to 10 kpc. These may be stars kicked out of the disc, perhaps analogous to other high latitude structures (Bergemann et al., 2018; Deason, Belokurov, and Koposov, 2018; Sheffield et al., 2018). The O-rich LPVs are so intrinsically luminous that they can trace far into the halo. We identify six candidate Mira probably reaching distances between 90 and 140 kpc, and a good fraction of these distant Mira appear to be associated with the Sgr Stream. In addition to the tentative detection of Magellanic debris associated with tidal disruption, we have also provided new detections of O-Miras in Milky Way satellites. Specifically, we found associations between likely O-Mira and the Fornax, Sculptor, Sextans and Leo II Galactic dwarf spheroidals, as well as the distant globular cluster Pal 4.

AGE DEMOGRAPHICS OF THE MILKY WAY DISC AND BULGE

This chapter is based on work originally published in Grady, Belokurov, and Evans (2020)

We exploit the extensive *Gaia* Data Release 2 set of Long Period Variables to select a sample of oxygen-rich Miras throughout the Milky Way disc and bulge for study. Exploiting the relation between Mira pulsation period and stellar age/chemistry, we slice the stellar density of the Galactic disc and bulge as a function of period. We find the morphology of both components evolves as a function of stellar age/chemistry with the stellar disc being stubby at old ages, becoming progressively thinner and more radially extended at younger stellar ages, consistent with the picture of inside-out and upside-down formation of the Milky Way's disc. We see evidence of a perturbed disc, with large-scale stellar over-densities visible both in and away from the stellar plane. We find the bulge is well modelled by a triaxial boxy distribution with an axis ratio of $\sim [1 : 0.4 : 0.3]$. The oldest of the Miras ($\sim 9 - 10$ Gyr) show little bar-like morphology, whilst the younger stars appear inclined at a viewing angle of $\sim 21^\circ$ to the Sun-Galactic Centre line. This suggests that bar formation and buckling took place $8 - 9$ Gyr ago, with the older Miras being hot enough to avoid being trapped by the growing bar. We find the youngest Miras to exhibit a strong peanut morphology, bearing the characteristic X-shape of an inclined bar structure.

3.1 DATA

We make use of the substantial DR2 LPV data set provided by the *Gaia* consortium Mowlavi et al. (2018). Specifically, we select all stars from the `vari_long_period_variable` table for which, crucially, the pulsation period is available and hence distance estimates afforded to us. We then cross-match with the 2MASS point source catalogue to obtain near infrared (NIR) JHK_s photometry yielding 89,555 sources. The cross-match was carried out using a 1 arcsec aperture. We correct for extinction using the map of Schlegel, Finkbeiner, and Davis (1998) and extinction coefficients from Yuan, Liu, and Xiang (2013). The spatial distribution of the sample is shown in Fig. 3.1 with LPVs

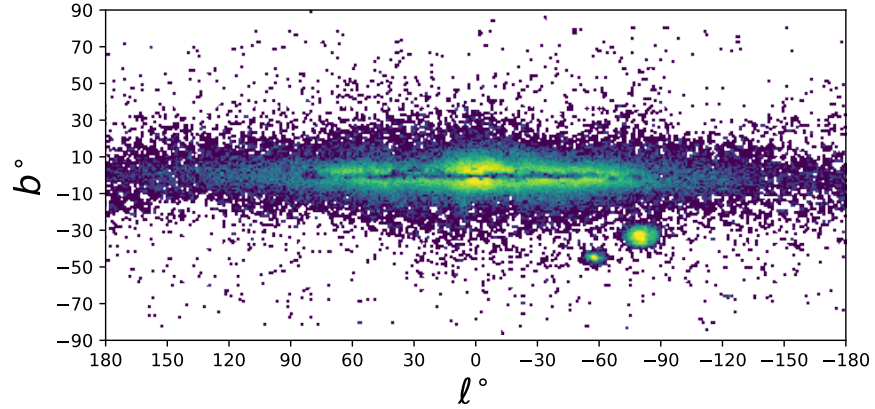


Figure 3.1: Logarithmic number density of the *Gaia* DR2+2MASS LPVs in Galactic coordinates. We clearly see the Magellanic Clouds as well as the Sgr dwarf galaxy. Otherwise, the majority of the LPV population is confined to the plane of the Galaxy.

pervading through the disc, bulge, Magellanic Clouds and the Sgr dwarf.

3.1.1 Selecting Miras

As discussed in the preceding chapters, Miras are high amplitude pulsators that have long been known to lie on precise PL sequences in the JHK_s system (see e.g. Feast et al., 1989; Glass and Feast, 1982). In Fig. 3.2 we plot the number density of our *Gaia* DR2+2MASS LPVs in amplitude¹ – colour space where we observe some important features. The bulk of stars inhabit two regions in amplitude space: there is a high amplitude population, and one of lower amplitude. Further, these two populations are largely confined to narrow regions of colour. Beyond this, we see a smearing toward redder and bluer colours. The blue-ward extensions are sources with large colour excess values lying in heavily extinguished regions. The sources flaring out to large red colours are the C-rich Miras. O-rich and C-rich Miras are known to separate in their near infrared (NIR) colours due to their differing circumstellar compositions (see e.g. Feast et al., 1982; Glass and Feast, 1982; Soszyński et al., 2009; Whitelock et al., 2006). The dusty outskirts of the C-rich Miras may impede our ability to obtain accurate distance estimates to them. Whitelock, Feast, and Van Leeuwen (2008b) note that whilst C-rich Miras are observed to lie on the same PL sequence as their counterpart, the O-rich Miras, they do so with higher uncertainty. Further, they can be difficult to separate from C-rich Semi Regular Variables (SRVs) and overtone pulsators and thus selection of this subset is prone to contamination. The O-

¹ We utilise the same amplitude definition from eqn (2.1) in Chapter 2

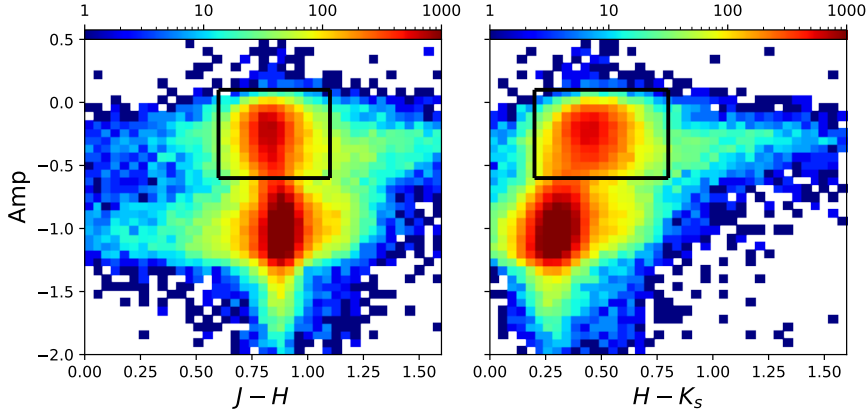


Figure 3.2: The logarithmic number density of stars in amplitude colour space for de-reddened $J - H$ and $H - K_s$. The Amp term defined in eqn (2.1) measures the amplitude of variability of the LPVs. We immediately observe a segregation between the high amplitude Miras and the lower amplitude SRVs in this projection. Solid black lines denote our selection boundaries.

rich Miras have less spread in their NIR colours and are identified as the stars bound by the black lines in Fig. 3.2. We select these stars as our sample, which we will henceforth simply refer to as Miras, leaving us with 24,533 stars. We employ the Mira PL relation of Yuan et al. (2017), with a minor calibration correction, as reported in Chapter. 2, to obtain:

$$M_{K_s} = -6.90 - 3.77 (\log P - 2.3) - 2.23 (\log P - 2.3)^2 - 0.17 \quad (3.1)$$

with M_{K_s} being the absolute magnitude of a Mira and P its pulsation period in days. Once we have computed the luminosity of each Mira using eqn (3.1), we can directly estimate the heliocentric distance via the standard relation:

$$\log \left(\frac{D}{\text{kpc}} \right) = \frac{K_s - M_{K_s}}{5} - 2 \quad (3.2)$$

3.1.2 Miras in the Large Magellanic Cloud

We test the efficacy of our selection method by analysing the *Gaia* DR2+2MASS LPVs towards the LMC. Selecting stars within a 15° aperture of the dwarf, we show their distribution in K_s magnitude – period space in the left panel of Fig. 3.3. Three main sequences are prominent with the middle of these being the high amplitude Mira sequence that we wish to select from (see Wood et al., 1999). On imposing the selection of Fig. 3.2 upon the LMC sample, we select stars mainly from the Mira sequence, as demonstrated in the right hand panel of Fig. 3.3. We overlay our PL relation of eqn (3.1), corrected for

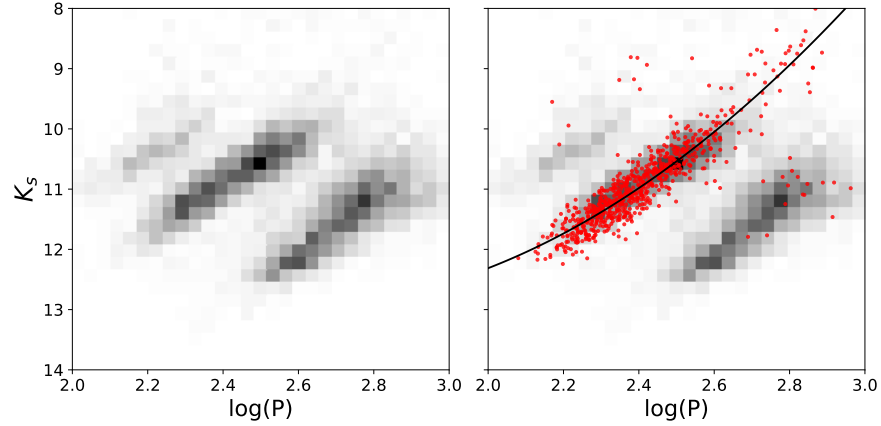


Figure 3.3: *Left*: Number density of the *Gaia* DR2+2MASS LPVs selected within a 15° aperture of the LMC are shown in period magnitude space. Values for K_s have been corrected for extinction. Three distinct PL sequences are seen with the middle of these identified as the Mira sequence. The upper and lower sequences are predominately populated by SRVs. *Right*: We overlay our Mira candidates as red markers. These stars are selected from the amplitude – colour cuts shown in Fig. 3.2. We see that our selection acts well to pick out the Miras for which we can obtain accurate distance estimates. The solid black line shows our PL relation of eqn (3.1) adjusted to the LMC’s distance modulus.

the LMC distance modulus of Elgueta et al. (2016), as a solid black line. There is a degree of contamination, as shown by the stars deviating from the Mira sequence for which we are unable to obtain accurate distances. We estimate the contaminant fraction by taking the ratio of the number of Miras deviating from our PL relation by > 0.5 magnitudes with the total number of selected LMC Miras. This yields a contamination estimate of $\sim 7\%$. Utilising the sample of LMC LPVs of Soszyński et al. (2009), we estimate the purity of our O-rich Mira sample to be 72% with the major contaminant being high amplitude stars classified as SRVs by OGLE. We recover 47% of the OGLE-III O-Miras in the cross-match, a completeness value consistent with that of the full *Gaia* DR2 LPV catalogue with respect to the OGLE-III LPVs towards the Magellanic Clouds (see Mowlavi et al., 2018).

3.1.3 Galactic Sample

Upon selecting our full sample of Mira, we assign distances by the procedure outlined in Sec. 3.1.1 and compute the Galactocentric (X, Y, Z) Cartesian coordinates for each star. We then remove stars lying towards the Magellanic Clouds by excising regions on the sky located within 15° and 10° of the LMC and SMC respectively. We further restrict our analysis to Miras in the period range of 100 – 400 days, beyond which there may be increased scatter about the PL relation,

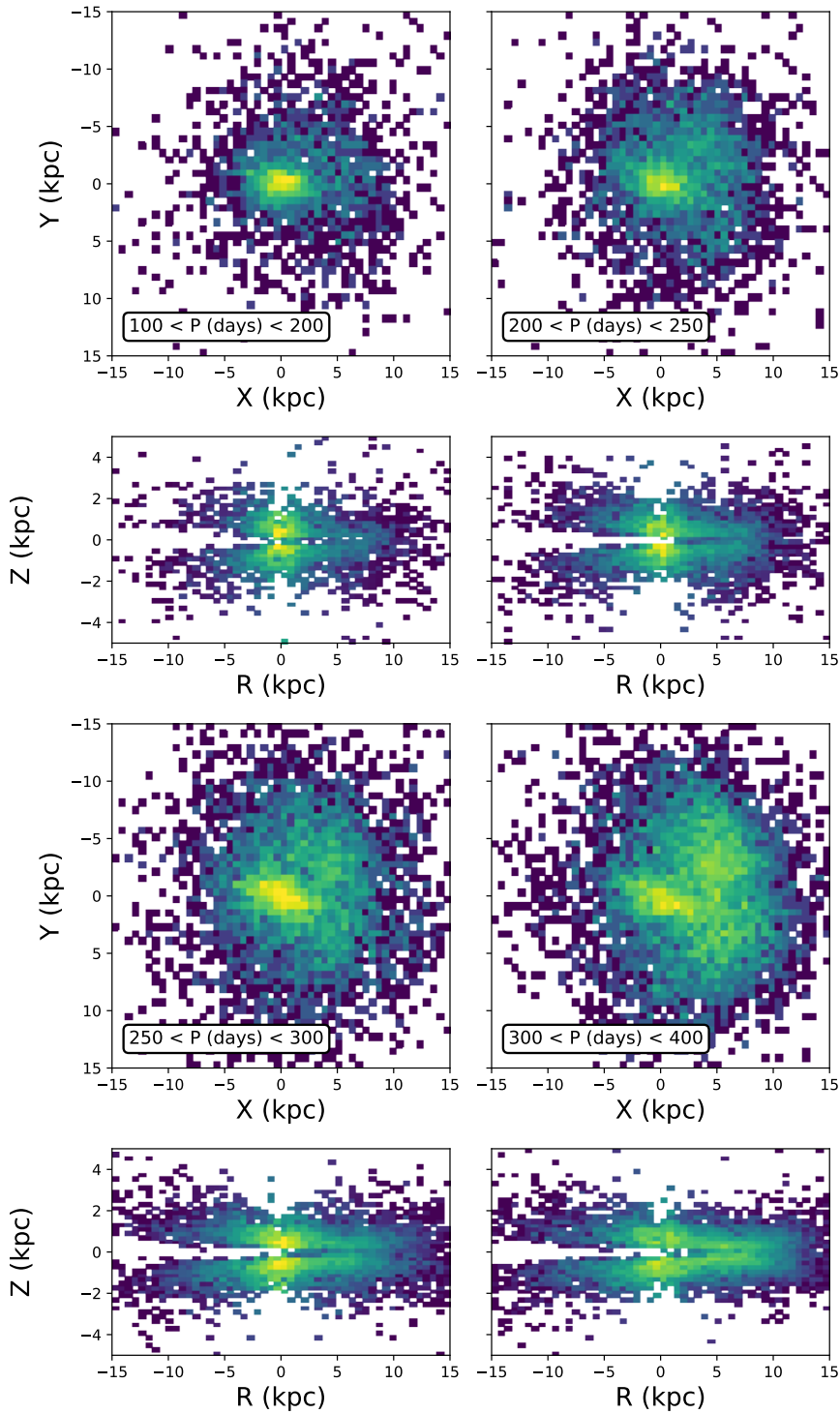


Figure 3.4: We show the spatial distribution of our Mira sample, subdivided into four period bins, in both Galactocentric $X - Y$ and cylindrical $R - Z$ projections. Solar position is at $(X_{\odot}, Y_{\odot}, Z_{\odot}) = (8.3, 0, 0)$ kpc. The bulge/bar is visible throughout, with the disc population becoming more populous with increasing Mira period. We further see most of the Miras to be vertically confined to within 2 kpc of the Galactic plane. For each $X - Y$ projection we show the corresponding $R - Z$ projection in the panel immediately below.

producing a sample size of 21,149 O-rich Miras. We choose 400 days as our upper limit as the *Gaia* DR2 data sample is based on data collected from a 22 month period. Thus, the number of candidate Mira with periods exceeding 400 days in *Gaia* DR2 is highly depleted (see Mowlavi et al., 2018).

The distribution of stars in Fig. 3.4 shows clear evolution as a function of period. The bulge grows in scale from low to high period with a distinct tilt being apparent at higher periods. The bulge dominates the Mira population at low periods, as expected for an older, metal poorer stellar population. For the longer period Miras, we see an extended bar stretching out to ~ 5 kpc either side of the galaxy. With regards to the disc, there is a plentiful stellar population local to the Sun at high periods, these being the young, low latitude, nearby Miras. Their vertical extent is restricted and they extend to beyond ~ 10 kpc radially. The lower period stars are less restricted to the plane, demonstrating a fluffier disc component for the older/metal poorer Miras. At the lowest periods, we observe the disc to be radially truncated in comparison to the higher period stars. This is suggestive of a progression from a thin, radially extensive disc at young ages to a thicker, stubbier disc at older stellar ages.

3.2 STELLAR DENSITY PROFILES

3.2.1 Modelling the Galactic Disc and Bulge

Each star is modelled as the realisation of a Poisson process at its spatial position. Thus, for a given density model, the likelihood has the general form²:

$$\ln \mathcal{L} = - \int_V \rho(\mathbf{r}|\Theta) S(\mathbf{r}) dV + \sum_{i=1} \ln \rho(\mathbf{r}_i|\Theta) \quad (3.3)$$

where $\rho(\mathbf{r}|\Theta)$ is the number density defined by model parameters Θ and \mathbf{r} the Galactocentric position vector. The integral part of the likelihood is a normalising term which equates to the number of Miras within the total volume V and the right hand summation is conducted over all stars bound by the volume. Any general selection function $S(\mathbf{r})$ depending on the spatial coordinates can in principle be incorporated. In our application, the selection function is highly non-trivial being a convolution of the individual selection functions of 2MASS and *Gaia*, the latter being unknown. We remark that the distribution of LPVs in Fig. 3.1 is encouragingly smooth. That is, there is no obvious spatial dependence on detection efficiency through the

² See A.2 for derivation of this likelihood function

Galaxy for the *Gaia* LPVs. We therefore only account for the footprint over which we can observe our Miras, as detailed later in this section.

The presence of a strong bulge/bar in the Miras seen in Fig. 3.4 motivates us to adopt a two component model to describe the data: a disc and a bar/bulge. We model the disc component by a simple double exponential function in Galactocentric cylindrical polar coordinates (R, Z) . The bulge/bar component is modelled as a triaxial boxy Gaussian distribution as in Dwek et al. (1995). Explicitly, these are:

$$\rho_{\text{disc}}(R, Z) = \rho_0^{\text{disc}} \exp(-R/R_s) \exp(-|Z|/Z_s) \quad (3.4a)$$

$$\rho_{\text{bulge}}(x, y, z) = \rho_0^{\text{bulge}} \exp(-0.5 m^2(x, y, z)) \quad (3.4b)$$

where R_s and Z_s denote the scale length and scale height of the Galactic disc. The terms ρ_0^{disc} and ρ_0^{bar} are the central number densities determined by the total number of stars included in the normalising volume integral of eqn (3.3). The term m in eqn (3.4b) is computed as:

$$m = \left[\left(\left(\frac{x}{x_0} \right)^2 + \left(\frac{y}{y_0} \right)^2 \right)^2 + \left(\frac{z}{z_0} \right)^4 \right]^{\frac{1}{4}} \quad (3.5)$$

where (x_0, y_0, z_0) represent the principal semi-axes of the bar. The Cartesian coordinates (x, y, z) are aligned along the major, intermediate and minor axes of the bar. Fig. 3.4 shows the major axis of the bar to be misaligned with the line of sight from the Sun to the Galactic Centre (GC). We transform from Galactocentric (X, Y, Z) to bar aligned coordinates (x, y, z) through a rotation in the (X, Y) plane defined as:

$$\begin{pmatrix} x \\ y \\ z \end{pmatrix} = \begin{pmatrix} \cos \theta & -\sin \theta & 0 \\ \sin \theta & \cos \theta & 0 \\ 0 & 0 & 1 \end{pmatrix} \begin{pmatrix} X \\ Y \\ Z \end{pmatrix} \quad (3.6)$$

where the angle θ is defined anti-clockwise about the Z axis from our line of sight to the Galactic Centre (X axis). Our model then has 5 parameters denoted as $\Theta = (R_s, Z_s, x_0, y_0, z_0, \beta, \theta)$, where we have introduced β to represent the central density fraction of bar to disc: $\rho_0^{\text{bar}}/\rho_0^{\text{disc}}$. We will hereafter refer to this as model 1 (M1). For the purposes of generality, we also consider a disc model of the form:

$$\rho_{\text{disc}}(R, Z) = \rho_0^{\text{disc}} \exp\left(-\sqrt{(R^2 + R_0^2)/R_s^2}\right) \exp(-|Z|/Z_s) \quad (3.7)$$

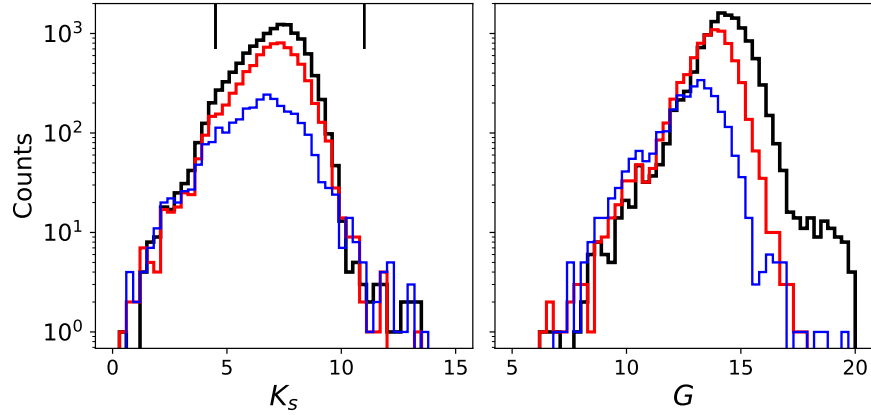


Figure 3.5: Distributions of apparent magnitude for our Mira sample, without any extinction corrections applied, in both the 2MASS K_s and *Gaia* G photometric bands. Black histograms show the Miras lying in the latitude range $0^\circ < |b| < 5^\circ$. The high extinction in this region is visible as an excess of stars at faint optical magnitudes. The red (blue) histograms correspond to those lying at $5^\circ < |b| < 10^\circ$ ($10^\circ < |b| < 20^\circ$).

now including a softening parameter R_0 . The combination of this softened exponential disc model with the boxy bulge model above will be referred to as model 2 (M2).

To transform from heliocentric coordinates (D, ℓ, b) to Galactocentric cylindrical polar (R, ϕ, Z) or bulge-aligned Cartesian coordinates (x, y, z) , we require the Jacobians:

$$\frac{\partial (R, Z, \phi)}{\partial (D, \ell, b)} = \frac{D^2 \cos b}{R}, \quad \frac{\partial (x, y, z)}{\partial (D, \ell, b)} = D^2 \cos b \quad (3.8)$$

We must also account for the spatial footprint over which we can efficiently observe Miras. Given that we are adopting photometric distance estimates, this will be a function of the survey photometry. In Fig. 3.5, we show the apparent magnitude distribution of our Miras in both the 2MASS K_s and *Gaia* G bands for different Galactic latitude bins. No reddening correction has been applied for this figure, so we can assess latitude dependence of the luminosity function. In both the 2MASS K_s and *Gaia* G bands, we see at low latitudes there is an excess of faint sources, those suffering from regions of high extinction. Accordingly, we only consider stars with $|b| > 5^\circ$ in our analysis, removing highly extinguished sources together with the region in which the extinction maps of Schlegel, Finkbeiner, and Davis (1998) become highly unreliable. We make use of the González-Fernández et al. (2012) IR bulge extinction map, which covers the VVV footprint, to further assess the extinction effects of our sample. We find that $\sim 1\%$ of our Miras have A_{K_s} values greater than 0.15 at latitudes beyond 5° .

We further restrict our analysis to stars bound by $K_s^{\max} = 11$ to mitigate any source detection deficiencies at faint magnitudes. We also see the luminosity functions truncate at bright magnitudes, as sources saturate, and thus we define a lower limiting magnitude for our sample at $K_s^{\min} = 4.5$. The volume over which we compute our likelihood in eqn (3.3) is bound by these imposed magnitude limits, with corresponding distance limits obtained from eqn (3.2). Further, though the contribution of high latitude halo stars is small, as is evident from Fig. 3.1, we also restrict our analysis to stars lying at $|b| < 20^\circ$. No Galactic longitudinal restriction is made in this analysis. Thus, our selection function is simply:

$$S(D, \ell, b) = \begin{cases} 1 & \text{if } D \in (D_{\min}, D_{\max}) \text{ and } b \in (b_{\min}, b_{\max}), \\ 0 & \text{else.} \end{cases} \quad (3.9)$$

The bounding volume is a function of Mira luminosity, which itself depends on pulsation period. Thus, the variation of volume as a function of Mira period must be accounted for in our likelihood calculation, achieved by splitting our likelihood into sub-period bins.

A further important consideration is the uncertainty in the distance assigned to each Mira, stemming from the width of the PL sequence in Fig. 3.3. We neglect errors on the periods assigned to the Miras by *Gaia* as they are typically less than 1% for our sample. We model the distance modulus distribution of our LMC Miras as a Gaussian and fit using least squares regression, obtaining a standard deviation of $\sigma = 0.23$. This distribution width is then convolved into our likelihood computation. We note that the distance uncertainty accounted for in this convolution outweighs that required for sources with $A_{K_s} \sim 0.15$. As mentioned earlier in the text, a negligible fraction of our Miras bear values larger than this, based on the extinction map of González-Fernández et al. (2012).

We sample our posterior distribution in Markov Chain Monte Carlo (MCMC) fashion, applying flat priors, to make an inference on our model parameters. To do so, we implement the *emcee* sampler provided by Foreman-Mackey et al. (2013). Numerical computation of the normalising integral is expensive and so we initially do so over a regular grid in our model parameter space. We then linearly interpolate over the grid, enabling posterior samples to be drawn for each MCMC step in parameter space. We choose to model the four period bins shown in Fig. 3.4 separately. Applying the selection criteria outlined in this section, we retrieve 1,198 Miras to model with periods in the range of 100 – 200 days. For the two intermediate period bins, we obtain 1,175 and 2,942 Miras respectively with 3,155 stars in our

high period bin. Hereon we will reference these bins as P1, P2, P3 and P4 in order of increasing period.

Using the period age relations of Feast (2009) and Wyatt and Cahn (1983), we estimate stars belonging to P1 bear ages of ~ 10 Gyr and older. For stars in P2 and P3, we reckon ages to lie from ~ 10 Gyr down to ~ 7 Gyr. For the long period Miras in P4, we estimate their ages to lie in the range $\sim 5 - 7$ Gyr. Given that we have no metallicity information for the Miras in our sample, we probed its effect on age estimation using the period-metallicity relation of Feast and White-lock (2000b). Drawing mock metallicity values from a Gaussian with a standard deviation of 0.3 dex (as judged from Hayden et al. (2015) and Gonzalez et al. (2015)), we estimate this to impact the age estimates by ~ 1 Gyr. We acknowledge the inherent uncertainty in these age estimates, but assign them to provide a sense of the age distribution of our Mira sample. Irrespective of metallicity uncertainties, it remains true that the development from short period to long period tracks Miras from old and metal poorer to young and metal richer. We use the nomenclature "old" and "young" purely in the context of our sample.

It has been observed by Kordopatis et al. (2013) that at metallicities less than $[\text{Fe}/\text{H}] = -1.5$, halo stars can dominate over disc stars in the solar neighbourhood. Recently, Arentsen et al. (2020) posit this may also be the case in the inner galaxy by analysing the kinematics of metal poor bulge stars. Stars of such low metallicity are extremely rare however and very few M giants have been observed with metallicities broaching this regime (see e.g. Rich and Origlia, 2005; Schultheis, Ryde, and Nandakumar, 2016). We therefore expect such effects to be negligible in our sample, even for our lowest period Miras in P1.

3.2.2 *Simulated data*

We first implement our inference method on a mock data set. We generate a population of stars comprised of a disc and a bar component. For the disc population, we draw cylindrical coordinates (R, Z) from exponential distributions with parameters $R_s = 3.5$ kpc and $Z_s = 1.0$ kpc to mimic the double exponential model of eqn (3.4a). Similarly for the bar, we draw (x, y, z) coordinates from the triaxial Gaussian distribution in eqn (3.4b) fixing the parameters at $(x_0, y_0, z_0) = (2.0, 1.0, 0.7)$ in units of kpc. We prescribe the stars period values ranging from 100 – 200 days, drawn from a narrow Gaussian centred on $P = 150$ days with a width of 50 days. Further, we fix the ratio of bar stars to disc stars to approximate that of our real data set in this

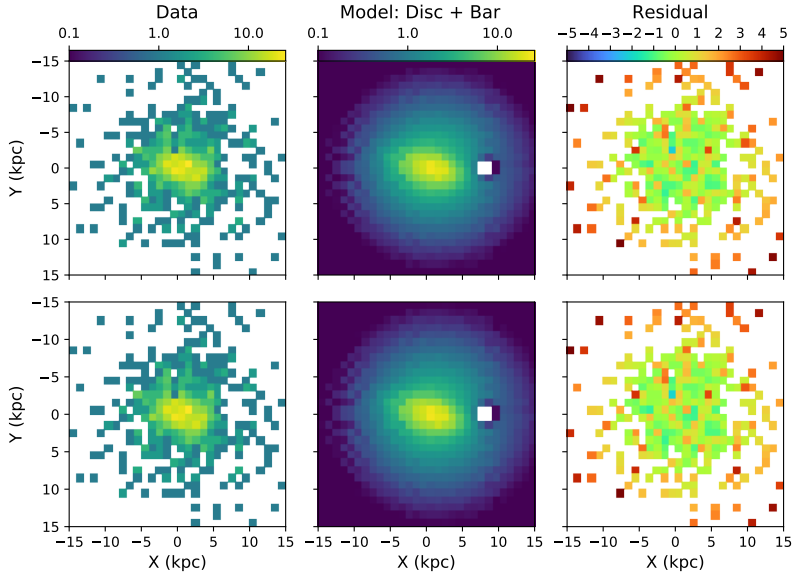


Figure 3.6: Comparisons of our simulated data with two models: the initial simulated model with parameters Θ_{sim} (top row) and that recovered from our MCMC inference procedure (bottom row). The left (middle) column shows the stellar number density projected into the Galactocentric (X, Y) plane for the simulated data (model). The lack of stars around the Solar position in the model panels stems from the limiting magnitude mask imposed when modelling the stellar density. The right columns shows the residual, scaled by the Poisson error in each corresponding model pixel.

	Input	Recovered
R_s (kpc)	3.5	$3.61^{+0.14}_{-0.16}$
Z_s (kpc)	1.0	$1.10^{+0.05}_{-0.05}$
x_0 (kpc)	2.0	$2.05^{+0.14}_{-0.15}$
y_0 (kpc)	1.0	$0.95^{+0.08}_{-0.07}$
z_0 (kpc)	0.7	$0.73^{+0.05}_{-0.04}$
β	2.04	$2.12^{+0.47}_{-0.39}$
θ (deg)	20	$17.48^{+3.7}_{-3.5}$

Table 3.1: Table shows the simulated input parameters used to generate our mock data and the recovered parameters from our fitting procedure.

period range, providing a simulated value for β as 2.04. We simulate 1,000 stars lying in the latitude range of $5^\circ < |b| < 20^\circ$.

Following the methods of Section 3.2.1, we infer the density profile parameters of our simulated data and make a comparison to those that we initially implemented in the generation of the mock data. We do so in Fig. 3.6 where we show the two sets of residuals in the $X - Y$ plane; the top row being that of simulated model and the bottom row

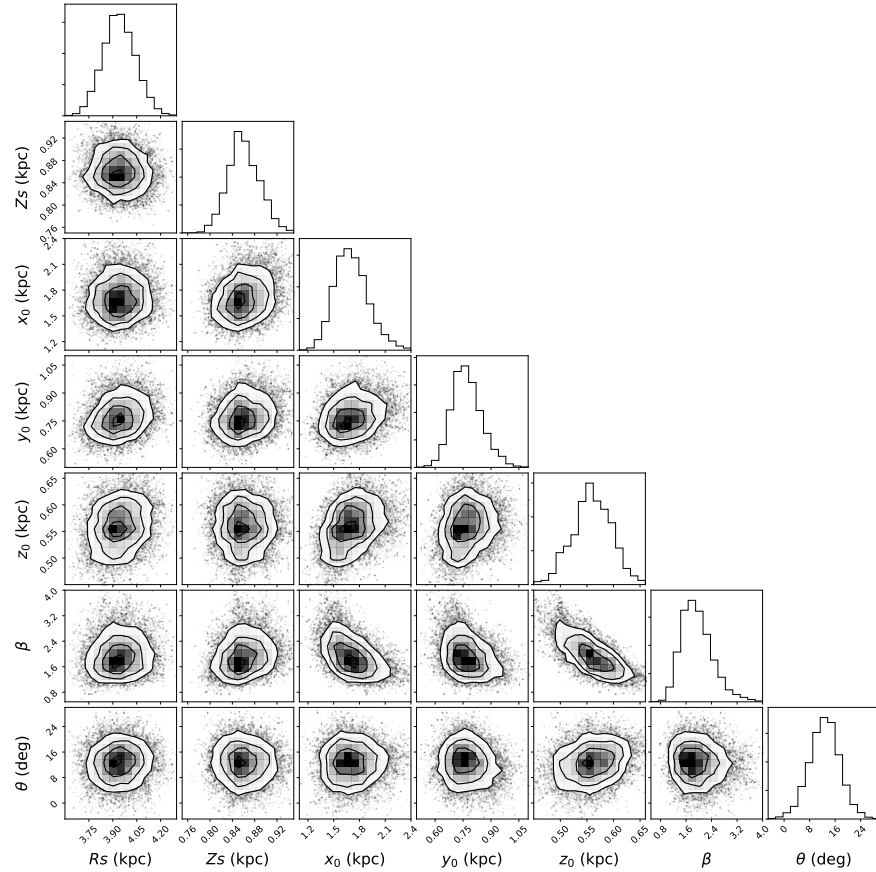


Figure 3.7: Marginalised posterior distributions for the model parameters of the Mira population in the period range 200-250 days recovered from our MCMC inference.

using the model parameters recovered from our inference procedure. The figure demonstrates excellent agreement between the two rows with negligible difference between the two residuals and in Table 3.1 we list the input and inferred simulated model parameters.

3.3 RESULTS

We apply our parameter fitting procedure to each of the three sub-populations of Miras shown in Fig. 3.4, probing the evolution of disc and bar morphology with pulsation period. Fig. 3.7 demonstrates the resultant posterior distributions obtained from our fits, with the figure being representative of the intermediate period population P2, and we list the full set of parameters for each of the period bins in Table 3.2. We show the full evolution of our model parameters in each period bin in Fig. 3.8 with our main model, M1, identified by red markers.

Period bin	R_s (kpc)	Z_s (kpc)	x_0 (kpc)	y_0 (kpc)	z_0 (kpc)	β	θ (deg)
P1	$3.78^{+0.13}_{-0.13}$	$1.01^{+0.05}_{-0.04}$	$1.85^{+0.23}_{-0.15}$	$0.81^{+0.07}_{-0.06}$	$0.64^{+0.04}_{-0.03}$	$3.29^{+0.65}_{-0.55}$	$1.27^{+3.20}_{-2.80}$
P2	$3.96^{+0.10}_{-0.11}$	$0.86^{+0.03}_{-0.03}$	$1.69^{+0.19}_{-0.17}$	$0.76^{+0.08}_{-0.06}$	$0.56^{+0.04}_{-0.04}$	$1.95^{+0.51}_{-0.47}$	$12.71^{+4.68}_{-4.60}$
P3	$4.47^{+0.11}_{-0.09}$	$0.66^{+0.02}_{-0.01}$	$1.68^{+0.12}_{-0.11}$	$0.73^{+0.05}_{-0.05}$	$0.55^{+0.02}_{-0.03}$	$1.59^{+0.36}_{-0.26}$	$21.16^{+3.27}_{-3.41}$
P4	$4.52^{+0.10}_{-0.10}$	$0.51^{+0.01}_{-0.01}$	$2.02^{+0.32}_{-0.28}$	$0.56^{+0.07}_{-0.07}$	$0.55^{+0.04}_{-0.04}$	$0.54^{+0.17}_{-0.11}$	$21.08^{+2.28}_{-2.66}$

Table 3.2: We list the recovered parameters of our model, for each Mira period bin, following the procedure detailed in Section 3.2.1. For the old stars (P1), they have age estimates of ~ 10 Gyr. Stars in P2 and P3 bear ages of $7 - 10$ Gyr. For the youngest Miras, we estimate their ages to be $\sim 5 - 7$ Gyr. We base these values on the Mira age estimates of Wyatt and Cahn (1983) and Feast (2009).

3.3.1 Miras in the Disc

From Fig. 3.8, the disc parameters of our main model (M1) show an evolution in agreement with the qualitative picture obtained from Fig. 3.4; as we progress from a high to low period population of stars, the thickness of the disc increases reaching a scale height of ~ 1 kpc, comparable to traditional estimates for the thick disc. Similarly, we see an evolution in the radial scale length of the disc, originating at low values for low periods and growing on increasing period. Such

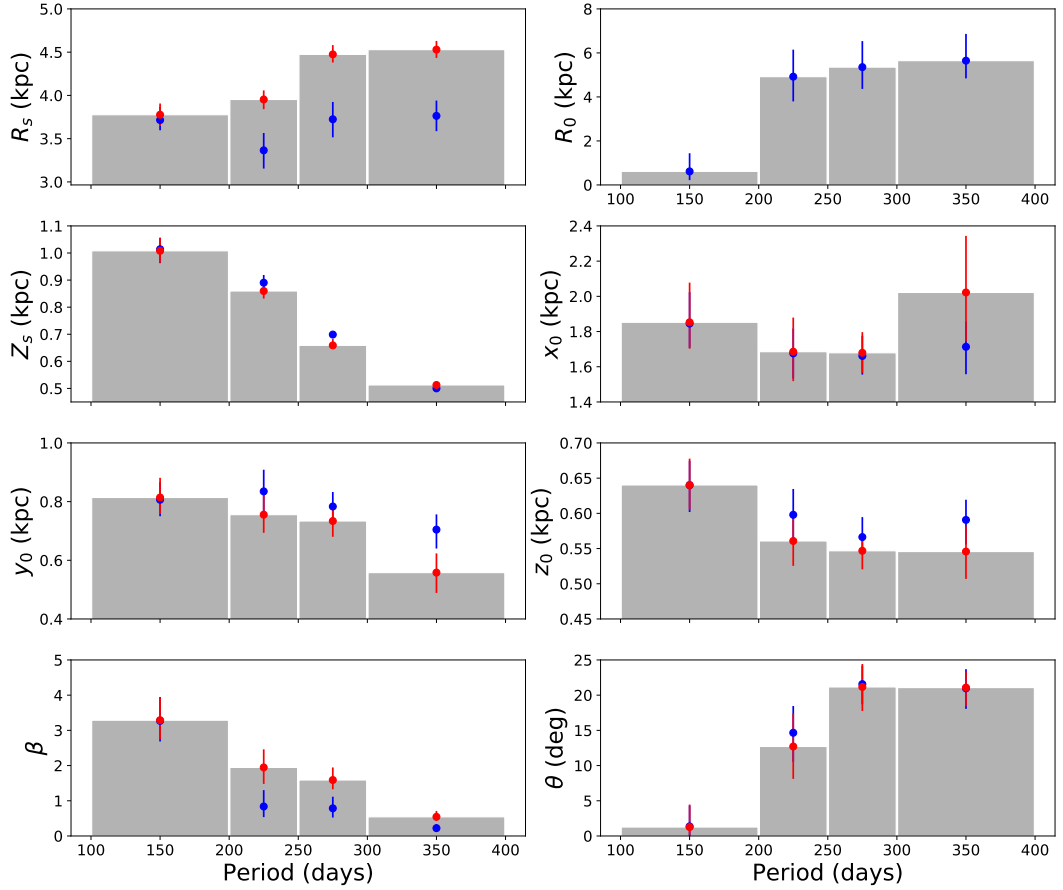


Figure 3.8: We show the evolution of recovered model parameters as a function of Mira pulsation period. Red scatter points correspond to the values given in Table 3.2, being the parameters of our main model, M1. The parameters show strong evolution as the older Miras make up a more radially concentrated and thicker disc, evolving toward a thinner and more extensive disc for younger stars. The bulge/bar length is consistent with being constant across all bins, but appears to narrow, becoming thinner for the youngest of Miras. The bar angle shows strong progression from being very nearly aligned with the Solar line of view at old ages up to $\theta \sim 21^\circ$ for the younger Miras. Blue scatter points correspond to our softened exponential disc M2, and largely show the same distribution as those of M1. This differs in the case of the radial scale length of the disc, for which we see a largely constant value across all period bins. This is compounded with the progression of the R_0 parameter evolving from near zero to 5 – 6 kpc. The grey bars indicate the width of each period bin with the scatter points located at the central value.

a smooth evolution of the disc’s stellar profile complements the findings of Bovy et al. (2012), who show there is a continuous change of the disc scale parameters as a function of stellar position in the $[\alpha/\text{Fe}]$ versus $[\text{Fe}/\text{H}]$ plane. As discussed in Chapter 1, Hayden et al. (2015) mapped out the stellar distribution in the $[\alpha/\text{Fe}]$ versus $[\text{Fe}/\text{H}]$ abundance space across the Galaxy, spanning a radial range of 3 – 15 kpc in the plane and up to 2 kpc vertically away from the plane. They observed a progression in which α -rich stars dominate in the inner disc

at large heights but α -poor stars dominate further out and closer to the disc plane. This behaviour was explained by Minchev et al. (2015) as the effect of disc flaring in mono-age stellar populations, observed in simulations wherein the discs form inside-out. Such a scenario also predicts a strong age gradient in the thick disc as seen by Martig et al. (2016b) and Grady, Belokurov, and Evans (2019). This is consistent with the distribution of our disc parameters. We may physically interpret our results to demonstrate the changing morphology of the Galactic disc as a function of chemistry and stellar age, given that the pulsation period of Miras acts as a proxy for both. The older, metal poor stellar population resides in a stubby disc; it is radially restricted but bloated high above the disc plane. As the age of the stellar population decreases and becomes metal enhanced, the stars reside closer to the Galactic plane but stretch out radially. This is a clear signal of inside-out, upside-down formation of the Milky Way disc over a stellar age spanning $\sim 5 - 10$ Gyr. The study of Milky Way-like galaxies in the Eris simulations catalogue by Bird et al. (2013) found the oldest of stellar populations to reside in centrally concentrated, puffy configurations with younger cohorts continuously populating radially more extended and vertically thinner discs. Tracing the star formation history of these sub-populations backward, they saw the older stars to have formed during active merging phases in the galaxy's history, dynamically heating the stellar orbits. The larger scale heights of the older stars were seen to be largely inherited from the turbulence associated with the early star-forming disc, imprinted by the high supernova feedback rate and larger rate of dynamical heating by mergers and halo substructure. Younger stars are born out of cooler, more rotationally supported gas at calmer periods in the galaxy's lifetime, and the disc grows radially. Further, the evolution of disc structure we infer for the MW is very similar to that seen by Buck et al. (2019) in their recent study of MW like galaxies from the suite of NIHAO-UHD simulations. They observe the disc scale length to increase and disc scale height to decrease for progressively younger stellar populations residing in the disc, as in Fig. 3.8 of this work.

Looking at the Galactic (X, Y) residuals of our model M1 in Fig. 3.9, we see there exists a strong ring like over-density amongst the youngest of the Miras (P4). The ring coincides approximately with the Solar radius and stretches out to $Y \sim \pm 10$ kpc, being more prominent away from the direction of Galactic rotation (i.e negative Y). Galactic rings are a well known phenomenon observed in many external galaxies largely thought to be formed through secular evolutionary processes within the galaxy. In barred galaxies, the bar itself can drive gas radially until it is halted at a resonance. In the case of outer rings, this

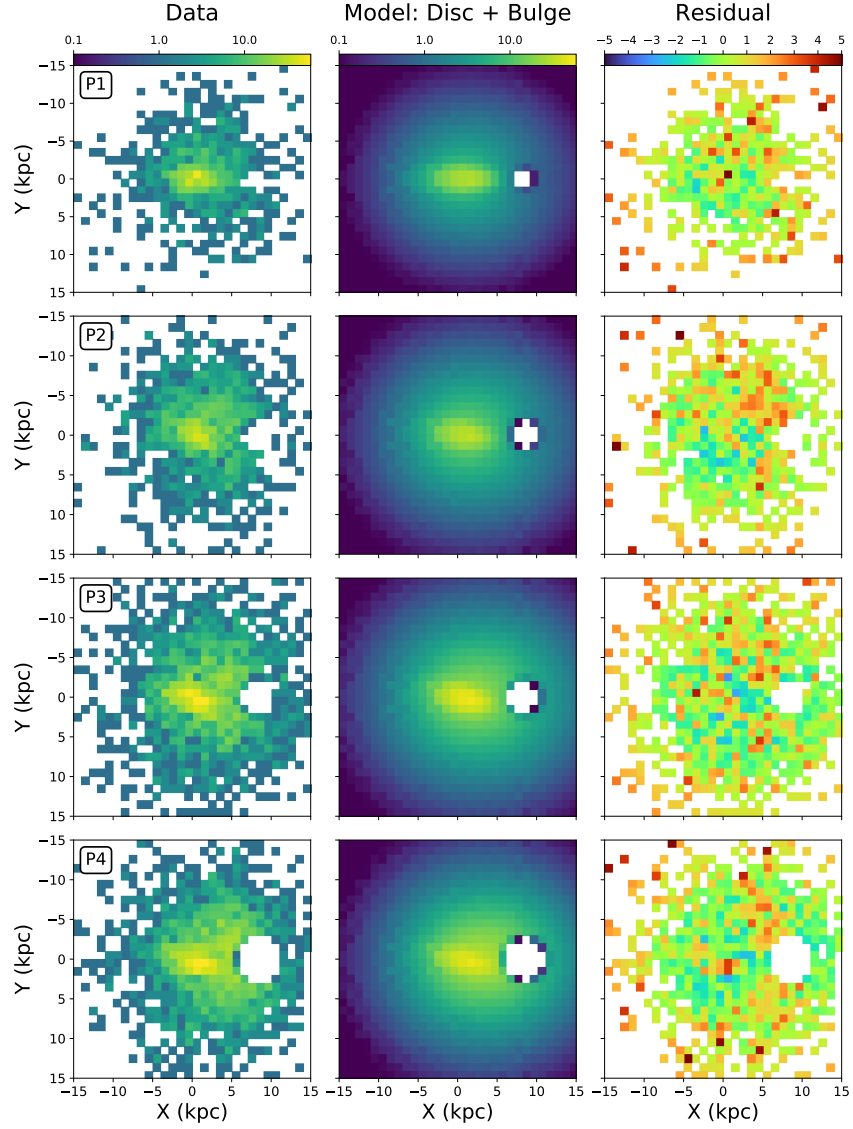


Figure 3.9: Comparison of our Mira sample modelled in each period bin with our recovered model from the MCMC fit in Galactocentric (X, Y) projection. The Solar position is at $(8.3, 0)$ with the Y axis aligned with the direction of Galactic rotation. Top to bottom panels run in order of low period to high period corresponding to stellar ages beyond 10 Gyr down to ~ 5 Gyr. The data column shows the logarithmic number density of the Miras and the model columns show the corresponding predicted number density based on the parameters in Table 3.2. The residuals are computed as the difference in data count and model count, weighted by the Poisson noise in each model.

occurs at the Outer Lindblad Resonance (OLR), with subsequent star formation yielding a stellar ring. For an approximately flat Galactic rotation curve, the OLR should reside at $R_{\text{OLR}} \sim 1.7 R_{\text{CR}}$ (Dehnen, 2000) where R_{CR} is the co-rotation radius. This is believed to lie in the range of $\sim 3 - 6$ kpc (see e.g. Gerhard, 2011), with a recent value of 5.7 ± 0.4 kpc obtained by Sanders, Smith, and Evans (2019) using

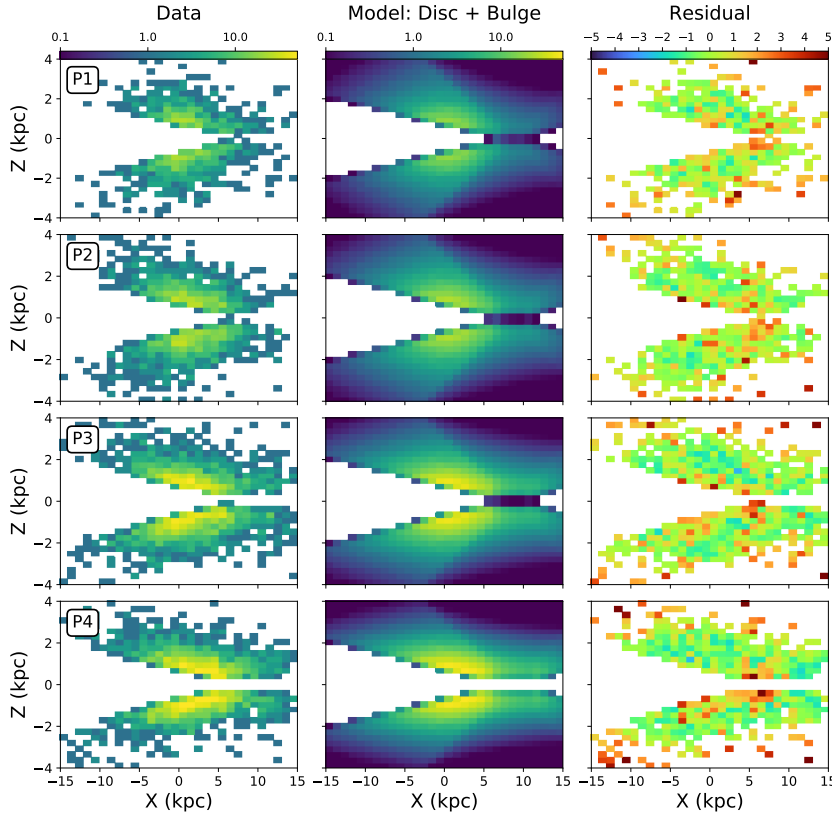


Figure 3.10: *Top*: Galactocentric $X - Z$ projections of our low period Mira sample. From left to right we show the recovered model from our fit, the data number density and the residuals scaled by the Poisson noise in each model pixel. The middle and bottom rows show the equivalent for the intermediate and high period Mira populations respectively.

a combined *Gaia* DR2 + VVV data set. Thus, the OLR is expected to reside somewhere between 6 kpc and 10 kpc, in the immediate neighbourhood of the Solar position. Given that the ring-like residual seen in the P4 Miras coincides with this radial range, it is plausible for it to be associated with trapping of stellar orbits around the OLR. Further, it can be gleaned from Figs. 3.10 and 3.11 that there are Miras lying beyond 2 kpc from the disc, manifesting as the fluffy residuals at these heights. We further see a long spur-like structure, constituted of Miras with periods in the range 200 – 250 days, in the (Y, Z) projection of Fig. 3.11. Its extent is large, stretching out to $Y \sim -5$ kpc and ~ 3 kpc below the plane of the disc. With the ever increasing wealth of stellar information provided by modern surveys, it is becoming evident that the Milky Way disc is not in dynamical equilibrium but displays various signatures of recent perturbations. A wave-like north-south asymmetry of stellar counts was observed by Widrow et al. (2012), who suggest an externally driven vertical perturbation may be the cause for such disc heating. With the advent of *Gaia* DR2, clear evidence of vertical phase space mixing was seen by Antoja et al. (2018)

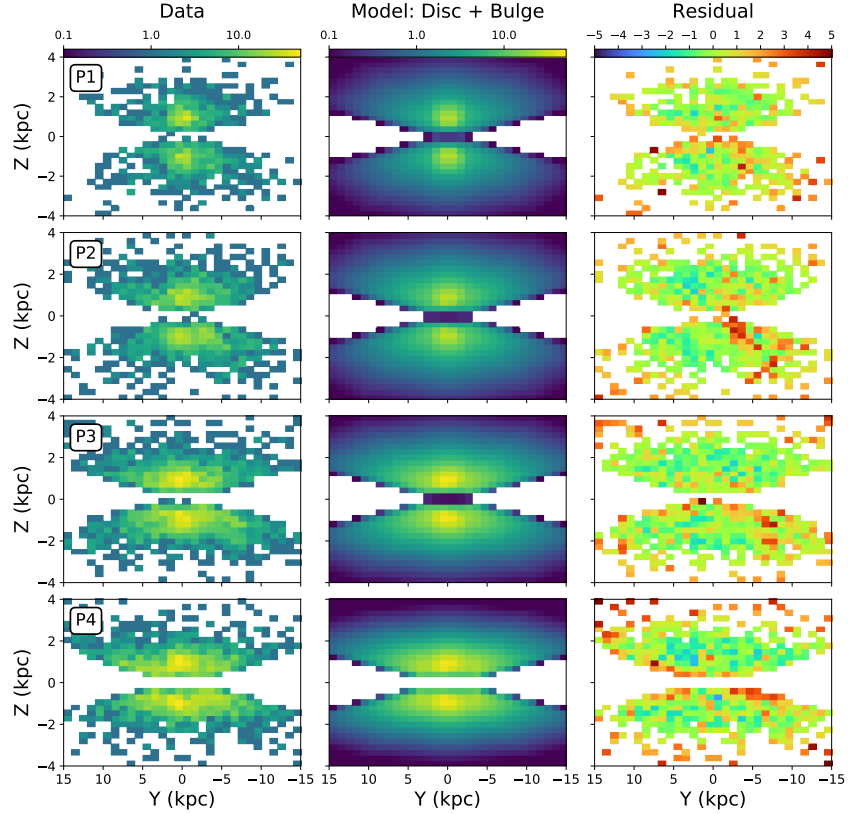


Figure 3.11: *Top*: Galactocentric (Y, Z) projections of our low period Mira sample. From left to right we show the recovered model from our fit, the data number density and the residuals scaled by the Poisson noise in each model pixel. The middle and bottom rows show the equivalent for the intermediate and high period Mira populations respectively.

within the Solar neighbourhood. The perpetrator of such a signature is still debated, with possibilities being a Sagittarius-like object plunging through the disc (see e.g. Binney and Schönrich, 2018; Laporte et al., 2019; Li and Shen, 2019) or even vertical oscillations induced by the buckling of the bar (see e.g. Khoperskov et al., 2019). Such heating events inevitably kick stars out of the disc to large heights and indeed stellar debris as high as ~ 10 kpc may have originated in the disc (Price-Whelan et al., 2015; Xu et al., 2015). As the Miras represent a thick disc stellar population, and thus in-plane perturbations due to spiral arms and giant molecular clouds etc are likely ineffective, it is reasonable to interpret the origin of the high lying Miras as that of external disc heating, kicking the stars to such heights. For our softened exponential model (M2), the general evolution of the parameters is equivalent, except in the case of the radial scale length which is consistent with being constant at all periods. The softening parameter R_0 shows a strong jump from near zero in P1, consistent with a simple double exponential disc, to $\sim 5 - 6$ kpc at higher periods. The interpretation for this is not clear and it may simply be that the soft-

ened model is acting to smooth out the stellar radial distribution at these periods. For consistency, we show the Galactocentric residuals of this model in the Appendix, but there is little difference to those of M1.

We note the presence of a model over-density at $(X, Y) \sim (-5, 4)$ kpc in our P2 residual panels. This likely stems from combined effects of the *Gaia* scanning law and sparse light curve sampling, inhibiting period recovery at periods of ~ 200 days (see Mowlavi et al., 2018). Checking the spatial distribution for each of our period bins, as in Fig. 3.1, we indeed see regions of low detection efficiency in P2, but largely at latitudes less than 5° , a region not included in our modelling.

3.3.2 *Miras in the Bulge*

Turning our attention to the bulge, we observe several interesting features in our recovered parameters of M1. Across all period bins, the bulge/bar length shows no clear evolution within the error, with a value of $\alpha_0 \sim 1.7 - 1.9$ kpc observed. Further, as the stellar age of

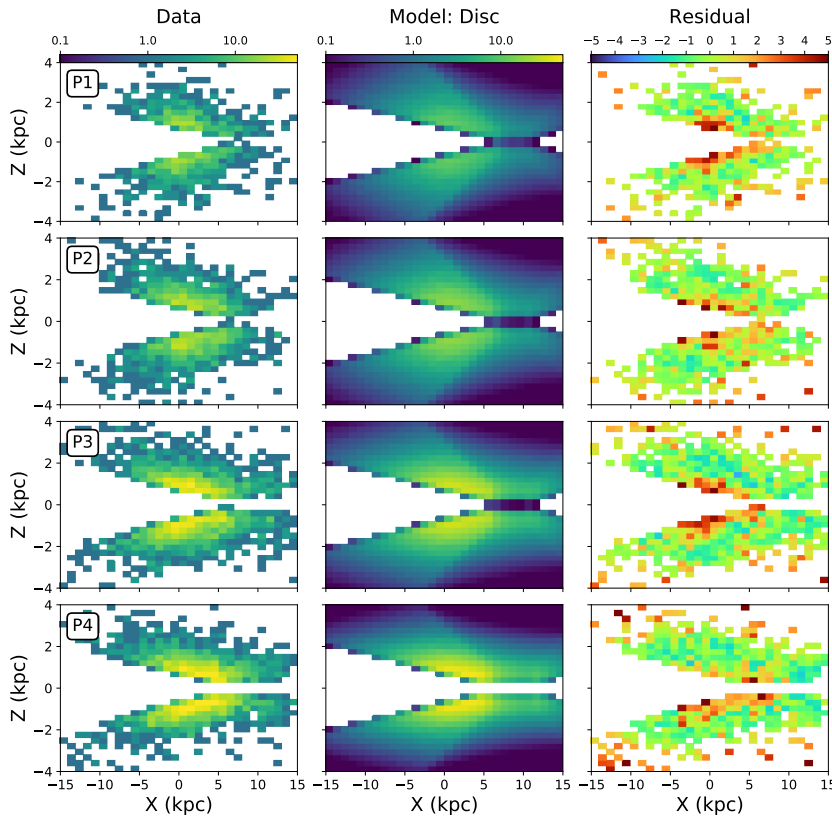


Figure 3.12: Equivalent to Fig. 3.10 but we now only show the exponential disc in our model. In doing so, we highlight the presence of the bulge Miras, made apparent by the strong central residuals in the right hand column.

the bulge decreases (on increasing period), it appears to become narrower and thinner. Based on the simulations of Debattista et al. (2017), this is an expected trend, one that they label ‘kinematic fractionation’. They show that through both purely N-body and high resolution, gas dynamical simulations, the resultant bulge morphology correlates strongly with the age of the stellar population in question, seeded by their initial in-plane random motions. The older, hotter stellar populations form a vertically thicker boxy bulge and the younger, cooler stars result in a thinner, peanut-like bulge (see Fig. 15 of Debattista et al. (2017)). This change in bulge morphology is true for the Miras. The bulge residuals when we model only for the disc in Fig. 3.12 and Fig. 3.13 clearly show the oldest Miras to extend vertically higher (i.e. thicker) than the younger Miras and our recovered model parameters in Fig. 3.8 clearly show the trend of decreasing width (i.e. become narrower) on increasing period. We note that whilst from Fig. 3.4 it appears that the bulge/bar length grows for the highest two period bins, our modelling is limited to $|b| > 5^\circ$ and so we are insensitive to this in plane bulge growth. Our latitudinal mask also inhibits the vertical extent over which we model the data (e.g. see Fig. 3.12) and this may be a reason why we do not observe a continuous decline in the bulge scale height.

For the oldest Miras, the scale length ratios of the bulge/bar are $[1 : 0.44 : 0.35]$ in the order of $[x_0 : y_0 : z_0]$. For the two intermediate populations, we obtain $[1 : 0.45 : 0.33]$ and $[1 : 0.43 : 0.33]$ with the youngest of Miras showing $[1 : 0.28 : 0.27]$. These values are comparable to the three dimensional structure of the Galactic bulge found by Pietrukowicz et al. (2015) in their study of OGLE-IV RR Lyrae, as well as the that of the RC bulge stars studied by Bissantz and Gerhard (2002) and Rattenbury et al. (2007). We find the elongation of the bar to be slightly less than that found by Wegg and Gerhard (2013), who utilised RC stars in the VVV survey to derive axis ratios of $[1 : 0.63 : 0.26]$ (see Zoccali, 2019, for discussion). This discrepancy may stem from the fact that they probe the bar region to lower latitudes ($|b| < 5^\circ$) than accessible to us here, though the extensive modelling efforts of VVV RC stars by Simion et al. (2017) yielded a best fitting bulge axis ratio of $[1 : 0.44 : 0.31]$. Further, Wegg, Gerhard, and Portail (2015) analysed a sample of RC stars residing outside of the bulge, highlighting the existence of a vertically ‘thin’ and ‘super-thin’ component associated with increasingly younger stellar populations, down to ~ 1 Gyr. They also see a smooth transition between the boxy bulge and long bar through the continuous decline in the scale heights of their fits. This is corroborated by Cabrera-Lavers et al. (2008, 2007) who find two triaxial structures residing in the inner

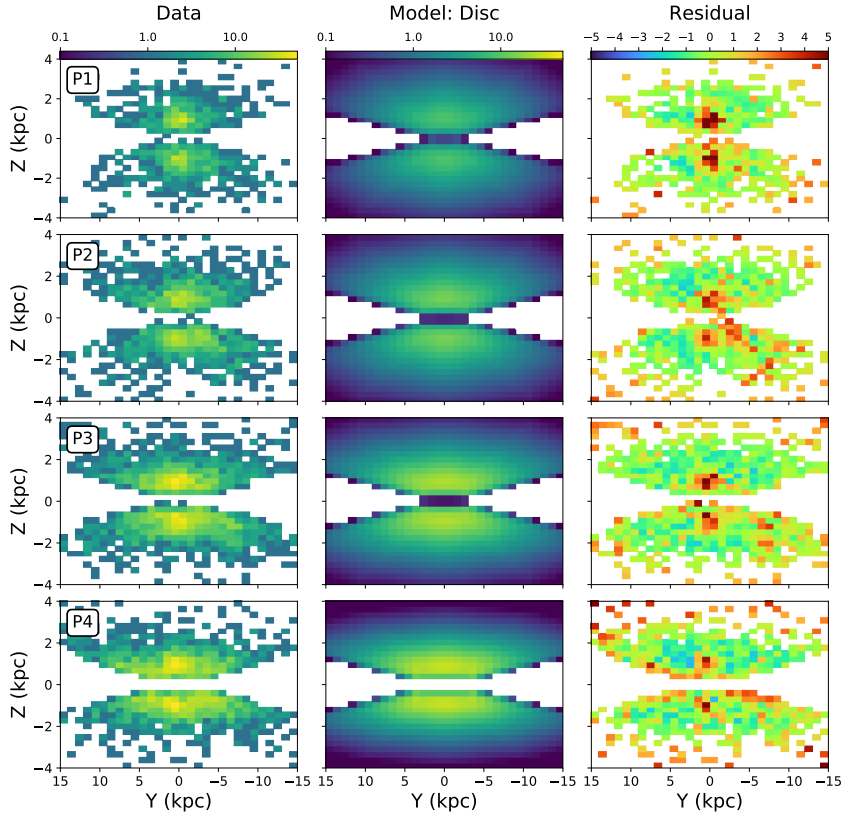


Figure 3.13: Again we only show the exponential disc in our model, highlighting the apparent decreasing vertical extent of the bulge Miras on increasing period.

galaxy: a thick BP bulge and a thinner long stellar bar. The claim of a long bar is not novel with Amôres et al. (2013), González-Fernández et al. (2012), Hammersley et al. (2000), and López-Corredoira et al. (2007) all finding such a structure, located at a position angle of $\sim 40^\circ - 45^\circ$, significantly offset from that typical of the main bar, inspiring the notion of two separate bulge/bar structures within the galaxy. However, the simulations of Martínez-Valpuesta and Gerhard (2011) and Romero-Gómez et al. (2011) imply that such an offset may be a result of volume projection effects in the stellar counts and possible asymmetries at the end of the bar, which develop leading ends induced by interactions with adjacent spiral arm heads. Such an effect appears to have been observed in Sloan Digital Sky Survey (SDSS) imaging of the galaxy MCG+07-28-064 where Peterken et al. (2019) observe a change in the bar angle at the youngest of stellar ages. They interpret this to be an effect of star formation occurring on the leading edge of the bar, wherein the young stars have not had ample time to fully mix in their orbits through the bar potential. It would therefore seem a single central structure may suffice; a central boxy bulge extending to a longer, thinner in-plane bar which can couple to the spiral arms yielding non-symmetric bar ends. In this context,

the evolution of the dimensions of our Mira populated bulge are consistent with known trends of the bulge/bar system in that the width and height of the structure decreases on decreasing stellar age, as observed by Wegg, Gerhard, and Portail (2015) and in the extensive simulations of Debattista et al. (2017). We note that, whilst less pronounced, the results of M2 are also consistent with this evolutionary picture of bulge/bar structure.

However, it is striking that the orientation of the bulge Miras evolves on increasing period; the oldest Miras orient themselves along our line of sight and the younger Miras reach an inclination angle of $\theta \sim 21^\circ$ as seen in Fig. 3.8. The OGLE-III bulge RR Lyrae studied by Dékány et al. (2013) using VVV photometry revealed a slightly elongated stellar structure, with an inclination angle of $\sim 12.5^\circ$ amongst a more spheroidal population. Further, the bulge OGLE-IV RR Lyrae sample studied by Pietrukowicz et al. (2015) resulted in an inclination angle of $\sim 20^\circ$. Previous analysis of bulge RC stars (see e.g. Babusi-*aux* and Gilmore, 2005; Bissantz and Gerhard, 2002; Rattenbury et al., 2007; Simion et al., 2017; Wegg and Gerhard, 2013) have constrained the angle of the bulge/bar to lie in the range of $\sim 20^\circ - 30^\circ$. Recent modelling of the bulge by Coleman et al. (2019) determines the bar angle to lie in the range $18^\circ - 32^\circ$ through both parametric and non-parametric modelling of VVV RC bulge stars. The two youngest Mira populations (P3 and P4) in our study are consistent with these findings and bear ages of $\sim 5 - 9$ Gyr. From Fig. 3.14, the presence of a central bulge/bar-like feature is evident at all periods from the large residuals in the centre of the galaxy when we fit only for an exponential disc. Curiously, these residuals are clearly very nearly aligned with our line of sight towards the Galactic centre for the lowest period population. Our best fit parameters for these old Miras do not suggest they are the most spheroidal of our sample, as we may expect for the oldest population. The extent of the residuals in the (X, Z) and (Y, Z) planes in Figs. 3.12 and 3.13 affirm this, with their vertical extent constrained below 2 kpc from the plane but reaching out to ~ 2.5 kpc along the Galactocentric X coordinate. An evolution of bar inclination angle with Mira pulsation period has been observed by Catchpole et al. (2016) who observe distinct bulge/bar structures occupied by the oldest and youngest of Miras in their sample. The ancient Miras show no apparent inclined structure, whereas the younger Miras form a tilted bar-like structure. This change of orientation is consistent with the difference we see between our shortest period bin and the longer period Miras. This too was observed by Debattista et al. (2017), who found that the oldest stars in their simulations showed very weak coupling to the inclined bulge/bar structure, as well as by

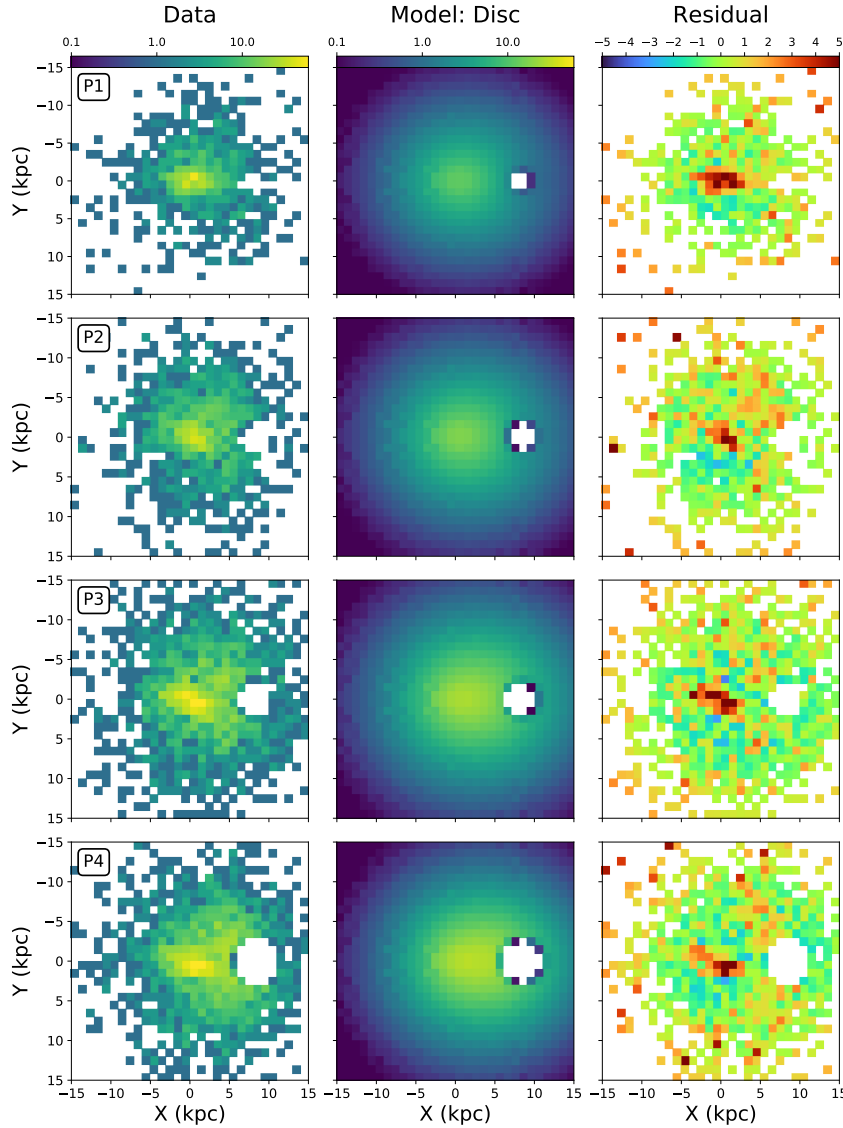


Figure 3.14: Equivalent to Fig. 3.9 but here we only show the exponential disc component of our model. On illuminating the bulge Miras, a curious evolution of bulge orientation is observed on increasing Mira period.

Dékány et al. (2013) in their bulge sample of RR Lyrae. This has been corroborated by Prudil et al. (2019) in their recent analysis of OGLE-IV RR Lyrae finding no evidence of a bar association. For the stars in P2, we find an inclination of $\sim 13^\circ$, comparable to that of the very central RR Lyrae distribution of Dékány et al. (2013). However, from Fig. 3.14, it is unclear how strong a bulge signal exists in this period bin. The bulge-like residual in the disc only fit is weak and confined only to the very central region. Thus our model may be suffering from the sparseness of the data in this narrow period range when fitting for the bulge/bar parameters, given our latitude restrictions. Alternatively, this period bin may be including Miras from two separate

bulge populations, one inclined at $\sim 21^\circ$ and another not, resulting in an intermediate bulge/bar angle. Aside from the uncertainty in this period range, the evolution of the bar angle from the oldest of Miras to the youngest is clear from the data where the ancient Miras look to be decoupled from the inclined boxy bulge/bar. It is possible therefore that these Miras are old enough to have been born before the formation of the bar and its subsequent buckling. If they were kinematically hot enough, it is possible they did not efficiently couple to the early bar thus maintaining their distinct structure. The prominent elongation of this structure may be a consequence of our imposed latitude cut or an observational bias due to potential incomplete latitudinal sampling of Miras in the *Gaia*+2MASS cross-match.

It has been predicted from both N-body and star forming simulations that upon observing younger/metal-richer bulge populations, their morphology should tend toward that of a peanut shape with a stronger X-shape signature compared to the older/metal poorer bulge stars (see e.g. Buck et al., 2018; Debattista et al., 2017; Fragkoudi et al., 2018). Indeed, observations have shown this to be the case with the older, metal poor stars being centrally concentrated and axisymmetric in their spatial distribution. The young and metal rich stars are consistent with belonging to a BP shaped bulge bearing the X-shape signature characteristic of such a structure inclined to the line of sight (see e.g. Rojas-Arriagada et al., 2014; Williams et al., 2016; Zoccali et al., 2017). Accordingly, we seek to find such a contrast in bulge spatial distribution in our Mira sample. Selecting only the oldest and youngest period bins of our sample, we show their density distribution in Fig. 3.15. On computing the residuals between these period bins, we can identify the regions in which the two sub-populations dominate the overall stellar density. Indeed, we see the old/metal poor Miras to lie centrally and extend vertically along the bulge/bar minor axis, whilst the young/metal rich Miras show four peaks in density, distributed asymmetrically about the Galactic centre. We interpret this as evidence that the young Miras lie in a BP configuration with a viewing angle of $\sim 21^\circ$ yielding the apparent X-shape. Our Galactic latitude mask at $|b| < 5^\circ$ inhibits us from making a direct comparison to our smooth bulge/bar model, as this signal exists primarily at low latitudes in a region of low stellar density. Regardless, the signal we recover is in excellent agreement with the predicted stellar age distribution of Debattista et al. (2017) (see their Fig. 22) and is reminiscent of the general X-shape morphology uncovered by Ness and Lang (2016).

Finally, we note that there has been long discussion of long period bulge Miras in the context of the apparent dearth of young stars seen

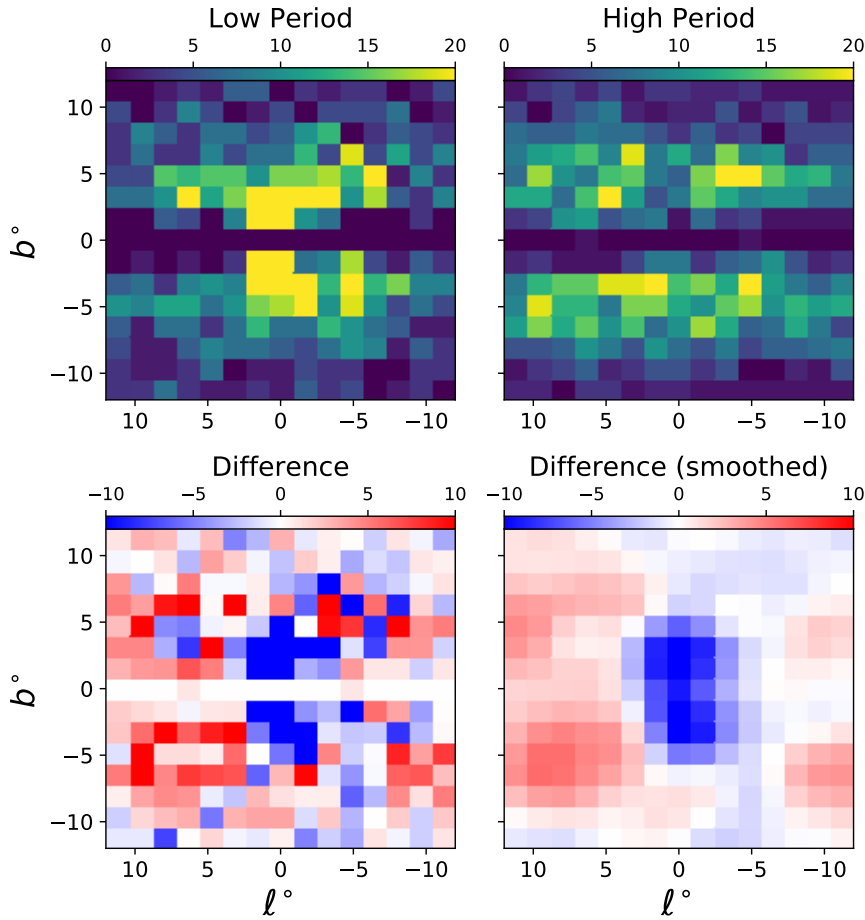


Figure 3.15: We show the distribution of the longest and shortest period Miras in our sample for the inner $12^\circ \times 12^\circ$ of the Galaxy in the top panels. The upper-left panel corresponds to the low period Miras and the upper-right to the long period Miras. We further restrict ourselves to stars within a Galactocentric cylindrical radius less than 5 kpc to reduce foreground contamination. Normalising the stellar number density across the two period bins, we compute the residual between the two. We smooth the image by applying a Gaussian filter of width 1.6° over the residual. This is displayed in the bottom-most panels. Red overdensities correspond to regions dominated by the long period (young/metal rich) Miras and blue those by the old (old/metal poor). The ancient Miras peak centrally, on the minor axis. Away from this region, the young Miras dominate in two fields either side of the Galactic centre, with greater vertical extent on the near side of the bulge. This is indicative of the younger Miras constituting an peanut-shaped bulge inclined to our line of sight.

to reside in the central region of the Galaxy (see e.g. Valenti et al., 2013; Zoccali et al., 2003). Both Renzini et al. (2018) and Clarkson et al. (2011) have set a limit on bulge stars younger than ~ 5 Gyr, coincident with our lower age limit. Miras covering a wide range of periods residing in the bulge/bar have been studied by Whitelock, Feast, and Catchpole (1991) who consider the possibility that the long period Mi-

ras are in fact the progeny of binary mergers rather than a distinctly young population, a notion put forth by Renzini and Greggio (1990). However, the majority of their Mira sample bear periods in excess of 400 days, a regime beyond our sample. Further, a likely candidate for such a process is that of the C-rich Mira discussed in Feast, Menzies, and Whitelock (2013) with a period of 551 days. Thus, we believe such effects are not at play in the age estimation of our longest period Miras.

3.4 SUMMARY

We take advantage of the, to date, underutilised sample of Miras provided by *Gaia* DR2. Selecting O-rich Miras based on their distinct infrared colour and considerable photometric amplitude of variability, we map the Mira population through the Galactic disc and into the bulge. We exploit the correlation between Mira pulsation period with stellar age/chemistry to date our Mira sample and slice the Galaxy chronologically. Spanning ages of $\sim 5 - 10$ Gyr, we can observe how the structure of the disc and bulge/bar has evolved over the Milky Way's lifetime.

We find the old, metal poor disc to be stubby; its vertical extent is large and is constricted radially. On increasing period, the disc settles into a thinner and radially more extensive formation. Modelling the disc as a simple double exponential, we see a progression in scale length from ~ 3.8 kpc to ~ 4.5 kpc for periods ranging from 100 to 400 days. Similarly, the vertical scale height of the disc plummets from ~ 1.0 kpc at low periods to ~ 0.5 kpc for our longer period Miras. This is entirely complementary to the findings of Bovy et al. (2012) who studied the stellar disc profile as a function of chemical abundance using a large sample of G-type dwarfs from the SDSS-SEGUE survey. They find the scale height of the disc to ascend from ~ 200 pc to ~ 1 kpc on increasing stellar age, as indicated by their metallicity and $[\alpha/\text{Fe}]$ abundance. The radial scale length of the disc decreases from > 4.5 kpc down to ~ 2 kpc also on increasing stellar age. The structure we see in the disc could be understood in terms of the early Galaxy being turbulent and dynamically active, heating the early star forming disc. As the Galaxy became more quiescent, the younger stellar populations were born out of progressively cooler and more rotationally supported gas, thinning and extending the stellar disc (see e.g. Bird et al., 2013; Bournaud, Elmegreen, and Martig, 2009).

Within the disc, we see evidence of disruption and heating. A large ring-like structure is observed in the youngest of disc Miras, coincident with the expected location of the Outer Lindblad Resonance and

indicative of secular evolutionary processes, mixing and restructuring the disc. Miras are observed to lie scattered from the plane, extending up to beyond 3 kpc likely due to vertical perturbations induced in the disc over their lifetime.

In the central regions of the Galaxy, we find the younger/metal-richer Miras to clearly inhabit an inclined bar-like structure. Fitting a boxy-bulge model to these Miras yields a viewing angle of $\sim 21^\circ$. The ancient Miras show little evidence for inclination, suggestive that they are a spatially distinct component from the bulge/bar. This is in accord with the findings of Dékány et al. (2013) who see the bulge RR Lyrae to lie detached from the bar with little evidence for an inclined population. Satisfyingly, the age of our eldest Miras are comparable to those of RR Lyrae at $\sim 9 - 10$ Gyr. This distinction is also seen in the simulations of Debattista et al. (2017) in which the disc is seeded by co-spatial populations of stars with differing velocity dispersion profiles. Bar formation occurs after ~ 2 Gyr, subsequently buckling into a bulge where the older, hotter stars form a boxy shape and the younger, cooler stars more easily trapped into X-shape orbits. When they studied the morphology of their oldest bulge stars, > 9.5 Gyr, they saw them to be decoupled from the bar structure. Thus, it is reasonable to interpret the RR Lyrae distribution of Dékány et al. (2013) and our ancient Miras to represent those stars that were born prior to bar formation, and were kinematically hot enough to avoid entrapment by the bar potential. Given that the lowest period bin to demonstrate a bulge/bar structure occurs at 250 – 300 days, we postulate that the bar must have buckled by $\sim 8 - 9$ Gyr ago, given the period age relations of Wyatt and Cahn (1983) and Feast (2009).

We find a bulge/bar half-length of $\sim 1.7 - 2$ kpc from our Miras, with an indication that the bulge/bar width and height decreases on stellar age. For the two period bins that clearly show the Miras to be bar-like, we see tentative evidence for an increase in the bar length. This is consistent with the trends seen by Wegg, Gerhard, and Portail (2015), who see the bar extending beyond the bulge to become longer and thinner for younger Red Clump stellar populations. Again our results are consistent with the findings of Debattista et al. (2017) who see the younger stars to constitute a narrower and thinner bulge/bar.

When comparing the spatial distributions of the oldest and youngest Miras in the inner Galaxy we see a clear distinction between the two. The old/metal-poor Miras dominate centrally, whilst the young/metal-rich Miras exhibit a boxy-peanut like morphology with a characteristic X-shape. This is consistent with the notion of ‘kinematic fractionation’ posited by Debattista et al. (2017) wherein the younger, initially

cooler stars couple more strongly to the buckling bar, exhibiting a more pronounced peanut-shape than the older stars.

By making use of the *Gaia* DR2 LPV data set, we have shown it is possible to cleanly select a large sample of O-rich Miras and assign them accurate distances. Owing to their impressive brightness in the near infrared regime, we are able to trace the Miras right across the disc and through the bulge. Seizing on the correlation between their pulsation period and stellar age/chemistry, we can, for the first time, chronologically slice through the Galactic disc and bulge at once. The Miras are not the only variable star to be utilised in mapping out the Milky Way. Cepheid variables and RR Lyrae have long been used to do so but the Miras are not limited to a single age bracket nor do they primarily trace a single structure as the Cepheids do in the spiral arms. Many studies have made excellent use of the vast Red Clump giant populations but these too lack the ability to act as chronometers in tracing the bulge/bar structure. Looking further afield, many Miras have already been resolved in M31 (see e.g. An et al., 2004), so it seems their ability to chronologically dissect a galaxy is not limited to the Milky Way.

MAGELLANIC MAYHEM: METALLICITIES AND MOTIONS

This chapter is based on work originally published in Grady, Belokurov, and Evans (2021).¹

We assemble a catalogue of Magellanic Cloud red giants from Data Release 2 of the *Gaia* mission and, utilising machine learning methods, obtain photometric metallicity estimates for them. In doing so, we are able to chemically map the entirety of the Magellanic System at once. Our maps reveal a plethora of substructure within our RG sample, with the LMC bar and spiral arm being readily apparent. We uncover a curious spiral-like feature in the southern portion of the LMC disc, hosting relatively metal-rich giants and likely a by-product of historic encounters with the SMC. Modelling the LMC as an inclined thin disc, we find a shallow metallicity gradient of -0.048 ± 0.001 dex/kpc out to $\sim 12^\circ$ from the centre of the dwarf. We see evidence that the Small Magellanic Cloud is disrupting, with its outer iso-density contours displaying the S-shape symptomatic of tidal stripping. On studying the proper motions of the SMC giants, we observe a population of them being violently dragged towards the larger Cloud. The perturbed stars predominately lie in front of the SMC, and we interpret that they exist as a tidal tail of the dwarf, trailing in its motion and undergoing severe disruption from the LMC. We find the metallicity structure in the Magellanic Bridge region to be complex, with evidence for a composite nature in this stellar population, consisting of both LMC and SMC debris.

4.1 DATA

We make use of the Magellanic RG catalogue compiled by Belokurov and Erkal (2019) from Data Release 2 (Gaia Collaboration et al., 2018d) of the *Gaia* mission (Gaia Collaboration et al., 2016), which holds 1,604,018 stars within 30° of the Clouds. In the top row of Fig. 4.1, we show the stellar density of these giants in two coordinate systems: the Magellanic Stream system (L,B) described by Nidever, Majewski, and Butler Burton (2008) and the Magellanic Bridge system as in Belokurov et al. (2017), both of which will be utilised in this work. A

¹ I note that Figs. 4.1 & 4.21 were created by Vasily Belokurov and appear here as they do in the submitted work.

plethora of substructure is seen in the giants, with the Clouds hosting multiple outer spiral-like arms such as the northern structure identified by Mackey et al. (2016). A complex ensemble of features present in the southern portion of the LMC; the claw like features, associated with "Substructure 1" and "Substructure 2" of Mackey et al. (2018), appear to wrap clockwise around the lower LMC disc. As noted in Belokurov and Erkal (2019), one of the most striking features is the thin stellar stream that appears connected to the SMC, arcing $\sim 90^\circ$ clockwise around the outer LMC. Curiously, hints of this structure may already be seen in the map of the Magellanic Mira built using *Gaia* DR1 data in combination with WISE and 2MASS photometry (Deason et al., 2017). The portion of the LMC disc nearest the SMC is truncated, with the morphology of the smaller dwarf appearing distorted, apparently stretching towards the LMC. The outskirts of the two galaxies are littered with stellar debris, and indeed a population of giants is observed to inhabit regions between the Clouds. In the lower two panels of the figure we show, for comparison, the distribution of RRL in the two coordinate systems, combining both the *Gaia* SOS (Specific Object Study Clementini et al., 2019) catalogue with stars classified as RRL in the general variability table `vari_classifier_result` (Holl et al., 2018). Requiring these RRL to have `phot_bp_rp_excess_factor < 3`, we correct for extinction and assign heliocentric distances as in Iorio and Belokurov (2019). Selecting those RRL whose distances are commensurate with the Clouds, we see in Fig. 4.1 a relatively clean selection can be made. The peripheries of the dwarfs are again scattered with diffuse structures, the LMC disc is truncated towards the SMC and most strikingly of all is the old stellar bridge spanning in the inter-Cloud region. Interestingly, the RR Lyrae distribution follows closely that of the giants, implying that in the LMC, many of these old pulsating stars represent the disc population. This is perhaps best reflected by the sharp disc truncation on the side nearest to the SMC. Both red giants and RR Lyrae show this dramatic near-linear cutoff in the disc density. The evacuated western portion of the LMC's disc emphasises strikingly the old bridge connection between the two Clouds.

We cross-match the Magellanic giant sample the 2MASS (Skrutskie et al., 2006) and WISE (Wright et al., 2010) surveys to build a sample with broad photometric coverage. We only select stars with the 2MASS quality flags `ph_qual = AAA`, `cc_flg = 000`, `gal_contam = 0` and the WISE quality flags `ext_flg \leq 1`, `ph_qual = AAA` to remove potential artefacts and sources with poor photometric measurements. Initially, we correct for extinction using the dust maps of Schlegel, Finkbeiner, and Davis (1998) and the 2MASS and WISE extinction

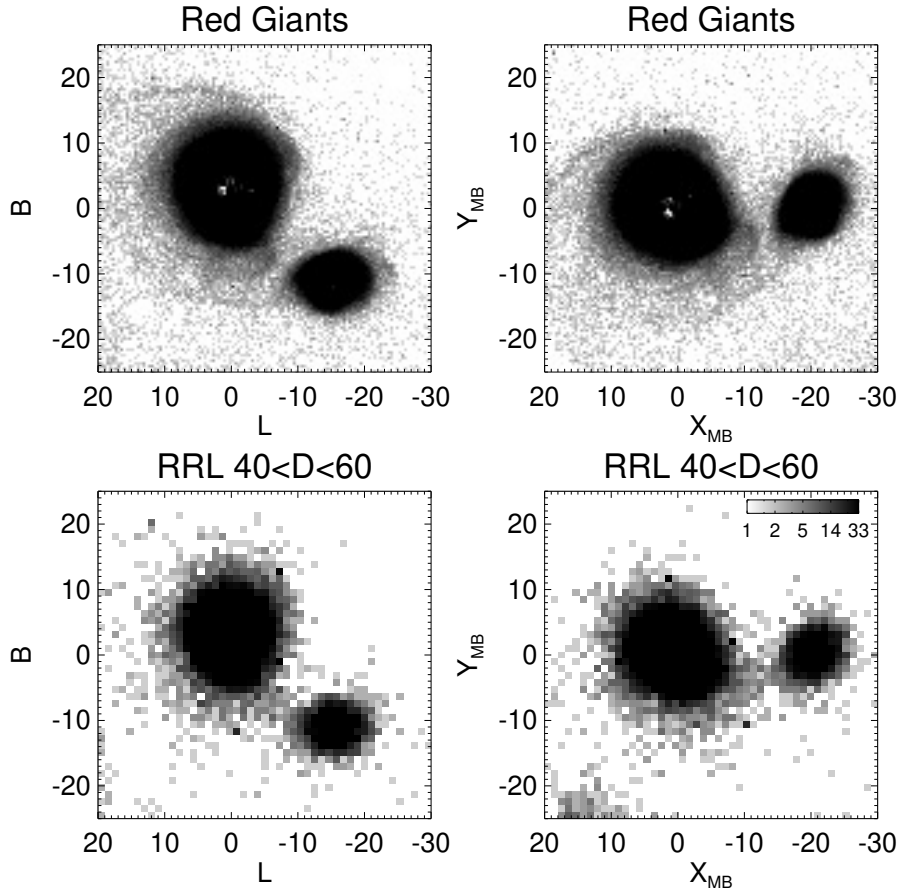


Figure 4.1: The top two panels show the red giant sample of Belokurov and Erkal (2019) shown in both Magellanic Stream and Magellanic Bridge coordinates. A myriad of diffuse stellar substructure can be seen in the outer regions of the system. Most prominent is the northern spiral like feature that was first observed by Mackey et al. (2016), alongside a host of complex thin streams in the southern portions of the outer LMC. The bottom two panels display *Gaia* DR2 RR Lyrae, whose selection we describe in the text. Note that the RR Lyrae distribution follows closely that of the giants, including the sharp cutoff in the disc density on the side of the LMC facing the SMC. With both stellar tracers, the old stellar bridge (Belokurov et al., 2017) is evident as the connecting feature of the two Clouds.

coefficients of Yuan, Liu, and Xiang (2013). For the *Gaia* photometry, we follow the de-reddening procedure of Gaia Collaboration et al. (2018c), using the first two terms in their eqn (1) to do so. The recent red clump calibration of Skowron et al. (2020) has provided reddening maps for the LMC and SMC with good resolution in the central parts of the Clouds, regions where those of Schlegel, Finkbeiner, and Davis (1998) suffer from high levels of dust. Consequently, we utilise these recent maps for the innermost regions of the Clouds ². We then require the giants to obey the relation of $\text{phot_bp_rp_excess_factor} < 1.3 + 0.06 (\text{BP} - \text{RP})^2$ and reject any

² We also applied this procedure to the RRL in Fig. 4.1

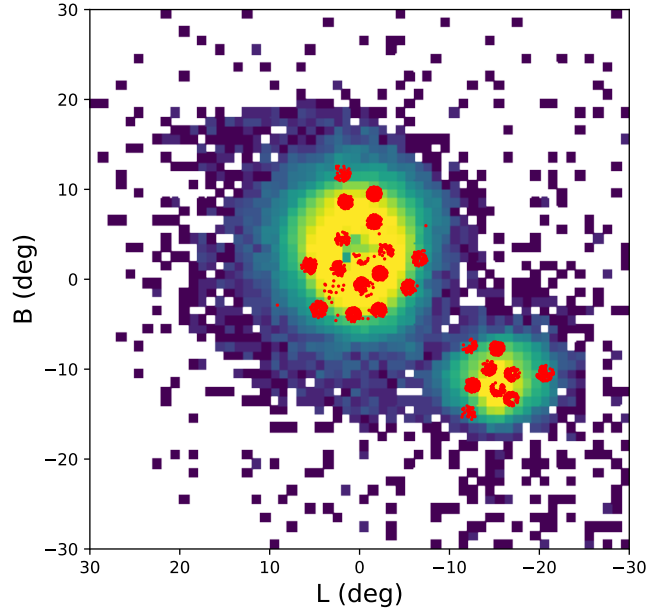


Figure 4.2: Spatial distribution of our giants in Magellanic Stream coordinates. Stars with an APOGEE spectroscopic metallicity measurement are shown in red and provide good coverage of both satellites. These stars will constitute our regression training set to predict the metallicities of all the Magellanic giants in our sample.

stars that now lie outside the CMD selection box of Belokurov and Erkal (2019), after correcting the extinctions in the inner regions, yielding a sample size of 226,119 Magellanic giants.

A subset of our sample are captured by the APOGEE-2 southern hemisphere observations (Majewski, APOGEE Team, and APOGEE-2 Team, 2016; Zasowski et al., 2017), the Magellanic Cloud targets of which provide a relatively unbiased sample of stars spanning a large metallicity range of $[\text{Fe}/\text{H}] = -0.2$ dex down to $[\text{Fe}/\text{H}] = -2.5$ dex (Nidever et al., 2020). This provides us with metallicity values for 3,077 giants. Fig. 4.2 shows the spatial distribution of our giant sample, with red markers indicating those stars with APOGEE measurements. Our full sample spans the entirety of the Magellanic region with the APOGEE stars also exhibiting good spatial coverage of the Clouds in both the radial and azimuthal sense. We will utilise this sub-sample as a training set to build a regression model that can accurately predict the metallicities for our full giant sample. In Fig. 4.3, we show the CMDs of our giants with the extent of the training APOGEE data indicated by the black contours. The WISE and 2MASS CMDs are relatively clean with clearly discernible red giant branches and asymptotic giant branches seen; the marked drop in stellar density at approximately $K_s < 12$ and $W1 < 12$ marks the

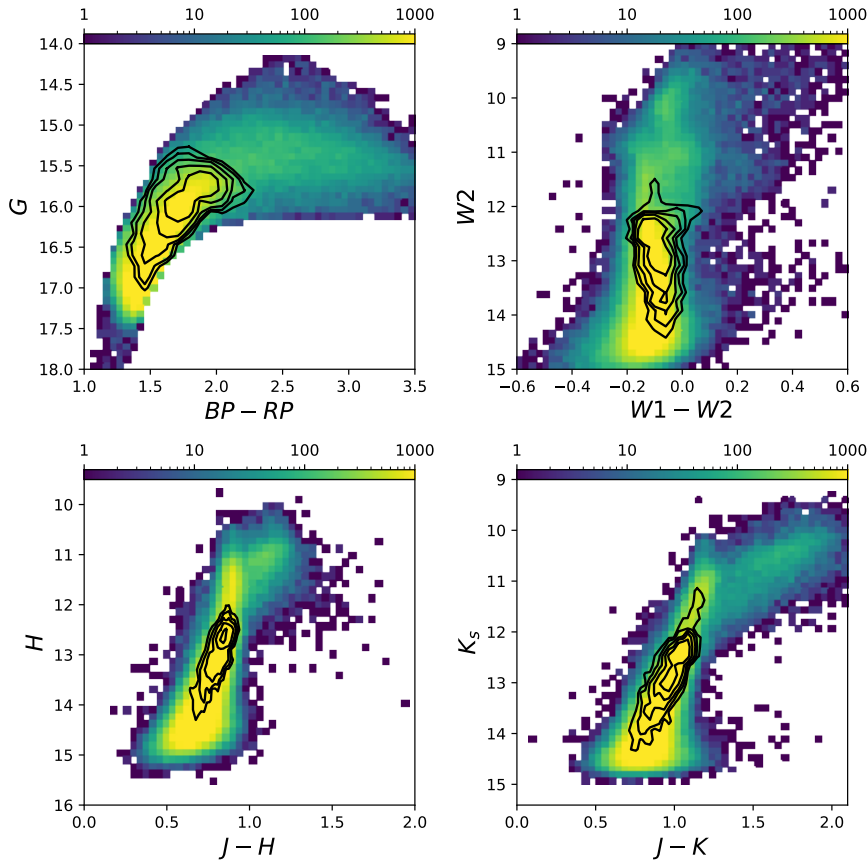


Figure 4.3: CMD diagrams of the full *Gaia*+2MASS+WISE giants for which we will predict metallicities. We see our giant sample encompasses the upper RGB out to the AGB stellar phase. The cleanliness of the *Gaia* CMD is a direct consequence of the methods employed by Belokurov and Erkal (2019) in their giant selection. In the other photometric systems, the CMDs look relatively clean and we overlay black contours spanning the 5th – 50th percentile levels of the APOGEE training sample, with logarithmic spacing. It can be seen that APOGEE generally obtains metallicity estimates for the brighter red giants, with the sample being particularly deficient at blue WISE colours. How this pertains to our regression analysis is discussed later in this work.

transition to the AGB stellar populations of which our sample encompasses both the O-rich and C-rich components of this phase. The stars for which APOGEE measurements exist are largely confined to bright RGs, with a noticeable lack of stars bluer than ~ -0.2 in the WISE colour $W1 - W2$ in comparison to the full sample. The effects that such colour offsets have on our ability to accurately predict metallicities is discussed later in this chapter. APOGEE DR16 has observed $\sim 23,000$ stars in the direction of the MCs, largely comprised of RGB, AGB and foreground dwarf stars (Zasowski et al., 2017). Recently, Nidever et al. (2020) selected Magellanic giants from APOGEE by utilising optical photometry to remove foreground dwarfs, and devised a 2MASS photometric selection to isolate likely Magellanic

giants. The authors acted to ensure there was minimal bias against selecting metal poor giants by employing a wide range in $J - K_s$ selection. We probed our APOGEE sample in relation to that of Nidever et al. (2020) by selecting all APOGEE+*Gaia*+2MASS+WISE stars within 40° of the LMC as a comparison sample. We then applied our photometric cleaning cuts outlined earlier in this section, as well as requiring parallax values to be less than 0.2 and employed a proper motion cut similar to that in Belokurov et al. (2017). We did not implement the CMD selection of Belokurov et al. (2017) but rather selected stars in the $J - K_s$ vs. H Magellanic red giant selection box of Nidever et al. (2020). We then assessed the level of bias that our *Gaia* CMD giant selection incurs against giant metallicity by assessing our sample completeness with respect to this comparison sample. In doing so, we estimate our sample completeness to be $\sim 80 - 90\%$ across our full metallicity range and conclude that no significant bias against any particular metallicity is present in the data we will use to build our regression model.

4.2 REGRESSION ANALYSIS

Through a process of experimentation, we choose a feature vector of $\mathbf{f} = [\text{BP} - \text{RP}, \text{RP} - \text{H}, \text{W1} - \text{W2}, \text{J} - \text{H}, \text{J} - \text{K}_s]$ to utilise in predicting photometric metallicities. The left column of Fig. 4.4 shows the distribution of the APOGEE training set across five CMDs. We assess the photometric correlation with metallicity in the middle column of the figure, where across the feature vector we see clear metallicity gradients in the CMDs, especially so in the WISE photometry owing to its near vertical RGB. Computing the pair-wise correlations between training set features and metallicities yields the correlation vector $[0.33, 0.45, -0.65, 0.46, 0.47]$, where elements are ordered in correspondence with feature vector \mathbf{f} . These correlations are shown explicitly in the rightmost column, where we see the strong correlation of the WISE colour with metallicity. The WISE W2 band covers the CO molecular absorption feature that is strongly dependent on stellar metallicity. Metal-rich giants are bright in the W1 band only whereas metal-poor giants are bright in both W1 and W2. Consequently, stars that are blue in $\text{W1} - \text{W2}$ are in fact metal richer, as seen in Fig. 4.4 (see e.g. Casey et al., 2018; Koposov et al., 2015; Schlafman and Casey, 2014). The *Gaia* features $\text{BP} - \text{RP}$ and $\text{RP} - \text{H}$ are included as both bear strong correlations with effective temperature, which itself affects the photometric colour of stars. We first set aside 30% of our *Gaia*+APOGEE+2MASS+WISE sample as a test set, unseen by the learning algorithm throughout the training process and used for

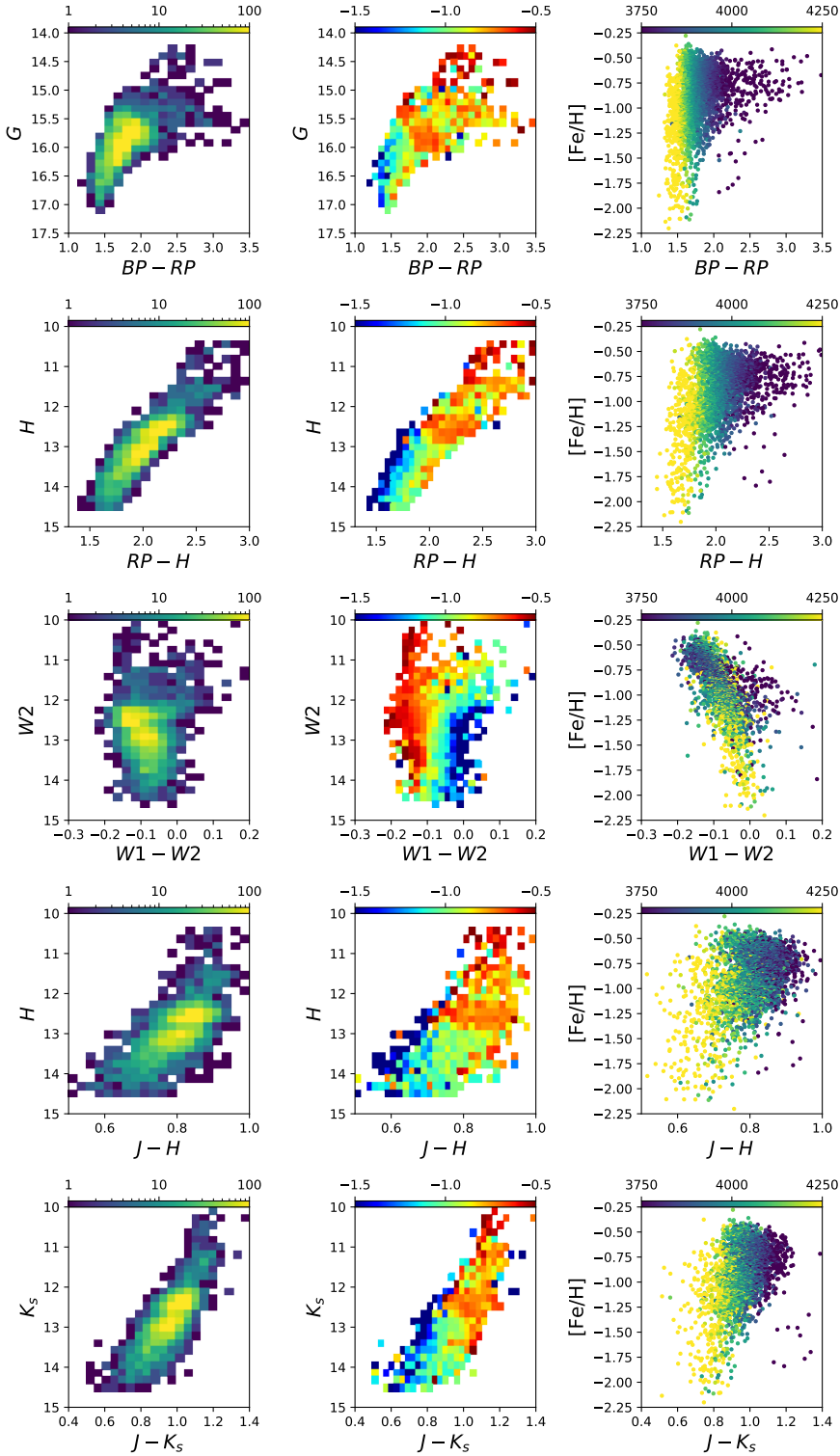


Figure 4.4: *Left*: CMD of our APOGEE training set across the *Gaia*, 2MASS and WISE photometric systems utilised in this work along with the addition of the *Gaia*+2MASS combination chosen as a feature in our regression analysis. The bulk of stars lie in the upper RGB with few AGB stars present. *Middle*: The colour scheme here shows the mean metallicity in each pixel. Gradients are clear across all colours, especially so in WISE owing to its near vertical RGB. *Right*: Scatter plots between each of our four chosen features and APOGEE metallicity are shown. Positive correlations are evident with the WISE band showing the tightest relation. Markers are coloured by effective temperature.

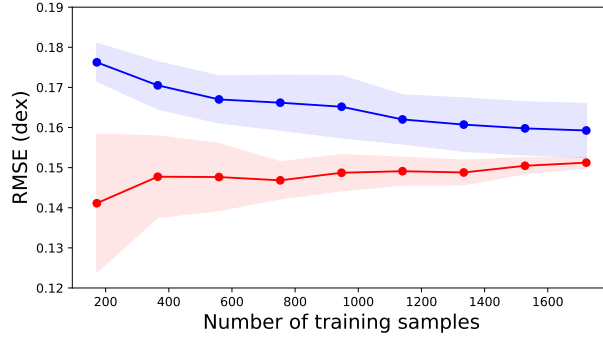


Figure 4.5: Learning curves for an SVR trained using a feature vector of $[BP - RP, RP - H, W1 - W2, J - H, J - K]$. A cross validation set is separated out and the algorithm is trained on incrementally increasing training set size. The root mean squared error score is then computed at each stage for both the training and validation set. The red (blue) line corresponds to the training (validation) set. Both curves tend toward each other smoothly to a sufficient accuracy of ~ 0.17 dex. The good convergence and low final accuracy indicates the learning scenario has sufficiently low bias and variance.

a final evaluation of the model’s performance. Utilising the Support Vector Regression (SVR) implementation of `scikit-learn` (Pedregosa et al., 2011), we implement a standard radial basis function (RBF) kernel of the form:

$$K(\mathbf{x}_1, \mathbf{x}_2) = \exp\left(-\gamma |\mathbf{x}_1 - \mathbf{x}_2|^2\right) \quad (4.1)$$

and optimize the algorithm’s parameters, namely γ and regularisation parameter C , through a K -fold cross validation grid search, with 10 splits, accepting parameter values that minimise the root mean squared error (RMSE). We choose to use a SVR algorithm as it has the ability to model complex, non-linear relations between the features with relatively few parameters to tune. The performance of the regressor is first assessed through the learning curve shown in Fig. 4.5 where the learning algorithm is trained on an incrementally increasing number of training points. A validation sample is set aside beforehand, from which we can evaluate the performance of the model with respect to our chosen metric (RMSE) at each incremental step. The general trend of the figure shows both curves tending towards a final RMSE of ~ 0.16 dex, an acceptably low value that validates the algorithm to be sufficiently unbiased. The convergence of the two curves also indicates relatively low variance – a regressor suffering from over-fitting would yield curves that tend toward convergence but still remain offset by a significant value even when maximal training data is available.

[Fe/H] bin	$\sigma_{[\text{Fe}/\text{H}]}$ (dex)
$[\text{Fe}/\text{H}] \leq -1.5$	0.25
$-1.5 < [\text{Fe}/\text{H}] \leq -1$	0.18
$-1 < [\text{Fe}/\text{H}] \leq -0.5$	0.13
$[\text{Fe}/\text{H}] > -0.5$	0.21

Table 4.1: Table lists the RMSE, computed from our test set predictions, in four metallicity bins. It is in the tails of the metallicity distribution that our predictions suffer greatest error, as demonstrated in Fig. 4.6.

4.2.1 Regression Performance

The upper middle panel of Fig. 4.6 shows good one to one agreement between the APOGEE spectroscopic [Fe/H] values and those predicted by our trained regressor. The upper right panel of the figure shows we are able to reasonably reproduce the metallicity distribution of the test data. The lower panels of the figure shows the mean squared error (MSE), squared bias and variance as a function of APOGEE metallicity for the predictions on our test set. The model suffers from relatively little bias across the full metallicity range, with most contribution occurring at $[\text{Fe}/\text{H}] < -1.25$ dex. Generally, the main contribution to the total error stems from variance in the predictions. This is particularly the case at the low metallicity end where data are sparse, leading the model to over-fit in this region. The predictions are biased high by ~ 0.15 dex for metallicities less than -1.5 dex and are biased slightly low by ~ 0.1 dex at the most metal-rich end. For metallicities less than -1.2 dex, the RMSE is approximately 0.2 dex and the RMSE across all metallicity values is 0.15 dex. We list our prediction errors in four metallicity bins in Table. 4.1. We stress that these are purely nominal error estimates and likely underestimated in some cases. We also note that the nominal errors we obtain from our test set analysis will naturally contain uncertainty invoked from the age-metallicity degeneracy, an effect which acts to make younger/older stars bluer/redder and hence our model would predict these stars to be more metal poor/rich than they actually are.

4.2.2 Regression Predictions

We use our trained SVR to predict metallicities of our full *Gaia*+2MASS+WISE giants, whose spatial distribution is shown in Fig. 4.2. We consider the fact that our full giant sample encompasses a much wider colour

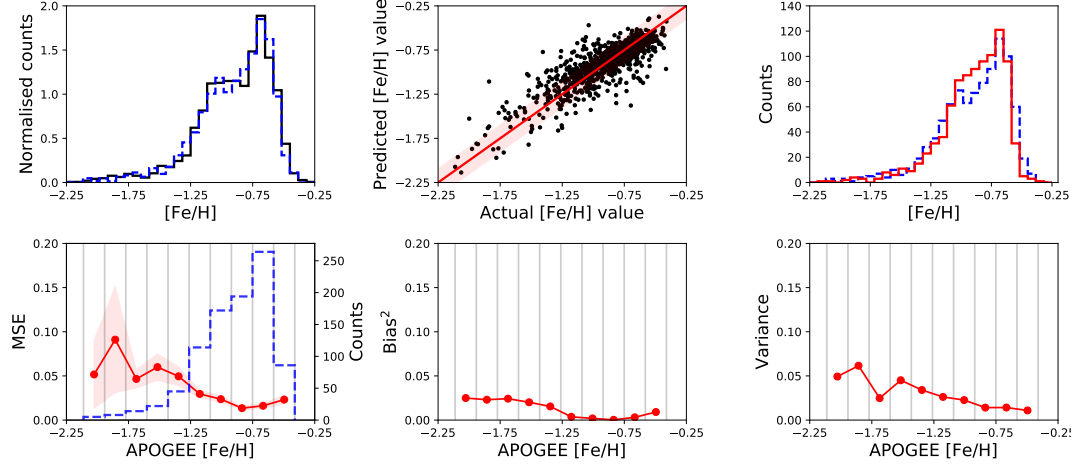


Figure 4.6: *Upper left panel:* Training data metallicity distribution in black solid line which is adequately representative of the test data distribution shown as blue hashed line. *Upper middle panel:* Scatter plot of the predicted and APOGEE measured metallicities for the stars in our test set. The solid red line indicates a one to one correspondence and the red shaded region bounds the RMSE of 0.15 dex recovered from the test set analysis. The majority of the scatter is present at the lowest of metallicities where the stellar density is extremely low. *Upper right panel:* The blue hashed line indicates the test set’s true metallicity distribution now overlaid with the predictions in solid red. Generally, the overall distribution is reproduced well. *Lower left:* The red line shows the estimated MSE binned by APOGEE metallicity values of our test data. The filled shaded region bounding this line shows the dispersion of this value weighted by the Poisson noise in each bin. The blue histogram shows the metallicity distribution of the test set in question with the faint grey vertical lines indicating the bin edges. At metallicities less than ~ -1.2 dex, the corresponding RMSE is 0.23 dex. *Lower middle:* The squared bias in each metallicity bin is seen to be relatively low across the full range with the greatest contribution being at the metal-poor end. *Lower right:* The variance of the predictions in each bin is shown. The largest contribution to total error is again seen at the metal-poor end owing to the dearth of training data in this region.

range than that of our APOGEE subset, particularly so for W1 – W2 as seen in comparison of Fig. 4.3 with Fig. 4.4. To account for this, we adopt a nearest neighbour approach, computing the mean Euclidean distance in feature space from each of our giants to those in the APOGEE sub-set using 5 nearest neighbours. We can then choose an appropriate upper limit cut on this mean feature distance, $\langle D_{NN} \rangle$, to reject stars whose photometry is not well represented in the training data. We also impose cuts in the 2MASS colours for which we require $J - H < 1$ and $J - K_s < 1.25$. In effect, this selection rejects the very red, likely C-rich, AGB stars from our sample. Such extremely red stars are poorly represented in the APOGEE training data and so the regression model will likely struggle to accurately interpolate values to this regime. We also further investigate the effect of

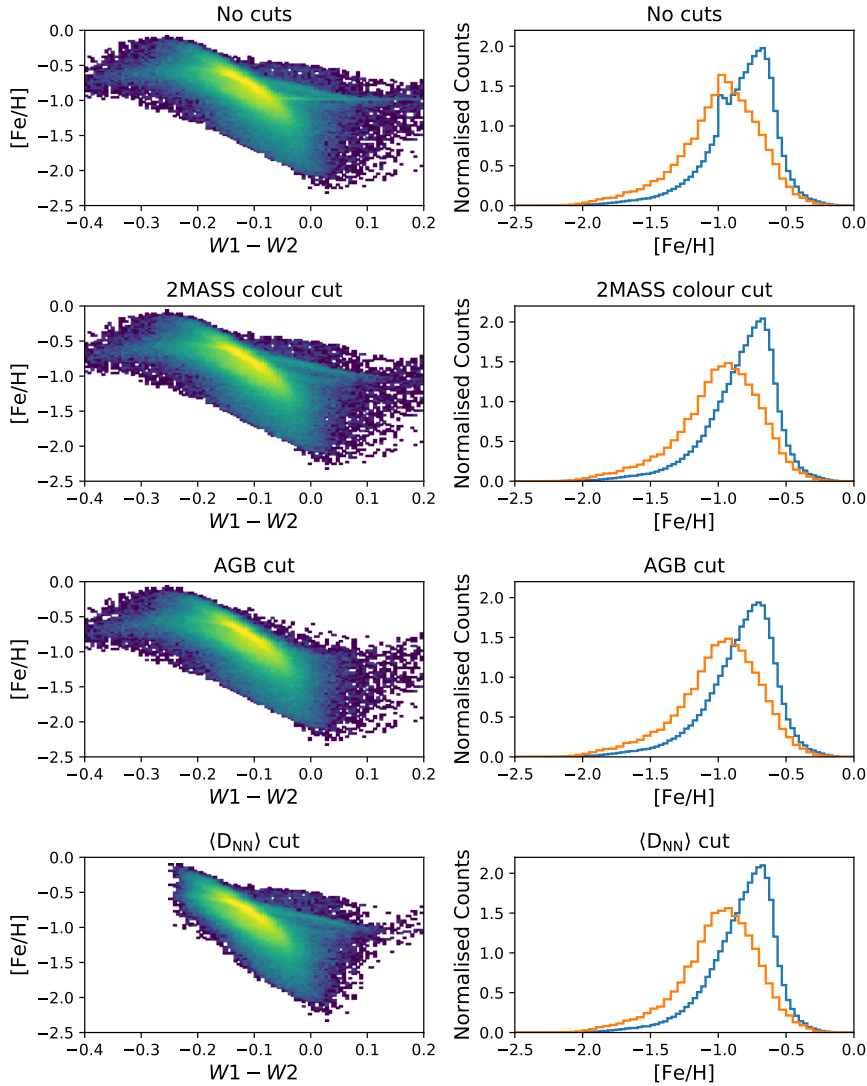


Figure 4.7: Predicted metallicities for our *Gaia*+2MASS+WISE giants as a function of WISE colour $W1 - W2$ are shown in the left column. The right column shows histograms of the predictions for LMC (SMC) in blue (orange) selecting stars that fall within a 12 (8) degree aperture of the respective Cloud. These histograms have been normalised to encompass an area of unity. In the top-leftmost panel, there is a population of stars for which our predictions are spurious, causing a pile up at ~ -1 dex. These stars are the reddest stars in our sample and can be removed through application of the 2MASS colour cuts described in the text. The AGB stars form a bifurcation in the metallicity-colour sequence owing to the unusual properties of the WISE isochrone tracks in which the AGB stars sharply turn red, crossing RGB tracks of lower metallicities. In turn, this causes a bi-modality in metallicity at fixed WISE colour. The bottom row shows the effect of requiring the mean feature space distance $\langle D_{NN} \rangle$ to be less than 0.06. It largely removes the stars that are extremely blue, culling those stars whose predictions spuriously converge to ~ -0.8 dex.

removing the AGB branch by only considering stars with $K_s > 12$ (this selection is tuned to the LMC AGB as it is the dominant contributor to our sample). The effects of these individual selections are

shown in Fig. 4.7, which shows the predicted metallicity as a function $W1 - W2$ colour for our *Gaia*+2MASS+WISE giants. The top panel clearly shows spurious predictions accumulating at $[\text{Fe}/\text{H}] \sim -1$ dex, towards red values of $W1 - W2$. On applying our 2MASS colour cuts we eliminate these entirely, as we cull the extremely red giants from our sample. The selection of stars fainter than $K_s > 12$ highlights the region occupied by likely AGB stars which consists of a spur branching out from the main colour-metallicity relation, an effect caused by the WISE AGB isochrone tracks turning red and crossing the RGB track at other fixed metallicities (see Fig. 1 of Koposov et al. (2015)). The bottom-most panels in the figure show the effect of requiring the nearest neighbour mean feature space distance $\langle D_{\text{NN}} \rangle$ to be less than 0.06, corresponding to a cull of stars within the largest 10th percentile. This selection acts to remove stars whose photometric colours deviates largely from the regime spanned by our APOGEE sample, thus eliminating spurious extrapolations in our metallicity estimates. This is evident from the panel, where stars extremely blue in $W1 - W2$, and whose predicted metallicities spuriously converge to ~ -0.8 dex, are effectively removed. The right column of the figure shows our predicted MDF in each of the cases. Aside from the most spurious deflections, these distributions behave well with both the LMC and SMC appearing negatively skewed with long tails towards the metal-poor end. Hereafter, we will only consider giants in our analysis whose 2MASS colours obey they cuts $J - H < 1$ and $J - K_s < 1.25$, as it is this selection that eliminates the most serious artefacts in our predictions, yielding a sample of 218,077 giants. We will note explicitly in the text when we apply further cleaning criteria to our giant sample. Considering stars within a 12° aperture of the LMC, we obtain a median metallicity value of -0.78 dex, with the peak of the (skewed) distribution occurring at ~ -0.67 dex. For stars falling within a 6° aperture of the SMC, we obtain a median metallicity value of -0.96 dex, with the distribution peaking at ~ -0.93 dex.

4.3 METALLICITY MAPS

We show the mean predicted metallicity across the Clouds in the top left panel of Fig. 4.8, using the Magellanic Stream coordinate system of (L, B). The LMC bar is strikingly clear as a central metal-rich structure in our giant sample. Outside of the bar region, diffuse arcs and spiral arm-like structures are seen both in the northern and southern portions of the LMC disc. We note that the structures apparent in this figure, and to be discussed later in this work, are viewed in projection and any reference to them will be done so with this in

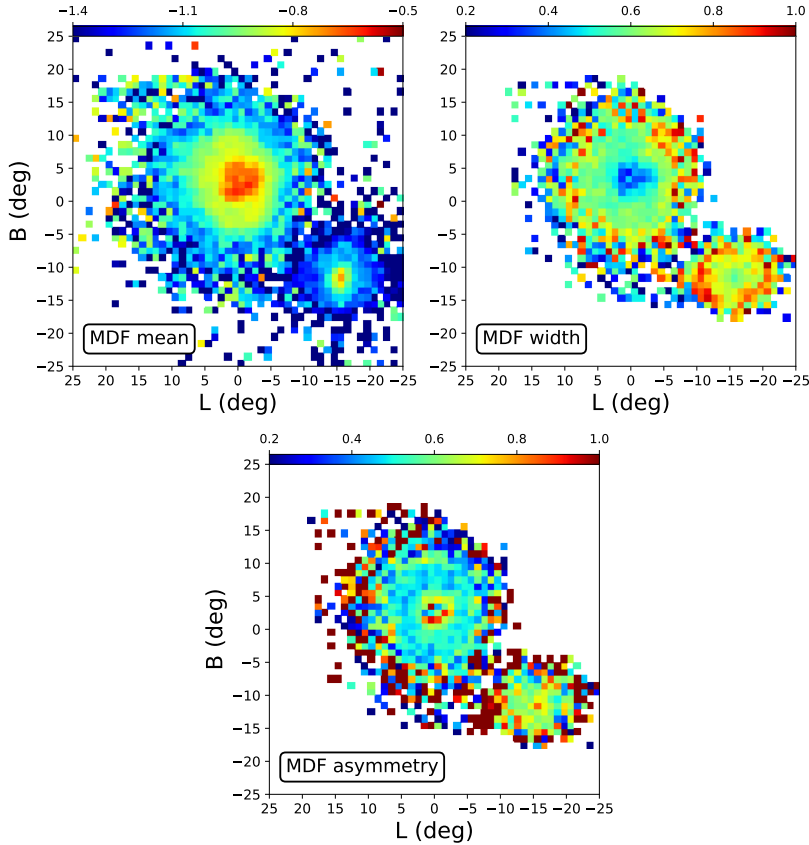


Figure 4.8: *Top-left*: Average metallicity maps of the Clouds coloured by mean metallicity per pixel. The central regions of the LMC are metal-rich, with the region occupied by the LMC bar and dominant spiral arm. Outside the bar region, diffuse metal-rich structures are seen with arc-like morphology in both the southern and northern regions. A negative metallicity gradient is seen through the LMC disc with apparent asymmetry; the northern and southern portions of the dwarf appear to have relatively more metal-rich stars at larger radii, and hence a flatter gradient, as opposed to the east-west direction. The outermost regions of the LMC are littered with metal-poor stars. Our metallicity predictions show the SMC to be distinctly more metal-poor, with a slight gradient and central enhancement visible. *Top-right*: We show the difference between the 90th and 10th percentile of $[\text{Fe}/\text{H}]$ in each pixel, effectively a width measure of the MDF. The central regions of the LMC appear to have a relatively narrow MDF where the metal-rich bar and spiral arm dominates. Generally, the MDF of the SMC appears to be broader throughout the dwarf, in comparison to the LMC, likely owing to its large extent along the line of sight such that we are viewing a projection of multiple populations within the galaxy. *Bottom*: We colour pixels by the ratio of the difference in the 95th and 50th to the difference in the 50th and 5th metallicity percentiles. A symmetric distribution would have a ratio of unity, with a left (right) skewed having values below (above) this. It can be seen that regions near the LMC bar have values close to unity, a consequence of metal-rich stars being relatively more prevalent in this region acting to reduce the left-skew of the MDF.

mind, unless otherwise stated. The LMC metallicity profile then decays into the outskirts, where it is littered with more metal-poor stars. The SMC giants are seen to be predominately metal-poor with only the most central region showing enhancement. The majority of substructure in the outskirts of the Clouds also appears to be relatively metal-poor, with the northern stream like substructure, identified first by Mackey et al. (2016), apparent in our sample. The Clouds appear to be connected, largely with metal-poor stars, in two regions: that of the Magellanic Bridge consisting of stars likely stripped from the SMC and dragged toward the LMC, as indicated by the proper motion analysis of Schmidt et al. (2020), and also in a region south of this at $L \sim 8^\circ$, at the end of a narrow tail like substructure that wraps around the eastern edge of the LMC (see Fig. 4.2 and Fig. 2 of Belokurov and Erkal (2019) also). Denoting the i^{th} percentile of the LMC/SMC MDF as p_i , we show in the top-right panel the difference of $p_{90} - p_{10}$ which represents the width of the distribution. The central regions of the LMC display a consistently narrow MDF with that of the SMC generally quite broad, likely a projection effect of its extensive line of sight depth. In the bottom panel, we show the ratio of $(p_{95} - p_{50}) / (p_{50} - p_5)$ which provides a sense of the direction of skew that the MDF possesses. The most central regions of the LMC show values close to unity, i.e. near symmetric, as metal rich stars dominate in this region and counteract the inherent left skew of the MDF (see Fig. 4.7). The outskirts of the Clouds show a tendency for the MDF to tend towards symmetry, which may be an indication of relatively metal-richer stars originating in the inner disc having migrated outward. This is particularly the case for the eastern most edge of the SMC indicated by the region of red pixels at a MS longitude of $\sim -8^\circ$. Curiously, this region coincides (in projection) with the point at which the outer southern LMC spiral arm structure appears to join with the SMC (see Fig. 4.1). On closer inspection, we see there is a population of giants with $[\text{Fe}/\text{H}] > -1$ dex in this region, relatively metal-rich for outer SMC stars which generally take on $[\text{Fe}/\text{H}] < -1.3$ dex in our sample. It is plausible therefore that there exists a stripped LMC giant population in the region, which is the continuation of the outer spiral-like arm seen in Fig. 4.1.

Considering both Clouds individually, we show mean metallicity, stellar density and associated extinction maps in Fig. 4.9. Here, we show our giants in coordinates offset from the respective Clouds, adopting an LMC centre of $(\alpha_0, \delta_0) = (82.25^\circ, -69.50^\circ)$ as determined by van der Marel and Cioni (2001) and an SMC centre of $(12.60^\circ, -73.09^\circ)$ from Rubele et al. (2015). Again the central bar is prominent and appears to display an extended metal-rich association just north of it;

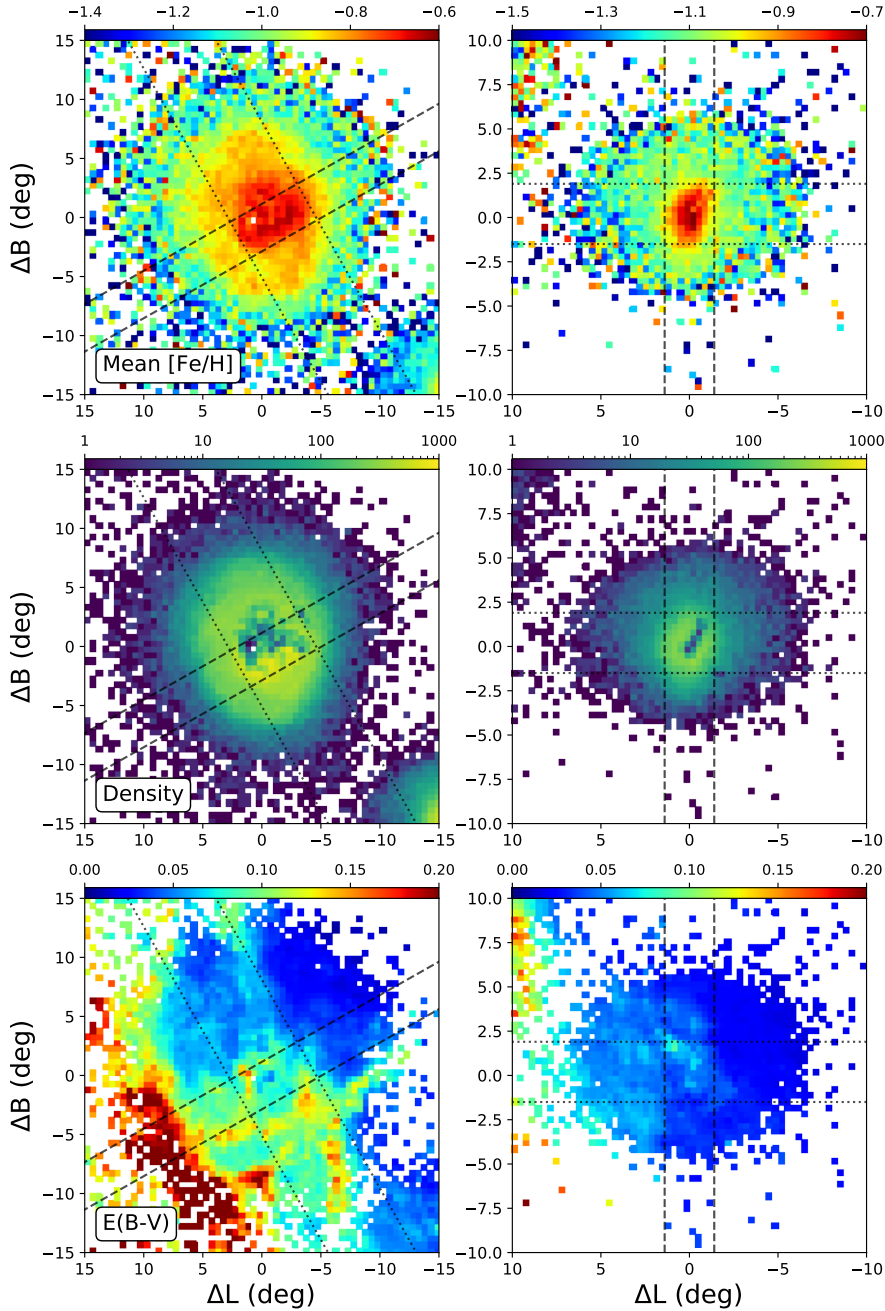


Figure 4.9: Left (right) column of the figure corresponds to the LMC (SMC). The top row shows mean metallicity per pixel. The same general features are seen as in Fig. 4.8 with the central regions of both Clouds being the most metal-rich and diffuse, metal enhanced structures seen in the outer LMC disc. The middle row shows the stellar density map of the Clouds, central regions of high extinction are most affected yielding gaps in the density profile. The SMC displays a stretched morphology with wings on the eastern and western side of the dwarf, a consequence of the tidal interactions with the LMC. The bottom row panels show the extinction map adopted in this work. Generally, the extinction is low aside from the eastern side of the LMC lying nearest the Galactic plane and various filamentary structures throughout it. Stars that fall between the dashed (dotted) lines are those shown in Fig. 4.11 to trace the metallicity profile of the LMC and SMC along the projected major and minor axes of their respective bars.

Assuming an LMC heliocentric distance of 49.9 kpc, the correspondence between on sky angular separation and distance is $1^\circ \leftrightarrow 0.87$ kpc. For the SMC at 60 kpc, the correspondence is $1^\circ \leftrightarrow 1.05$ kpc.

this extension is most likely the main spiral arm of the LMC. On slightly decreasing the dynamic range of the pixel colour, a plethora of diffuse metallicity features within the LMC is revealed in the figure, notably the strikingly spiral-like feature in the southern portion of the disc, reaching down to $\sim 6^\circ$ below the LMC centre. Its morphology is relatively smooth and coherent until $(\Delta L, \Delta B) \sim (2^\circ, -5^\circ)$, beyond which the metallicity structure becomes clumpy. This spiral-like feature, whilst faint, can also be seen in the corresponding stellar density map. The lack of correlation with any large scale extinction patterns, seen in the bottom left-most panel, supports the notion of this being a genuine feature of the LMC disc.

When comparing our LMC metallicity map with that of Choudhury, Subramaniam, and Cole (2016), the large scale features are generally consistent. In their analysis, they combined giants from the OGLE-III and Magellanic Cloud Photometric Survey (MCPS) out to a radius of $\sim 5^\circ$. Taking the slope of the RGB as proxy for average metallicity, calibrated against spectroscopic data, they estimated the metallicity of sub-regions through the Cloud. Both samples provide reasonable coverage of the central LMC with the OGLE-III (MCPS) footprint covering more of the east-west (north-south) regions. They observed the LMC bar to be the most metal-rich region and found evidence for a differing metallicity gradient through different regions of the disc; a shallower gradient was observed in the north-south regions in comparison to that in the east-west regions of the LMC. Both of these features are evident in Fig. 4.9, where the metal enhanced substructures in the top left panel are seen to reside largely in the north-south direction where they act to flatten any pre-existing gradient.

With regards to the SMC, it is only the core of the dwarf that displays any coherent metallicity structure, consistent with the spatial density patterns observed by El Youssoufi et al. (2019) and the recent SMC metallicity maps of Choudhury et al. (2020). The outskirts of the SMC appear to be stretched and show an elliptical appearance, likely a result of tidal stripping of material through LMC interactions (see also Belokurov et al., 2017; Massana et al., 2020). The black hashed (dotted) lines in the figure denote selection bounds to sample giants lying along the projected major (minor) axis of the Magellanic bars for use in Section 4.3.1. Owing to the complex three dimensional structure of the SMC, the exact orientation at which we are viewing it is highly uncertain, and so in this case, the bar selection is made simply to isolate the central most metal-rich feature. It is worthwhile to note that, whilst the stellar density of our data-set in the central regions of the Clouds is patchy and incomplete, we can still gain insight

into the structure of these regions through the lens of spatially averaged metallicity maps. The spatial incompleteness in these regions is likely an effect of the CMD giant selection employed by Belokurov and Erkal (2019).

4.3.1 Metallicity Gradients

We first attempt to quantify the presence of a metallicity gradient within the LMC by considering the dwarf as an inclined thin disc. The equations of van der Marel and Cioni (2001) provide the transformations into a Cartesian system of an inclined thin plane, from observed on-sky positions, defined by its inclination angle i and position angle θ measured anticlockwise from west. This allows us to assign each LMC giant an in-plane Galactocentric cylindrical radius R . We model the radial metallicity profile by the simple linear relationship:

$$[\text{Fe}/\text{H}]^{\text{model}} = \Theta_0 R(\alpha, \delta, i, \theta) + \Theta_1 \quad (4.2)$$

where we wish to infer the gradient and intercept contained in the parameter vector $\Theta = [\Theta_0, \Theta_1]$. The in-plane radius is a function of the plane geometry and thus dependent on the choice of (i, θ) for the LMC. We account for this in our inference by marginalising over these parameters. We fix the centre of the LMC to be at $(\alpha_0, \delta_0) = (82.25^\circ, -69.50^\circ)$ as in van der Marel and Cioni (2001) and specify a distance of 49.9 kpc (de Grijs, Wicker, and Bono, 2014) to the LMC centre. Writing the total likelihood as:

$$p([\text{Fe}/\text{H}] | \Theta, i, \theta, \alpha, \delta, \sigma_{\text{Fe}/\text{H}}, V) = \prod_n \frac{1}{\sqrt{2\pi s_n^2}} \exp\left(-\frac{([\text{Fe}/\text{H}]_n^{\text{model}} - [\text{Fe}/\text{H}]_n)^2}{2s_n^2}\right) \quad (4.3)$$

where $[\text{Fe}/\text{H}]_n$ is our metallicity prediction for the n^{th} giant. The term $s_n^2 = \sigma_n^2 + V$ encompasses the prediction error σ_n for each giant and some general intrinsic scatter in the model through the parameter V . The full posterior probability can then be written as:

$$p(\Theta, V | \alpha, \delta, [\text{Fe}/\text{H}], \sigma_{\text{Fe}/\text{H}}) \propto \iint p([\text{Fe}/\text{H}] | \Theta, i, \theta, \alpha, \delta, \sigma_{\text{Fe}/\text{H}}, V) p(\Theta, V) p(i, \theta) di d\theta \quad (4.4)$$

from which we can draw samples in an MCMC fashion, utilising the sampler emcee of Foreman-Mackey et al. (2013), for parameters Θ and V . In practice we compute the marginalisation over the nuisance parameters (i, θ) by summing the likelihood over a two dimensional

In this context, the position angle is that to the line of intersection between the disk plane of the LMC and the on-sky plane. The usual astronomical convention is to measure this angle eastward from north and is related to θ by $PA = \theta - 90^\circ$.

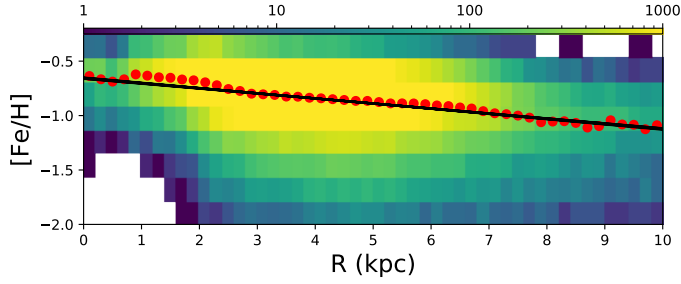


Figure 4.10: This shows the evolution of LMC giant predicted metallicity as a function of in-plane cylindrical radius. Pixels are coloured by stellar counts per pixel. The central regions are seen to be metal enhanced with respect to the outer regions of the LMC, where the metal-rich bar dominates. The red markers show the mean metallicity in bins of radius. A shallow negative metallicity gradient is evident. The solid black lines are samples drawn from our model. We only show giants with $\langle D_{\text{NN}} \rangle < 0.06$ in this figure to isolate stars that should have reasonable metallicity estimates given their colours. In this figure, we adopt the LMC viewing angles of Choi et al. (2018a)

Gaussian grid with mean (i, θ) values of 30° and 235° . The covariance matrix of the Gaussian prior was forced to be diagonal with respective widths of $\sigma_i = 5^\circ$ and $\sigma_\theta = 10^\circ$. These choices reflect range of values reported in the literature; recently Choi et al. (2018a) inferred an LMC inclination and position angle of $(25.86^\circ, 149.23^\circ)$ from photometric data alone whereas van der Marel and Kallivayalil (2014) infer viewing angles of $(34.0^\circ, 139.1^\circ)$ from field proper motions and old stellar line of sight velocities (note in both these cases, the quoted position angle is in the usual astronomical convention). We perform the fit on all giants within a 12° aperture of the LMC. We also exclude the most central giants within 3.5° so as to avoid the metal-rich bar and focus on stars primarily tracing the LMC disc. In doing so, we also mitigate the fact that our metallicity predictions for the most metal-rich stars, which dominate centrally, incur a degree of bias (at least $\sim 0.1 - 0.2$ dex) in our regression model. We further limit our analysis to giants with $\langle D_{\text{NN}} \rangle < 0.06$ to remove giants whose photometric colours lie in the domain in which our regression struggles to perform adequately. In doing so, we limit our sample to 196,216 red giants. We recover a metallicity gradient of -0.048 ± 0.001 dex/kpc for our giant sample, consistent with that of Choudhury, Subramaniam, and Cole (2016) who found a gradient of -0.049 ± 0.002 dex/kpc in their analysis of LMC RGBs, as well as that of Cioni (2009) whose value of -0.047 ± 0.003 dex/kpc was obtained from a sample of LMC AGB stars. For our intercept term we recover a value of -0.656 ± 0.004 dex.

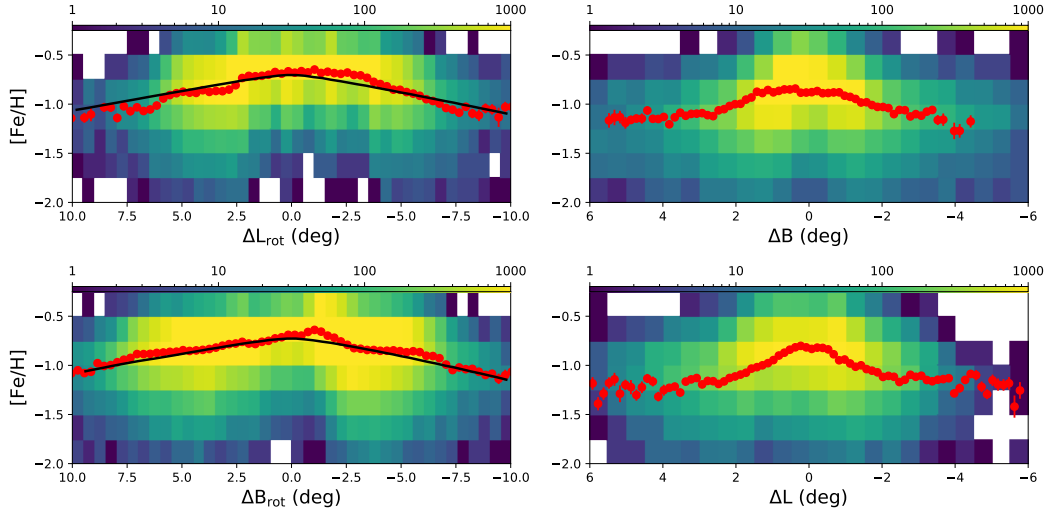


Figure 4.11: Stellar density maps tracing the metallicity profile along directions aligned with the projected axes of the bars. The left two panels corresponds to the LMC and the right panels to the SMC. The top (bottom) row shows the profile of stars that fall within the dashed (dotted) line in Fig. 4.9. In the case of the LMC, we have rotated the Magellanic Stream coordinate system clockwise by 30° so as to approximately align with the major axis of the bar. We only consider stars with $\langle D_{NN} \rangle < 0.06$ in this figure. Red markers correspond mean metallicity binned over angular offset relative to each Cloud’s centre with error bars representing standard errors in each bin. Both the LMC and SMC show a flattening in the metallicity profile centrally in the domain of the bar. Clear negative gradients are observed on increasing distance away from the central regions, with strong asymmetries and plateau like features present.

In Fig 4.10, we show the radial metallicity profile of our LMC giants. Our fit describes the negative profile well through the LMC disc, with the inner regions being the most metal enhanced. We show the metallicity profiles along the projected bar major and minor axes for both Clouds in Fig. 4.11; the giants used in the figure were selected to lie between the hashed and dotted lines in Fig. 4.9 respectively. For the LMC, we transform to a coordinate system that is approximately bar aligned through a clockwise rotation of 30° into the system we denote (L_{rot}, B_{rot}) . In the Magellanic Stream coordinate system, the major axis of the SMC bar is very nearly aligned with the vertical and so no rotation was performed. Both of the Clouds display a flattening of their metallicity profiles centrally in the bar dominated regions. Outside of this domain, the profiles show clear negative gradients outwards into the disc. This is consistent with the findings of Fraser-McKelvie et al. (2019), who studied a sample of 128 barred galaxies finding both the age and metallicity gradients to be flatter in the bar as opposed to the discs of the galaxies, indicative of bars being confined structures, efficient in radially mixing their stellar populations (see Seidel et al.

(2016) also). Through the LMC disc, complex structure is observed with asymmetric gradients and plateau features present. The black solid line in these panels shows our model projected into this coordinate system to highlight the large degree of asymmetric metallicity structure that exists throughout the LMC; the western portion of the disc (i.e. towards positive ΔL_{rot}) shows a depletion in metallicity with respect to the model whereas the northern and southern regions show mild excesses. Whilst we have hesitated to quantify the metallicity gradient in the SMC, owing to the uncertainty of the dwarf's morphology, Fig. 4.11 demonstrates asymmetric gradients in the smaller Cloud also.

In Fig. 4.12, we compare the mean metallicity maps of our LMC giants with that of an inclined disc whose radial metallicity profile follows that in our inference. The bottom-most panel shows the metallicity residual, obtained by subtracting the model from the data, in which the LMC bar and main spiral arm are clearly revealed as centrally enhanced regions. The main spiral arm of the LMC is a feature usually only observed in young stellar tracers (ages $\lesssim 1$ Gyr) such as main sequence stars and supergiants (e.g. Cepheid Variables), notably so in the recent morphological mapping of the LMC by El Yousoufi et al. (2019) using VMC data. Utilising stellar synthesis models to calibrate stellar ages, they obtain age estimates for LMC stellar populations right across the CMD. Panels B, C and H of their Fig. 5 show the extent of the main spiral arm, with an additional faint arm emerging to the north of it; such a bifurcation is revealed in our metallicity residuals also and is annotated in the figure as a spiral extension. In the northern regions of the outer disc we isolate an arc like area of metallicity enhancement. This portion of the LMC is coincident with the structure labelled "Arc" in Fig. 3 of Besla et al. (2016), lying $\sim 5 - 7^\circ$ above the LMC centre with no symmetric counterpart in the southern regions.

This feature is likely a remnant of tidal interactions between the Clouds. Indeed the simulations of Besla et al. (2016) suggest that it is repeated close encounters between the Clouds that seed such stellar arcs in the northern periphery of the LMC, in isolation of the Milky Way. This notion is supported by the observation of the Clouds appearing to be on their first infall (see e.g. Besla et al., 2007; Kallivayalil et al., 2013). The curious spiral/arc like feature seen in Fig. 4.9 is also revealed in Fig. 4.12, which we label as a Southern Arm, wrapping from $\sim -4^\circ$ to 2° in latitude and looks to emanate from the bar downwards by $\sim 6^\circ$. This feature is curious in its apparent asymmetry, with typical spiral galaxies possessing spiral arms emanating symmetrically from the bar. This residual feature is largely coinci-

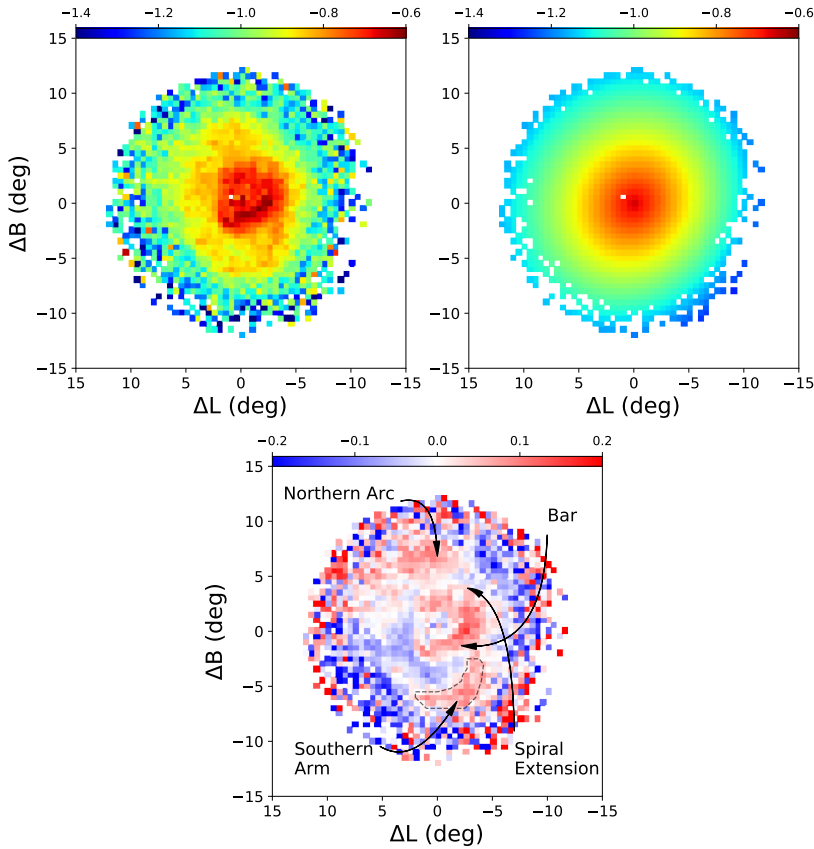


Figure 4.12: *Top-left*: Giants within 12° of the LMC are shown in Magellanic Stream coordinates (relative to the LMC centre) with pixels coloured by mean metallicity. The metal-rich central region traces the bar and the dominant spiral arm of the Cloud. The northern portions of the disc trace arc like features and the southern region shows a spiral like feature with moderately enhanced metallicity. *Top-right*: Mean metallicity map of an inclined disc with viewing angles of Choi et al. (2018a) and radial metallicity function defined by the parameters found by our fitting method. *Bottom*: We subtract the metallicity of the model pixels from that of our data to highlight regions that are enhanced/depleted with respect to a disc whose radial metallicity distribution follows the form of eqn (4.2). Red pixels correspond to metal-richer regions and blue pixels metal-poorer with respect to the model. The most striking revelation in doing this is that of the LMC’s metal-rich bar and inner northern spiral arm emanating from the north-west end of the bar. The giants used to make this figure were subject to our nearest neighbour selection in feature space. Prominent regions, other than the bar, of enhanced metallicity are annotated and labelled.

dent with the ring like over-density uncovered by Choi et al. (2018b). Through modelling the LMC stellar density with a disc and bar component, their residuals revealed a structure akin to ours composed of stars older than ~ 1 Gyr. They observe the feature to wrap around more extensively on the western side of the LMC in comparison to our metal-rich feature, which diminishes at $(\Delta L, \Delta B) \sim (2^\circ, -6^\circ)$ in

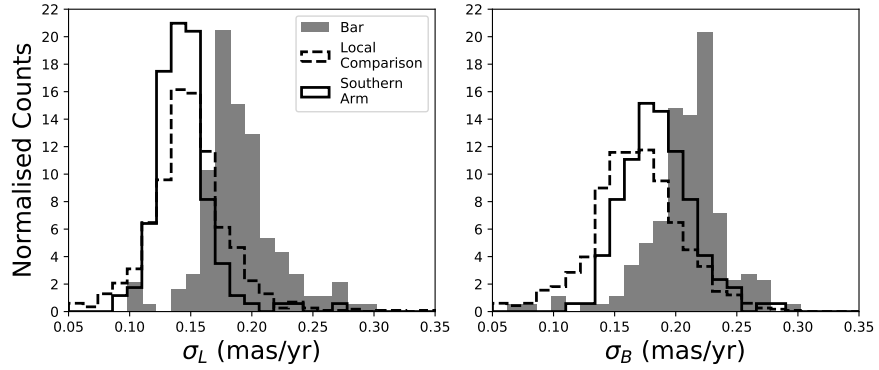


Figure 4.13: Histograms show reflex corrected proper motion dispersions in the Magellanic Stream coordinate system (L,B). We have normalised the histograms such that their areas integrate to unity. The black lined histogram corresponds to pixels bound by the polygon in Fig. 4.12 and the dashed line histogram are stars bound by the aperture described in the text. The grey histogram represents the metal-rich pixels in the LMC bar region which are distinctly hotter than the two disc populations. Stars in the Southern Arm appear to share similar dispersions to those lying at a similar (projected) radius across all azimuthal angles.

our residuals, and is more reminiscent of a spiral/arc as opposed to a ring. Curiously however, the signal of their over-density appears to diminish in strength near to the tip of our residual spiral. Beyond this, the Choi et al. (2018b) over-density becomes patchy as it continues to wrap around the LMC centre. Looking at our data in the left panel of Fig. 4.12, we observe similar behaviour; the coherent spiral-like structure emerges from the south-west end of the bar and wraps eastward until $(\Delta L, \Delta B) \sim (2^\circ, -6^\circ)$, beyond which we see a patchy continuation of slight [Fe/H] enhancement. We note however that, as can be gleaned from Fig. 4.9, the extinction pattern in this region of the LMC is itself patchy and may be influencing the small scale structure of the metallicity feature. El Youssoufi et al. (2019) also saw evidence of such a southern structure in their analysis of VMC data, with aging main sequence stars and sub-giants ($\sim 1 - 2.5$ Gyr) a faint extension from the south-west region of the bar. Bica et al. (2008) mapped the spatial distribution of Magellanic star clusters (ages < 4 Gyr), indeed observing a southern spiral/ring like structure that our metal rich feature is spatially coincident with.

We attempt to determine if our Southern Arm giants are kinematically distinct in any way by considering their proper motion dispersions. To do so, we first select all pixels bound by the polygon in Fig. 4.12. We further select all pixels within a $5 - 7.5^\circ$ aperture around the LMC centre, rejecting those within the polygon, to represent stars at a similar radius as the arm for a ‘local’ comparison. We also select metal-rich pixels associated with the LMC bar. As a simple

investigation, we plot the histograms of pixel proper motion dispersion in Fig. 4.13 where we see both disc populations to co-exist in proper motion dispersion, distinctly cooler than the bar region. This combined with the fact that this spiral like structure is a metal-rich feature is suggestive of it harbouring LMC disc stars. We conjecture that these stars may have been perturbed in some way, giving rise to the coherent, spiral like structure we see. Many barred galaxies display a symmetrical appearance, with spiral arms emerging from both ends of the bar. The LMC however has long been known to possess only one dominant spiral arm. Recently, Ruiz-Lara et al. (2020) determine the LMC spiral arm to be a spatially coherent structure that has been in place for the last ~ 2 Gyr, supporting the notion that it was seeded through a historic close encounter with the SMC, as observed in simulations (see e.g. Besla et al., 2012; Pearson et al., 2018). The N-body simulations of Berentzen et al. (2003) demonstrate that the collision of a small companion with a larger barred galaxy can seed complex structures such as spiral arms, stellar rings and stellar spurs, and those of Walker, Mihos, and Hernquist (1996) further display the prominence of one sided spiral features seeded by the accretion of a satellite galaxy onto a large disc galaxy; single spiral arms emanate from the bar and wrapped spiral arms form in the disc. It is likely that the southern spur we observe has arisen from the historic interactions between the LMC and SMC and is a metal-rich counterpart of the structure observed by Choi et al. (2018a). Our residual maps show the northern and southern portions of the LMC to be metal enhanced with respect to the eastern and western regions, an observation consistent with that of Choudhury, Subramaniam, and Cole (2016), indicative of the former regions being most disrupted by previous tidal interactions. The region of slight metallicity depletion, running interior to the Southern Arm, is evident in the top left panel of Fig. 4.11 as the plateauing region at $\Delta L_{\text{rot}} \sim 3^\circ - 5^\circ$, beyond which the metallicity diminishes as outer metal-poor stars begin to dominate. The two slight bumps in metallicity in the bottom left panel of Fig. 4.11 correspond to the northern arc and Southern Arm features we present in Fig. 4.12. Thus, whilst our giant sample is incomplete and much of the LMC structure difficult to discern from our density maps alone, we utilise our metallicity estimates as a probe into LMC disc structure. In considering the deviation away from a smooth, simple axisymmetric metallicity model, we readily observe the complex structures that are known to reside in the LMC disc at once, in effect overcoming the completeness limitations of our sample.

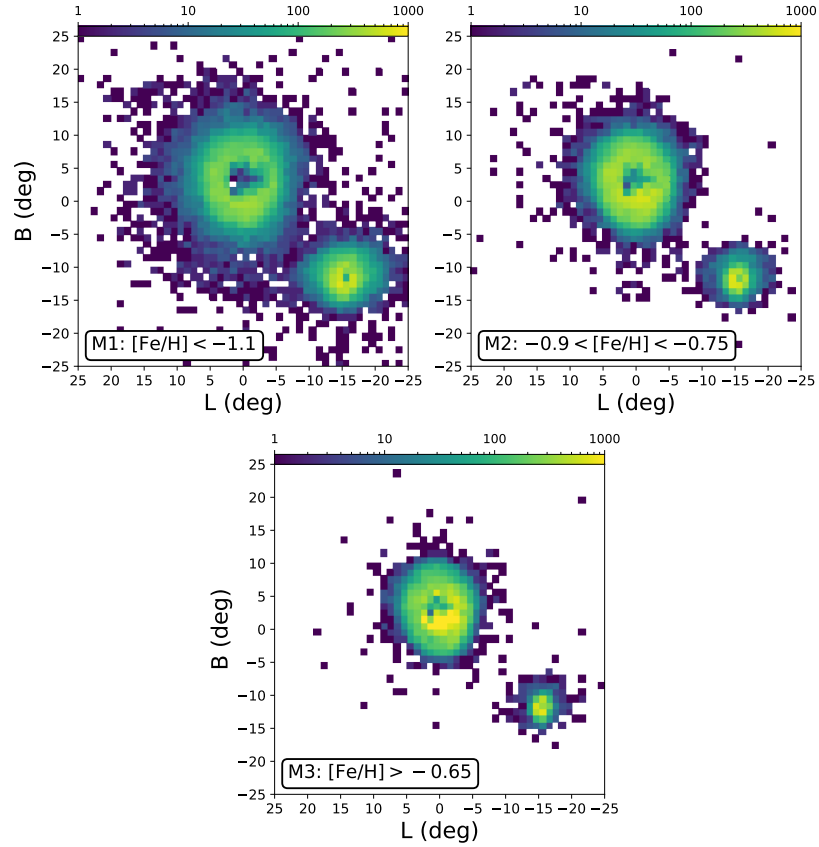


Figure 4.14: Stellar density maps of our red giants in the three metallicity bins described in the text with metal-poor in the leftmost panel and metal-rich in the right. The general evolution in morphology is a decrease in outer substructure in both Clouds on increasing stellar metallicity. The most metal-rich bin shows the LMC and SMC to be isolated, whereas the metal-poor bin shows the Clouds to be connected, both in the Magellanic Bridge region and further south where the outer stellar arc of the LMC attaches to the eastern edge of the SMC. The most metal-poor giants in the SMC shows a high central density with the outer regions appearing stretched horizontally, likely due to tidal interactions with the LMC. At the metal-rich end, the SMC is much more compact and shows a weaker signature of tidal disruption.

4.3.2 Slicing the Clouds by Metallicity

We consider the broad scale morphology of the Clouds as a function of metallicity in Fig. 4.14 where we show the stellar density in the three metallicity bins of: $[\text{Fe}/\text{H}] < -1.1$, $-0.9 < [\text{Fe}/\text{H}] < -0.75$ and $[\text{Fe}/\text{H}] > -0.65$, each containing $\sim 44,000$ giants. We will refer to these bins as M1, M2 and M3 hereafter. Although there exists a degree of scatter between the bins due to the uncertainty in our metallicity predictions, we present this map to provide a sense of the general structural trends of the Clouds on increasing metallicity. The majority of outer substructure around the Clouds is made of the metal-poorer

stars in M1. It is in this bin that the northern substructure identified by Mackey et al. (2016) is most prominent. A region at the base of this structure was recently analysed by Cullinane et al. (2020), finding it to be kinematically perturbed from an equilibrium disc, likely through SMC/MW interactions. Furthermore, the southern stellar stream like feature that connects to the SMC, first observed by Belokurov and Erkal (2019), is only apparent in this bin and appears to be the symmetric counterpart to the northern outer arc. The LMC+SMC+MW N-body simulations conducted by Belokurov and Erkal (2019) found that as recently as ~ 150 Myr after a close encounter with the SMC, such outer spiral-like features can be induced in the LMC. Indeed, the SMC is thought to have experienced a direct collision with the LMC on a timescale comparable to this from the kinematical modelling of Zivick et al. (2018). Another diminishing feature on increasing metallicity is the density of stars in the old stellar Magellanic Bridge region, likely composed of outer, tidally stripped stars originating from both the LMC and SMC. The general shape of both Clouds also appears to evolve in a sensible way, presenting themselves as extended, rather diffuse objects at the metal-poorer end in M1 through to much more centrally concentrated objects at the metal-rich end in M3. In the case of the SMC, it demonstrates a degree of ellipticity in M1 (and slightly so in M2), indicative of strong tidal disruption induced in the outer metal-poor regions.

We consider the proper motions of our giants in the three bins in Fig. 4.15 and Fig. 4.16. We correct for the solar reflex motion assuming a constant heliocentric distance of 49.9 kpc (with the main focus being the LMC). The dominant signal is that of rotation within the LMC disc, apparent by the gradient across the Cloud. As in Belokurov and Erkal (2019), the northern and southern arm like features display a coherent rotation signal, lagging that of the LMC disc; both arms bear motions that are consistent with the bulk of the LMC and appear distinct from the proper motions of the SMC. In Fig. 4.15, a significant portion of the SMC nearest to the LMC shows prominent motion towards the larger Cloud, with the signal appearing to persist across the three metallicity bins. The lower left panel of Fig. 4.15 shows there to be significant dispersion in M1, precisely at the SMC edge of enhanced proper motion and at the LMC-SMC interface, where a mixture of Cloud populations is to be expected. The SMC is known to be disrupting (see e.g. De Leo et al., 2020; Zivick et al., 2018) and the perturbed motions we observe here are likely a result of this, with the LMC violently dragging the eastern edge of the SMC towards it. The fact that we observe this signature in all three of the top panels indicates that the disruption is severe, penetrating through to the

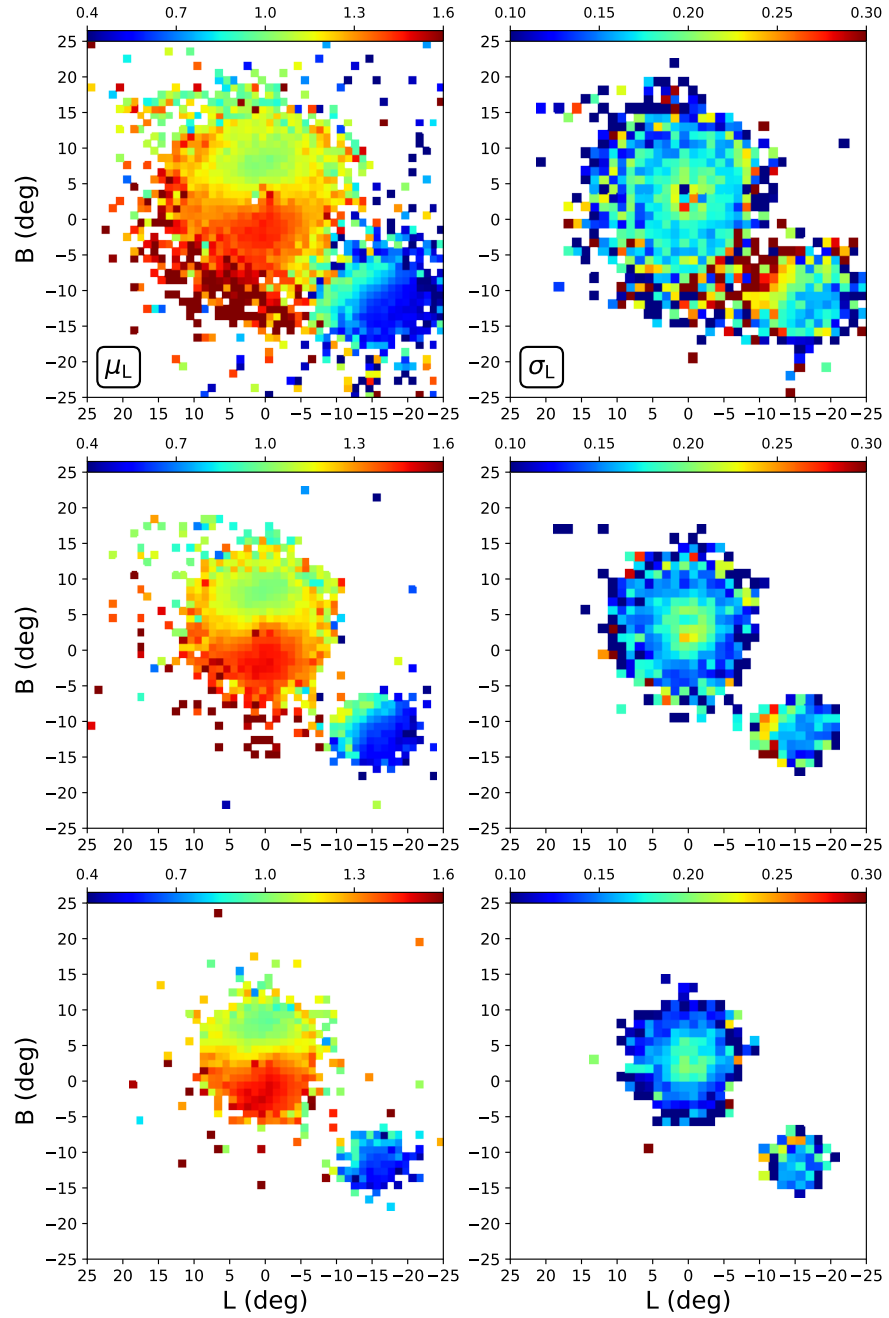


Figure 4.15: In the left-hand panels, we show reflex corrected mean μ_L in three metallicity bins M1, M2 and M3 from top to bottom. The right-hand panels show the respective dispersion in each pixel. The LMC displays a coherent rotation signal across all the metallicity bins, with the two outer arms appearing to lag somewhat behind the inner disc. The SMC shows a gradient in its motion, with the edge nearest the LMC displaying prominent motion towards the larger Cloud. The greatest dispersion in the motion of the giants appears in the metal-poorest bin at the interface between the Clouds – a region where we expect mixing of stellar populations and turbulent motion due to tidal interactions within the system. The central-most region of the LMC, in the vicinity of the bar and spiral arm, is mildly visible as a region of enhanced dispersion.

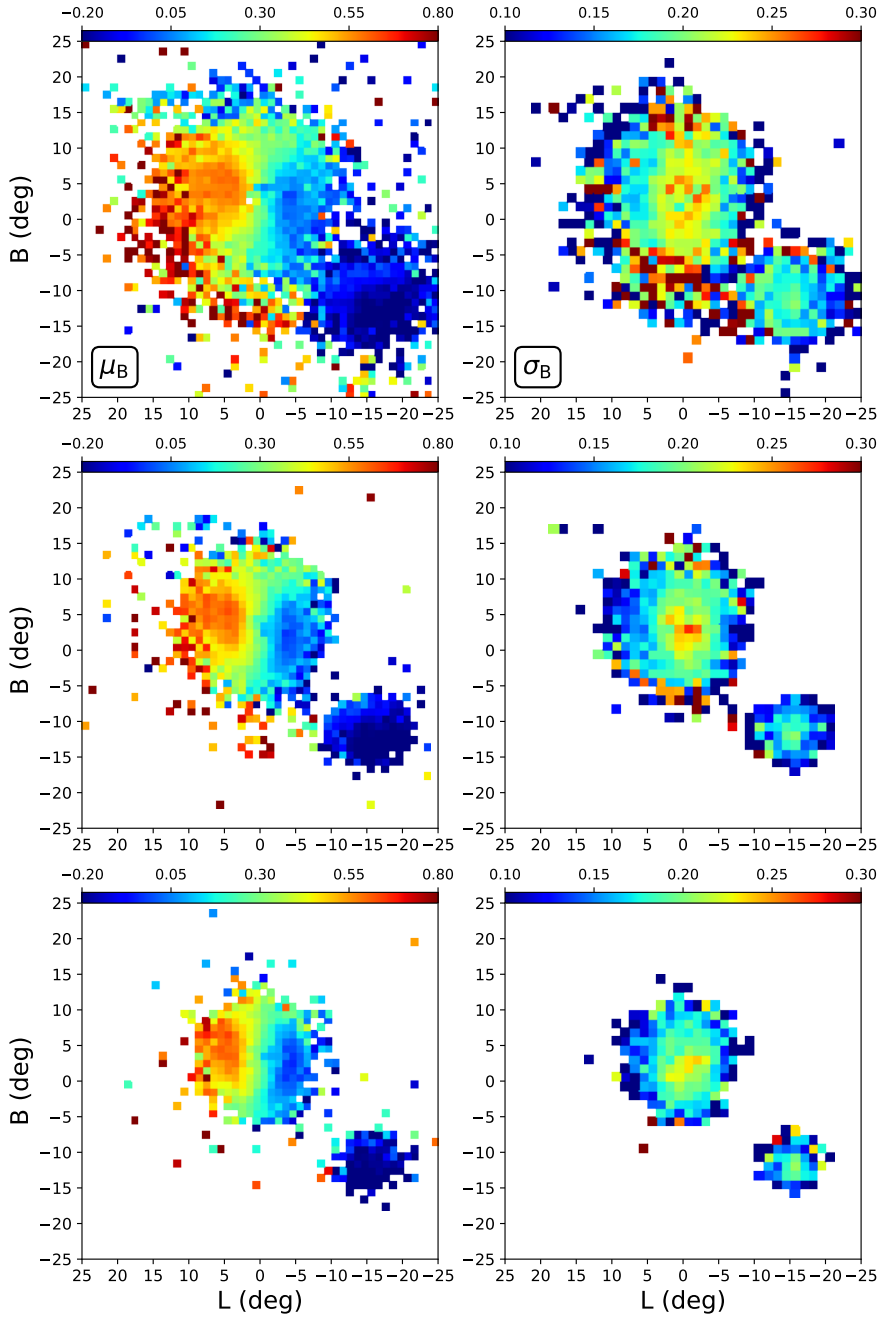


Figure 4.16: As in Fig. 4.15 but pixels now coloured by mean μ_B in the left panels and corresponding dispersions in the right panels. Again the dominant signal within the LMC is that of ordered rotation within the disc. The regions of most turbulent motion appear to exist at the bases of the two outer spiral like features. Through the inner regions of the disc, there also appears to be enhanced dispersion in this direction in comparison to that of μ_L . This is perhaps indicative of the tidal disruption endured by the LMC occurring mostly in the north-south regions where the majority of stellar substructure is observed (see Fig. 4.12).

more centrally concentrated metal-rich giants in M3. With respect to the motions of μ_B , the two main regions of significant heating appear in M1: at the base of the northern arm and another diametrically op-

posed to this in the southern region. Between these two points we also observe a vertical region of moderate dispersion in the LMC. That is, the dispersion in μ_B is greater along north-south direction than so along east-west. This may be a consequence of how the LMC has been perturbed by the SMC, as the majority of substructure observed in Sec. 4.3.1 is observed to lie in the northern and southern regions of the LMC disc. In each bin, the central bar region also displays a degree of enhanced dispersion, both in μ_L and μ_B , owing to the complex orbits hosted by galactic bars.

4.3.3 SMC shape and disruption

In Fig. 4.17, we show the density of stars lying around the SMC in Magellanic Bridge coordinates. The top left panel of the figure shows an ellipse fitted to an outer SMC density contour for which a mild ellipticity value of ~ 0.21 is obtained. Upon plotting a set of iso-density contours to the SMC giants in the top right panel, a distinctive twisting is seen, with the outer regions displaying an S-shape that is characteristic of a tidally perturbed system. Similar SMC morphology was observed by Belokurov et al. (2017) in the *Gaia* DR1 data. They found that the orientation of the S-shaped tails aligned conspicuously with the SMC's proper motions vector (relative to the LMC). Based on this, they designated the tail nearest to the LMC to be the trailing arm and that stretching towards the top right in Fig. 4.17 to be leading. In the lower panels of the figure, we have sliced the stars into two metallicity bins, symmetrically offset from the mean of our SMC metallicity distribution, so as to investigate the morphology of a relatively metal-poorer and metal-richer subset of SMC giants. The bottom left panel of Fig. 4.17 shows the stellar density of stars with $[\text{Fe}/\text{H}] < -1.25$ dex. These metal-poorer giants constitute a relatively diffuse, fluffy population with their outermost contour again showing the tidally symptomatic S-shape. The bottom right panel of the figure shows stars with predicted metallicities $[\text{Fe}/\text{H}] > -0.75$ dex and we show the same iso-density contours as in the metal-poor bin in black for comparison. The bulk of these metal-richer giants are confined to the most central regions, with little extent beyond $\sim 5^\circ$ of the Cloud centre. The red solid line traces the outer-most contour level of the metal-poorer bin which highlights that the outskirts of these relatively metal-richer giants also show symptoms of tidal disruption.

We consider the motion of the SMC in a simple fashion by first studying the spatially averaged proper motion components in Fig. 4.18. In the figure, we have set the origin of the coordinate system to the SMC centre. The pixels in the left (right) panel are coloured by

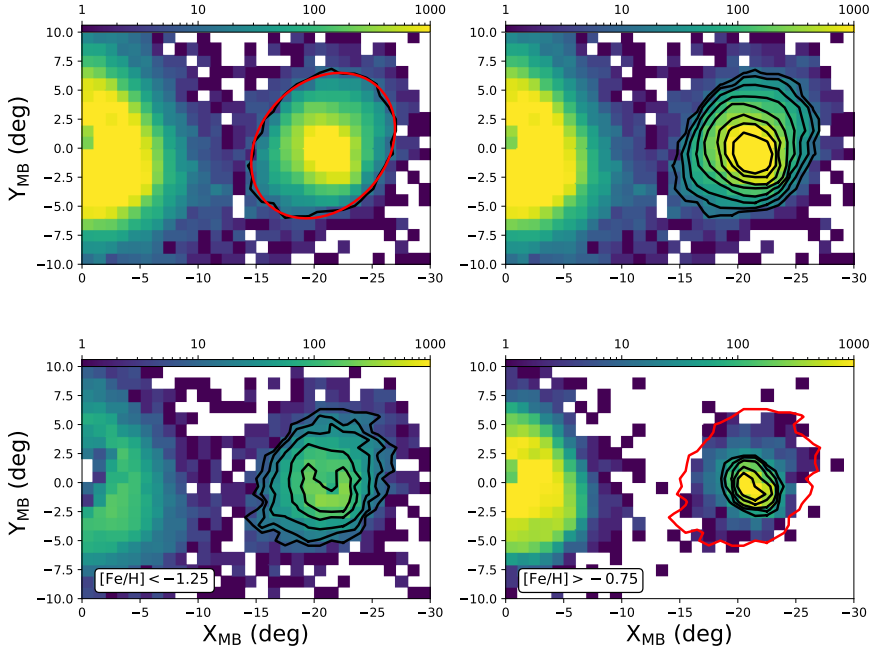


Figure 4.17: We show the stellar density of stars near to the SMC in Magellanic Bridge coordinates. *Top left*: Black solid line is an outer isodensity contour corresponding to 10 stars per square degree. We fit an ellipse to this contour, shown by the solid red line, whose ellipticity is mild at ~ 0.21 . *Top right*: We overlay logarithmically spaced isodensity contours on the SMC where a clear S-shape is apparent, reminiscent of tidal tails and consistent with the RR Lyrae SMC morphology observed by Belokurov et al. (2017). *Bottom left*: We now only show giants with predicted metallicities of $[\text{Fe}/\text{H}] < -1.25$ dex and contours trace pixels corresponding to the 2.5th, 5th, 10th, 25th and 50th percent contour levels for stars around the SMC. *Bottom right*: We only consider stars with $[\text{Fe}/\text{H}] > -0.75$ dex and trace the same contour levels with black solid lines. The red line corresponds to the outermost contour of the metal-poor SMC giants. Whilst the metal-rich giants are located much more centrally within the SMC, the outer regions still bear the signature of tidal disruption, indicating that the SMC has been significantly disrupted across a range of stellar populations.

mean $\mu_{X_{\text{MB}}}(\mu_{Y_{\text{MB}}})$, where we have centred the proper motion distributions around the bulk values for our SMC giants. We compute these based on the mean proper motions of giants lying within a 3° aperture of the SMC for which we obtain the SMC motion to be $(\mu_\alpha, \mu_\delta) = (0.65, -1.21)$ mas yr⁻¹, consistent with the recent determination of De Leo et al. (2020) and similar to that of Zivick et al. (2018). We note that the RA component of our measured proper motion is smaller than that of recent ground based measurements, with Niederhofer et al. (2018) measuring $(1.087 \pm 0.192, -1.187 \pm 0.008)$ mas yr⁻¹ from VMC data. We have also corrected the proper motions for the perspective expansion/contraction induced by the systematic centre

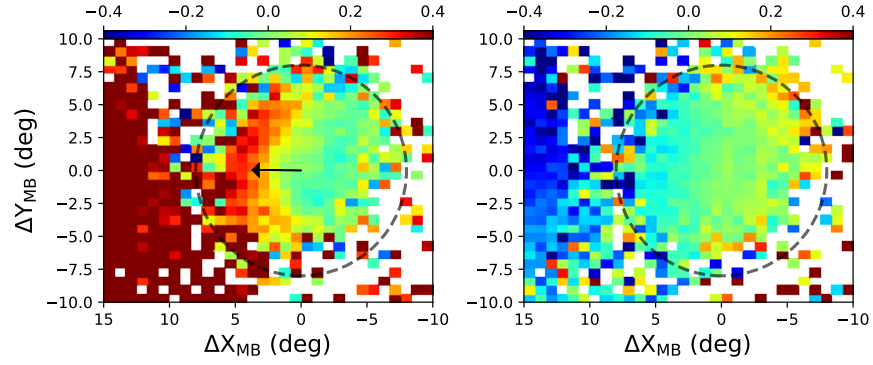


Figure 4.18: SMC giants shown in the Magellanic Bridge coordinate system. Pixels in the left (right) panel are coloured by mean proper motion along X_{MB} (Y_{MB}). The black arrow in the left panel points towards the centre of the LMC in this system. There is little sign of internal motion in $\mu_{Y_{MB}}$ with a distinct lack of rotation signal. In the left panel, a clear gradient is seen with SMC giants residing on the side nearest the LMC clearly being disrupted toward the larger Cloud.

of mass motion along the line of sight, following van de Ven et al. (2006). The left panel of the figure shows stars residing on the edge nearest the LMC (on the side of the trailing tail), being pulled directly towards the larger Cloud, with giants on the opposite leading edge of the dwarf showing little sign of such effects. Further, the motion of the giants in $\mu_{Y_{MB}}$ shows very little structure, with no indication of ordered rotation. Note that the faint vertical, banding structure seen in this panel is an artefact of the *Gaia* scanning law (see Gaia Collaboration et al. (2018b)). Thus, in the picture we present here, it would seem that the region of the SMC nearest the LMC, and coincident with the trailing arm, is being violently hauled towards the LMC. Recent detailed kinematic analysis of SMC RGB stars by De Leo et al. (2020) found the dwarf to be undergoing strong tidal disruption, with a net outward motion of RGB stars in the direction of the LMC. The giants display strong tangential anisotropy in their proper motion dispersions, right down to the SMC centre. Through comparison to a suite of N-body simulations of the Clouds in orbit about the MW, they argued this effect is due to unbound material lying in front of the SMC, distinct in their kinematics due to tidal stripping by the LMC. The proper motion analysis of Zivick et al. (2018) also showed the SMC to bear little sign of ordered rotation, but rather mean ordered motion radially away from the galaxy in its outer regions, consistent with heavy disruption.

The geometry of the SMC is complex, with a substantial line of sight depth. The north-eastern regions of the dwarf appear to lie

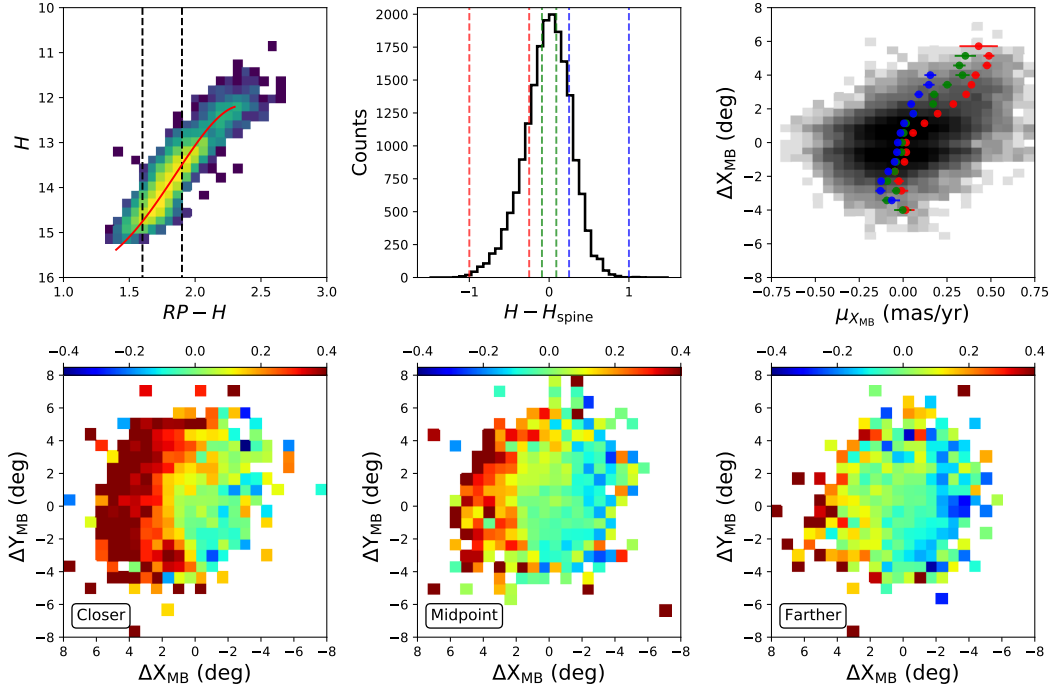


Figure 4.19: *Upper left*: CMD of SMC giants within a fixed metallicity range of $-1 < [\text{Fe}/\text{H}] < -0.9$ dex. The solid red line shows the polynomial fitted to the RGB in this bin, offsets from which are taken as a proxy for heliocentric distance. As described in the text, we have fitted such polynomials to SMC giants lying in the range $-1.2 < [\text{Fe}/\text{H}] < -0.5$ dex, over metallicity bins of width 0.1 dex. In computing the magnitude offset of our giants, we only consider those falling between the black hashed lines in the panel. *Upper middle*: We show the distribution of the magnitude offset of the SMC giants we select to analyse. The distribution is centred about zero and appears to be relatively symmetric about its peak, with a slight tail to negative values with these stars likely lying in front of the dwarf. Three bins in this distance proxy where selected to study the behaviour of giants lying in front of, coincident with and behind the centre of the SMC. The boundaries of these bins are shown by the red, green and blue hashed lines respectively. *Upper right*: Grey scale pixels show the logarithmic density of stars in their relative offset from the SMC centre as a function of their motion in $\mu_{X_{\text{MB}}}$. There is a distinct population of stars with excessive motion in $\mu_{X_{\text{MB}}}$ along increasing ΔX_{MB} , towards the LMC. The scatter points are coloured by their respective distances, and show mean proper motion values as a function of ΔX_{MB} . We see that it is those giants lying predominately in front of the SMC who exhibit such perturbed motion. This sequence becomes distinct in its behaviour very centrally, and rapidly evolves out to high values of $\mu_{X_{\text{MB}}}$ on increasing angular distance away from the SMC core. Error bars represent the standard error weighted by the Poisson noise in each bin. *Lower panels*: We show the SMC giants in the three distance bins, with the closet in the left panel and the most distant in the right. Pixel colours correspond to mean values of $\mu_{X_{\text{MB}}}$. This view of the SMC reinforces the result of the upper right panel, where we can clearly see the giants lying closer to use being those most heavily disrupted in the direction of the LMC.

closer to us than its western edge, as perceived through numerous stellar tracers including star clusters, red clump stars, Cepheid Variables and RR Lyrae (see e.g. Crowl et al., 2001; Deb et al., 2019, 2015; Haschke, Grebel, and Duffau, 2012; Muraveva et al., 2018; Scowcroft et al., 2016; Subramanian and Subramaniam, 2012). The SMC red clump analysis of Nidever et al. (2013) revealed a stellar structure lying eastward at ~ 10 kpc in front of the dwarf, a structure they interpret to have been tidally stripped and dragged toward the LMC/Magellanic Bridge region. Further to this, Subramanian et al. (2017) also found evidence for such a tidally stripped stellar structure in identifying a population of VMC red clump stars lying ~ 12 kpc in front of the main SMC body, tracing them from the direction of the Magellanic Bridge right down to $\sim 2.5^\circ - 4^\circ$ of the SMC centre. Very recently, Omkumar et al. (2020) identified this foreground red clump population in *Gaia*, tracing it from the inner 2.5° out to $\sim 6^\circ$ from the centre of the SMC.

We attempt to discern whether those giants whose on-sky motion is prominently towards the LMC in Fig. 4.18, are indeed lying closer to us as a result of tidal stripping by the larger Cloud. To do so we first select all SMC giants lying within the 8° aperture shown in Fig. 4.18. We then attempt to use each star's relative position within the observed CMD as a proxy for heliocentric distance. We first select stars for which we have predicted metallicities in the range of $-1.2 < [\text{Fe}/\text{H}] < -0.5$ dex, a region where there is sufficiently low bias and variance in our predictions that our estimates are reasonable. We then divide these giants into metallicity bins of width 0.2 dex and, considering each metallicity bin independently, fit a polynomial to the CMD of the giants, an example of which is shown by the solid red line in the upper left panel of Fig. 4.19. We choose to utilise the CMD of $\text{RP} - \text{H}$ vs H owing to the limited spread it displays at fixed metallicity and clear correlation in the CMD. We do this to minimise the broadening of the CMD due to the spread in metallicities of the SMC population. Utilising these polynomial fits as base 'spines', we compute the magnitude offset $\text{H} - \text{H}_{\text{spine}}$ for the selected SMC stars relative to the spine, such that stars with a negative (positive) offset are likely closer (farther) in distance. We only use stars which fall in the range $1.6 < \text{RP} - \text{H} < 1.9$, a region where the polynomial fits appear most reasonable and indicated in Fig. 4.19 by the vertical black hashed lines. The upper middle panel of Fig. 4.19 shows the distribution of this magnitude offset, where we see it to be centred at zero and approximately symmetric. The histogram shows a slight skew towards negative values, indicative of a higher relative proportion of SMC giants lying in front of the dwarf's core. We then

choose three bins in $H - H_{\text{spine}}$ initially centred at -0.3 mag, 0 mag and 0.3 mag, corresponding to $\sim \pm 10$ kpc in front of and behind the SMC, with the bin edges shown by the red, green and blue lines respectively. We have then allowed the widths of the two outer bins to be broad so as to roughly equalise the counts per bin ($\sim 3,000$) and to encompass stars lying in the tails of the distribution. The upper right panel of the figure shows the logarithmic density of our selected SMC stars' spatial coordinate X_{MB} as function of their motion in $\mu_{X_{\text{MB}}}$ (approximately) towards the LMC. From this density plot alone, there is a clear population of stars with high $\mu_{X_{\text{MB}}}$ values, deviating from the bulk beyond $\mu_{X_{\text{MB}}} \sim 2^\circ$. For the three distance bins we have defined, we show the mean proper motion binned over coordinate X_{MB} where a clear distinction is observed between the different distance bins. At a value of $X_{\text{MB}} \sim 2^\circ$, the stars most likely lying in front of the SMC display a sharp turn toward stronger motion in the LMC direction, dominating the population of stars exhibiting high values of $\mu_{X_{\text{MB}}}$. It therefore seems that the stars apparently being ripped from the SMC are predominately those lying closer to us, tracing the disruption of the trailing arm down to the inner regions of the SMC. On increasing heliocentric distance, the signal diminishes with little sign of a companion leading arm in the proper motions. The bottom panels of the figure are coloured by mean $\mu_{X_{\text{MB}}}$ where we show each of the three distance bins independently, with stars lying in front (behind) of the SMC in the left (right) panel and stars approximately at the SMC distance in the middle panel. The evolution of disruption on increasing distance is evident, with the closer stars being those most strongly dragged towards the LMC.

Thus, our interpretation is that the portion of the SMC in which we see strong motion towards the LMC in Fig. 4.15 and Fig. 4.18 consists largely of tidally stripped stars; stars that have been dragged outwards to closer heliocentric distances with their motions disrupted towards the larger Cloud, in effect forming a tidal tail trailing the SMC. We observe the signature down to angular separations of $\sim 2^\circ - 3^\circ$ from the SMC centre, indicative of heavy disruption of SMC stars lying along our line of sight. The fact that we do not observe a significant kinematic counterpart to the trailing tail lying beyond the SMC (i.e the leading arm) is somewhat at odds with simulation models of the Magellanic system. Whilst the majority of simulations in the literature aim to primarily trace the gaseous features of the Clouds, those of Diaz and Bekki (2012) do well in replicating the general properties of the Magellanic bridge region, with signs of stars being drawn eastward and towards the LMC (see Nidever et al., 2013, for discussion). However, these models also predict a 'counter-bridge', lying at large

heliocentric distances and predominately directly behind the SMC (see also Belokurov et al., 2017). Such a feature is predicted to be much more diffuse than its bridge counterpart which may indicate why no stellar detection has been made, either in this work or by Nidever et al. (2013) and Subramanian et al. (2017). Indeed, the counter-bridge, if present, may be so diffuse that it exists as a purely gaseous feature with minimal stellar counterpart (see Diaz and Bekki (2012)). Interestingly, however, in their analysis of SMC Cepheids, Ripepi et al. (2017) found evidence for a population of variables located toward the anticipated region of the counter-bridge.

We note that the stellar content of the SMC is complex, with stars spanning a range of metallicities and ages. In our above analysis, we have alleviated the effect that metallicity has in broadening the CMD. We cannot, however, account for the fact that giants of differing ages, at fixed metallicity and distance, will induce a magnitude offset in $H - H_{\text{spine}}$. Thus our distance proxy is rather a convolution of heliocentric distance, stellar age as well as reddening effects along the line of sight. Nonetheless, the results are tantalising, and appear in agreement with previous studies of SMC debris. As a consistency check, we applied our procedure to subsamples of LMC giants lying in the north-east and south-west regions of the disc. Given the viewing angles of the LMC, the north-east disc is lying at a closer heliocentric distance to us than the south-western edge. Thus, this should be detectable in our method; indeed we find a median magnitude offset of -0.12 mag for the giants located in the north-east and one of 0.03 mag for those in the south-west. These offset values are comparable to those of Li et al. (2016) who applied a similar method to M-giants in the LMC.

4.3.4 *Old stellar Bridge*

Given that we have found evidence for a population of stars within 8° of the SMC centre, lying in front of the dwarf, and displaying a kinematic signature of tidal disruption, a natural avenue of exploration is to now assess the stars lying directly in the inter-Cloud region. Historically, the detection of a continuous path between the Clouds in intermediate and old stellar populations has proved elusive. Utilising 2MASS and WISE photometry, Bagheri, Cioni, and Napiwotzki (2013) selected a sample of giants with ages ranging from ~ 400 Myr – 5 Gyr in the bridge region at low stellar density. The analysis of OGLE RGB and RC stars by Skowron et al. (2014) found little evidence of a coherent stellar bridge, but rather posited that the presence of evolved stellar populations in this region stems from overlap of the MC's ha-

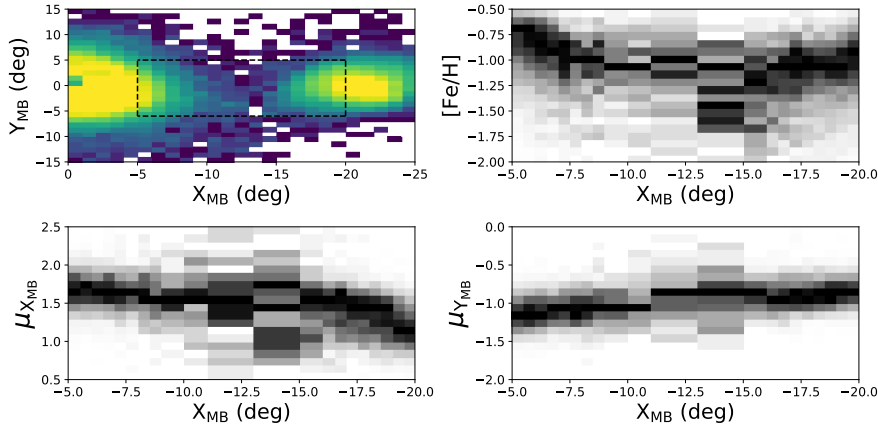


Figure 4.20: The top left panel shows the logarithmic density of giants in Magellanic Bridge coordinates. In the region between the Clouds, there exists a population of stars whose nature we would like to probe. On selecting stars falling within the black rectangle, we show their metallicity along the bridge in the top right panel. The column normalised density shows the evolution of giant metallicity upon the passage from the SMC to the LMC. Between the Clouds, it appears as if they are joined by a constant ridge at ~ -1 dex, a value consistent with both the outer regions of the LMC and the median value of all SMC giants. On moving outwards from the SMC, there appears to be two sequences: the ridge that connects to the LMC and a metal-poorer population that extends out to $X_{MB} \sim -13^\circ$. The lower two panels show the column normalised proper motions of the stars through the bridge region, with a relatively smooth transition between the Clouds being apparent. The motion along $\mu_{X_{MB}}$ shows a degree of dispersion that is consistent with Fig. 4.15.

los. They did, however, observe the diffuse structure of giants to lie predominately south of the young bridge. This is consistent with the findings of Belokurov et al. (2017) who, on selecting RR Lyrae out of the *Gaia* DR1 catalogue, were able to trace a continuous structure between the Clouds, offset by $\sim 5^\circ$ south of the young Magellanic Bridge. They argued this offset was formed under the scenario that both the gas and old RR Lyrae were stripped coevally from the SMC. The stripped gas was accosted by the hot gas of the Milky Way corona in the form of ram pressure, essentially pushing it back and forming the offset. The spectroscopic study of inter-Cloud red giants by Carrera et al. (2017) found the chemistry and kinematics of their intermediate aged sample to be consistent with that of an tidally stripped SMC population, adding weight to the notion that an older stellar bridge exists in some form. Subsequently, the deep Dark Energy Camera imaging of Mackey et al. (2018) and the highly-pure giant sample of Belokurov and Erkal (2019) revealed the presence of a tangled mix of ancient stellar populations between the Clouds and confirming the earlier discovery of Belokurov et al. (2017).

In the top panel of Fig. 4.20, we show the stellar density of our giants in MB coordinates, with the black dashed box indicating the selection of stars lying in the bridge region. In the panel below, we show the distribution of metallicity of these giants progressively through the bridge. On moving through the outer LMC disc, the metallicity shows a steady decline, with the SMC profile remaining relatively flat out to $X_{\text{MB}} \sim -15^\circ$, just beyond which appears to lie a metal-poor sample of stars with $[\text{Fe}/\text{H}] \sim -1.5$ dex. Moving through the region of $-15^\circ < X_{\text{MB}} < -10^\circ$, the metallicity structure becomes more complex and difficult to discern owing to the low stellar density in this region. Interestingly, however, there does appear to be a continuous ridge of constant metallicity, $[\text{Fe}/\text{H}] \sim -1$ dex, running through this region, connecting to the outer edge of the LMC out toward $X_{\text{MB}} \sim -15^\circ$. It is noteworthy that the metallicity along this ridge is consistent with the mean value of SMC giant's lying within the inner 4° of the dwarf, as well as that of the outer regions of the LMC. The lower two panels of the figure trace the proper motions through the bridge region, with $\mu_{Y_{\text{MB}}}$ showing a relatively coherent structure that smoothly links the motions of the SMC to the LMC. The motion in $\mu_{X_{\text{MB}}}$ is less well defined through the bridge region, with greater scatter about the general trend. This is consistent with the high level of dispersion we see in the lower left panel of Fig. 4.15 at the interface of the two Clouds, as well as our results from Section 4.3.3. The signature of a flow of stars through the bridge region is consistent with the findings of Zivick et al. (2019) whose proper motion analysis of red giants through the bridge closely resembles our findings (see their Fig. 8). The relatively complex metallicity distribution in the inter-Cloud region, alongside the high dispersion in $\mu_{X_{\text{MB}}}$ render it difficult to exactly discern the origin of the stars lying in this region. Further to this, the MB region is composed of giants tending toward the metal poor end of our sample where our regression predictions are inherently more uncertain. This adds to the difficulty in drawing firm conclusions on the metallicity distribution through the MB. It is, however, highly likely that the population of stars in this region are a mixture of both LMC and SMC giants. The origin of LMC debris in the bridge could be attributed to the effect of Milky Way tides acting on the larger dwarf, with the N-body simulation of Belokurov et al. (2017) and Belokurov and Erkal (2019) demonstrating that such an effect can quite easily strip LMC debris to align well with the old stellar bridge.

In Fig. 4.21, we show the sample of *Gaia* DR2 RRL described in Sec. 4.1 for which we are afforded heliocentric distance estimates. The left panel of the figure shows the Clouds in MB coordinates with pixels coloured by mean heliocentric distance, where we see RRL lying

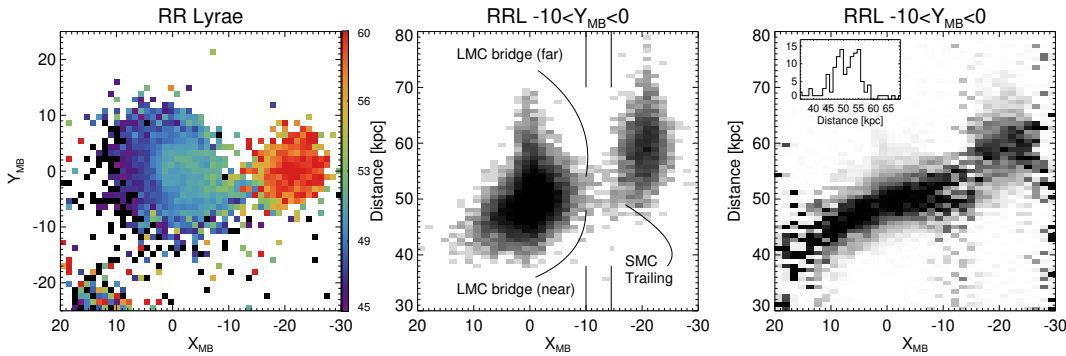


Figure 4.21: We show the *Gaia* DR2 RR Lyrae whose selection was described in Sec. 4.1. *Left*: Pixels are coloured by mean RRL heliocentric distance. A gradient is observed across the face of the LMC disc owing to its inclination. We also see RRL residing in the eastern portion of the SMC to lie at closer heliocentric distances. Between the Clouds, we see the old stellar bridge with stars lying at distances consistent with both Clouds. *Middle*: RRL distance is shown along X_{MB} for stars lying in the slice of $-10^\circ < Y_{\text{MB}} < 0^\circ$. The SMC morphology is cigar-like, stretching along our line of sight. There appears to be two distinct structures lying between the Clouds at heliocentric distances of ~ 50 kpc and ~ 55 kpc. The inset panel shows the distance distribution for RRL lying in the slice $-14^\circ < X_{\text{MB}} < -10^\circ$ in which we observe a bi-modality, with the two peaks associated with the dual structures stretching between the Clouds.

at distances consistent with both the LMC and SMC in the old stellar bridge. Selecting RRL in the slice of $-10^\circ < Y_{\text{MB}} < 0^\circ$, we show the distance distribution of these stars along X_{MB} , revealing three interesting structures that pervade through the bridge region. First, two distinct filaments peel away from the LMC’s western edge; one sits at ~ 50 kpc, while the other some 5 kpc farther away. The closer RR Lyrae sequence stretching from the LMC meets half way with the trailing tail of the SMC, emanating from the near end of the dwarf in the direction of the LMC. This appears to be consistent with our findings in Sec. 4.3.3, where we saw evidence for (likely unbound) giants lying in front of the SMC and kinematically disrupted towards the larger Cloud. The interpretation of the nature of the second (more distant) part of the bifurcated structure attached to the LMC at ~ 55 kpc is more challenging. Are these LMC stars that have been stripped towards the SMC or vice versa? In the right panel, we show a column-normalised version of this representation. The distance gradient as mapped by the RR Lyrae appears to run almost uninterrupted from the east side of the LMC to the far side of the SMC. This is akin to the findings of Wagner-Kaiser and Sarajedini (2017) who observed a smooth transition in the distances of OGLE RR Lyrae between the Clouds. In this view of the line-of-sight distance distribution, the bifurcation in the LMC side of the old bridge is even more evident

(also see the 1D slice shown in the inset). Whilst the exact nature of the old bridge is still unclear, it appears from the RRL that both Clouds are joined by a population of stars over heliocentric distance, whose nature is likely dual, with debris having been stripped from both galaxies. The metallicity distribution of our giants between the Clouds supports this notion; giants with a wide range of metallicities appear to inhabit this region with two main structures apparent. We observe a metal poor continuation of the outer SMC, appearing to extend out to $X_{\text{MB}} \sim -15^\circ$, consistent with the SMC RRL we observe peeling away from the dwarf's trailing tail. Second to this is the ridge of $[\text{Fe}/\text{H}] \sim -1$ dex that looks to span far into the bridge region, where from the RRL we see such LMC debris exists. We have seen the proper motion distribution of the giants to be turbulent through the bridge region, as stars from both Clouds are being stripped and thrust towards each other in a complex way.

4.4 SUMMARY

We have amassed a sample of Magellanic red giants, drawn from *Gaia* DR2, demonstrating the ability to predict accurate photometric metallicities for such stars utilising machine learning methods. In doing so, we have produced some of the largest scale metallicity maps of the Clouds to date. Utilising our metallicity predictions in conjunction with the proper motions of our giants, we produced a chemokinematical mapping of the Magellanic system, which shows it to be fraught with intricacy as a consequence of its severe disruption.

We observe negative metallicity gradients on moving outwards through both Clouds. In modelling the LMC as a thin inclined disc, we infer a metallicity gradient of -0.048 ± 0.01 dex/kpc, a value in good agreement other estimates in the literature (see e.g. Choudhury, Subramaniam, and Cole, 2016; Cioni, 2009). Centrally, the profiles flatten as this region becomes dominated by the metal-rich bars. Various asymmetries are present in the metallicity profiles when considering different regions of each galaxy. Such features are readily visible in the LMC, where we observe the stellar bar, main spiral arm and diffuse regions of metallicity enhancement in the disc. The most striking example is perhaps the southern spiral arm feature seen in the inner regions, a metal-rich component appearing to emanate from the western end of the bar and wrapping clockwise through the LMC disc. Spatially, this spiral-like feature is coincident with the stellar overdensity observed by Choi et al. (2018b) and it is very likely that historic LMC-SMC interactions have given rise to this intermediate aged stellar structure. We further observe a northern arc-like region of rela-

tive metal enhancement, coincident with the stellar feature observed by Besla et al. (2016) in their optical images of the LMC periphery. In their simulations of the Magellanic system, they concluded it is the repeated close encounters with the SMC that primarily seeds such one-sided stellar structures in the northern portion of the LMC, with the tidal field of the SMC alone able to induce one-armed spirals within the larger Cloud.

On slicing the Clouds by metallicity, we observe global evolution in the morphology of the two galaxies. Naturally, the majority of outer substructure is observed in the more metal-poor giants, with those that are metal-richer residing much more centrally in both instances. The outer northern and southern thin spiral-like arms in the LMC are again observed to rotate with the Cloud, lagging in their orbits, as was first noted by Belokurov and Erkal (2019). The metal poor SMC giants located nearest to the LMC are hot in their motions with high dispersion observed at the interface between the two dwarfs, a region where we naturally expect a mixture of stars originating from both the LMC and SMC. Further to this, in Fig. 4.15, we observe the eastern portion of the SMC to bear increased motion in the direction of its larger counterpart. On studying the iso-density contours of the SMC, we observe them to display the S-shape signature characteristic of tidal disruption, a feature that appears to persist at all metallicities. We probe the SMC disruption further through a simple consideration of the proper motions of our giants. Utilising each star's relative position in the CMD as a proxy for heliocentric distance, we ascertain that it is those giants likely lying closer to us that exhibit such fervent motion towards the larger Cloud. Our interpretation is that we are observing a tidal tail trailing the SMC, projected along our line of sight, that has been stripped away from the dwarf's core by the LMC. We trace this disruption down to the inner $\sim 2^\circ - 3^\circ$ of the SMC, consistent with the foreground red clump population observed by Subramanian et al. (2017) and traced down to the inner ~ 2 kpc of the dwarf (see Nidever et al., 2013, also). In essence, this stripped population constitutes the start of the old stellar bridge emanating away from the SMC towards the LMC. We do not observe any leading counterpart, and it may simply be that we do not possess enough distant giants in our sample to do so, as such debris is expected to lie ~ 20 kpc directly behind the SMC (Diaz and Bekki, 2012).

Finally, we consider giants lying in between the Clouds in the Magellanic Bridge region. We, for the first time, trace the metallicity distribution through the region and find its nature to be dual; we observe a metal-poor component of $[\text{Fe}/\text{H}] \sim -1.5$ dex lying just beyond the eastern edge of the SMC, with a continuous metallicity ridge of ap-

proximately -1 dex appearing to span much of the distance between the two Clouds. We further consider the *Gaia* DR2 RR Lyrae around this region, with the added benefit that we can easily estimate the heliocentric distances for such stars. Two thin appendages appear to link the Clouds, lying at distances of ~ 50 and 55 kpc. The SMC morphology appears cigar-like, with stellar debris appearing to peel away from the near-end of the dwarf, warping towards the LMC. It also appears that a population of LMC stars extend into the bridge region, indicating that the old stellar populations inhabiting the bridge are a mixture of stripped stars from both the LMC and the SMC.

CONCLUSIONS AND OUTLOOK

In this thesis I have studied Galactic structure in both the Milky Way and the Magellanic Clouds. For the former, I have utilised O-rich Mira variables on a scale, to the knowledge of this author, not done so before in the astronomical literature. The works published in Grady, Belokurov, and Evans (2019) and Grady, Belokurov, and Evans (2020) form the basis of Chapters 2 and 3 in this thesis. With respect to the Clouds, I have produced large scale metallicity maps from photometric information which, when coupled with *Gaia's* proper motion measurements, provides the basis for a chemo-kinematic analysis of the system. The work published in Grady, Belokurov, and Evans (2021) forms the basis for Chapter 4 of this thesis.

5.1 CONCLUSIONS

The goal of Galactic research is to understand the origins of the Milky Way; how has it evolved from the cosmological initial conditions that seeded it, through to its current state today? *Gaia* has provided us with astrometric measurements for over a billion stars, information on both how far away stars are from us and how they are moving through space; a Galactic census. Modern spectroscopic surveys provide us with abundance data for stars in the Galaxy, allowing a glimpse into the chemical enrichment history of the Milky Way. Constraints on the ages of stars in the Galaxy are invaluable; in slicing the Milky Way chronologically, one can build a picture of its assembly and test predictions of Galactic models in a temporal fashion. Many studies of Galactic structure have limited ability to age date their stellar samples, even on a relative basis, and largely rely on chemo-dynamical analyses, itself a powerful tool. The study of Galactic structure as a function of stellar age is a key ingredient to understanding the history of formation, dynamics and enrichment.

The first two chapters of this thesis are directly concerned with the view of the Galaxy as a function of stellar age. In Chapter 2 I assembled a catalogue of O-rich LPVs, mostly Miras, from the CRTS and ASAS-SN data-sets. Under the interpretation that the pulsation periods of such stars correlates inversely with their stellar ages, as has been observed kinematically (Feast and Whitelock, 2000b) and in cluster associations (see Fig. 2.7), I trace age gradients through the

Galactic disc and out into the halo. On increasing radius through the disc the period profile is observed to show a negative gradient consistent with the notion of inside-out disc formation. The transition to the halo is marked by a plummeting in the profile with a population of relatively younger stars observed far from the plane, likely kicked to such heights by some disc perturbation. The overall theme of this chapter is to establish O-rich LPVs and Miras as useful Galactic tracers. For these we can obtain accurate distance estimates, observe them to great distances, owing to their intrinsic brightness, and exploit the ability to stratify the sample by relative age based on their observed periods.

Developing on these ideas I utilise the *Gaia* DR2 LPV data-set in Chapter 3, extracting a clean sample of Miras for which *Gaia* obtained period estimates. Miras pervade through the Galactic disc and bulge and I model the stellar density profiles of both components simultaneously. Afforded the ability to slice the sample by relative age, I chronologically dissect the disc and bulge at once for the first time. The picture of inside-out disc formation in the Miras is evident again; the older stars form a stubby disc, radially constricted and vertically extended. On increasing period the disc settles into a thinner and more radially extensive structure. The bulge is modelled well by a triaxial boxy distribution inclined at a bar angle of $\sim 21^\circ$. Interestingly, the most ancient Miras do not appear to trace the bar, echoing previous results of metal poor RR Lyrae in the bulge region. Indeed it is only the youngest Miras that are observed to show the characteristic X-shape of a bar having buckled.

With respect to the Clouds, the discussion in Sec. 1.4, and references therein, highlights the fact that the influence of the satellites on the Milky Way is indeed non-negligible. That is, to understand our Galaxy we must also understand the nature of the Magellanic Clouds. Furthermore, they represent an ideal laboratory to study interacting dwarf galaxies; a great deal of substructure has been observed within the system, largely attributed to their self interaction. Dedicated spectroscopic surveys are ongoing, e.g. The Magellanic Edges Survey (Cullinane et al., 2020), to ascertain the nature of such substructures observed in the periphery of the LMC. The Clouds are important for detailed study of how interactions affect galaxy evolution.

In Chapter 4 I study the chemo-kinematics of the Magellanic Clouds. In combining photometry from *Gaia*, 2MASS and WISE for a sample of Magellanic red giants, I estimate photometric metallicities for them, calibrated by APOGEE spectroscopic measurements. A shallow, radial metallicity gradient is confirmed in the LMC. Residual to this is

much of the diffuse substructure known to reside in the Cloud, seen to correlate with regions of relatively enhanced metallicity. Combining my metallicity estimates with *Gaia* proper motion measurements I observe the SMC to be disrupting, with giants lying in front of the dwarf showing strong apparent motion towards the larger Cloud. The the inter-Cloud region shows complex metallicity structure with the *Gaia* DR2 RRL further indicating the old stellar bridge region is populated with a mixture of stripped stars.

5.2 OUTLOOK

Much of the work undertaken in this thesis has been done so in the era of *Gaia* DR2. The third data release from *Gaia* is expected in the first half of 2022 with the sample of classified variables set to be an order of magnitude greater (millions) than currently available. Furthermore, the release of the *Gaia* EDR3 data-set occurred on 3rd December 2020 now providing improved astrometry and photometry for ~ 1.8 billion sources. The advancement in our Galactic understanding continues to progress with the ever increasing precision and accuracy provided by *Gaia*.

An interesting future project would be the search for stars that have migrated between the Magellanic Clouds. It is known that the Clouds have experienced historic close encounters, though the exact details are still to be ascertained, and the degree to which stars are accreted between the Clouds is not well understood. The kinematically distinct and metal poor sample of LMC giants identified by Olsen et al. (2011) were postulated to be such a population of stars, those having been accreted from the SMC. *Gaia* provides good proper motion measurements for bright giants in the Clouds. It is yet to be determined whether it is possible from the apparent motion of stars alone (i. e. without radial velocity measurements) to identify kinematic outliers within the system. One could devise an algorithm whereby the proper motions of individual stars are compared to the local bulk motion in the LMC, searching for those differing significantly. In Chapter 4 I demonstrated that one can obtain accurate photometric metallicity estimates for Magellanic giants. In principle one could combine such estimates with proper motion measurements and use a classifying scheme, e.g. a mixture model, to hunt for stars in the LMC that are distinct in their motion and chemistry. Such a line of inquiry is interesting in the perspective of constraining the historic encounters between the Clouds. For example, the simulations of Besla et al. (2012) show the degree of accretion of SMC debris onto the larger Cloud to

be dependent on the number of passages the smaller dwarf has completed about the LMC.

An important aspect in the study of Mira variables is the calibration of the period-age relation. An empirical investigation could be conducted utilising the velocity dispersion relations provided by Sharma et al. (2020), functions separable in stellar age, metallicity, angular momentum and height above the plane. Currently only ~ 650 high amplitude LPVs with radial velocity measurements exist in the *Gaia* DR2 catalogue. Future data releases should bolster this number providing a sample of LPVs with full velocity information and whose distances can be accurately predicted from the Mira period-luminosity relation or, for nearby stars, from their parallaxes. One could then probe the velocity dispersion of the sample as a function of pulsation period and attempt to calibrate the latter with stellar age. This would immediately add large value to Miras as tracers of Galactic structure as one could then, based purely on their measured pulsation period, age date swathes of the Galaxy and potentially do so in the Magellanic Clouds and Sgr dwarf galaxy too.

A note of consideration regarding Miras is their ability to act as cosmic distance indicators. The successor to Hubble, the James Webb Space Telescope, will observe the sky in the infra-red, the domain in which Miras shine their brightest. Thus they have the potential to act as independent anchors of the Type Ia supernovae distance scale. Miras are evolved stars and visible in the haloes of galaxies and thus can be observed across all galaxy types with varying degrees of on-sky inclinations. They should act to bolster the sample of Type Ia supernovae calibrators, with Huang et al. (2019) recently demonstrating the feasibility of utilising Miras in such a way.

Another, more exploratory, avenue of investigation would be to assess how feasible it is to attain photometric distance estimates for red giants; a regression problem in predicting the absolute magnitude of RG's from their photometric colours. Red giants are numerous throughout the Galaxy, produced in populations of varying metallicity and stellar age. Studies such as mapping MW halo substructure in three dimensions would be greatly aided by such distance estimates. An initial investigation into this subject was conducted wherein a sample of local giants, with good parallaxes, was paired with the Magellanic giant sample of Belokurov and Erkal (2019) and the Sgr dwarf giant sample of Vasiliev and Belokurov (2020). Cross-matching these with the 2MASS survey yields a training set with broad photometric coverage and reasonable distance estimates. A regression model was trained on this data to predict M_{K_s} . Vasiliev, Belokurov, and Erkal (2021) provide a sample of Sgr giants pervading through

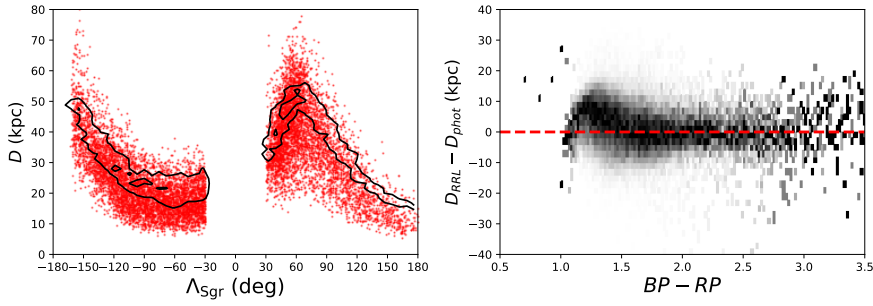


Figure 5.1: *Left*: Red markers show the photometric heliocentric distance estimates of giants along the Sgr stream. Each giant has a corresponding distance estimate from nearby RRL as provided by Vasiliev, Belokurov, and Erkal (2021). The black contours delineate the stream with these RRL distances assigned to the giants. *Right*: Column normalised distance offset as a function of *Gaia* $BP - RP$ colour; there is a portion of giants for which there is little bias in the photometric distance method.

both tidal arms associated with the dwarf, painted with distances of nearby RRL. In Fig. 5.1 I show the results of such a preliminary analysis where, in the left panel, the red markers delineate the photometric distance estimates assigned to the giants across the stream. The right panel shows the column normalised offset in these prediction, as compared to those of the nearby RRL, as a function of *Gaia* $BP - RP$ colour. Whilst preliminary, the result is encouraging with a relatively small degree of bias present; it may be plausible that such methods could be employed to study halo structure out to large distances.

APPENDIX

A.1 MIRA CLUSTER ASSOCIATIONS

Mira RA (deg)	Mira Dec (deg)	Cluster RA (deg)	Cluster Dec (deg)	Cluster Name
75.3828	-68.6918	75.3729	-68.7117	KMHK448
76.1248	-69.3232	76.1625	-69.3409	NGC1830
76.2188	-69.4008	76.2779	-69.4042	NGC1835
76.4310	-69.1061	76.3887	-69.1164	HS112
76.4538	-68.6334	76.3987	-68.6283	NGC1836
76.6068	-68.7011	76.6079	-68.7033	HS117
77.4052	-69.0758	77.4554	-69.0842	HS141
77.5206	-69.3357	77.4917	-69.3531	SL276
77.5597	-69.1029	77.5254	-69.0888	OGLE-LMC0169
78.2803	-69.0481	78.2646	-69.0505	HS177
78.7717	-68.9685	78.7750	-68.9792	NGC1885
79.2006	-70.2146	79.1558	-70.2108	BSDL1102
79.3180	-69.3416	79.3417	-69.3381	NGC1903
79.3224	-69.3485	79.3417	-69.3381	NGC1903
79.4868	-69.6439	79.4550	-69.6441	H2
79.7282	-69.0660	79.6737	-69.0796	H88-269
80.0841	-69.5624	80.0983	-69.5851	SL402
80.4405	-69.9429	80.3629	-69.9504	NGC1939
84.6330	-68.7837	84.5917	-68.7807	SL629
87.0700	-71.4776	87.0483	-71.4808	NGC2121

Table A.1: LMC pairs of clusters and Mira shown in Fig. 2.7. We provide heliocentric coordinates and cluster names for each of the pairings. Coordinates are given to 0.0001° to show the angular separations.

Mira RA (deg)	Mira Dec (deg)	Cluster RA (deg)	Cluster Dec (deg)	Cluster Name
271.5503	-27.8131	271.5269	-27.7507	NGC6540
268.4649	-32.3238	268.4760	-32.4662	ESO 456-09
232.0031	-50.7856	231.9916	-50.6716	NGC5927
273.4691	-28.6639	273.5120	-28.6342	vdBergh-Hagen 261
215.5882	-71.9603	215.4072	-72.0828	FSR 1667
247.3279	-35.3601	247.1580	-35.3527	Terzan 3
262.9789	-39.8512	262.8952	-39.8401	FSR 1758
264.8100	-35.6040	264.6566	-35.6506	ESO 393-12
247.3693	-27.9688	247.2783	-27.9610	FSR 1761

Table A.2: As Table A.1, but for the Milky Way Mira cluster pairs in Fig. 2.7

A.2 DENSITY PROFILE LIKELIHOOD

For stars observed at position vectors \mathbf{r}_i and for some density profile model $\rho(\mathbf{r}|\Theta)$ for parameter vector Θ over volume V , we seek the likelihood of observing the data. Splitting the observed volume into a grid of pixels, the expected number of points observed in the i^{th} pixel is:

$$N_i = \rho(\mathbf{r}_i|\Theta) \delta V \quad (\text{A.1})$$

Denoting the number of observed data points in the i^{th} pixel as x_i , the associated probability of such an observation is given by the Poisson distribution as:

$$P(x_i|N_i) = \frac{N_i^{x_i} e^{-N_i}}{x_i!} \quad (\text{A.2})$$

Thus the likelihood of observing the total data over all pixels is:

$$\mathcal{L} = \prod_i \frac{N_i^{x_i} e^{-N_i}}{x_i!} \quad (\text{A.3})$$

In the limit that $\delta V \mapsto 0$, $x_i \mapsto 1$ if a star is observed is at the associated position and $x_i \mapsto 0$ if absent. As such, the total likelihood can be split over pixels that are occupied and empty pixels as:

$$\mathcal{L} = \prod_i e^{-N_i} \prod_j N_j e^{-N_j} \quad (\text{A.4})$$

where the product over i corresponds to empty pixels and that over j to occupied pixels. Taking the natural logarithm in this limit then yields:

$$\ln \mathcal{L} = - \int_V \rho(\mathbf{r}|\Theta) dV + \sum_i \ln \rho(\mathbf{r}_i|\Theta) \quad (\text{A.5})$$

with the right hand summation occurring over all observed data points. Any selection function can be incorporated into the normalising integral above.

A.3 MODEL M2 RESIDUALS

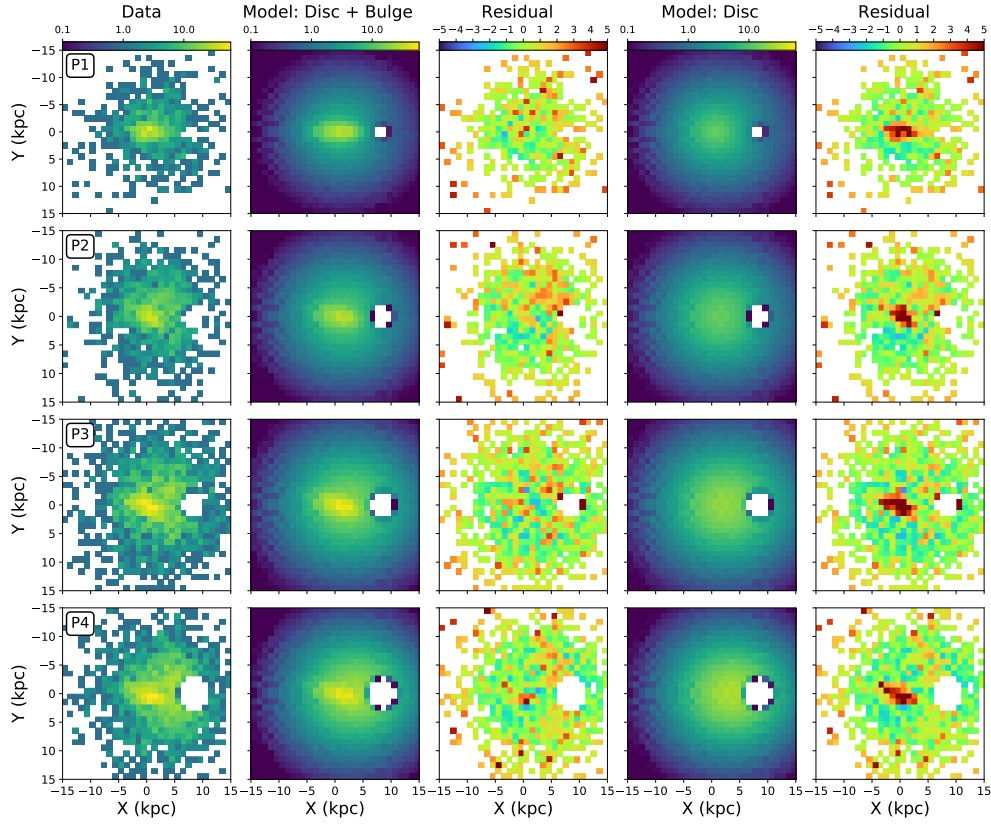


Figure A.1: Comparison of our Mira sample in each period bin with model M2, as in Eq. 3.7, in Galactocentric (X, Y) projection. We show residuals, weighted by Poisson noise, for two instances: that with a disc + bulge and that for a disc component only. In the latter case, the bulge residual is stronger than in Fig. 3.9 owing to the flattening of the model.

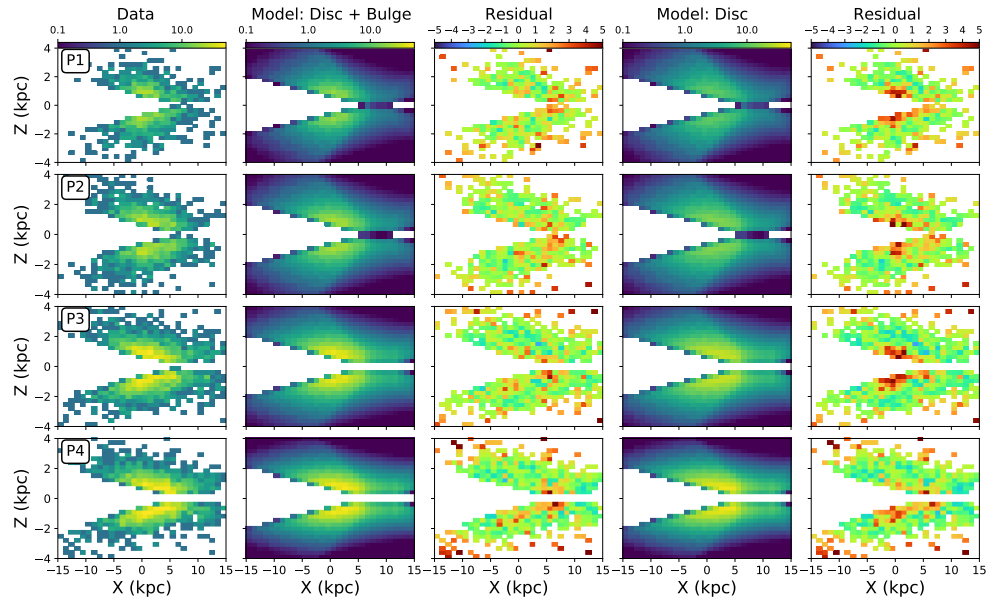


Figure A.2: Equivalent to Fig. A.1 but in Galactocentric (X, Z) projection.

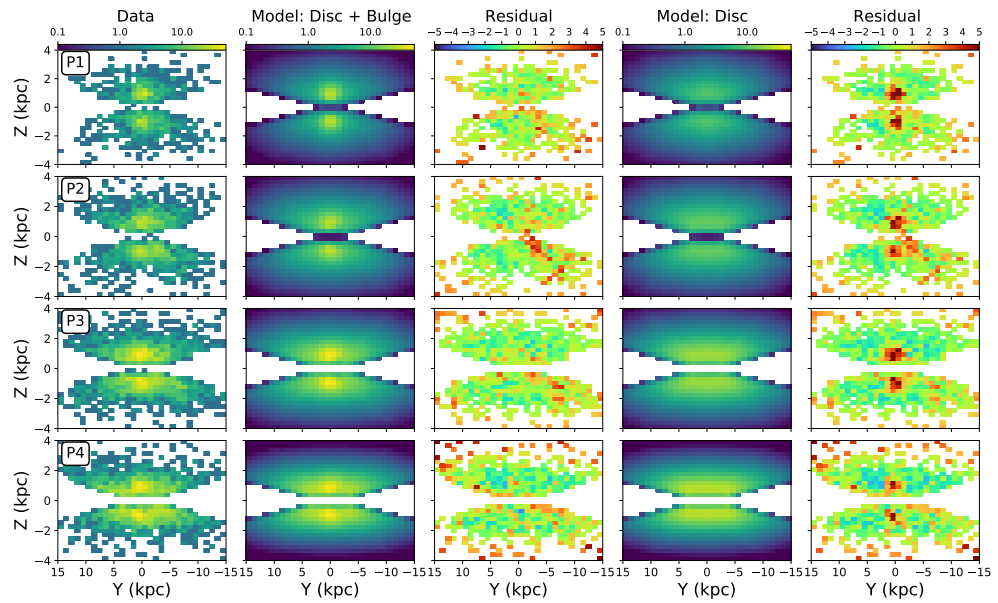


Figure A.3: Equivalent to Fig. A.2 but in Galactocentric (Y, Z) projection.

BIBLIOGRAPHY

- Adibekyan, V. Z., N. C. Santos, S. G. Sousa, and G. Israelian (Nov. 2011). “A new α -enhanced super-solar metallicity population.” In: *A&A* 535, L11, p. L11. DOI: [10.1051/0004-6361/201118240](https://doi.org/10.1051/0004-6361/201118240). arXiv: [1111.4936](https://arxiv.org/abs/1111.4936) [astro-ph.GA].
- Adibekyan, V. Z., S. G. Sousa, N. C. Santos, E. Delgado Mena, J. I. González Hernández, G. Israelian, M. Mayor, and G. Khachatrian (Sept. 2012). “Chemical abundances of 1111 FGK stars from the HARPS GTO planet search program. Galactic stellar populations and planets.” In: *A&A* 545, A32, A32. DOI: [10.1051/0004-6361/201219401](https://doi.org/10.1051/0004-6361/201219401). arXiv: [1207.2388](https://arxiv.org/abs/1207.2388) [astro-ph.EP].
- Amôres, E. B., M. López-Corredoira, C. González-Fernández, A. Moitinho, D. Minniti, and S. Gurovich (Nov. 2013). “The long bar as seen by the VVV Survey. II. Star counts.” In: *A&A* 559, A11, A11. DOI: [10.1051/0004-6361/201219846](https://doi.org/10.1051/0004-6361/201219846). arXiv: [1308.6022](https://arxiv.org/abs/1308.6022) [astro-ph.GA].
- Amôres, E. B., A. C. Robin, and C. Reylé (June 2017). “Evolution over time of the Milky Way’s disc shape.” In: *A&A* 602, A67, A67. DOI: [10.1051/0004-6361/201628461](https://doi.org/10.1051/0004-6361/201628461). arXiv: [1701.00475](https://arxiv.org/abs/1701.00475).
- An, J. H. et al. (July 2004). “The POINT-AGAPE Survey - I. The variable stars in M31.” In: *MNRAS* 351, pp. 1071–1098. DOI: [10.1111/j.1365-2966.2004.07853.x](https://doi.org/10.1111/j.1365-2966.2004.07853.x). eprint: [astro-ph/0401374](https://arxiv.org/abs/astro-ph/0401374).
- Antoja, T. et al. (Sept. 2018). “A dynamically young and perturbed Milky Way disk.” In: *Nature* 561.7723, pp. 360–362. DOI: [10.1038/s41586-018-0510-7](https://doi.org/10.1038/s41586-018-0510-7). arXiv: [1804.10196](https://arxiv.org/abs/1804.10196) [astro-ph.GA].
- Arentsen, A. et al. (Jan. 2020). “The Pristine Inner Galaxy Survey (PIGS) I: tracing the kinematics of metal-poor stars in the Galactic bulge.” In: *MNRAS* 491.1, pp. L11–L16. DOI: [10.1093/mnrasl/slz156](https://doi.org/10.1093/mnrasl/slz156). arXiv: [1910.06337](https://arxiv.org/abs/1910.06337) [astro-ph.GA].
- Aumer, Michael and James J. Binney (Aug. 2009). “Kinematics and history of the solar neighbourhood revisited.” In: *MNRAS* 397.3, pp. 1286–1301. DOI: [10.1111/j.1365-2966.2009.15053.x](https://doi.org/10.1111/j.1365-2966.2009.15053.x). arXiv: [0905.2512](https://arxiv.org/abs/0905.2512) [astro-ph.GA].
- Aumer, Michael, James Binney, and Ralph Schönrich (Oct. 2016). “Age-velocity dispersion relations and heating histories in disc galaxies.” In: *MNRAS* 462.2, pp. 1697–1713. DOI: [10.1093/mnras/stw1639](https://doi.org/10.1093/mnras/stw1639). arXiv: [1607.01972](https://arxiv.org/abs/1607.01972) [astro-ph.GA].
- Baade, W. (Aug. 1946). “A Search For the Nucleus of Our Galaxy.” In: *PASP* 58.343, pp. 249–252. DOI: [10.1086/125835](https://doi.org/10.1086/125835).

- Babusiaux, C. and G. Gilmore (Apr. 2005). “The structure of the Galactic bar.” In: *MNRAS* 358.4, pp. 1309–1319. DOI: [10.1111/j.1365-2966.2005.08828.x](https://doi.org/10.1111/j.1365-2966.2005.08828.x). arXiv: [astro-ph/0501383](https://arxiv.org/abs/astro-ph/0501383) [astro-ph].
- Bagheri, G., M. R. L. Cioni, and R. Napiwotzki (Mar. 2013). “The detection of an older population in the Magellanic Bridge.” In: *A&A* 551, A78, A78. DOI: [10.1051/0004-6361/201118236](https://doi.org/10.1051/0004-6361/201118236). arXiv: [1209.0216](https://arxiv.org/abs/1209.0216) [astro-ph.GA].
- Battinelli, P. and S. Demers (Aug. 2014). “Miras among C stars.” In: *A&A* 568, A100, A100. DOI: [10.1051/0004-6361/201423900](https://doi.org/10.1051/0004-6361/201423900).
- Baumgardt, H., G. Parmentier, P. Anders, and E. K. Grebel (Mar. 2013). “The star cluster formation history of the LMC.” In: *MNRAS* 430, pp. 676–685. DOI: [10.1093/mnras/sts667](https://doi.org/10.1093/mnras/sts667).
- Bekki, Kenji and Snežana Stanimirović (May 2009). “The total mass and dark halo properties of the Small Magellanic Cloud.” In: *MNRAS* 395.1, pp. 342–350. DOI: [10.1111/j.1365-2966.2009.14514.x](https://doi.org/10.1111/j.1365-2966.2009.14514.x). arXiv: [0807.2102](https://arxiv.org/abs/0807.2102) [astro-ph].
- Belokurov, V., D. Erkal, A. J. Deason, S. E. Koposov, F. De Angeli, D. W. Evans, F. Fraternali, and D. Mackey (Apr. 2017). “Clouds, Streams and Bridges. Redrawing the blueprint of the Magellanic System with Gaia DR1.” In: *MNRAS* 466, pp. 4711–4730. DOI: [10.1093/mnras/stw3357](https://doi.org/10.1093/mnras/stw3357). arXiv: [1611.04614](https://arxiv.org/abs/1611.04614).
- Belokurov, V., D. Erkal, N. W. Evans, S. E. Koposov, and A. J. Deason (July 2018). “Co-formation of the disc and the stellar halo.” In: *MNRAS* 478.1, pp. 611–619. DOI: [10.1093/mnras/sty982](https://doi.org/10.1093/mnras/sty982). arXiv: [1802.03414](https://arxiv.org/abs/1802.03414) [astro-ph.GA].
- Belokurov, V. et al. (Jan. 2014). “Precession of the Sagittarius stream.” In: *MNRAS* 437, pp. 116–131. DOI: [10.1093/mnras/stt1862](https://doi.org/10.1093/mnras/stt1862). arXiv: [1301.7069](https://arxiv.org/abs/1301.7069) [astro-ph.GA].
- Belokurov, Vasily A. and Denis Erkal (Jan. 2019). “Clouds in arms.” In: *MNRAS* 482.1, pp. L9–L13. DOI: [10.1093/mnrasl/sly178](https://doi.org/10.1093/mnrasl/sly178). arXiv: [1808.00462](https://arxiv.org/abs/1808.00462) [astro-ph.GA].
- Bennett, Morgan and Jo Bovy (Jan. 2019). “Vertical waves in the solar neighbourhood in Gaia DR2.” In: *MNRAS* 482.1, pp. 1417–1425. DOI: [10.1093/mnras/sty2813](https://doi.org/10.1093/mnras/sty2813). arXiv: [1809.03507](https://arxiv.org/abs/1809.03507) [astro-ph.GA].
- Bensby, T., S. Feltzing, and I. Lundström (Nov. 2003). “Elemental abundance trends in the Galactic thin and thick disks as traced by nearby F and G dwarf stars.” In: *A&A* 410, pp. 527–551. DOI: [10.1051/0004-6361:20031213](https://doi.org/10.1051/0004-6361:20031213).
- Bensby, T. et al. (Sept. 2017). “Chemical evolution of the Galactic bulge as traced by microlensed dwarf and subgiant stars. VI. Age and abundance structure of the stellar populations in the central subpc of the Milky Way.” In: *A&A* 605, A89, A89. DOI: [10.1051/0004-6361/201730560](https://doi.org/10.1051/0004-6361/201730560). arXiv: [1702.02971](https://arxiv.org/abs/1702.02971) [astro-ph.GA].

- Berentzen, I., E. Athanassoula, C. H. Heller, and K. J. Fricke (May 2003). “Numerical simulations of interacting gas-rich barred galaxies: vertical impact of small companions.” In: *MNRAS* 341.1, pp. 343–360. DOI: [10.1046/j.1365-8711.2003.06417.x](https://doi.org/10.1046/j.1365-8711.2003.06417.x). arXiv: [astro-ph/0301300](https://arxiv.org/abs/astro-ph/0301300) [astro-ph].
- Bergemann, M. et al. (Mar. 2018). “Two chemically similar stellar overdensities on opposite sides of the plane of the Galactic disk.” In: *Nature* 555, pp. 334–337. DOI: [10.1038/nature25490](https://doi.org/10.1038/nature25490). arXiv: [1803.00563](https://arxiv.org/abs/1803.00563).
- Besla, Gurtina, Nitya Kallivayalil, Lars Hernquist, Brant Robertson, T. J. Cox, Roeland P. van der Marel, and Charles Alcock (Oct. 2007). “Are the Magellanic Clouds on Their First Passage about the Milky Way?” In: *ApJ* 668.2, pp. 949–967. DOI: [10.1086/521385](https://doi.org/10.1086/521385). arXiv: [astro-ph/0703196](https://arxiv.org/abs/astro-ph/0703196) [astro-ph].
- Besla, Gurtina, Nitya Kallivayalil, Lars Hernquist, Roeland P. van der Marel, T. J. Cox, and Dušan Kereš (Apr. 2012). “The role of dwarf galaxy interactions in shaping the Magellanic System and implications for Magellanic Irregulars.” In: *MNRAS* 421.3, pp. 2109–2138. DOI: [10.1111/j.1365-2966.2012.20466.x](https://doi.org/10.1111/j.1365-2966.2012.20466.x). arXiv: [1201.1299](https://arxiv.org/abs/1201.1299) [astro-ph.GA].
- Besla, Gurtina, David Martínez-Delgado, Roeland P. van der Marel, Yuri Beletsky, Mark Seibert, Edward F. Schlafly, Eva K. Grebel, and Fabian Neyer (July 2016). “Low Surface Brightness Imaging of the Magellanic System: Imprints of Tidal Interactions between the Clouds in the Stellar Periphery.” In: *ApJ* 825.1, 20, p. 20. DOI: [10.3847/0004-637X/825/1/20](https://doi.org/10.3847/0004-637X/825/1/20). arXiv: [1602.04222](https://arxiv.org/abs/1602.04222) [astro-ph.GA].
- Bica, E., C. Bonatto, C. M. Dutra, and J. F. C. Santos (Sept. 2008). “A general catalogue of extended objects in the Magellanic System.” In: *MNRAS* 389.2, pp. 678–690. DOI: [10.1111/j.1365-2966.2008.13612.x](https://doi.org/10.1111/j.1365-2966.2008.13612.x). arXiv: [0806.3049](https://arxiv.org/abs/0806.3049) [astro-ph].
- Binney, James and Ralph Schönrich (2018). “The origin of the Gaia phase-plane spiral.” In: *MNRAS* 481.2, pp. 1501–1506. DOI: [10.1093/mnras/sty2378](https://doi.org/10.1093/mnras/sty2378). arXiv: [1807.09819](https://arxiv.org/abs/1807.09819) [astro-ph.GA].
- Bird, Jonathan C., Stelios Kazantzidis, David H. Weinberg, Javiera Guedes, Simone Callegari, Lucio Mayer, and Piero Madau (Aug. 2013). “Inside out and Upside down: Tracing the Assembly of a Simulated Disk Galaxy Using Mono-age Stellar Populations.” In: *ApJ* 773.1, 43, p. 43. DOI: [10.1088/0004-637X/773/1/43](https://doi.org/10.1088/0004-637X/773/1/43). arXiv: [1301.0620](https://arxiv.org/abs/1301.0620) [astro-ph.GA].
- Bissantz, Nicolai and Ortwin Gerhard (Mar. 2002). “Spiral arms, bar shape and bulge microlensing in the Milky Way.” In: *MNRAS* 330.3, pp. 591–608. DOI: [10.1046/j.1365-8711.2002.05116.x](https://doi.org/10.1046/j.1365-8711.2002.05116.x). arXiv: [astro-ph/0110368](https://arxiv.org/abs/astro-ph/0110368) [astro-ph].

- Blommaert, J. A. D. L. and M. A. T. Groenewegen (Dec. 2007). “The Galactic Bulge Mira Population.” In: *From Stars to Galaxies: Building the Pieces to Build Up the Universe*. Ed. by A. Vallenari, R. Tantaló, L. Portinari, and A. Moretti. Vol. 374. Astronomical Society of the Pacific Conference Series, p. 193.
- Bochanski, J. J., B. Willman, N. Caldwell, R. Sanderson, A. A. West, J. Strader, and W. Brown (July 2014). “The Most Distant Stars in the Milky Way.” In: *ApJ* 790, L5, p. L5. DOI: [10.1088/2041-8205/790/1/L5](https://doi.org/10.1088/2041-8205/790/1/L5). arXiv: [1407.2610](https://arxiv.org/abs/1407.2610) [astro-ph.SR].
- Bournaud, F., B. G. Elmegreen, and M. Martig (Dec. 2009). “The Thick Disks of Spiral Galaxies as Relics from Gas-rich, Turbulent, Clumpy Disks at High Redshift.” In: *ApJ* 707, pp. L1–L5. DOI: [10.1088/0004-637X/707/1/L1](https://doi.org/10.1088/0004-637X/707/1/L1). arXiv: [0910.3677](https://arxiv.org/abs/0910.3677).
- Bovy, J., H.-W. Rix, C. Liu, D. W. Hogg, T. C. Beers, and Y. S. Lee (July 2012). “The Spatial Structure of Mono-abundance Sub-populations of the Milky Way Disk.” In: *ApJ* 753, 148, p. 148. DOI: [10.1088/0004-637X/753/2/148](https://doi.org/10.1088/0004-637X/753/2/148). arXiv: [1111.1724](https://arxiv.org/abs/1111.1724) [astro-ph.GA].
- Bovy, J., H.-W. Rix, E. F. Schlafly, D. L. Nidever, J. A. Holtzman, M. Shetrone, and T. C. Beers (May 2016). “The Stellar Population Structure of the Galactic Disk.” In: *ApJ* 823, 30, p. 30. DOI: [10.3847/0004-637X/823/1/30](https://doi.org/10.3847/0004-637X/823/1/30). arXiv: [1509.05796](https://arxiv.org/abs/1509.05796).
- Buck, Tobias, Melissa K. Ness, Andrea V. Macciò, Aura Obreja, and Aaron A. Dutton (July 2018). “Stars Behind Bars. I. The Milky Way’s Central Stellar Populations.” In: *ApJ* 861.2, 88, p. 88. DOI: [10.3847/1538-4357/aac890](https://doi.org/10.3847/1538-4357/aac890). arXiv: [1711.04765](https://arxiv.org/abs/1711.04765) [astro-ph.GA].
- Buck, Tobias, Aura Obreja, Andrea V. Macciò, Ivan Minchev, Aaron A. Dutton, and Jeremiah P. Ostriker (Nov. 2019). “NIHAO-UHD: The properties of MW-like stellar disks in high resolution cosmological simulations.” In: *MNRAS*, p. 2827. DOI: [10.1093/mnras/stz3241](https://doi.org/10.1093/mnras/stz3241).
- Bureau, M. and K. C. Freeman (July 1999). “The Nature of Boxy/Peanut-Shaped Bulges in Spiral Galaxies.” In: *AJ* 118.1, pp. 126–138. DOI: [10.1086/300922](https://doi.org/10.1086/300922). arXiv: [astro-ph/9904015](https://arxiv.org/abs/astro-ph/9904015) [astro-ph].
- Cabrera-Lavers, A., C. González-Fernández, F. Garzón, P. L. Hammersley, and M. López-Corredoira (2008). “The long Galactic bar as seen by UKIDSS Galactic plane survey.” In: *A&A* 491.3, pp. 781–787. DOI: [10.1051/0004-6361:200810720](https://doi.org/10.1051/0004-6361:200810720). arXiv: [0809.3174](https://arxiv.org/abs/0809.3174) [astro-ph].
- Cabrera-Lavers, A., P. L. Hammersley, C. González-Fernández, M. López-Corredoira, F. Garzón, and T. J. Mahoney (Apr. 2007). “Tracing the long bar with red-clump giants.” In: *A&A* 465.3, pp. 825–838. DOI: [10.1051/0004-6361:20066185](https://doi.org/10.1051/0004-6361:20066185). arXiv: [astro-ph/0702109](https://arxiv.org/abs/astro-ph/0702109) [astro-ph].

- Callingham, Thomas M., Marius Cautun, Alis J. Deason, Carlos S. Frenk, Wenting Wang, Facundo A. Gómez, Robert J. J. Grand, Federico Marinacci, and Ruediger Pakmor (Apr. 2019). “The mass of the Milky Way from satellite dynamics.” In: *MNRAS* 484.4, pp. 5453–5467. DOI: [10.1093/mnras/stz365](https://doi.org/10.1093/mnras/stz365). arXiv: [1808.10456](https://arxiv.org/abs/1808.10456) [astro-ph.GA].
- Carollo, D., T. C. Beers, V. M. Placco, R. M. Santucci, P. Denissenkov, P. B. Tissera, G. Lentner, S. Rossi, Y. S. Lee, and J. Tumlinson (Dec. 2016). “The age structure of the Milky Way’s halo.” In: *Nature Physics* 12, pp. 1170–1176. DOI: [10.1038/nphys3874](https://doi.org/10.1038/nphys3874). arXiv: [1607.08628](https://arxiv.org/abs/1607.08628).
- Carpenter, J. M. (May 2001). “Color Transformations for the 2MASS Second Incremental Data Release.” In: *AJ* 121, pp. 2851–2871. DOI: [10.1086/320383](https://doi.org/10.1086/320383). eprint: [astro-ph/0101463](https://arxiv.org/abs/astro-ph/0101463).
- Carraro, Giovanni, Ruben A. Vázquez, Edgardo Costa, Gabriel Perren, and André Moitinho (Aug. 2010). “The Edge of the Young Galactic Disk.” In: *ApJ* 718.2, pp. 683–694. DOI: [10.1088/0004-637X/718/2/683](https://doi.org/10.1088/0004-637X/718/2/683). arXiv: [1006.1277](https://arxiv.org/abs/1006.1277) [astro-ph.GA].
- Carrera, Ricardo, Blair C. Conn, Noelia E. D. Noël, Justin I. Read, and Ángel R. López Sánchez (Nov. 2017). “The Magellanic Inter-Cloud Project (MAGIC) III: first spectroscopic evidence of a dwarf stripping a dwarf.” In: *MNRAS* 471.4, pp. 4571–4578. DOI: [10.1093/mnras/stx1932](https://doi.org/10.1093/mnras/stx1932). arXiv: [1707.08397](https://arxiv.org/abs/1707.08397) [astro-ph.GA].
- Casetti-Dinescu, Dana I., Katherine Vieira, Terrence M. Girard, and William F. van Altena (July 2012). “Constraints on the Magellanic Clouds’ Interaction from the Distribution of OB Stars and the Kinematics of Giants.” In: *ApJ* 753.2, 123, p. 123. DOI: [10.1088/0004-637X/753/2/123](https://doi.org/10.1088/0004-637X/753/2/123). arXiv: [1205.0989](https://arxiv.org/abs/1205.0989) [astro-ph.GA].
- Casey, A. R., G. M. Kennedy, T. R. Hartle, and Kevin C. Schlafman (Aug. 2018). “Infrared colours and inferred masses of metal-poor giant stars in the Kepler field.” In: *MNRAS* 478.2, pp. 2812–2818. DOI: [10.1093/mnras/sty1208](https://doi.org/10.1093/mnras/sty1208). arXiv: [1805.12133](https://arxiv.org/abs/1805.12133) [astro-ph.SR].
- Catchpole, Robin M., Patricia A. Whitelock, Michael W. Feast, Shaun M. G. Hughes, Mike Irwin, and Christophe Alard (Jan. 2016). “The age and structure of the Galactic bulge from Mira variables.” In: *MNRAS* 455.2, pp. 2216–2227. DOI: [10.1093/mnras/stv2372](https://doi.org/10.1093/mnras/stv2372). arXiv: [1510.03295](https://arxiv.org/abs/1510.03295) [astro-ph.SR].
- Chiappini, C., F. Matteucci, and R. Gratton (Mar. 1997). “The Chemical Evolution of the Galaxy: The Two-Infall Model.” In: *ApJ* 477.2, pp. 765–780. DOI: [10.1086/303726](https://doi.org/10.1086/303726). arXiv: [astro-ph/9609199](https://arxiv.org/abs/astro-ph/9609199) [astro-ph].
- Choi, Yumi et al. (Oct. 2018a). “SMASHing the LMC: A Tidally Induced Warp in the Outer LMC and a Large-scale Reddening

- Map." In: *ApJ* 866.2, 90, p. 90. DOI: [10.3847/1538-4357/aae083](https://doi.org/10.3847/1538-4357/aae083). arXiv: [1804.07765](https://arxiv.org/abs/1804.07765) [[astro-ph.GA](#)].
- Choi, Yumi et al. (Dec. 2018b). "SMASHing the LMC: Mapping a Ring-like Stellar Overdensity in the LMC Disk." In: *ApJ* 869.2, 125, p. 125. DOI: [10.3847/1538-4357/aaed1f](https://doi.org/10.3847/1538-4357/aaed1f). arXiv: [1805.00481](https://arxiv.org/abs/1805.00481) [[astro-ph.GA](#)].
- Choudhury, Samyaday, Annapurni Subramaniam, and Andrew A. Cole (Jan. 2016). "Photometric metallicity map of the Large Magellanic Cloud." In: *MNRAS* 455.2, pp. 1855–1880. DOI: [10.1093/mnras/stv2414](https://doi.org/10.1093/mnras/stv2414). arXiv: [1510.05769](https://arxiv.org/abs/1510.05769) [[astro-ph.GA](#)].
- Choudhury, Samyaday, Richard de Grijs, Stefano Rubele, Kenji Bekki, Maria-Rosa L. Cioni, Valentin D. Ivanov, Jacco Th van Loon, Florian Niederhofer, Joana M. Oliveira, and Vincenzo Ripepi (July 2020). "The VMC survey - XXXIX. Mapping metallicity trends in the Small Magellanic Cloud using near-infrared passbands." In: *MNRAS* 497.3, pp. 3746–3760. DOI: [10.1093/mnras/staa2140](https://doi.org/10.1093/mnras/staa2140). arXiv: [2007.08753](https://arxiv.org/abs/2007.08753) [[astro-ph.GA](#)].
- Cignoni, M. et al. (Oct. 2015). "Hubble Tarantula Treasury Project. II. The Star-formation History of the Starburst Region NGC 2070 in 30 Doradus." In: *ApJ* 811.2, 76, p. 76. DOI: [10.1088/0004-637X/811/2/76](https://doi.org/10.1088/0004-637X/811/2/76). arXiv: [1505.04799](https://arxiv.org/abs/1505.04799) [[astro-ph.SR](#)].
- Cioni, M. R. L. (Nov. 2009). "The metallicity gradient as a tracer of history and structure: the Magellanic Clouds and M33 galaxies." In: *A&A* 506.3, pp. 1137–1146. DOI: [10.1051/0004-6361/200912138](https://doi.org/10.1051/0004-6361/200912138). arXiv: [0904.3136](https://arxiv.org/abs/0904.3136) [[astro-ph.CO](#)].
- Cioni, M.-R. L., J.-B. Marquette, C. Loup, M. Azzopardi, H. J. Habing, T. Lasserre, and E. Lesquoy (Oct. 2001). "Variability and spectral classification of LMC giants: Results from DENIS and EROS." In: *A&A* 377, pp. 945–954. DOI: [10.1051/0004-6361:20011143](https://doi.org/10.1051/0004-6361:20011143). eprint: [astro-ph/0109014](https://arxiv.org/abs/astro-ph/0109014).
- Clarkson, W. I. et al. (July 2011). "The First Detection of Blue Straggler Stars in the Milky Way Bulge." In: *ApJ* 735.1, 37, p. 37. DOI: [10.1088/0004-637X/735/1/37](https://doi.org/10.1088/0004-637X/735/1/37). arXiv: [1105.4176](https://arxiv.org/abs/1105.4176) [[astro-ph.GA](#)].
- Clarkson, Will et al. (Sept. 2008). "Stellar Proper Motions in the Galactic Bulge from Deep Hubble Space Telescope ACS WFC Photometry." In: *ApJ* 684.2, pp. 1110–1142. DOI: [10.1086/590378](https://doi.org/10.1086/590378). arXiv: [0809.1682](https://arxiv.org/abs/0809.1682) [[astro-ph](#)].
- Clementini, G. et al. (Feb. 2019). "Gaia Data Release 2. Specific characterisation and validation of all-sky Cepheids and RR Lyrae stars." In: *A&A* 622, A60, A60. DOI: [10.1051/0004-6361/201833374](https://doi.org/10.1051/0004-6361/201833374). arXiv: [1805.02079](https://arxiv.org/abs/1805.02079) [[astro-ph.SR](#)].
- Coleman, Brendan, Dylan Paterson, Chris Gordon, Oscar Macias, and Harrison Ploeg (Nov. 2019). "Maximum Entropy Estimation of

- the Galactic Bulge Morphology via the VVV Red Clump.” In: *arXiv e-prints*, arXiv:1911.04714, arXiv:1911.04714. arXiv: [1911.04714](#) [astro-ph.GA].
- Comerón, S. et al. (Nov. 2012). “Breaks in Thin and Thick Disks of Edge-on Galaxies Imaged in the Spitzer Survey Stellar Structure in Galaxies (S⁴G).” In: *ApJ* 759, 98, p. 98. DOI: [10.1088/0004-637X/759/2/98](#). arXiv: [1209.1513](#).
- Crowl, Hugh H., Ata Sarajedini, Andrés E. Piatti, Doug Geisler, Eduardo Bica, Juan J. Clariá, and Jr. Santos João F. C. (July 2001). “The Line-of-Sight Depth of Populous Clusters in the Small Magellanic Cloud.” In: *AJ* 122.1, pp. 220–231. DOI: [10.1086/321128](#). arXiv: [astro-ph/0104227](#) [astro-ph].
- Cullinane, L. R., A. D. Mackey, G. S. Da Costa, S. E. Koposov, V. Belokurov, D. Erkal, A. Koch, A. Kunder, and D. M. Nataf (July 2020). “The Magellanic Edges Survey I: Description and first results.” In: *MNRAS* 497.3, pp. 3055–3075. DOI: [10.1093/mnras/staa2048](#). arXiv: [2007.06780](#) [astro-ph.GA].
- De Leo, Michele, Ricardo Carrera, Noelia E. D. Noël, Justin I. Read, Denis Erkal, and Carme Gallart (Apr. 2020). “Revealing the tidal scars of the Small Magellanic Cloud.” In: *MNRAS* 495.1, pp. 98–113. DOI: [10.1093/mnras/staa1122](#). arXiv: [2002.11138](#) [astro-ph.GA].
- De Marchi, Guido et al. (Sept. 2011). “Star Formation in 30 Doradus.” In: *ApJ* 739.1, 27, p. 27. DOI: [10.1088/0004-637X/739/1/27](#). arXiv: [1106.2801](#) [astro-ph.SR].
- Deason, A. J., V. Belokurov, D. Erkal, S. E. Koposov, and D. Mackey (May 2017). “The Clouds are breaking: tracing the Magellanic system with Gaia DR1 Mira variables.” In: *MNRAS* 467, pp. 2636–2647. DOI: [10.1093/mnras/stx263](#). arXiv: [1611.04600](#).
- Deason, A. J., V. Belokurov, N. W. Evans, S. E. Koposov, R. J. Cooke, J. Peñarrubia, C. F. P. Laporte, M. Fellhauer, M. G. Walker, and E. W. Olszewski (Oct. 2012). “The cold veil of the Milky Way stellar halo.” In: *MNRAS* 425, pp. 2840–2853. DOI: [10.1111/j.1365-2966.2012.21639.x](#). arXiv: [1205.6203](#).
- Deason, A. J., V. Belokurov, and S. E. Koposov (Jan. 2018). “Cresting the wave: proper motions of the Eastern Banded Structure.” In: *MNRAS* 473, pp. 2428–2433. DOI: [10.1093/mnras/stx2528](#). arXiv: [1709.08633](#).
- Deason, Alis J., Vasily Belokurov, Sergey E. Koposov, and Lachlan Lancaster (July 2018). “Apocenter Pile-up: Origin of the Stellar Halo Density Break.” In: *ApJ* 862.1, L1, p. L1. DOI: [10.3847/2041-8213/aad0ee](#). arXiv: [1805.10288](#) [astro-ph.GA].

- Deason, Alis J. et al. (Mar. 2021). "The mass of the Milky Way out to 100 kpc using halo stars." In: *MNRAS* 501.4, pp. 5964–5972. DOI: [10.1093/mnras/staa3984](https://doi.org/10.1093/mnras/staa3984). arXiv: [2010.13801](https://arxiv.org/abs/2010.13801) [astro-ph.GA].
- Deb, Sukanta, Kerdaris Kurbah, Harinder P. Singh, Shashi M. Kanbur, Chow-Choong Ngeow, Biman J. Medhi, and Subhash Kumar (Nov. 2019). "Morphology of the Small Magellanic Cloud using multiwavelength photometry of classical Cepheids." In: *MNRAS* 489.3, pp. 3725–3738. DOI: [10.1093/mnras/stz2328](https://doi.org/10.1093/mnras/stz2328).
- Deb, Sukanta, Harinder P. Singh, Subhash Kumar, and Shashi M. Kanbur (May 2015). "Morphology and metallicity of the Small Magellanic Cloud using RRab stars." In: *MNRAS* 449.3, pp. 2768–2783. DOI: [10.1093/mnras/stv358](https://doi.org/10.1093/mnras/stv358). arXiv: [1502.05824](https://arxiv.org/abs/1502.05824) [astro-ph.SR].
- Debattista, Victor P., Melissa Ness, Oscar A. Gonzalez, K. Freeman, Manuela Zoccali, and Dante Minniti (Aug. 2017). "Separation of stellar populations by an evolving bar: implications for the bulge of the Milky Way." In: *MNRAS* 469.2, pp. 1587–1611. DOI: [10.1093/mnras/stx947](https://doi.org/10.1093/mnras/stx947). arXiv: [1611.09023](https://arxiv.org/abs/1611.09023) [astro-ph.GA].
- Dehnen, Walter (Feb. 2000). "The Effect of the Outer Lindblad Resonance of the Galactic Bar on the Local Stellar Velocity Distribution." In: *AJ* 119.2, pp. 800–812. DOI: [10.1086/301226](https://doi.org/10.1086/301226). arXiv: [astro-ph/9911161](https://arxiv.org/abs/astro-ph/9911161) [astro-ph].
- Dékány, I., D. Minniti, M. Catelan, M. Zoccali, R. K. Saito, M. Hempel, and O. A. Gonzalez (Oct. 2013). "VVV Survey Near-infrared Photometry of Known Bulge RR Lyrae Stars: The Distance to the Galactic Center and Absence of a Barred Distribution of the Metal-poor Population." In: *ApJ* 776.2, L19, p. L19. DOI: [10.1088/2041-8205/776/2/L19](https://doi.org/10.1088/2041-8205/776/2/L19). arXiv: [1309.5933](https://arxiv.org/abs/1309.5933) [astro-ph.GA].
- Diaz, Jonathan D. and Kenji Bekki (May 2012). "The Tidal Origin of the Magellanic Stream and the Possibility of a Stellar Counterpart." In: *ApJ* 750.1, 36, p. 36. DOI: [10.1088/0004-637X/750/1/36](https://doi.org/10.1088/0004-637X/750/1/36). arXiv: [1112.6191](https://arxiv.org/abs/1112.6191) [astro-ph.GA].
- Downes, R. A., B. Margon, S. F. Anderson, H. C. Harris, G. R. Knapp, J. Schroeder, D. P. Schneider, D. G. York, J. R. Pier, and J. Brinkmann (May 2004). "Faint High-Latitude Carbon Stars Discovered by the Sloan Digital Sky Survey: An Initial Catalog." In: *AJ* 127, pp. 2838–2849. DOI: [10.1086/383211](https://doi.org/10.1086/383211). eprint: [astro-ph/0402118](https://arxiv.org/abs/astro-ph/0402118).
- Drake, A. J. et al. (Mar. 2013). "Evidence for a Milky Way Tidal Stream Reaching Beyond 100 kpc." In: *ApJ* 765, 154, p. 154. DOI: [10.1088/0004-637X/765/2/154](https://doi.org/10.1088/0004-637X/765/2/154). arXiv: [1301.6168](https://arxiv.org/abs/1301.6168).
- Drake, A. J. et al. (July 2014). "The Catalina Surveys Periodic Variable Star Catalog." In: *ApJS* 213, 9, p. 9. DOI: [10.1088/0067-0049/213/1/9](https://doi.org/10.1088/0067-0049/213/1/9). arXiv: [1405.4290](https://arxiv.org/abs/1405.4290) [astro-ph.SR].

- Drake, A. J. et al. (2017). "The Catalina Surveys Southern periodic variable star catalogue." In: *Monthly Notices of the Royal Astronomical Society* 469.3, pp. 3688–3712. DOI: [10.1093/mnras/stx1085](https://doi.org/10.1093/mnras/stx1085). eprint: [/oup/backfile/content_public/journal/mnras/469/3/10.1093_mnras_stx1085/4/stx1085.pdf](https://oup/backfile/content_public/journal/mnras/469/3/10.1093_mnras_stx1085/4/stx1085.pdf). URL: [+http://dx.doi.org/10.1093/mnras/stx1085](http://dx.doi.org/10.1093/mnras/stx1085).
- Du, Hangci, Shude Mao, E. Athanassoula, Juntao Shen, and Pawel Pietrukowicz (Aug. 2020). "Kinematics of RR Lyrae stars in the Galactic bulge with OGLE-IV and Gaia DR2." In: *MNRAS* 498.4, pp. 5629–5642. DOI: [10.1093/mnras/staa2601](https://doi.org/10.1093/mnras/staa2601). arXiv: [2007.01102](https://arxiv.org/abs/2007.01102) [astro-ph.GA].
- Dwek, E., R. G. Arendt, M. G. Hauser, T. Kelsall, C. M. Lisse, S. H. Moseley, R. F. Silverberg, T. J. Sodroski, and J. L. Weiland (June 1995). "Morphology, near-infrared luminosity, and mass of the Galactic bulge from COBE DIRBE observations." In: *ApJ* 445, pp. 716–730. DOI: [10.1086/175734](https://doi.org/10.1086/175734).
- El Youssoufi, Dalal et al. (Nov. 2019). "The VMC survey - XXXIV. Morphology of stellar populations in the Magellanic Clouds." In: *MNRAS* 490.1, pp. 1076–1093. DOI: [10.1093/mnras/stz2400](https://doi.org/10.1093/mnras/stz2400). arXiv: [1908.08545](https://arxiv.org/abs/1908.08545) [astro-ph.GA].
- Elgueta, S. S. et al. (Aug. 2016). "The Orbital and Physical Parameters, and the Distance of the Eclipsing Binary System OGLE-LMC-ECL-25658 in the Large Magellanic Cloud." In: *AJ* 152, 29, p. 29. DOI: [10.3847/0004-6256/152/2/29](https://doi.org/10.3847/0004-6256/152/2/29). arXiv: [1605.00909](https://arxiv.org/abs/1605.00909) [astro-ph.SR].
- Erkal, D. et al. (Aug. 2019). "The total mass of the Large Magellanic Cloud from its perturbation on the Orphan stream." In: *MNRAS* 487.2, pp. 2685–2700. DOI: [10.1093/mnras/stz1371](https://doi.org/10.1093/mnras/stz1371). arXiv: [1812.08192](https://arxiv.org/abs/1812.08192) [astro-ph.GA].
- Erkal, Denis and Vasily A. Belokurov (July 2020). "Limit on the LMC mass from a census of its satellites." In: *MNRAS* 495.3, pp. 2554–2563. DOI: [10.1093/mnras/staa1238](https://doi.org/10.1093/mnras/staa1238). arXiv: [1907.09484](https://arxiv.org/abs/1907.09484) [astro-ph.GA].
- Erkal, Denis et al. (Oct. 2020). "Detection of the LMC-induced sloshing of the Galactic halo." In: *arXiv e-prints*, arXiv:2010.13789, arXiv:2010.13789. arXiv: [2010.13789](https://arxiv.org/abs/2010.13789) [astro-ph.GA].
- Erwin, Peter and Victor P. Debattista (June 2013). "Peanuts at an angle: detecting and measuring the three-dimensional structure of bars in moderately inclined galaxies." In: *MNRAS* 431.4, pp. 3060–3086. DOI: [10.1093/mnras/stt385](https://doi.org/10.1093/mnras/stt385). arXiv: [1301.0638](https://arxiv.org/abs/1301.0638) [astro-ph.CO].
- Fabricius, Maximilian H., Roberto P. Saglia, David B. Fisher, Niv Drory, Ralf Bender, and Ulrich Hopp (July 2012). "Kinematic Signatures of Bulges Correlate with Bulge Morphologies and Sérsic

- Index." In: *ApJ* 754.1, 67, p. 67. DOI: [10.1088/0004-637X/754/1/67](https://doi.org/10.1088/0004-637X/754/1/67). arXiv: [1204.5188](https://arxiv.org/abs/1204.5188) [astro-ph.CO].
- Feast, M. W. (Jan. 2009). "The Ages, Masses, Evolution and Kinematics of Mira Variables." In: *AGB Stars and Related Phenomena*. Ed. by Toshiya Ueta, Noriyuki Matsunaga, and Yoshifusa Ita, p. 48. arXiv: [0812.0250](https://arxiv.org/abs/0812.0250) [astro-ph].
- Feast, M. W., I. S. Glass, P. A. Whitelock, and R. M. Catchpole (Nov. 1989). "A period-luminosity-colour relation for Mira variables." In: *MNRAS* 241, pp. 375–392. DOI: [10.1093/mnras/241.3.375](https://doi.org/10.1093/mnras/241.3.375).
- Feast, M. W., B. S. C. Robertson, R. M. Catchpole, T. L. Evans, I. S. Glass, and B. S. Carter (Nov. 1982). "The infrared properties of Mira-type variables and other cool stars as determined from JHKL photometry." In: *MNRAS* 201, pp. 439–450. DOI: [10.1093/mnras/201.2.439](https://doi.org/10.1093/mnras/201.2.439).
- Feast, M. W. and P. A. Whitelock (Sept. 2000a). "Mira kinematics from Hipparcos data: a Galactic bar to beyond the Solar circle." In: *MNRAS* 317, pp. 460–487. DOI: [10.1046/j.1365-8711.2000.03629.x](https://doi.org/10.1046/j.1365-8711.2000.03629.x). eprint: [astro-ph/0004107](https://arxiv.org/abs/astro-ph/0004107).
- Feast, M. W., P. A. Whitelock, and J. W. Menzies (June 2006). "Carbon-rich Mira variables: kinematics and absolute magnitudes." In: *MNRAS* 369, pp. 791–797. DOI: [10.1111/j.1365-2966.2006.10324.x](https://doi.org/10.1111/j.1365-2966.2006.10324.x). eprint: [astro-ph/0603506](https://arxiv.org/abs/astro-ph/0603506).
- Feast, M. (Nov. 2007). "C- and O-Rich Miras and Galactic Structure." In: *Why Galaxies Care About AGB Stars: Their Importance as Actors and Probes*. Ed. by F. Kerschbaum, C. Charbonnel, and R. F. Wing. Vol. 378. Astronomical Society of the Pacific Conference Series, p. 479. eprint: [astro-ph/0609318](https://arxiv.org/abs/astro-ph/0609318).
- Feast, M. and P. Whitelock (2000b). "Can Mira Variables Tell us the Chemical Abundances in Stellar Systems?" In: *Astrophysics and Space Science Library*. Ed. by F. Matteucci and F. Giovannelli. Vol. 255. Astrophysics and Space Science Library, p. 229. DOI: [10.1007/978-94-010-0938-6_22](https://doi.org/10.1007/978-94-010-0938-6_22). eprint: [astro-ph/9911393](https://arxiv.org/abs/astro-ph/9911393).
- Feast, Michael W., John W. Menzies, Noriyuki Matsunaga, and Patricia A. Whitelock (May 2014). "Cepheid variables in the flared outer disk of our galaxy." In: *Nature* 509.7500, pp. 342–344. DOI: [10.1038/nature13246](https://doi.org/10.1038/nature13246). arXiv: [1406.7660](https://arxiv.org/abs/1406.7660) [astro-ph.GA].
- Feast, Michael W., John W. Menzies, and Patricia A. Whitelock (Jan. 2013). "A carbon-rich Mira variable in a globular cluster: a stellar merger." In: *MNRAS* 428.1, pp. L36–L38. DOI: [10.1093/mnrasl/sls009](https://doi.org/10.1093/mnrasl/sls009). arXiv: [1210.0415](https://arxiv.org/abs/1210.0415) [astro-ph.GA].
- Fisher, D. B. and N. Drory (Oct. 2008). "Distinguishing Pseudobulges and Classical Bulges." In: *Formation and Evolution of Galaxy Disks*.

- Ed. by J. G. Funes and E. M. Corsini. Vol. 396. Astronomical Society of the Pacific Conference Series, p. 309.
- Foreman-Mackey, D., D. W. Hogg, D. Lang, and J. Goodman (Mar. 2013). “emcee: The MCMC Hammer.” In: *PASP* 125, p. 306. DOI: [10.1086/670067](https://doi.org/10.1086/670067). arXiv: [1202.3665](https://arxiv.org/abs/1202.3665) [astro-ph.IM].
- Fragkoudi, F., P. Di Matteo, M. Haywood, M. Schultheis, S. Khoperskov, A. Gómez, and F. Combes (Sept. 2018). “The disc origin of the Milky Way bulge. Dissecting the chemo-morphological relations using N-body simulations and APOGEE.” In: *A&A* 616, A180, A180. DOI: [10.1051/0004-6361/201732509](https://doi.org/10.1051/0004-6361/201732509). arXiv: [1802.00453](https://arxiv.org/abs/1802.00453) [astro-ph.GA].
- Frankel, Neige, Jason Sanders, Yuan-Sen Ting, and Hans-Walter Rix (June 2020). “Keeping It Cool: Much Orbit Migration, yet Little Heating, in the Galactic Disk.” In: *ApJ* 896.1, 15, p. 15. DOI: [10.3847/1538-4357/ab910c](https://doi.org/10.3847/1538-4357/ab910c). arXiv: [2002.04622](https://arxiv.org/abs/2002.04622) [astro-ph.GA].
- Fraser-McKelvie, Amelia et al. (Sept. 2019). “SDSS-IV MaNGA: stellar population gradients within barred galaxies.” In: *MNRAS* 488.1, pp. L6–L11. DOI: [10.1093/mnrasl/slz085](https://doi.org/10.1093/mnrasl/slz085). arXiv: [1906.00643](https://arxiv.org/abs/1906.00643) [astro-ph.GA].
- Fuhrmann, Klaus (Oct. 1998). “Nearby stars of the Galactic disk and halo.” In: *A&A* 338, pp. 161–183.
- Gaia Collaboration, A. G. A. Brown, A. Vallenari, T. Prusti, J. H. J. de Bruijne, C. Babusiaux, and C. A. L. Bailer-Jones (Apr. 2018a). “Gaia Data Release 2. Summary of the contents and survey properties.” In: *ArXiv e-prints*. arXiv: [1804.09365](https://arxiv.org/abs/1804.09365).
- Gaia Collaboration et al. (Nov. 2016). “The Gaia mission.” In: *A&A* 595, A1, A1. DOI: [10.1051/0004-6361/201629272](https://doi.org/10.1051/0004-6361/201629272). arXiv: [1609.04153](https://arxiv.org/abs/1609.04153) [astro-ph.IM].
- Gaia Collaboration et al. (Aug. 2018b). “Gaia Data Release 2. Kinematics of globular clusters and dwarf galaxies around the Milky Way.” In: *A&A* 616, A12, A12. DOI: [10.1051/0004-6361/201832698](https://doi.org/10.1051/0004-6361/201832698). arXiv: [1804.09381](https://arxiv.org/abs/1804.09381) [astro-ph.GA].
- Gaia Collaboration et al. (Aug. 2018c). “Gaia Data Release 2. Observational Hertzsprung-Russell diagrams.” In: *A&A* 616, A10, A10. DOI: [10.1051/0004-6361/201832843](https://doi.org/10.1051/0004-6361/201832843). arXiv: [1804.09378](https://arxiv.org/abs/1804.09378) [astro-ph.SR].
- Gaia Collaboration et al. (Aug. 2018d). “Gaia Data Release 2. Summary of the contents and survey properties.” In: *A&A* 616, A1, A1. DOI: [10.1051/0004-6361/201833051](https://doi.org/10.1051/0004-6361/201833051). arXiv: [1804.09365](https://arxiv.org/abs/1804.09365) [astro-ph.GA].
- Gaia Collaboration et al. (Dec. 2020). “Gaia Early Data Release 3: Structure and properties of the Magellanic Clouds.” In: *arXiv*

- e-prints*, arXiv:2012.01771, arXiv:2012.01771. arXiv: [2012.01771](#) [[astro-ph.GA](#)].
- Gaposchkin, C. P. (1954). *Variable stars & galactic structure*.
- Gardiner, L. T. and M. R. S. Hawkins (July 1991). “Stellar populations and large-scale structure of the SMC - III. The geometry of the northern and north-western outlying regions.” In: *MNRAS* 251, p. 174. DOI: [10.1093/mnras/251.1.174](#).
- Gerhard, O. (Jan. 2011). “Pattern speeds in the Milky Way.” In: *Memorie della Societa Astronomica Italiana Supplementi* 18, p. 185. arXiv: [1003.2489](#) [[astro-ph.GA](#)].
- Gillessen, S., F. Eisenhauer, T. K. Fritz, H. Bartko, K. Dodds-Eden, O. Pfuhl, T. Ott, and R. Genzel (Dec. 2009). “The Orbit of the Star S2 Around SGR A* from Very Large Telescope and Keck Data.” In: *ApJ* 707.2, pp. L114–L117. DOI: [10.1088/0004-637X/707/2/L114](#). arXiv: [0910.3069](#) [[astro-ph.GA](#)].
- Gilmore, G. and N. Reid (Mar. 1983). “New light on faint stars. III - Galactic structure towards the South Pole and the Galactic thick disc.” In: *MNRAS* 202, pp. 1025–1047. DOI: [10.1093/mnras/202.4.1025](#).
- Glass, I. S. and M. W. Feast (Apr. 1982). “Infrared Photometry of Mira Variables in the Large Magellanic Cloud and the Pulsational Properties of Miras.” In: *MNRAS* 199, p. 245. DOI: [10.1093/mnras/199.2.245](#).
- Glass, I. S., P. A. Whitelock, R. M. Catchpole, and M. W. Feast (Mar. 1995). “Long-period variables in the SGR I field of the Galactic Bulge.” In: *MNRAS* 273, pp. 383–400. DOI: [10.1093/mnras/273.2.383](#).
- Goldman, S. R. et al. (May 2019). “An Infrared Census of DUST in Nearby Galaxies with Spitzer (DUSTiNGS). V. The Period-Luminosity Relation for Dusty Metal-poor AGB Stars.” In: *ApJ* 877.1, 49, p. 49. DOI: [10.3847/1538-4357/ab0965](#). arXiv: [1902.07362](#) [[astro-ph.SR](#)].
- González-Fernández, C., M. López-Corredoira, E. B. Amôres, D. Minniti, P. Lucas, and I. Toledo (Oct. 2012). “The long bar as seen by the VVV survey. I. Colour-magnitude diagrams.” In: *A&A* 546, A107, A107. DOI: [10.1051/0004-6361/201219756](#). arXiv: [1209.4370](#) [[astro-ph.GA](#)].
- Gonzalez, O. A. et al. (2015). “The GIRAFFE Inner Bulge Survey (GIBS). II. Metallicity distributions and alpha element abundances at fixed Galactic latitude.” In: *A&A* 584, A46, A46. DOI: [10.1051/0004-6361/201526737](#). arXiv: [1508.02576](#) [[astro-ph.GA](#)].
- Grady, J., V. Belokurov, and N. W. Evans (Mar. 2019). “Age gradients throughout the Galaxy with long-period variables.” In: *MNRAS*

- 483, pp. 3022–3035. DOI: [10.1093/mnras/sty3284](https://doi.org/10.1093/mnras/sty3284). arXiv: [1804.09186](https://arxiv.org/abs/1804.09186).
- Grady, J., V. Belokurov, and N. W. Evans (Feb. 2020). “Age demographics of the Milky Way disc and bulge.” In: *MNRAS* 492.3, pp. 3128–3142. DOI: [10.1093/mnras/stz3617](https://doi.org/10.1093/mnras/stz3617). arXiv: [1912.02816](https://arxiv.org/abs/1912.02816) [[astro-ph.GA](#)].
- Grady, J., V. Belokurov, and N. W. Evans (Mar. 2021). “Magellanic Mayhem: Metallicities and Motions.” In: *ApJ* 909.2, 150, p. 150. DOI: [10.3847/1538-4357/abd4e4](https://doi.org/10.3847/1538-4357/abd4e4). arXiv: [2010.05956](https://arxiv.org/abs/2010.05956) [[astro-ph.GA](#)].
- Grand, Robert J. J., Sebastián Bustamante, Facundo A. Gómez, Daisuke Kawata, Federico Marinacci, Rüdiger Pakmor, Hans-Walter Rix, Christine M. Simpson, Martin Sparre, and Volker Springel (Mar. 2018). “Origin of chemically distinct discs in the Auriga cosmological simulations.” In: *MNRAS* 474.3, pp. 3629–3639. DOI: [10.1093/mnras/stx3025](https://doi.org/10.1093/mnras/stx3025). arXiv: [1708.07834](https://arxiv.org/abs/1708.07834) [[astro-ph.GA](#)].
- Grand, Robert J. J., Daisuke Kawata, Vasily Belokurov, Alis J. Deason, Azadeh Fattahi, Francesca Fragkoudi, Facundo A. Gómez, Federico Marinacci, and Rüdiger Pakmor (July 2020). “The dual origin of the Galactic thick disc and halo from the gas-rich Gaia-Enceladus Sausage merger.” In: *MNRAS* 497.2, pp. 1603–1618. DOI: [10.1093/mnras/staa2057](https://doi.org/10.1093/mnras/staa2057). arXiv: [2001.06009](https://arxiv.org/abs/2001.06009) [[astro-ph.GA](#)].
- Grisoni, V., E. Spitoni, F. Matteucci, A. Recio-Blanco, P. de Laverny, M. Hayden, Š. Mikolaitis, and C. C. Worley (Dec. 2017). “The AMBRE project: chemical evolution models for the Milky Way thick and thin discs.” In: *MNRAS* 472.3, pp. 3637–3647. DOI: [10.1093/mnras/stx2201](https://doi.org/10.1093/mnras/stx2201). arXiv: [1706.02614](https://arxiv.org/abs/1706.02614) [[astro-ph.GA](#)].
- Guglielmo, Magda, Richard R. Lane, Blair C. Conn, Anna Y. Q. Ho, Rodrigo A. Ibata, and Geraint F. Lewis (Mar. 2018). “On the origin of the Monoceros Ring - I. Kinematics, proper motions, and the nature of the progenitor.” In: *MNRAS* 474.4, pp. 4584–4593. DOI: [10.1093/mnras/stx3048](https://doi.org/10.1093/mnras/stx3048). arXiv: [1711.06682](https://arxiv.org/abs/1711.06682) [[astro-ph.GA](#)].
- Habing, H. J. and H. Olofsson, eds. (2003). *Asymptotic giant branch stars*.
- Hammersley, P. L., F. Garzón, T. J. Mahoney, M. López-Corredoira, and M. A. P. Torres (Sept. 2000). “Detection of the old stellar component of the major Galactic bar.” In: *MNRAS* 317.3, pp. L45–L49. DOI: [10.1046/j.1365-8711.2000.03858.x](https://doi.org/10.1046/j.1365-8711.2000.03858.x). arXiv: [astro-ph/0007232](https://arxiv.org/abs/astro-ph/0007232) [[astro-ph](#)].
- Harris, W. E. (Oct. 1996). “A Catalog of Parameters for Globular Clusters in the Milky Way.” In: *AJ* 112, p. 1487. DOI: [10.1086/118116](https://doi.org/10.1086/118116).
- Haschke, Raoul, Eva K. Grebel, and Sonia Duffau (Oct. 2012). “Three-dimensional Maps of the Magellanic Clouds using RR Lyrae Stars and Cepheids. II. The Small Magellanic Cloud.” In: *AJ* 144.4, 107,

- p. 107. DOI: [10.1088/0004-6256/144/4/107](https://doi.org/10.1088/0004-6256/144/4/107). arXiv: [1209.3769](https://arxiv.org/abs/1209.3769) [astro-ph.GA].
- Hasselquist, Sten et al. (Oct. 2020). “Exploring the Stellar Age Distribution of the Milky Way Bulge Using APOGEE.” In: *ApJ* 901.2, 109, p. 109. DOI: [10.3847/1538-4357/abaeee](https://doi.org/10.3847/1538-4357/abaeee). arXiv: [2008.03603](https://arxiv.org/abs/2008.03603) [astro-ph.GA].
- Hayden, M. R. et al. (Aug. 2015). “Chemical Cartography with APOGEE: Metallicity Distribution Functions and the Chemical Structure of the Milky Way Disk.” In: *ApJ* 808, 132, p. 132. DOI: [10.1088/0004-637X/808/2/132](https://doi.org/10.1088/0004-637X/808/2/132). arXiv: [1503.02110](https://arxiv.org/abs/1503.02110).
- Haywood, Misha, Paola Di Matteo, Matthew D. Lehnert, David Katz, and Ana Gómez (Dec. 2013). “The age structure of stellar populations in the solar vicinity. Clues of a two-phase formation history of the Milky Way disk.” In: *A&A* 560, A109, A109. DOI: [10.1051/0004-6361/201321397](https://doi.org/10.1051/0004-6361/201321397). arXiv: [1305.4663](https://arxiv.org/abs/1305.4663) [astro-ph.GA].
- Hindman, J. V., F. J. Kerr, and R. X. McGee (Jan. 1963). “A Low Resolution Hydrogen-line Survey of the Magellanic System. II. Interpretation of Results.” In: *Australian Journal of Physics* 16, p. 570. DOI: [10.1071/PH630570](https://doi.org/10.1071/PH630570).
- Holl, B. et al. (Oct. 2018). “Gaia Data Release 2. Summary of the variability processing and analysis results.” In: *A&A* 618, A30, A30. DOI: [10.1051/0004-6361/201832892](https://doi.org/10.1051/0004-6361/201832892). arXiv: [1804.09373](https://arxiv.org/abs/1804.09373) [astro-ph.SR].
- Holmberg, J., B. Nordström, and J. Andersen (July 2009). “The Geneva-Copenhagen survey of the solar neighbourhood. III. Improved distances, ages, and kinematics.” In: *A&A* 501.3, pp. 941–947. DOI: [10.1051/0004-6361/200811191](https://doi.org/10.1051/0004-6361/200811191). arXiv: [0811.3982](https://arxiv.org/abs/0811.3982) [astro-ph].
- Howard, Christian D., R. Michael Rich, David B. Reitzel, Andreas Koch, Roberto De Propris, and HongSheng Zhao (Dec. 2008). “The Bulge Radial Velocity Assay (BRAVA). I. Sample Selection and a Rotation Curve.” In: *ApJ* 688.2, pp. 1060–1077. DOI: [10.1086/592106](https://doi.org/10.1086/592106). arXiv: [0807.3967](https://arxiv.org/abs/0807.3967) [astro-ph].
- Huang, C. D. et al. (Apr. 2018). “A Near-infrared Period-Luminosity Relation for Miras in NGC 4258, an Anchor for a New Distance Ladder.” In: *ApJ* 857, 67, p. 67. DOI: [10.3847/1538-4357/aab6b3](https://doi.org/10.3847/1538-4357/aab6b3). arXiv: [1801.02711](https://arxiv.org/abs/1801.02711).
- Huang, Caroline D., Adam G. Riess, Wenlong Yuan, Lucas M. Macri, Nadia L. Zakamska, Stefano Casertano, Patricia A. Whitelock, Samantha L. Hoffmann, Alexei V. Filippenko, and Daniel Scolnic (Aug. 2019). “Hubble Space Telescope Observations of Mira Variables in the Type Ia Supernova Host NGC 1559: An Alternative Candle to Measure the Hubble Constant.” In: *arXiv e-prints*, arXiv:1908.10883, arXiv:1908.10883. arXiv: [1908.10883](https://arxiv.org/abs/1908.10883) [astro-ph.CO].

- Huxor, A. P. and E. K. Grebel (Nov. 2015). "Tracing the tidal streams of the Sagittarius dSph, and halo Milky Way features, with carbon-rich long-period variables." In: *MNRAS* 453, pp. 2653–2681. DOI: [10.1093/mnras/stv1631](https://doi.org/10.1093/mnras/stv1631). arXiv: [1507.06776](https://arxiv.org/abs/1507.06776).
- Ibata, R., G. F. Lewis, M. Irwin, E. Totten, and T. Quinn (Apr. 2001). "Great Circle Tidal Streams: Evidence for a Nearly Spherical Massive Dark Halo around the Milky Way." In: *ApJ* 551, pp. 294–311. DOI: [10.1086/320060](https://doi.org/10.1086/320060). eprint: [astro-ph/0004011](https://arxiv.org/abs/astro-ph/0004011).
- Indu, Gopalakrishnan and Annapurni Subramaniam (Jan. 2015). "HI kinematics of the Large Magellanic Cloud revisited: Evidence of possible infall and outflow." In: *A&A* 573, A136, A136. DOI: [10.1051/0004-6361/201321133](https://doi.org/10.1051/0004-6361/201321133). arXiv: [1410.6650](https://arxiv.org/abs/1410.6650) [[astro-ph.GA](https://arxiv.org/abs/1410.6650)].
- Iorio, Giuliano and Vasily Belokurov (Jan. 2019). "The shape of the Galactic halo with Gaia DR2 RR Lyrae. Anatomy of an ancient major merger." In: *MNRAS* 482.3, pp. 3868–3879. DOI: [10.1093/mnras/sty2806](https://doi.org/10.1093/mnras/sty2806). arXiv: [1808.04370](https://arxiv.org/abs/1808.04370) [[astro-ph.GA](https://arxiv.org/abs/1808.04370)].
- Irwin, M. J. (Jan. 1991). "Optical Surveys of the Magellanic Bridge, Stream and Outer Halos." In: *The Magellanic Clouds*. Ed. by Raymond Haynes and Douglas Milne. Vol. 148. IAU Symposium, p. 453.
- Irwin, M. J., Serge Demers, and W. E. Kunkel (Jan. 1990). "A Blue Stellar Link Between the Magellanic Clouds." In: *AJ* 99, p. 191. DOI: [10.1086/115319](https://doi.org/10.1086/115319).
- Irwin, M. J., W. E. Kunkel, and S. Demers (Nov. 1985). "A blue stellar population in the HI bridge between the two Magellanic Clouds." In: *Nature* 318.6042, pp. 160–161. DOI: [10.1038/318160a0](https://doi.org/10.1038/318160a0).
- Ita, Y. et al. (Jan. 2004). "Variable stars in the Magellanic Clouds: results from OGLE and SIRIUS." In: *MNRAS* 347, pp. 720–728. DOI: [10.1111/j.1365-2966.2004.07257.x](https://doi.org/10.1111/j.1365-2966.2004.07257.x). eprint: [astro-ph/0310083](https://arxiv.org/abs/astro-ph/0310083).
- Jacyszyn-Dobrzaniecka, A. M. et al. (Mar. 2017). "OGLE-ing the Magellanic System: Three-Dimensional Structure of the Clouds and the Bridge using RR Lyrae Stars." In: *Acta Astron.* 67.1, pp. 1–35. DOI: [10.32023/0001-5237/67.1.1](https://doi.org/10.32023/0001-5237/67.1.1). arXiv: [1611.02709](https://arxiv.org/abs/1611.02709) [[astro-ph.GA](https://arxiv.org/abs/1611.02709)].
- Jayaraman, A., G. Gilmore, R. F. G. Wyse, J. E. Norris, and V. Belokurov (May 2013). "A 10 000 star spectroscopic survey of the thick disc-halo interface: phase-space sub-structure in the thick disc." In: *MNRAS* 431, pp. 930–953. DOI: [10.1093/mnras/stt221](https://doi.org/10.1093/mnras/stt221). arXiv: [1302.4913](https://arxiv.org/abs/1302.4913).
- Jayasinghe, T. et al. (Mar. 2018). "The ASAS-SN Catalog of Variable Stars I: The Serendipitous Survey." In: *ArXiv e-prints*. arXiv: [1803.01001](https://arxiv.org/abs/1803.01001) [[astro-ph.SR](https://arxiv.org/abs/1803.01001)].

- Johnston, K. V., L. Hernquist, and M. Bolte (July 1996). "Fossil Signatures of Ancient Accretion Events in the Halo." In: *ApJ* 465, p. 278. DOI: [10.1086/177418](https://doi.org/10.1086/177418). eprint: [astro-ph/9602060](https://arxiv.org/abs/astro-ph/9602060).
- Jurić, M. et al. (Feb. 2008). "The Milky Way Tomography with SDSS. I. Stellar Number Density Distribution." In: *ApJ* 673, 864-914, pp. 864-914. DOI: [10.1086/523619](https://doi.org/10.1086/523619). eprint: [astro-ph/0510520](https://arxiv.org/abs/astro-ph/0510520).
- Kallivayalil, Nitya, Roeland P. van der Marel, Gurtina Besla, Jay Anderson, and Charles Alcock (Feb. 2013). "Third-epoch Magellanic Cloud Proper Motions. I. Hubble Space Telescope/WFC3 Data and Orbit Implications." In: *ApJ* 764.2, 161, p. 161. DOI: [10.1088/0004-637X/764/2/161](https://doi.org/10.1088/0004-637X/764/2/161). arXiv: [1301.0832](https://arxiv.org/abs/1301.0832) [[astro-ph.CO](https://arxiv.org/abs/astro-ph.CO)].
- Kamath, D., P. R. Wood, I. Soszyński, and T. Lebzelter (Oct. 2010). "The pulsation of AGB stars in the Magellanic Cloud clusters NGC1978 and 419." In: *MNRAS* 408, pp. 522-534. DOI: [10.1111/j.1365-2966.2010.17137.x](https://doi.org/10.1111/j.1365-2966.2010.17137.x). arXiv: [1006.3121](https://arxiv.org/abs/1006.3121) [[astro-ph.SR](https://arxiv.org/abs/astro-ph.SR)].
- Kepner, J. V. (July 1999). "Inside-out Galaxy Formation." In: *ApJ* 520, pp. 59-66. DOI: [10.1086/307419](https://doi.org/10.1086/307419). eprint: [astro-ph/9710329](https://arxiv.org/abs/astro-ph/9710329).
- Kharchenko, N. V., A. E. Piskunov, E. Schilbach, S. Röser, and R. D. Scholz (Jan. 2016). "Global survey of star clusters in the Milky Way. V. Integrated JHK_S magnitudes and luminosity functions." In: *A&A* 585. DOI: [10.1051/0004-6361/201527292](https://doi.org/10.1051/0004-6361/201527292).
- Khoperskov, Sergey, Paola Di Matteo, Ortwin Gerhard, David Katz, Misha Haywood, Françoise Combes, Peter Berczik, and Ana Gomez (Feb. 2019). "The echo of the bar buckling: Phase-space spirals in Gaia Data Release 2." In: *A&A* 622, L6, p. L6. DOI: [10.1051/0004-6361/201834707](https://doi.org/10.1051/0004-6361/201834707).
- Kilic, M., J. A. Munn, H. C. Harris, T. von Hippel, J. W. Liebert, K. A. Williams, E. Jeffery, and S. DeGennaro (Mar. 2017). "The Ages of the Thin Disk, Thick Disk, and the Halo from Nearby White Dwarfs." In: *ApJ* 837, 162, p. 162. DOI: [10.3847/1538-4357/aa62a5](https://doi.org/10.3847/1538-4357/aa62a5). arXiv: [1702.06984](https://arxiv.org/abs/1702.06984) [[astro-ph.SR](https://arxiv.org/abs/astro-ph.SR)].
- Kobayashi, Naoto, Chikako Yasui, Alan T. Tokunaga, and Masao Saito (Aug. 2008). "Star Formation in the Most Distant Molecular Cloud in the Extreme Outer Galaxy: A Laboratory of Star Formation in an Early Epoch of the Galaxy's Formation." In: *ApJ* 683.1, pp. 178-188. DOI: [10.1086/588421](https://doi.org/10.1086/588421). arXiv: [0803.3369](https://arxiv.org/abs/0803.3369) [[astro-ph](https://arxiv.org/abs/astro-ph)].
- Koposov, S. E., V. Belokurov, D. B. Zucker, G. F. Lewis, R. A. Ibata, E. W. Olszewski, Á. R. López-Sánchez, and E. A. Hyde (Jan. 2015). "Exposing Sgr tidal debris behind the Galactic disc with M giants selected in WISE \cap 2MASS." In: *MNRAS* 446.3, pp. 3110-3117. DOI: [10.1093/mnras/stu2263](https://doi.org/10.1093/mnras/stu2263). arXiv: [1410.6482](https://arxiv.org/abs/1410.6482) [[astro-ph.GA](https://arxiv.org/abs/astro-ph.GA)].

- Kordopatis, G. et al. (2013). “In the thick of it: metal-poor disc stars in RAVE.” In: *MNRAS* 436.4, pp. 3231–3246. DOI: [10.1093/mnras/stt1804](https://doi.org/10.1093/mnras/stt1804). arXiv: [1310.1919](https://arxiv.org/abs/1310.1919) [[astro-ph.GA](https://arxiv.org/archive/astro-ph)].
- Kormendy, J. and G. Illingworth (May 1982). “Rotation of the bulge components of disk galaxies.” In: *ApJ* 256, p. 460. DOI: [10.1086/159923](https://doi.org/10.1086/159923).
- Kormendy, John and Jr. Kennicutt Robert C. (Sept. 2004). “Secular Evolution and the Formation of Pseudobulges in Disk Galaxies.” In: *ARA&A* 42.1, pp. 603–683. DOI: [10.1146/annurev.astro.42.053102.134024](https://doi.org/10.1146/annurev.astro.42.053102.134024). arXiv: [astro-ph/0407343](https://arxiv.org/abs/astro-ph/0407343) [[astro-ph](https://arxiv.org/archive/astro-ph)].
- Kunder, Andrea et al. (Mar. 2012). “The Bulge Radial Velocity Assay (BRAVA). II. Complete Sample and Data Release.” In: *AJ* 143.3, 57, p. 57. DOI: [10.1088/0004-6256/143/3/57](https://doi.org/10.1088/0004-6256/143/3/57). arXiv: [1112.1955](https://arxiv.org/abs/1112.1955) [[astro-ph.SR](https://arxiv.org/archive/astro-ph)].
- Laporte, Chervin F. P., Kathryn V. Johnston, and Anastasios Tzanidakis (Feb. 2019). “Stellar disc streams as probes of the Galactic potential and satellite impacts.” In: *MNRAS* 483.2, pp. 1427–1436. DOI: [10.1093/mnras/sty2362](https://doi.org/10.1093/mnras/sty2362). arXiv: [1803.11198](https://arxiv.org/abs/1803.11198) [[astro-ph.GA](https://arxiv.org/archive/astro-ph)].
- Laporte, Chervin F. P., Ivan Minchev, Kathryn V. Johnston, and Facundo A. Gómez (May 2019). “Footprints of the Sagittarius dwarf galaxy in the Gaia data set.” In: *MNRAS* 485.3, pp. 3134–3152. DOI: [10.1093/mnras/stz583](https://doi.org/10.1093/mnras/stz583). arXiv: [1808.00451](https://arxiv.org/abs/1808.00451) [[astro-ph.GA](https://arxiv.org/archive/astro-ph)].
- Larson, R. B. (July 1976). “Models for the formation of disc galaxies.” In: *MNRAS* 176, pp. 31–52. DOI: [10.1093/mnras/176.1.31](https://doi.org/10.1093/mnras/176.1.31).
- Li, Jing et al. (May 2016). “Selecting M Giants with Infrared Photometry: Distances, Metallicities, and the Sagittarius Stream.” In: *ApJ* 823.1, 59, p. 59. DOI: [10.3847/0004-637X/823/1/59](https://doi.org/10.3847/0004-637X/823/1/59). arXiv: [1603.00262](https://arxiv.org/abs/1603.00262) [[astro-ph.GA](https://arxiv.org/archive/astro-ph)].
- Li, Zhao-Yu and Juntao Shen (Apr. 2019). “Dissecting the Phase Space Snail Shell.” In: *arXiv e-prints*, arXiv:1904.03314, arXiv:1904.03314. arXiv: [1904.03314](https://arxiv.org/abs/1904.03314) [[astro-ph.GA](https://arxiv.org/archive/astro-ph)].
- Licquia, Timothy C. and Jeffrey A. Newman (June 2015). “Improved Estimates of the Milky Way’s Stellar Mass and Star Formation Rate from Hierarchical Bayesian Meta-Analysis.” In: *ApJ* 806.1, 96, p. 96. DOI: [10.1088/0004-637X/806/1/96](https://doi.org/10.1088/0004-637X/806/1/96). arXiv: [1407.1078](https://arxiv.org/abs/1407.1078) [[astro-ph.GA](https://arxiv.org/archive/astro-ph)].
- Liu, W. M. and B. Chaboyer (Dec. 2000). “The Relative Age of the Thin and Thick Galactic Disks.” In: *ApJ* 544, pp. 818–829. DOI: [10.1086/317231](https://doi.org/10.1086/317231). eprint: [astro-ph/0007193](https://arxiv.org/abs/astro-ph/0007193).
- López-Corredoira, M. (Feb. 2017). “Absence of an X-shaped Structure in the Milky Way Bulge Using Mira Variable Stars.” In: *ApJ* 836, 218, p. 218. DOI: [10.3847/1538-4357/836/2/218](https://doi.org/10.3847/1538-4357/836/2/218). arXiv: [1702.02539](https://arxiv.org/abs/1702.02539).

- López-Corredoira, M., A. Cabrera-Lavers, T. J. Mahoney, P. L. Hammersley, F. Garzón, and C. González-Fernández (Jan. 2007). “The Long Bar in the Milky Way: Corroboration of an Old Hypothesis.” In: *AJ* 133.1, pp. 154–161. DOI: [10.1086/509605](https://doi.org/10.1086/509605). arXiv: [astro-ph/0606201](https://arxiv.org/abs/astro-ph/0606201) [astro-ph].
- López-Corredoira, M., Y. W. Lee, F. Garzón, and D. Lim (July 2019). “Distribution of red clump stars does not support the X-shaped Galactic bulge.” In: *A&A* 627, A3, A3. DOI: [10.1051/0004-6361/201935571](https://doi.org/10.1051/0004-6361/201935571). arXiv: [1905.13592](https://arxiv.org/abs/1905.13592) [astro-ph.GA].
- Lorenz, D., T. Lebzelter, W. Nowotny, J. Telting, F. Kerschbaum, H. Olofsson, and H. E. Schwarz (Aug. 2011). “Long-period variables in NGC 147 and NGC 185.” In: *A&A* 532, A78, A78. DOI: [10.1051/0004-6361/201116951](https://doi.org/10.1051/0004-6361/201116951). arXiv: [1106.5280](https://arxiv.org/abs/1106.5280) [astro-ph.SR].
- Lynden-Bell, D. and R. M. Lynden-Bell (July 1995). “Ghostly streams from the formation of the Galaxy’s halo.” In: *MNRAS* 275, pp. 429–442. DOI: [10.1093/mnras/275.2.429](https://doi.org/10.1093/mnras/275.2.429).
- Mackey, A. D., S. E. Koposov, G. S. Da Costa, V. Belokurov, D. Erkal, F. Fraternali, N. M. McClure-Griffiths, and M. Fraser (Dec. 2017). “Structured star formation in the Magellanic inter-Cloud region.” In: *MNRAS* 472.3, pp. 2975–2989. DOI: [10.1093/mnras/stx2035](https://doi.org/10.1093/mnras/stx2035). arXiv: [1708.04363](https://arxiv.org/abs/1708.04363) [astro-ph.GA].
- Mackey, A. D., S. E. Koposov, D. Erkal, V. Belokurov, G. S. Da Costa, and F. A. Gómez (June 2016). “A 10 kpc stellar substructure at the edge of the Large Magellanic Cloud: perturbed outer disc or evidence for tidal stripping?” In: *MNRAS* 459.1, pp. 239–255. DOI: [10.1093/mnras/stw497](https://doi.org/10.1093/mnras/stw497). arXiv: [1508.01356](https://arxiv.org/abs/1508.01356) [astro-ph.GA].
- Mackey, Dougal, Sergey Koposov, Gary Da Costa, Vasily Belokurov, Denis Erkal, and Pete Kuzma (May 2018). “Substructures and Tidal Distortions in the Magellanic Stellar Periphery.” In: *ApJ* 858.2, L21, p. L21. DOI: [10.3847/2041-8213/aac175](https://doi.org/10.3847/2041-8213/aac175). arXiv: [1804.06431](https://arxiv.org/abs/1804.06431) [astro-ph.GA].
- Majewski, S. R., APOGEE Team, and APOGEE-2 Team (Sept. 2016). “The Apache Point Observatory Galactic Evolution Experiment (APOGEE) and its successor, APOGEE-2.” In: *Astronomische Nachrichten* 337.8-9, p. 863. DOI: [10.1002/asna.201612387](https://doi.org/10.1002/asna.201612387).
- Majewski, S. R., M. F. Skrutskie, M. D. Weinberg, and J. C. Ostheimer (Dec. 2003). “A Two Micron All Sky Survey View of the Sagittarius Dwarf Galaxy. I. Morphology of the Sagittarius Core and Tidal Arms.” In: *ApJ* 599, pp. 1082–1115. DOI: [10.1086/379504](https://doi.org/10.1086/379504). eprint: [astro-ph/0304198](https://arxiv.org/abs/astro-ph/0304198).
- Martig, M., M. Fouesneau, H.-W. Rix, M. Ness, S. Mészáros, D. A. García-Hernández, M. Pinsonneault, A. Serenelli, V. Silva Aguirre, and O. Zamora (Mar. 2016a). “Red giant masses and ages de-

- rived from carbon and nitrogen abundances." In: *MNRAS* 456, pp. 3655–3670. DOI: [10.1093/mnras/stv2830](https://doi.org/10.1093/mnras/stv2830). arXiv: [1511.08203](https://arxiv.org/abs/1511.08203) [astro-ph.SR].
- Martig, M., I. Minchev, M. Ness, M. Fouesneau, and H.-W. Rix (Nov. 2016b). "A Radial Age Gradient in the Geometrically Thick Disk of the Milky Way." In: *ApJ* 831, 139, p. 139. DOI: [10.3847/0004-637X/831/2/139](https://doi.org/10.3847/0004-637X/831/2/139). arXiv: [1609.01168](https://arxiv.org/abs/1609.01168).
- Martinez-Valpuesta, Inma and Ortwin Gerhard (June 2011). "Unifying A Boxy Bulge and Planar Long Bar in the Milky Way." In: *ApJ* 734.1, L20, p. L20. DOI: [10.1088/2041-8205/734/1/L20](https://doi.org/10.1088/2041-8205/734/1/L20). arXiv: [1105.0928](https://arxiv.org/abs/1105.0928) [astro-ph.GA].
- Massana, Pol et al. (Aug. 2020). "SMASHing the low surface brightness SMC." In: *MNRAS* 498.1, pp. 1034–1049. DOI: [10.1093/mnras/staa2451](https://doi.org/10.1093/mnras/staa2451). arXiv: [2008.00012](https://arxiv.org/abs/2008.00012) [astro-ph.GA].
- Mateu, C., G. Bruzual, L. Aguilar, A. G. A. Brown, O. Valenzuela, L. Carigi, H. Velázquez, and F. Hernández (July 2011). "Detection of satellite remnants in the Galactic Halo with Gaia - II. A modified great circle cell method." In: *MNRAS* 415, pp. 214–224. DOI: [10.1111/j.1365-2966.2011.18690.x](https://doi.org/10.1111/j.1365-2966.2011.18690.x). arXiv: [1103.0283](https://arxiv.org/abs/1103.0283).
- Matsunaga, N., J. W. Menzies, M. W. Feast, P. A. Whitelock, H. Onozato, S. Barway, and E. Aydi (Aug. 2017). "Discovery of carbon-rich Miras in the Galactic bulge." In: *MNRAS* 469, pp. 4949–4956. DOI: [10.1093/mnras/stx1213](https://doi.org/10.1093/mnras/stx1213). arXiv: [1705.05485](https://arxiv.org/abs/1705.05485) [astro-ph.SR].
- Matsuura, M. et al. (June 2009). "The global gas and dust budget of the Large Magellanic Cloud: AGB stars and supernovae, and the impact on the ISM evolution." In: *MNRAS* 396, pp. 918–934. DOI: [10.1111/j.1365-2966.2009.14743.x](https://doi.org/10.1111/j.1365-2966.2009.14743.x). arXiv: [0903.1123](https://arxiv.org/abs/0903.1123).
- Mauron, N. (Apr. 2008). "New observations of cool carbon stars in the halo." In: *A&A* 482, pp. 151–163. DOI: [10.1051/0004-6361:200809378](https://doi.org/10.1051/0004-6361:200809378). arXiv: [0803.2650](https://arxiv.org/abs/0803.2650).
- Mauron, N., K. S. Gigoyan, and G. R. Kostandyan (Mar. 2018). "New Asymptotic Giant Branch Carbon Stars in the Galactic Halo." In: *Astrophysics* 61, pp. 83–90. DOI: [10.1007/s10511-018-9517-x](https://doi.org/10.1007/s10511-018-9517-x).
- McConnachie, A. W. (July 2012). "The Observed Properties of Dwarf Galaxies in and around the Local Group." In: *AJ* 144, 4, p. 4. DOI: [10.1088/0004-6256/144/1/4](https://doi.org/10.1088/0004-6256/144/1/4). arXiv: [1204.1562](https://arxiv.org/abs/1204.1562).
- McWilliam, Andrew and R. Michael Rich (Apr. 1994). "The First Detailed Abundance Analysis of Galactic Bulge K Giants in Baade's Window." In: *ApJS* 91, p. 749. DOI: [10.1086/191954](https://doi.org/10.1086/191954).
- McWilliam, Andrew and Manuela Zoccali (2010). "Two Red Clumps and the X-shaped Milky Way Bulge." In: *ApJ* 724.2, pp. 1491–1502. DOI: [10.1088/0004-637X/724/2/1491](https://doi.org/10.1088/0004-637X/724/2/1491). arXiv: [1008.0519](https://arxiv.org/abs/1008.0519) [astro-ph.GA].

- Medina, G. E. et al. (Mar. 2018). "Discovery of Distant RR Lyrae Stars in the Milky Way Using DECam." In: *ApJ* 855, 43, p. 43. DOI: [10.3847/1538-4357/aaad02](https://doi.org/10.3847/1538-4357/aaad02). arXiv: [1802.01581](https://arxiv.org/abs/1802.01581).
- Menzies, J. W., M. W. Feast, P. A. Whitelock, and N. Matsunaga (July 2011). "Asymptotic giant branch stars in the Sculptor dwarf spheroidal galaxy." In: *MNRAS* 414, pp. 3492–3500. DOI: [10.1111/j.1365-2966.2011.18649.x](https://doi.org/10.1111/j.1365-2966.2011.18649.x). arXiv: [1103.1739](https://arxiv.org/abs/1103.1739).
- Minchev, I., B. Famaey, F. Combes, P. Di Matteo, M. Mouhcine, and H. Wozniak (Mar. 2011). "Radial migration in galactic disks caused by resonance overlap of multiple patterns: Self-consistent simulations." In: *A&A* 527, A147, A147. DOI: [10.1051/0004-6361/201015139](https://doi.org/10.1051/0004-6361/201015139). arXiv: [1006.0484](https://arxiv.org/abs/1006.0484) [[astro-ph.GA](https://arxiv.org/abs/1006.0484)].
- Minchev, I., M. Martig, D. Streich, C. Scannapieco, R. S. de Jong, and M. Steinmetz (May 2015). "On the Formation of Galactic Thick Disks." In: *ApJ* 804.1, L9, p. L9. DOI: [10.1088/2041-8205/804/1/L9](https://doi.org/10.1088/2041-8205/804/1/L9). arXiv: [1502.06606](https://arxiv.org/abs/1502.06606) [[astro-ph.GA](https://arxiv.org/abs/1502.06606)].
- Minniti, Dante, Edward W. Olszewski, James Liebert, Simon D. M. White, John M. Hill, and Michael J. Irwin (Dec. 1995). "The metallicity gradient of the Galactic bulge*." In: *MNRAS* 277.4, pp. 1293–1311. DOI: [10.1093/mnras/277.4.1293](https://doi.org/10.1093/mnras/277.4.1293).
- Mishenina, T. V., C. Soubiran, V. V. Kovtyukh, and S. A. Korotin (May 2004). "On the correlation of elemental abundances with kinematics among galactic disk stars." In: *A&A* 418, pp. 551–562. DOI: [10.1051/0004-6361:20034454](https://doi.org/10.1051/0004-6361:20034454). eprint: [astro-ph/0401234](https://arxiv.org/abs/astro-ph/0401234).
- Mo, H., F. C. van den Bosch, and S. White (May 2010). *Galaxy Formation and Evolution*.
- Molaeinezhad, A., J. Falcón-Barroso, I. Martínez-Valpuesta, H. G. Khoshahahi, M. Balcells, and R. F. Peletier (Feb. 2016). "Establishing the level of cylindrical rotation in boxy/peanut bulges." In: *MNRAS* 456.1, pp. 692–709. DOI: [10.1093/mnras/stv2697](https://doi.org/10.1093/mnras/stv2697). arXiv: [1511.05572](https://arxiv.org/abs/1511.05572) [[astro-ph.GA](https://arxiv.org/abs/1511.05572)].
- Moni Bidin, C., D. I. Casetti-Dinescu, T. M. Girard, L. Zhang, R. A. Méndez, K. Vieira, V. I. Korchagin, and W. F. van Altena (Apr. 2017). "Young stars in the periphery of the Large Magellanic Cloud." In: *MNRAS* 466.3, pp. 3077–3087. DOI: [10.1093/mnras/stw3242](https://doi.org/10.1093/mnras/stw3242). arXiv: [1612.03072](https://arxiv.org/abs/1612.03072) [[astro-ph.GA](https://arxiv.org/abs/1612.03072)].
- Mowlavi, N. et al. (Oct. 2018). "Gaia Data Release 2. The first Gaia catalogue of long-period variable candidates." In: *A&A* 618, A58, A58. DOI: [10.1051/0004-6361/201833366](https://doi.org/10.1051/0004-6361/201833366). arXiv: [1805.02035](https://arxiv.org/abs/1805.02035) [[astro-ph.SR](https://arxiv.org/abs/1805.02035)].
- Muraveva, T. et al. (Jan. 2018). "The VMC survey - XXVI. Structure of the Small Magellanic Cloud from RR Lyrae stars." In: *MNRAS*

- 473.3, pp. 3131–3146. DOI: [10.1093/mnras/stx2514](https://doi.org/10.1093/mnras/stx2514). arXiv: [1709.09064](https://arxiv.org/abs/1709.09064) [astro-ph.SR].
- Myeong, G. C., N. W. Evans, V. Belokurov, J. L. Sanders, and S. E. Koposov (Aug. 2018a). “Discovery of new retrograde substructures: the shards of ω Centauri?” In: *MNRAS* 478.4, pp. 5449–5459. DOI: [10.1093/mnras/sty1403](https://doi.org/10.1093/mnras/sty1403).
- Myeong, G. C., N. W. Evans, V. Belokurov, J. L. Sanders, and S. E. Koposov (Apr. 2018b). “The Milky Way Halo in Action Space.” In: *ApJ* 856.2, L26, p. L26. DOI: [10.3847/2041-8213/aab613](https://doi.org/10.3847/2041-8213/aab613). arXiv: [1802.03351](https://arxiv.org/abs/1802.03351) [astro-ph.GA].
- Myeong, G. C., N. W. Evans, V. Belokurov, J. L. Sanders, and S. E. Koposov (Aug. 2018c). “The Sausage Globular Clusters.” In: *ApJ* 863.2, L28, p. L28. DOI: [10.3847/2041-8213/aad7f7](https://doi.org/10.3847/2041-8213/aad7f7). arXiv: [1805.00453](https://arxiv.org/abs/1805.00453) [astro-ph.GA].
- Ness, M., K. Freeman, E. Athanassoula, E. Wylie-de-Boer, J. Bland-Hawthorn, M. Asplund, G. F. Lewis, D. Yong, R. R. Lane, and L. L. Kiss (Apr. 2013a). “ARGOS - III. Stellar populations in the Galactic bulge of the Milky Way.” In: *MNRAS* 430.2, pp. 836–857. DOI: [10.1093/mnras/sts629](https://doi.org/10.1093/mnras/sts629). arXiv: [1212.1540](https://arxiv.org/abs/1212.1540) [astro-ph.GA].
- Ness, M., D. W. Hogg, H.-W. Rix, M. Martig, M. H. Pinsonneault, and A. Y. Q. Ho (June 2016). “Spectroscopic Determination of Masses (and Implied Ages) for Red Giants.” In: *ApJ* 823, 114, p. 114. DOI: [10.3847/0004-637X/823/2/114](https://doi.org/10.3847/0004-637X/823/2/114). arXiv: [1511.08204](https://arxiv.org/abs/1511.08204) [astro-ph.SR].
- Ness, M. et al. (Sept. 2012). “The Origin of the Split Red Clump in the Galactic Bulge of the Milky Way.” In: *ApJ* 756.1, 22, p. 22. DOI: [10.1088/0004-637X/756/1/22](https://doi.org/10.1088/0004-637X/756/1/22). arXiv: [1207.0888](https://arxiv.org/abs/1207.0888) [astro-ph.GA].
- Ness, M. et al. (July 2013b). “ARGOS - IV. The kinematics of the Milky Way bulge.” In: *MNRAS* 432.3, pp. 2092–2103. DOI: [10.1093/mnras/stt533](https://doi.org/10.1093/mnras/stt533). arXiv: [1303.6656](https://arxiv.org/abs/1303.6656) [astro-ph.GA].
- Ness, Melissa and Dustin Lang (July 2016). “The X-shaped Bulge of the Milky Way Revealed by WISE.” In: *AJ* 152.1, 14, p. 14. DOI: [10.3847/0004-6256/152/1/14](https://doi.org/10.3847/0004-6256/152/1/14). arXiv: [1603.00026](https://arxiv.org/abs/1603.00026) [astro-ph.GA].
- Nidever, D. L., S. R. Majewski, and W. Butler Burton (May 2008). “The Origin of the Magellanic Stream and Its Leading Arm.” In: *ApJ* 679, pp. 432–459. DOI: [10.1086/587042](https://doi.org/10.1086/587042).
- Nidever, David L., Antonela Monachesi, Eric F. Bell, Steven R. Majewski, Ricardo R. Muñoz, and Rachael L. Beaton (Dec. 2013). “A Tidally Stripped Stellar Component of the Magellanic Bridge.” In: *ApJ* 779.2, 145, p. 145. DOI: [10.1088/0004-637X/779/2/145](https://doi.org/10.1088/0004-637X/779/2/145). arXiv: [1310.4824](https://arxiv.org/abs/1310.4824) [astro-ph.GA].
- Nidever, David L. et al. (June 2020). “The Lazy Giants: APOGEE Abundances Reveal Low Star Formation Efficiencies in the Mag-

- ellanic Clouds." In: *ApJ* 895.2, 88, p. 88. DOI: [10.3847/1538-4357/ab7305](https://doi.org/10.3847/1538-4357/ab7305). arXiv: [1901.03448](https://arxiv.org/abs/1901.03448) [astro-ph.GA].
- Niederhofer, F. et al. (May 2018). "The VMC survey. XXX. Stellar proper motions in the central parts of the Small Magellanic Cloud." In: *A&A* 613, L8, p. L8. DOI: [10.1051/0004-6361/201833144](https://doi.org/10.1051/0004-6361/201833144). arXiv: [1804.04689](https://arxiv.org/abs/1804.04689) [astro-ph.GA].
- Nikolaev, S., A. J. Drake, S. C. Keller, K. H. Cook, N. Dalal, K. Griest, D. L. Welch, and S. M. Kanbur (Jan. 2004). "Geometry of the Large Magellanic Cloud Disk: Results from MACHO and the Two Micron All Sky Survey." In: *ApJ* 601.1, pp. 260–276. DOI: [10.1086/380439](https://doi.org/10.1086/380439).
- Nishida, S., T. Tanabé, Y. Nakada, S. Matsumoto, K. Sekiguchi, and I. S. Glass (Mar. 2000). "The variability of Magellanic cluster infrared stars." In: *MNRAS* 313, pp. 136–140. DOI: [10.1046/j.1365-8711.2000.03189.x](https://doi.org/10.1046/j.1365-8711.2000.03189.x).
- Nissen, P. E. and W. J. Schuster (Feb. 2010). "Two distinct halo populations in the solar neighborhood. Evidence from stellar abundance ratios and kinematics." In: *A&A* 511, L10, p. L10. DOI: [10.1051/0004-6361/200913877](https://doi.org/10.1051/0004-6361/200913877). arXiv: [1002.4514](https://arxiv.org/abs/1002.4514) [astro-ph.GA].
- Ochsendorf, Bram B., Hans Zinnecker, Omnarayani Nayak, John Bally, Margaret Meixner, Olivia C. Jones, Remy Indebetouw, and Mubdi Rahman (Oct. 2017). "The star-forming complex LMC-N79 as a future rival to 30 Doradus." In: *Nature Astronomy* 1, pp. 784–790. DOI: [10.1038/s41550-017-0268-0](https://doi.org/10.1038/s41550-017-0268-0). arXiv: [1710.00805](https://arxiv.org/abs/1710.00805) [astro-ph.GA].
- Ojha, D. K. (Apr. 2001). "Radial scalelengths of the galactic thin and thick disc with 2MASS data." In: *MNRAS* 322, pp. 426–432. DOI: [10.1046/j.1365-8711.2001.04155.x](https://doi.org/10.1046/j.1365-8711.2001.04155.x).
- Olsen, K. A. G. and C. Salyk (Oct. 2002). "A Warp in the Large Magellanic Cloud Disk?" In: *AJ* 124.4, pp. 2045–2053. DOI: [10.1086/342739](https://doi.org/10.1086/342739).
- Olsen, Knut A. G., Dennis Zaritsky, Robert D. Blum, Martha L. Boyer, and Karl D. Gordon (Aug. 2011). "A Population of Accreted Small Magellanic Cloud Stars in the Large Magellanic Cloud." In: *ApJ* 737.1, 29, p. 29. DOI: [10.1088/0004-637X/737/1/29](https://doi.org/10.1088/0004-637X/737/1/29). arXiv: [1106.0044](https://arxiv.org/abs/1106.0044) [astro-ph.GA].
- Omkumar, Abinaya O., Smitha Subramanian, Florian Niederhofer, Jonathan Diaz, Maria-Rosa L. Cioni, Dalal El Youssoufi, Kenji Bekki, Richard de Grijs, and Jacco Th. van Loon (Oct. 2020). "Gaia view of a stellar sub-structure in front of the Small Magellanic Cloud." In: *arXiv e-prints*, arXiv:2010.02687, arXiv:2010.02687. arXiv: [2010.02687](https://arxiv.org/abs/2010.02687) [astro-ph.GA].

- Pearson, Sarah, George C. Privon, Gurtina Besla, Mary E. Putman, David Martínez-Delgado, Kathryn V. Johnston, R. Jay Gabany, David R. Patton, and Nitya Kallivayalil (Nov. 2018). “Modelling the baryon cycle in low-mass galaxy encounters: the case of NGC 4490 and NGC 4485.” In: *MNRAS* 480.3, pp. 3069–3090. DOI: [10.1093/mnras/sty2052](https://doi.org/10.1093/mnras/sty2052). arXiv: [1807.03791](https://arxiv.org/abs/1807.03791) [astro-ph.GA].
- Pedregosa, F. et al. (2011). “Scikit-learn: Machine Learning in Python.” In: *Journal of Machine Learning Research* 12, pp. 2825–2830.
- Peterken, Thomas, Amelia Fraser-McKelvie, Alfonso Aragón-Salamanca, Michael Merrifield, Katarina Kraljic, Johan H. Knapen, Rogério Riffel, Joel Brownstein, and Niv Drory (Aug. 2019). “Time-slicing spiral galaxies with SDSS-IV MaNGA.” In: *MNRAS*, p. 2135. DOI: [10.1093/mnras/stz2204](https://doi.org/10.1093/mnras/stz2204). arXiv: [1908.05013](https://arxiv.org/abs/1908.05013) [astro-ph.GA].
- Piatti, Andrés E. (Feb. 2018). “Stellar density distribution along the minor axis of the Large Magellanic Cloud.” In: *MNRAS* 473.4, pp. 4410–4416. DOI: [10.1093/mnras/stx2686](https://doi.org/10.1093/mnras/stx2686). arXiv: [1710.04053](https://arxiv.org/abs/1710.04053) [astro-ph.GA].
- Pietrukowicz, P. et al. (Oct. 2015). “Deciphering the 3D Structure of the Old Galactic Bulge from the OGLE RR Lyrae Stars.” In: *ApJ* 811.2, 113, p. 113. DOI: [10.1088/0004-637X/811/2/113](https://doi.org/10.1088/0004-637X/811/2/113). arXiv: [1412.4121](https://arxiv.org/abs/1412.4121) [astro-ph.GA].
- Pohlen, M., S. Zaroubi, R. F. Peletier, and R.-J. Dettmar (June 2007). “On the three-dimensional structure of edge-on disc galaxies.” In: *MNRAS* 378, pp. 594–616. DOI: [10.1111/j.1365-2966.2007.11790.x](https://doi.org/10.1111/j.1365-2966.2007.11790.x). eprint: [astro-ph/0703768](https://arxiv.org/abs/astro-ph/0703768).
- Price-Whelan, Adrian M., Kathryn V. Johnston, Allyson A. Sheffield, Chervin F. P. Laporte, and Branimir Sesar (Sept. 2015). “A reinterpretation of the Triangulum-Andromeda stellar clouds: a population of halo stars kicked out of the Galactic disc.” In: *MNRAS* 452.1, pp. 676–685. DOI: [10.1093/mnras/stv1324](https://doi.org/10.1093/mnras/stv1324). arXiv: [1503.08780](https://arxiv.org/abs/1503.08780) [astro-ph.GA].
- Prudil, Z., I. Dékány, M. Catelan, R. Smolec, E. K. Grebel, and M. Skarka (Apr. 2019). “On the Oosterhoff dichotomy in the Galactic bulge: I. Spatial distribution.” In: *MNRAS* 484.4, pp. 4833–4848. DOI: [10.1093/mnras/stz311](https://doi.org/10.1093/mnras/stz311). arXiv: [1901.09726](https://arxiv.org/abs/1901.09726) [astro-ph.SR].
- Ramírez, Solange V., Andrew W. Stephens, Jay A. Frogel, and D. L. DePoy (Aug. 2000). “Metallicity of Red Giants in the Galactic Bulge from Near-Infrared Spectroscopy.” In: *AJ* 120.2, pp. 833–844. DOI: [10.1086/301466](https://doi.org/10.1086/301466). arXiv: [astro-ph/0003116](https://arxiv.org/abs/astro-ph/0003116) [astro-ph].
- Rattenbury, Nicholas J., Shude Mao, Takahiro Sumi, and Martin C. Smith (July 2007). “Modelling the Galactic bar using OGLE-II red clump giant stars.” In: *MNRAS* 378.3, pp. 1064–1078. DOI: [10.1111/j.1365-2966.2007.11843.x](https://doi.org/10.1111/j.1365-2966.2007.11843.x). arXiv: [0704.1614](https://arxiv.org/abs/0704.1614) [astro-ph].

- Reddy, B. E., D. L. Lambert, and C. Allende Prieto (Apr. 2006). “Elemental abundance survey of the Galactic thick disc.” In: *MNRAS* 367, pp. 1329–1366. DOI: [10.1111/j.1365-2966.2006.10148.x](https://doi.org/10.1111/j.1365-2966.2006.10148.x). eprint: [astro-ph/0512505](https://arxiv.org/abs/astro-ph/0512505).
- Rejkuba, M., D. Minniti, and D. R. Silva (July 2003). “Long period variables in NGC 5128. I. Catalogue.” In: *A&A* 406, pp. 75–85. DOI: [10.1051/0004-6361:20030683](https://doi.org/10.1051/0004-6361:20030683). eprint: [astro-ph/0305432](https://arxiv.org/abs/astro-ph/0305432).
- Rejkuba, M., D. Minniti, D. R. Silva, and T. R. Bedding (Dec. 2003). “Long Period Variables in NGC 5128 . II. Near-IR properties.” In: *A&A* 411, pp. 351–360. DOI: [10.1051/0004-6361:20034056](https://doi.org/10.1051/0004-6361:20034056). eprint: [astro-ph/0309358](https://arxiv.org/abs/astro-ph/0309358).
- Renzini, Alvio, Mario Gennaro, Manuela Zoccali, Thomas M. Brown, Jay Anderson, Dante Minniti, Kailash C. Sahu, Elena Valenti, and Don A. Vandenberg (Aug. 2018). “The WFC3 Galactic Bulge Treasury Program: Relative Ages of Bulge Stars of High and Low Metallicity.” In: *ApJ* 863.1, 16, p. 16. DOI: [10.3847/1538-4357/aad09b](https://doi.org/10.3847/1538-4357/aad09b). arXiv: [1806.11556](https://arxiv.org/abs/1806.11556) [[astro-ph.GA](https://arxiv.org/abs/astro-ph.GA)].
- Renzini, Alvio and Laura Greggio (Jan. 1990). “The Evolution of Bulge and Super Metal Rich Stars - a.” In: *European Southern Observatory Conference and Workshop Proceedings*. Vol. 35. European Southern Observatory Conference and Workshop Proceedings, p. 47.
- Rich, R. Michael and Livia Origlia (2005). “The First Detailed Abundances for M Giants in Baade’s Window from Infrared Spectroscopy.” In: *ApJ* 634.2, pp. 1293–1299. DOI: [10.1086/432592](https://doi.org/10.1086/432592). arXiv: [astro-ph/0506051](https://arxiv.org/abs/astro-ph/0506051) [[astro-ph](https://arxiv.org/abs/astro-ph)].
- Ripepi, Vincenzo et al. (Nov. 2017). “The VMC survey - XXV. The 3D structure of the Small Magellanic Cloud from Classical Cepheids.” In: *MNRAS* 472.1, pp. 808–827. DOI: [10.1093/mnras/stx2096](https://doi.org/10.1093/mnras/stx2096). arXiv: [1707.04500](https://arxiv.org/abs/1707.04500) [[astro-ph.GA](https://arxiv.org/abs/astro-ph.GA)].
- Rocha-Pinto, H. J., S. R. Majewski, M. F. Skrutskie, J. D. Crane, and R. J. Patterson (Nov. 2004). “Exploring Halo Substructure with Giant Stars: A Diffuse Star Cloud or Tidal Debris around the Milky Way in Triangulum-Andromeda.” In: *ApJ* 615, pp. 732–737. DOI: [10.1086/424585](https://doi.org/10.1086/424585). eprint: [astro-ph/0405437](https://arxiv.org/abs/astro-ph/0405437).
- Rojas-Arriagada, A. et al. (Sept. 2014). “The Gaia-ESO Survey: metallicity and kinematic trends in the Milky Way bulge.” In: *A&A* 569, A103, A103. DOI: [10.1051/0004-6361/201424121](https://doi.org/10.1051/0004-6361/201424121). arXiv: [1408.4558](https://arxiv.org/abs/1408.4558).
- Romero-Gómez, M., E. Athanassoula, T. Antoja, and F. Figueras (2011). “Modelling the inner disc of the Milky Way with manifolds - I. A first step.” In: *MNRAS* 418.2, pp. 1176–1193. DOI: [10.1111/j.1365-2966.2011.19569.x](https://doi.org/10.1111/j.1365-2966.2011.19569.x). arXiv: [1108.0660](https://arxiv.org/abs/1108.0660) [[astro-ph.GA](https://arxiv.org/abs/astro-ph.GA)].

- Roškar, R., V. P. Debattista, G. S. Stinson, T. R. Quinn, T. Kaufmann, and J. Wadsley (Mar. 2008). “Beyond Inside-Out Growth: Formation and Evolution of Disk Outskirts.” In: *ApJ* 675, L65, p. L65. DOI: [10.1086/586734](https://doi.org/10.1086/586734). arXiv: [0710.5523](https://arxiv.org/abs/0710.5523).
- Roškar, Rok, Victor P. Debattista, Thomas R. Quinn, Gregory S. Stinson, and James Wadsley (Sept. 2008). “Riding the Spiral Waves: Implications of Stellar Migration for the Properties of Galactic Disks.” In: *ApJ* 684.2, p. L79. DOI: [10.1086/592231](https://doi.org/10.1086/592231). arXiv: [0808.0206](https://arxiv.org/abs/0808.0206) [astro-ph].
- Rubele, Stefano et al. (May 2015). “The VMC survey - XIV. First results on the look-back time star formation rate tomography of the Small Magellanic Cloud.” In: *MNRAS* 449.1, pp. 639–661. DOI: [10.1093/mnras/stv141](https://doi.org/10.1093/mnras/stv141). arXiv: [1501.05347](https://arxiv.org/abs/1501.05347) [astro-ph.SR].
- Ruiz-Lara, T. et al. (July 2020). “The Large Magellanic Cloud stellar content with SMASH. I. Assessing the stability of the Magellanic spiral arms.” In: *A&A* 639, L3, p. L3. DOI: [10.1051/0004-6361/202038392](https://doi.org/10.1051/0004-6361/202038392). arXiv: [2006.10759](https://arxiv.org/abs/2006.10759) [astro-ph.GA].
- Sadler, Elaine M., R. Michael Rich, and D. M. Terndrup (July 1996). “K Giants in Baade’s Window. II. The Abundance Distribution.” In: *AJ* 112, p. 171. DOI: [10.1086/117998](https://doi.org/10.1086/117998). arXiv: [astro-ph/9604045](https://arxiv.org/abs/astro-ph/9604045) [astro-ph].
- Sakamoto, T., N. Matsunaga, T. Hasegawa, and Y. Nakada (Dec. 2012). “Discovery of Mira Variable Stars in the Metal-poor Sextans Dwarf Spheroidal Galaxy.” In: *ApJ* 761, L10, p. L10. DOI: [10.1088/2041-8205/761/1/L10](https://doi.org/10.1088/2041-8205/761/1/L10). arXiv: [1210.7481](https://arxiv.org/abs/1210.7481).
- Salem, Munier, Gurtina Besla, Greg Bryan, Mary Putman, Roeland P. van der Marel, and Stephanie Tonnesen (Dec. 2015). “Ram Pressure Stripping of the Large Magellanic Cloud’s Disk as a Probe of the Milky Way’s Circumgalactic Medium.” In: *ApJ* 815.1, 77, p. 77. DOI: [10.1088/0004-637X/815/1/77](https://doi.org/10.1088/0004-637X/815/1/77). arXiv: [1507.07935](https://arxiv.org/abs/1507.07935) [astro-ph.GA].
- Sanders, Jason L. and Payel Das (Dec. 2018). “Isochrone ages for ~3 million stars with the second Gaia data release.” In: *MNRAS* 481.3, pp. 4093–4110. DOI: [10.1093/mnras/sty2490](https://doi.org/10.1093/mnras/sty2490). arXiv: [1806.02324](https://arxiv.org/abs/1806.02324) [astro-ph.GA].
- Sanders, Jason L., Leigh Smith, and N. Wyn Evans (Oct. 2019). “The pattern speed of the Milky Way bar from transverse velocities.” In: *MNRAS* 488.4, pp. 4552–4564. DOI: [10.1093/mnras/stz1827](https://doi.org/10.1093/mnras/stz1827). arXiv: [1903.02009](https://arxiv.org/abs/1903.02009) [astro-ph.GA].
- Sanders, Jason L., Leigh Smith, N. Wyn Evans, and Philip Lucas (Aug. 2019). “Transverse kinematics of the Galactic bar-bulge from VVV and Gaia.” In: *MNRAS* 487.4, pp. 5188–5208. DOI: [10.1093/mnras/stz1630](https://doi.org/10.1093/mnras/stz1630). arXiv: [1903.02008](https://arxiv.org/abs/1903.02008) [astro-ph.GA].

- Savchenko, S. S., N. Ya. Sotnikova, A. V. Mosenkov, V. P. Reshetnikov, and D. V. Bizyaev (Nov. 2017). "Measuring the X-shaped structures in edge-on galaxies." In: *MNRAS* 471.3, pp. 3261–3272. DOI: [10.1093/mnras/stx1802](https://doi.org/10.1093/mnras/stx1802). arXiv: [1707.04700](https://arxiv.org/abs/1707.04700) [astro-ph.GA].
- Schlaufman, Kevin C. and Andrew R. Casey (Dec. 2014). "The Best and Brightest Metal-poor Stars." In: *ApJ* 797.1, 13, p. 13. DOI: [10.1088/0004-637X/797/1/13](https://doi.org/10.1088/0004-637X/797/1/13). arXiv: [1409.4775](https://arxiv.org/abs/1409.4775) [astro-ph.SR].
- Schlegel, David J., Douglas P. Finkbeiner, and Marc Davis (June 1998). "Maps of Dust Infrared Emission for Use in Estimation of Reddening and Cosmic Microwave Background Radiation Foregrounds." In: *ApJ* 500.2, pp. 525–553. DOI: [10.1086/305772](https://doi.org/10.1086/305772). arXiv: [astro-ph/9710327](https://arxiv.org/abs/astro-ph/9710327) [astro-ph].
- Schmidt, Thomas et al. (June 2020). "The VMC survey – XXXVIII. Proper motion of the Magellanic Bridge." In: *arXiv e-prints*, arXiv:2006.03163, arXiv:2006.03163. arXiv: [2006.03163](https://arxiv.org/abs/2006.03163) [astro-ph.GA].
- Schönrich, Ralph and James Binney (June 2009a). "Chemical evolution with radial mixing." In: *MNRAS* 396.1, pp. 203–222. DOI: [10.1111/j.1365-2966.2009.14750.x](https://doi.org/10.1111/j.1365-2966.2009.14750.x). arXiv: [0809.3006](https://arxiv.org/abs/0809.3006) [astro-ph].
- Schönrich, Ralph and James Binney (Nov. 2009b). "Origin and structure of the Galactic disc(s)." In: *MNRAS* 399.3, pp. 1145–1156. DOI: [10.1111/j.1365-2966.2009.15365.x](https://doi.org/10.1111/j.1365-2966.2009.15365.x). arXiv: [0907.1899](https://arxiv.org/abs/0907.1899) [astro-ph.GA].
- Schultheis, M., N. Ryde, and G. Nandakumar (May 2016). "Temperatures and metallicities of M giants in the Galactic bulge from low-resolution K-band spectra." In: *A&A* 590, A6, A6. DOI: [10.1051/0004-6361/201628266](https://doi.org/10.1051/0004-6361/201628266). arXiv: [1603.02633](https://arxiv.org/abs/1603.02633) [astro-ph.SR].
- Scowcroft, Victoria, Wendy L. Freedman, Barry F. Madore, Andy Monson, S. E. Persson, Jeff Rich, Mark Seibert, and Jane R. Rigby (Jan. 2016). "The Carnegie Hubble Program: The Distance and Structure of the SMC as Revealed by Mid-infrared Observations of Cepheids." In: *ApJ* 816.2, 49, p. 49. DOI: [10.3847/0004-637X/816/2/49](https://doi.org/10.3847/0004-637X/816/2/49). arXiv: [1502.06995](https://arxiv.org/abs/1502.06995) [astro-ph.GA].
- Seidel, M. K., J. Falcón-Barroso, I. Martínez-Valpuesta, P. Sánchez-Blázquez, I. Pérez, R. Peletier, and A. Vazdekis (Aug. 2016). "The BaLROG project - II. Quantifying the influence of bars on the stellar populations of nearby galaxies." In: *MNRAS* 460.4, pp. 3784–3828. DOI: [10.1093/mnras/stw1209](https://doi.org/10.1093/mnras/stw1209). arXiv: [1605.06500](https://arxiv.org/abs/1605.06500) [astro-ph.GA].
- Sellwood, J. A. and J. J. Binney (Nov. 2002). "Radial mixing in galactic discs." In: *MNRAS* 336.3, pp. 785–796. DOI: [10.1046/j.1365-8711.2002.05806.x](https://doi.org/10.1046/j.1365-8711.2002.05806.x). arXiv: [astro-ph/0203510](https://arxiv.org/abs/astro-ph/0203510) [astro-ph].
- Sesar, B. et al. (May 2017). "Machine-learned Identification of RR Lyrae Stars from Sparse, Multi-band Data: The PS1 Sample." In:

- AJ* 153, 204, p. 204. DOI: [10.3847/1538-3881/aa661b](https://doi.org/10.3847/1538-3881/aa661b). arXiv: [1611.08596](https://arxiv.org/abs/1611.08596).
- Shapley, Harlow (Dec. 1940). "An Extension of the Small Magellanic Cloud." In: *Harvard College Observatory Bulletin* 914, pp. 8–9.
- Sharma, Sanjib, Michael R. Hayden, and Joss Bland-Hawthorn (May 2020). "Chemical Enrichment and Radial Migration in the Galactic Disk – the origin of the $[\alpha/\text{Fe}]$ Double Sequence." In: *arXiv e-prints*, arXiv:2005.03646, arXiv:2005.03646. arXiv: [2005.03646](https://arxiv.org/abs/2005.03646) [[astro-ph.GA](https://arxiv.org/archive/astro)].
- Sharma, Sanjib et al. (Apr. 2020). "Fundamental relations for the velocity dispersion of stars in the Milky Way." In: *arXiv e-prints*, arXiv:2004.06556, arXiv:2004.06556. arXiv: [2004.06556](https://arxiv.org/abs/2004.06556) [[astro-ph.GA](https://arxiv.org/archive/astro)].
- Sheffield, A. A., A. M. Price-Whelan, A. Tzanidakis, K. V. Johnston, C. F. P. Laporte, and B. Sesar (Feb. 2018). "A Disk Origin for the Monoceros Ring and A13 Stellar Overdensities." In: *ApJ* 854, 47, p. 47. DOI: [10.3847/1538-4357/aaa4b6](https://doi.org/10.3847/1538-4357/aaa4b6). arXiv: [1801.01171](https://arxiv.org/abs/1801.01171).
- Shen, Juntai, R. Michael Rich, John Kormendy, Christian D. Howard, Roberto De Propris, and Andrea Kunder (Sept. 2010). "Our Milky Way as a Pure-disk Galaxy—A Challenge for Galaxy Formation." In: *ApJ* 720.1, pp. L72–L76. DOI: [10.1088/2041-8205/720/1/L72](https://doi.org/10.1088/2041-8205/720/1/L72). arXiv: [1005.0385](https://arxiv.org/abs/1005.0385) [[astro-ph.CO](https://arxiv.org/archive/astro)].
- Silva Aguirre, V. et al. (Apr. 2018). "Confirming chemical clocks: asteroseismic age dissection of the Milky Way disc(s)." In: *MNRAS* 475.4, pp. 5487–5500. DOI: [10.1093/mnras/sty150](https://doi.org/10.1093/mnras/sty150). arXiv: [1710.09847](https://arxiv.org/abs/1710.09847) [[astro-ph.GA](https://arxiv.org/archive/astro)].
- Simion, I. T., V. Belokurov, M. Irwin, S. E. Koposov, C. Gonzalez-Fernandez, A. C. Robin, J. Shen, and Z. Y. Li (Nov. 2017). "A parametric description of the 3D structure of the Galactic bar/bulge using the VVV survey." In: *MNRAS* 471.4, pp. 4323–4344. DOI: [10.1093/mnras/stx1832](https://doi.org/10.1093/mnras/stx1832). arXiv: [1707.06660](https://arxiv.org/abs/1707.06660) [[astro-ph.GA](https://arxiv.org/archive/astro)].
- Sit, Tawny and M. K. Ness (Sept. 2020). "The Age Distribution of Stars in the Milky Way Bulge." In: *ApJ* 900.1, 4, p. 4. DOI: [10.3847/1538-4357/ab9ff6](https://doi.org/10.3847/1538-4357/ab9ff6). arXiv: [2006.01158](https://arxiv.org/abs/2006.01158) [[astro-ph.SR](https://arxiv.org/archive/astro)].
- Skowron, D. M. et al. (Nov. 2014). "OGLE-ING the Magellanic System: Stellar Populations in the Magellanic Bridge." In: *ApJ* 795.2, 108, p. 108. DOI: [10.1088/0004-637X/795/2/108](https://doi.org/10.1088/0004-637X/795/2/108). arXiv: [1405.7364](https://arxiv.org/abs/1405.7364) [[astro-ph.SR](https://arxiv.org/archive/astro)].
- Skowron, D. M. et al. (June 2020). "OGLE-ing the Magellanic System: Optical Reddening Maps of the Large and Small Magellanic Cloud from Red Clump Stars." In: *arXiv e-prints*, arXiv:2006.02448, arXiv:2006.02448. arXiv: [2006.02448](https://arxiv.org/abs/2006.02448) [[astro-ph.SR](https://arxiv.org/archive/astro)].
- Skrutskie, M. F. et al. (Feb. 2006). "The Two Micron All Sky Survey (2MASS)." In: *AJ* 131.2, pp. 1163–1183. DOI: [10.1086/498708](https://doi.org/10.1086/498708).

- Snaith, O., M. Haywood, P. Di Matteo, M. D. Lehnert, F. Combes, D. Katz, and A. Gómez (June 2015). “Reconstructing the star formation history of the Milky Way disc(s) from chemical abundances.” In: *A&A* 578, A87, A87. DOI: [10.1051/0004-6361/201424281](https://doi.org/10.1051/0004-6361/201424281). arXiv: [1410.3829](https://arxiv.org/abs/1410.3829) [[astro-ph.GA](#)].
- Sohn, Y.-J., J.-H. Park, S.-C. Rey, Y.-W. Lee, H.-I. Kim, S. J. Oh, S.-G. Lee, M. G. Lee, and W. Han (Aug. 2003). “Wide-Field Stellar Distributions around the Remote Young Galactic Globular Clusters Palomar 3 and Palomar 4.” In: *AJ* 126, pp. 803–814. DOI: [10.1086/375907](https://doi.org/10.1086/375907).
- Soszynski, I., A. Udalski, M. Kubiak, M. K. Szymanski, G. Pietrzynski, K. Zebrun, O. Szewczyk, L. Wyrzykowski, and W. A. Dziembowski (Dec. 2004a). “The Optical Gravitational Lensing Experiment. Ellipsoidal Variability of Red Giants in the Large Magellanic Cloud.” In: *Acta Astron.* 54, pp. 347–362. eprint: [astro-ph/0412505](https://arxiv.org/abs/astro-ph/0412505).
- Soszynski, I., A. Udalski, M. Kubiak, M. Szymanski, G. Pietrzynski, K. Zebrun, O. Szewczyk, and L. Wyrzykowski (June 2004b). “The Optical Gravitational Lensing Experiment. Small Amplitude Variable Red Giants in the Magellanic Clouds.” In: *Acta Astron.* 54, pp. 129–152. eprint: [astro-ph/0407057](https://arxiv.org/abs/astro-ph/0407057).
- Soszyński, I., A. Udalski, M. K. Szymański, M. Kubiak, G. Pietrzyński, Ł. Wyrzykowski, O. Szewczyk, K. Ulaczyk, and R. Poleski (Sept. 2009). “The Optical Gravitational Lensing Experiment. The OGLE-III Catalog of Variable Stars. IV. Long-Period Variables in the Large Magellanic Cloud.” In: *Acta Astron.* 59, pp. 239–253.
- Soszyński, I. and P. R. Wood (Feb. 2013). “Semiregular Variables with Periods Lying between the Period-Luminosity Sequences C', C, and D.” In: *ApJ* 763, 103, p. 103. DOI: [10.1088/0004-637X/763/2/103](https://doi.org/10.1088/0004-637X/763/2/103). arXiv: [1212.0549](https://arxiv.org/abs/1212.0549) [[astro-ph.SR](#)].
- Soubiran, C., O. Bienaymé, and A. Siebert (Jan. 2003). “Vertical distribution of Galactic disk stars. I. Kinematics and metallicity.” In: *A&A* 398, pp. 141–151. DOI: [10.1051/0004-6361:20021615](https://doi.org/10.1051/0004-6361:20021615). eprint: [astro-ph/0210628](https://arxiv.org/abs/astro-ph/0210628).
- Spano, M., N. Mowlavi, L. Eyer, G. Burki, J.-B. Marquette, I. Lecoœur-Taïbi, and P. Tisserand (Dec. 2011). “Long period variables in the Large Magellanic Cloud from the EROS-2 survey.” In: *A&A* 536, A60, A60. DOI: [10.1051/0004-6361/201117302](https://doi.org/10.1051/0004-6361/201117302). arXiv: [1109.6132](https://arxiv.org/abs/1109.6132) [[astro-ph.SR](#)].
- Spitoni, E., V. Silva Aguirre, F. Matteucci, F. Calura, and V. Grisoni (Mar. 2019). “Galactic Archaeology with asteroseismic ages: Evidence for delayed gas infall in the formation of the Milky Way

- disc." In: *A&A* 623, A60, A60. DOI: [10.1051/0004-6361/201834188](https://doi.org/10.1051/0004-6361/201834188). arXiv: [1809.00914](https://arxiv.org/abs/1809.00914) [astro-ph.GA].
- Stanimirović, S., L. Staveley-Smith, and P. A. Jones (Mar. 2004). "A New Look at the Kinematics of Neutral Hydrogen in the Small Magellanic Cloud." In: *ApJ* 604.1, pp. 176–186. DOI: [10.1086/381869](https://doi.org/10.1086/381869). arXiv: [astro-ph/0312223](https://arxiv.org/abs/astro-ph/0312223) [astro-ph].
- Stebbins, Joel and A. E. Whitford (Jan. 1947). "Infrared radiation from the region of the galactic center." In: *AJ* 52, p. 130. DOI: [10.1086/106022](https://doi.org/10.1086/106022).
- Subramanian, Smitha and Annapurni Subramaniam (Jan. 2012). "The Three-dimensional Structure of the Small Magellanic Cloud." In: *ApJ* 744.2, 128, p. 128. DOI: [10.1088/0004-637X/744/2/128](https://doi.org/10.1088/0004-637X/744/2/128). arXiv: [1109.3980](https://arxiv.org/abs/1109.3980) [astro-ph.CO].
- Subramanian, Smitha et al. (May 2017). "The VMC Survey - XXIV. Signatures of tidally stripped stellar populations from the inner Small Magellanic Cloud." In: *MNRAS* 467.3, pp. 2980–2995. DOI: [10.1093/mnras/stx205](https://doi.org/10.1093/mnras/stx205). arXiv: [1701.05722](https://arxiv.org/abs/1701.05722) [astro-ph.GA].
- Tian, Hai-Jun, Chao Liu, Yue Wu, Mao-Sheng Xiang, and Yong Zhang (Oct. 2018). "Time Stamps of Vertical Phase Mixing in the Galactic Disk from LAMOST/Gaia Stars." In: *ApJ* 865.2, L19, p. L19. DOI: [10.3847/2041-8213/aaef3](https://doi.org/10.3847/2041-8213/aaef3). arXiv: [1809.06510](https://arxiv.org/abs/1809.06510) [astro-ph.GA].
- Totten, E. J. and M. J. Irwin (Feb. 1998). "The APM survey for cool carbon stars in the Galactic halo. I." In: *MNRAS* 294, p. 1. DOI: [10.1046/j.1365-8711.1998.01086.x](https://doi.org/10.1046/j.1365-8711.1998.01086.x).
- Trabucchi, Michele, Peter R. Wood, Nami Mowlavi, Giada Pastorelli, Paola Marigo, Léo Girardi, and Thomas Lebzelter (Jan. 2021). "Modelling long-period variables - II. Fundamental mode pulsation in the non-linear regime." In: *MNRAS* 500.2, pp. 1575–1591. DOI: [10.1093/mnras/staa3356](https://doi.org/10.1093/mnras/staa3356). arXiv: [2010.13654](https://arxiv.org/abs/2010.13654) [astro-ph.SR].
- Valenti, E., M. Zoccali, A. Renzini, T. M. Brown, O. A. Gonzalez, D. Minniti, V. P. Debattista, and L. Mayer (Nov. 2013). "Stellar ages through the corners of the boxy bulge." In: *A&A* 559, A98, A98. DOI: [10.1051/0004-6361/201321962](https://doi.org/10.1051/0004-6361/201321962). arXiv: [1309.4570](https://arxiv.org/abs/1309.4570) [astro-ph.GA].
- Vasiliev, Eugene and Vasily Belokurov (Aug. 2020). "The last breath of the Sagittarius dSph." In: *MNRAS* 497.4, pp. 4162–4182. DOI: [10.1093/mnras/staa2114](https://doi.org/10.1093/mnras/staa2114). arXiv: [2006.02929](https://arxiv.org/abs/2006.02929) [astro-ph.GA].
- Vasiliev, Eugene, Vasily Belokurov, and Denis Erkal (Feb. 2021). "Tango for three: Sagittarius, LMC, and the Milky Way." In: *MNRAS* 501.2, pp. 2279–2304. DOI: [10.1093/mnras/staa3673](https://doi.org/10.1093/mnras/staa3673). arXiv: [2009.10726](https://arxiv.org/abs/2009.10726) [astro-ph.GA].
- Velazquez, Hector and Simon D. M. White (Apr. 1999). "Sinking satellites and the heating of galaxy discs." In: *MNRAS* 304.2, pp. 254–

270. DOI: [10.1046/j.1365-8711.1999.02354.x](https://doi.org/10.1046/j.1365-8711.1999.02354.x). arXiv: [astro-ph/9809412](https://arxiv.org/abs/astro-ph/9809412) [astro-ph].
- Wagner-Kaiser, R. and Ata Sarajedini (Apr. 2017). “The properties of the Magellanic Bridge based on OGLE IV RR Lyrae variables.” In: *MNRAS* 466.4, pp. 4138–4146. DOI: [10.1093/mnras/stw3206](https://doi.org/10.1093/mnras/stw3206). arXiv: [1612.01811](https://arxiv.org/abs/1612.01811) [astro-ph.GA].
- Walker, Ian R., J. Christopher Mihos, and Lars Hernquist (Mar. 1996). “Quantifying the Fragility of Galactic Disks in Minor Mergers.” In: *ApJ* 460, p. 121. DOI: [10.1086/176956](https://doi.org/10.1086/176956). arXiv: [astro-ph/9510052](https://arxiv.org/abs/astro-ph/9510052) [astro-ph].
- Wegg, Christopher and Ortwin Gerhard (Nov. 2013). “Mapping the three-dimensional density of the Galactic bulge with VVV red clump stars.” In: *MNRAS* 435.3, pp. 1874–1887. DOI: [10.1093/mnras/stt1376](https://doi.org/10.1093/mnras/stt1376). arXiv: [1308.0593](https://arxiv.org/abs/1308.0593) [astro-ph.GA].
- Wegg, Christopher, Ortwin Gerhard, and Matthieu Portail (July 2015). “The structure of the Milky Way’s bar outside the bulge.” In: *MNRAS* 450.4, pp. 4050–4069. DOI: [10.1093/mnras/stv745](https://doi.org/10.1093/mnras/stv745). arXiv: [1504.01401](https://arxiv.org/abs/1504.01401) [astro-ph.GA].
- Weiland, J. L. et al. (Apr. 1994). “COBE Diffuse Background Experiment Observations of the Galactic Bulge.” In: *ApJ* 425, p. L81. DOI: [10.1086/187315](https://doi.org/10.1086/187315).
- Whitelock, P. A., M. W. Feast, F. Marang, and M. A. T. Groenewegen (June 2006). “Near-infrared photometry of carbon stars.” In: *MNRAS* 369, pp. 751–782. DOI: [10.1111/j.1365-2966.2006.10322.x](https://doi.org/10.1111/j.1365-2966.2006.10322.x). eprint: [astro-ph/0603504](https://arxiv.org/abs/astro-ph/0603504).
- Whitelock, P. A., M. W. Feast, and F. Van Leeuwen (May 2008a). “AGB variables and the Mira period-luminosity relation.” In: *MNRAS* 386, pp. 313–323. DOI: [10.1111/j.1365-2966.2008.13032.x](https://doi.org/10.1111/j.1365-2966.2008.13032.x). arXiv: [0801.4465](https://arxiv.org/abs/0801.4465).
- Whitelock, P. A., J. W. Menzies, M. W. Feast, N. Matsunaga, T. Tanabé, and Y. Ita (Apr. 2009). “Asymptotic giant branch stars in the Fornax dwarf spheroidal galaxy.” In: *MNRAS* 394, pp. 795–809. DOI: [10.1111/j.1365-2966.2008.14365.x](https://doi.org/10.1111/j.1365-2966.2008.14365.x). arXiv: [0812.0903](https://arxiv.org/abs/0812.0903).
- Whitelock, P., J. Menzies, M. Feast, F. Marang, B. Carter, G. Roberts, R. Catchpole, and J. Chapman (Apr. 1994). “High-mass-loss AGB stars in the South Galactic Cap.” In: *MNRAS* 267, pp. 711–742. DOI: [10.1093/mnras/267.3.711](https://doi.org/10.1093/mnras/267.3.711).
- Whitelock, Patricia A., Michael W. Feast, and Floor Van Leeuwen (May 2008b). “AGB variables and the Mira period-luminosity relation.” In: *MNRAS* 386, pp. 313–323. DOI: [10.1111/j.1365-2966.2008.13032.x](https://doi.org/10.1111/j.1365-2966.2008.13032.x). arXiv: [0801.4465](https://arxiv.org/abs/0801.4465) [astro-ph].

- Whitelock, Patricia, Michael Feast, and Robin Catchpole (Jan. 1991). "IRAS sources and the nature of the Galactic Bulge." In: *MNRAS* 248, p. 276. DOI: [10.1093/mnras/248.2.276](https://doi.org/10.1093/mnras/248.2.276).
- Widrow, Lawrence M., Susan Gardner, Brian Yanny, Scott Dodelson, and Hsin-Yu Chen (May 2012). "Galactoseismology: Discovery of Vertical Waves in the Galactic Disk." In: *ApJ* 750.2, L41, p. L41. DOI: [10.1088/2041-8205/750/2/L41](https://doi.org/10.1088/2041-8205/750/2/L41). arXiv: [1203.6861](https://arxiv.org/abs/1203.6861) [astro-ph.GA].
- Williams, Angus A. et al. (June 2016). "The Gaia-ESO Survey: Metal-rich Bananas in the Bulge." In: *ApJ* 824.2, L29, p. L29. DOI: [10.3847/2041-8205/824/2/L29](https://doi.org/10.3847/2041-8205/824/2/L29). arXiv: [1605.09684](https://arxiv.org/abs/1605.09684) [astro-ph.GA].
- Wood, P. R. (Apr. 2000). "Variable Red Giants in the LMC: Pulsating Stars and Binaries?" In: *Publ. Astron. Soc. Australia* 17, pp. 18–21. DOI: [10.1071/AS00018](https://doi.org/10.1071/AS00018).
- Wood, P. R. et al. (1999). "MACHO observations of LMC red giants: Mira and semi-regular pulsators, and contact and semi-detached binaries." In: *Asymptotic Giant Branch Stars*. Ed. by T. Le Bertre, A. Lebre, and C. Waelkens. Vol. 191. IAU Symposium, p. 151.
- Wright, Edward L. et al. (Dec. 2010). "The Wide-field Infrared Survey Explorer (WISE): Mission Description and Initial On-orbit Performance." In: *AJ* 140.6, pp. 1868–1881. DOI: [10.1088/0004-6256/140/6/1868](https://doi.org/10.1088/0004-6256/140/6/1868). arXiv: [1008.0031](https://arxiv.org/abs/1008.0031) [astro-ph.IM].
- Wyatt, S. P. and J. H. Cahn (1983). "Kinematics and ages of Mira variables in the greater solar neighborhood." In: *ApJ* 275, pp. 225–239. DOI: [10.1086/161527](https://doi.org/10.1086/161527).
- Wyse, Rosemary F. G. and Gerard Gilmore (May 1988). "The Galactic Spheroid: What is Population II?" In: *AJ* 95, p. 1404. DOI: [10.1086/114738](https://doi.org/10.1086/114738).
- Xu, Yan, Heidi Jo Newberg, Jeffrey L. Carlin, Chao Liu, Licai Deng, Jing Li, Ralph Schönrich, and Brian Yanny (Mar. 2015). "Rings and Radial Waves in the Disk of the Milky Way." In: *ApJ* 801.2, 105, p. 105. DOI: [10.1088/0004-637X/801/2/105](https://doi.org/10.1088/0004-637X/801/2/105). arXiv: [1503.00257](https://arxiv.org/abs/1503.00257) [astro-ph.GA].
- Yoachim, P. and J. J. Dalcanton (Jan. 2006). "Structural Parameters of Thin and Thick Disks in Edge-on Disk Galaxies." In: *AJ* 131, pp. 226–249. DOI: [10.1086/497970](https://doi.org/10.1086/497970). eprint: [astro-ph/0508460](https://arxiv.org/abs/astro-ph/0508460).
- Yuan, H. B., X. W. Liu, and M. S. Xiang (Apr. 2013). "Empirical extinction coefficients for the GALEX, SDSS, 2MASS and WISE passbands." In: *MNRAS* 430.3, pp. 2188–2199. DOI: [10.1093/mnras/stt039](https://doi.org/10.1093/mnras/stt039). arXiv: [1301.1427](https://arxiv.org/abs/1301.1427) [astro-ph.SR].
- Yuan, W., L. M. Macri, S. He, J. Z. Huang, S. M. Kanbur, and C.-C. Ngeow (Oct. 2017). "Large Magellanic Cloud Near-infrared Synoptic Survey. V. Period-Luminosity Relations of Miras." In:

- AJ* 154, 149, p. 149. DOI: [10.3847/1538-3881/aa86f1](https://doi.org/10.3847/1538-3881/aa86f1). arXiv: [1708.04742](https://arxiv.org/abs/1708.04742) [astro-ph.SR].
- Yuan, W., L. M. Macri, A. Javadi, Z. Lin, and J. Z. Huang (Sept. 2018). “Near-infrared Mira Period-Luminosity Relations in M33.” In: *AJ* 156, 112, p. 112. DOI: [10.3847/1538-3881/aad330](https://doi.org/10.3847/1538-3881/aad330). arXiv: [1807.03544](https://arxiv.org/abs/1807.03544) [astro-ph.SR].
- Zaritsky, Dennis, Jason Harris, Eva K. Grebel, and Ian B. Thompson (May 2000). “The Morphologies of the Small Magellanic Cloud.” In: *ApJ* 534.1, pp. L53–L56. DOI: [10.1086/312649](https://doi.org/10.1086/312649). arXiv: [astro-ph/0003155](https://arxiv.org/abs/astro-ph/0003155) [astro-ph].
- Zasowski, G. et al. (Nov. 2017). “Target Selection for the SDSS-IV APOGEE-2 Survey.” In: *AJ* 154.5, 198, p. 198. DOI: [10.3847/1538-3881/aa8df9](https://doi.org/10.3847/1538-3881/aa8df9). arXiv: [1708.00155](https://arxiv.org/abs/1708.00155) [astro-ph.GA].
- Zhao, HongSheng and N. Wyn Evans (Dec. 2000). “The So-called “Bar” in the Large Magellanic Cloud.” In: *ApJ* 545.1, pp. L35–L38. DOI: [10.1086/317324](https://doi.org/10.1086/317324). arXiv: [astro-ph/0009155](https://arxiv.org/abs/astro-ph/0009155) [astro-ph].
- Zivick, Paul, Nitya Kallivayalil, Gurtina Besla, Sangmo Tony Sohn, Roeland P. van der Marel, Andrés del Pino, Sean T. Linden, Tobias K. Fritz, and J. Anderson (Mar. 2019). “The Proper-motion Field along the Magellanic Bridge: A New Probe of the LMC-SMC Interaction.” In: *ApJ* 874.1, 78, p. 78. DOI: [10.3847/1538-4357/ab0554](https://doi.org/10.3847/1538-4357/ab0554). arXiv: [1811.09318](https://arxiv.org/abs/1811.09318) [astro-ph.GA].
- Zivick, Paul et al. (Sept. 2018). “The Proper Motion Field of the Small Magellanic Cloud: Kinematic Evidence for Its Tidal Disruption.” In: *ApJ* 864.1, 55, p. 55. DOI: [10.3847/1538-4357/aad4b0](https://doi.org/10.3847/1538-4357/aad4b0). arXiv: [1804.04110](https://arxiv.org/abs/1804.04110) [astro-ph.GA].
- Zoccali, M. (Aug. 2019). “The Stellar Population, 3D structure, and kinematics of the Galactic bulge.” In: *Boletin de la Asociacion Argentina de Astronomia La Plata Argentina* 61, pp. 137–144.
- Zoccali, M., V. Hill, A. Lecureur, B. Barbuy, A. Renzini, D. Minniti, A. Gómez, and S. Ortolani (July 2008). “The metal content of bulge field stars from FLAMES-GIRAFFE spectra. I. Stellar parameters and iron abundances.” In: *A&A* 486.1, pp. 177–189. DOI: [10.1051/0004-6361:200809394](https://doi.org/10.1051/0004-6361:200809394). arXiv: [0805.1218](https://arxiv.org/abs/0805.1218) [astro-ph].
- Zoccali, M., A. Renzini, S. Ortolani, L. Greggio, I. Saviane, S. Cassisi, M. Rejkuba, B. Barbuy, R. M. Rich, and E. Bica (Mar. 2003). “Age and metallicity distribution of the Galactic bulge from extensive optical and near-IR stellar photometry.” In: *A&A* 399, pp. 931–956. DOI: [10.1051/0004-6361:20021604](https://doi.org/10.1051/0004-6361:20021604). arXiv: [astro-ph/0210660](https://arxiv.org/abs/astro-ph/0210660) [astro-ph].
- Zoccali, M. et al. (Mar. 2017). “The GIRAFFE Inner Bulge Survey (GIBS). III. Metallicity distributions and kinematics of 26 Galac-

- tic bulge fields." In: *A&A* 599, A12, A12. DOI: [10.1051/0004-6361/201629805](https://doi.org/10.1051/0004-6361/201629805). arXiv: [1610.09174](https://arxiv.org/abs/1610.09174) [[astro-ph.GA](#)].
- de Boer, T. J. L., V. Belokurov, and S. E. Koposov (Jan. 2018). "The fall of the Northern Unicorn: tangential motions in the Galactic anticentre with SDSS and Gaia." In: *MNRAS* 473, pp. 647–662. DOI: [10.1093/mnras/stx2391](https://doi.org/10.1093/mnras/stx2391). arXiv: [1706.09468](https://arxiv.org/abs/1706.09468).
- de Grijs, Richard, James E. Wicker, and Giuseppe Bono (May 2014). "Clustering of Local Group Distances: Publication Bias or Correlated Measurements? I. The Large Magellanic Cloud." In: *AJ* 147.5, 122, p. 122. DOI: [10.1088/0004-6256/147/5/122](https://doi.org/10.1088/0004-6256/147/5/122). arXiv: [1403.3141](https://arxiv.org/abs/1403.3141) [[astro-ph.GA](#)].
- de Vaucouleurs, G. (May 1955). "Studies of Magellanic Clouds. I. Dimensions and structure of the Large Cloud." In: *AJ* 60, p. 126. DOI: [10.1086/107173](https://doi.org/10.1086/107173).
- de Vaucouleurs, G. and K. C. Freeman (Jan. 1972). "Structure and dynamics of barred spiral galaxies, in particular of the Magellanic type." In: *Vistas in Astronomy* 14.1, pp. 163–294. DOI: [10.1016/0083-6656\(72\)90026-8](https://doi.org/10.1016/0083-6656(72)90026-8).
- van Gelder, M. L. et al. (Apr. 2020). "VLT/X-shooter spectroscopy of massive young stellar objects in the 30 Doradus region of the Large Magellanic Cloud." In: *A&A* 636, A54, A54. DOI: [10.1051/0004-6361/201936361](https://doi.org/10.1051/0004-6361/201936361). arXiv: [2002.02690](https://arxiv.org/abs/2002.02690) [[astro-ph.SR](#)].
- van de Ven, G., R. C. E. van den Bosch, E. K. Verolme, and P. T. de Zeeuw (Jan. 2006). "The dynamical distance and intrinsic structure of the globular cluster ω Centauri." In: *A&A* 445.2, pp. 513–543. DOI: [10.1051/0004-6361:20053061](https://doi.org/10.1051/0004-6361:20053061). arXiv: [astro-ph/0509228](https://arxiv.org/abs/astro-ph/0509228) [[astro-ph](#)].
- van der Marel, Roeland P. and Maria-Rosa L. Cioni (Oct. 2001). "Magellanic Cloud Structure from Near-Infrared Surveys. I. The Viewing Angles of the Large Magellanic Cloud." In: *AJ* 122.4, pp. 1807–1826. DOI: [10.1086/323099](https://doi.org/10.1086/323099). arXiv: [astro-ph/0105339](https://arxiv.org/abs/astro-ph/0105339) [[astro-ph](#)].
- van der Marel, Roeland P. and Nitya Kallivayalil (Feb. 2014). "Third-epoch Magellanic Cloud Proper Motions. II. The Large Magellanic Cloud Rotation Field in Three Dimensions." In: *ApJ* 781.2, 121, p. 121. DOI: [10.1088/0004-637X/781/2/121](https://doi.org/10.1088/0004-637X/781/2/121). arXiv: [1305.4641](https://arxiv.org/abs/1305.4641) [[astro-ph.CO](#)].

COLOPHON

This document was typeset using the typographical look-and-feel classicthesis developed by André Miede.

Final Version as of April 9, 2021 (classicthesis version 4.2).